ALMA MATER STUDIORUM - UNIVERSITÀ DI BOLOGNA

SCUOLA DI INGEGNERIA E ARCHITETTURA

DIPARTIMENTO DIN

CORSO DI LAUREA MAGISTRALE IN INGEGNERIA ENERGETICA

TESI DI LAUREA

In

TERMOTECNICA E IMPIANTI TERMOTECNICI M

HARDWARE-IN-THE-LOOP EXPERIMENTS FOR HEAT PUMP CONTROLLER OPTIMIZATION

CANDIDATO:
Mara Magni

RELATORE:
Prof. Ing. Gian Luca Morini

CORRELATORI:
Dr.-Ing. Fabian Ochs
Dipl.-Ing. Dietmar Siegele BSc MSc

Anno Accademico 2014/2015

Sessione III

LEOPOLD-FRANZENS-UNIVERSITÄT INNSBRUCK
FAKULTÄT FÜR TECHNISCHE WISSENSCHAFTEN

HARDWARE-IN-THE-LOOP EXPERIMENTS FOR HEAT PUMP CONTROLLER OPTIMIZATION

Student:
Mara Magni

Supervisor:
Prof. Ing. Gian Luca Morini

Co-Supervisors:
Dr.-Ing. Fabian Ochs
Dipl.-Ing. Dietmar Siegele BSc MSc

AKNOWLEDGMENT

After an intensive period of six months, today is the day: writing this note of thanks is the finishing touch on my thesis. It has been a period of intense learning for me, not only in the scientific area, but also on a personal level. Writing this thesis has had a big impact on me. I would like to reflect on the people who have supported and helped me so much throughout this period.

I am thankful to all my colleagues of the department "Energieeffizientes Bauen" of the Innsbruck University.
The door to Dipl.-Ing. Dietmar Siegele office was always open whenever I ran into a trouble spot or had a question about my research or writing. He consistently allowed this paper to be my own work, but steered me in the right direction whenever he thought I needed it.
My sincere gratitude to Dr. Ing. Fabian Ochs for the continuous support, and knowledge. I am also thankful to him for encouraging the use of correct grammar and consistent notation in my writings and for carefully reading and commenting on countless revisions of this manuscript.

I am also grateful to my supervisor Gian Luca Morini. I want to thank you for encouraging and supporting me in this experience.

A very special thanks goes to my friend and colleague Eleonora Leonardi for sharing with me this experience from every point of view. Your support was essential.

I am also thankful to my boyfriend Giacomo for supporting and standing me in all the moment of crisis and for giving me all the necessary time to achieve my university goals. Thank you for always being willing to listen when I need to talk.

Finally, I must express my very profound gratitude to my parents for providing me with unfailing support and continuous encouragement throughout my years of study. This accomplishment would not have been possible without them. Thank you

RINGRAZIAMENTI

Dopo un intenso periodo di sei mesi oggi è il giorno, scrivere queste note di ringraziamento è il tocco finale alla mia tesi. In questo periodo ho imparato molto, non solo nell'ambito scientifico ma anche a livello personale. Vorrei riflettere sulle persone che mi hanno supportato ed aiutato in questo periodo.

Vorrei ringraziare i colleghi del dipartimento "Energieeffizientes Bauen" dell'Università di Innsbruck.
La porta dell'ufficio del dottorando Dipl.-Ing. Dietmar Siegele è sempre stata aperta a ricevermi ogni qualvolta avessi avuto problemi o domande. Dietmar ha permesso che questo lavoro fosse mio ma mi ha guidato nella giusta direzione quando ne ho avuto bisogno.
La mia gratitudine va a Dr. Ing. Fabian Ochs per il suo supporto e le sue conoscenze. Lo ringrazio per avermi incoraggiato nell'uso di una grammatica corretta e per aver letto attentamente e commentato le diverse versioni di questo lavoro.

Ringrazio in mio professore Gian Luca Morini per avermi incoraggiato ad intraprendere questa strada e supportato lungo il percorso.

Un ringraziamento speciale va alla mia amica e collega Eleonora Leonardi per aver condiviso con me ogni momento di questa esperienza sotto tutti i punti di vista. Il tuo supporto è stato essenziale.

Grazie al mio ragazzo Giacomo per avermi supportato e sopportato nei momenti di isteria pre-esame e per avermi sempre lasciato tutto il tempo necessario al mio percorso universitario. Grazie per avermi sempre ascoltato anche nei momenti di pazzia.

Infine, voglio esprimere la mia più profonda gratitudine per i miei genitori che mi hanno sempre supportato e continuamente incoraggiato durante questo lungo percorso. Non avrei potuto realizzare questo obbiettivo senza di voi. Grazie.

ABSTRACT

The goal of this master thesis is to optimize the micro-heat pump controller by means of software and hardware in the loop (HiL) simulations. An optimized controller is important to ensure comfortable condition in the building, a high energy efficiency, and a long life of the mechanical components. The HiL simulations are essential for the analysis of the heat pump behaviour and for the detection of the implementation error and bugs.

A façade-integrated mechanical ventilation with heat recovery (MVHR) in combination with a micro-heat pump (m-HP) is developed within the framework of the European project iNSPiRe. A functional model of the MVHR and micro-heat pump is developed and integrated in a test façade. This experimental work is done using PASSYS test cell (Passive Solar System and Component Testing) and a dynamic Simulink model of a demo building in order to be able to test the m-HP under different conditions. The HiL simulations involve the hardware (the PASSYS test cell) and the software (Simulink). The data exchange between these two actors is done with BCVTB (Building Control Virtual Test Bed). With this experimental setup, it is possible to reproduce the internal and external ambient conditions with which the m-HP operates. The PASSYS test cell environment permits to get measured data of the m-HP behaviour and of the airflows used by the m-HP. The temperature deviations between the set point temperatures (set by the simulation) and the measured temperatures in the coldbox and test room are analysed in order to ensure the quality of the HiL simulations results. A performances map of the heat pump working points (power and performances) is defined by using the PASSYS test cell dynamic behaviour.

A dynamic Simulink model of the controller and of the heat pump based on lookup tables is developed within this work and validated by means of HiL simulations. This model is used in order to optimize the parameter of the controller and to test different types of controller. The parameters of the controller are determined by studying the dynamic behaviour of the system with an open loop configuration.

From the analysis of the dynamic behaviour of the simple (lumped capacity) and complex (two star nodes) building models, it turns out that the simple building model is not accurate enough in order to be used for the simulations and analysis of the controller behaviour.

From the comparison between experimental and simulation results, it can be seen that the model of the heat pump and controller delivers accurate results when the extract air is dry while the deviation between the Simulink model and the measured data increases when the relative humidity of the extract air increases. This effect is caused by the enhanced power of the heat pump when it operates with high level of relative humidity in the extract air. The model can be improved by measuring more working points of the heat pump with different level of relative humidity in the extract airflow.

ABSTRACT

L’obiettivo di questa tesi è l’ottimizzazione del controllo della micro-pompa di calore tramite l’uso di simulazioni software e simulazioni Hardware in the Loop (HiL). Un controllo ottimizzato garantisce un elevato livello di comfort all’interno dell’abitazione, un’elevata efficienza energetica ed una vita longeva dei componenti meccanici della pompa di calore. Le simulazioni HiL sono essenziali per la caratterizzazione della pompa di calore e per la detenzione di eventuali errori di implementazione.

Grazie al progetto europeo iNSPIRe è stato sviluppato un sistema di ventilazione meccanica controllata con recuperatore di calore e micro-pompa di calore integrato alla facciata, tale sistema è stato studiato all’interno di questo lavoro. La parte sperimentale di questa tesi è basata sull’utilizzo della PASSYS test cell (Passive Solar System and Component Testing) e di un modello di simulazione dinamico implementato in Simulink.

Il funzionamento della pompa di calore in diverse condizioni è stato testato mediante HiL (Hardware in the Loop). I due attori coinvolti nelle simulazioni HiL sono la PASSYS test cell (hardware) e Simulink (software) per lo scambio di dati è stato usato l’ambiente software BCVTB (Building Control Virtual Test Bed). All’interno della PASSYS test cell è possibile riprodurre le condizioni dell’aria negli ambienti esterno ed interno tra i quali la micro-pompa di calore lavora. L’ambiente della PASSYS test cell, grazie ai sensori installati, permette di misurare diverse variabili che caratterizzano il comportamento della pompa di calore. Le deviazioni tra le temperature di set point determinate dal software e le temperature misurate all’interno della coldbox e della test room sono state analizzate in modo da garantire la qualità dei risultati ottenuti con le simulazioni HiL. Grazie ai dati misurati nella PASSYS test cell è stato possibile definire una mappa delle prestazioni della pompa di calore. Il modello della pompa di calore e del sistema di controllo, basato sull’uso delle lookup tables, è stato implementato in Simulink e validato mediante l’uso di simulazioni HiL. Questo modello è stato usato per l’ottimizzazione dei parametri di controllo della pompa di calore e per l’analisi di diverse tipologie di controllo.

Dall’analisi delle due diverse tipologie di modello di edificio “Simple” (a parametri concentrati) e “Complex” (a due nodi) è stato riscontrato che il modello “Simple” non è abbastanza accurato per essere utilizzato nella simulazione ed analisi del sistema di controllo.

Dalla comparazione di risultati ottenuti mediante simulazioni HiL e dei risultati ottenuti dal modello Simulink della pompa di calore e del sistema di controllo si può concludere che il modello Simulink implementato genera risultati realistici in particolar modo quando si considerano situazioni in cui la pompa di calore lavora con aria estratta con basso grado di umidità. La potenza che la pompa può produrre aumenta quando l’aria estratta ha un elevato tasso di umidità. Questo effetto può essere considerato nel modello ampliando la mappa dei punti di funzionamento della pompa di calore con diversi livelli di umidità relativa.

TABLE OF CONTENTS

LIST OF SYMBOLS AND UNITS

λ	Thermal conductivity	$\left[\frac{\mathrm{W}}{\mathrm{m \cdot K}}\right]$
ϑ	Relative temperature	$[°\mathrm{C}]$
T	Absolute temperature	$[\mathrm{K}]$
ρ	Density of the material	$\left[\frac{\mathrm{kg}}{\mathrm{m}^3}\right]$
c_v	Specific heat capacity at constant volume	$\left[\frac{\mathrm{J}}{\mathrm{kg \cdot K}}\right]$
c_p	Specific heat capacity at constant pressure	$\left[\frac{\mathrm{J}}{\mathrm{kg \cdot K}}\right]$
h	Heat transfer coefficient	$\left[\frac{\mathrm{W}}{\mathrm{m}^2\ \mathrm{K}}\right]$
r	Radius	$[\mathrm{m}]$
l	Length	$[\mathrm{m}]$
$\dot{C}$	Heat capacity rate	$\left[\frac{\mathrm{W}}{\mathrm{K}}\right]$
C	Capacity	$\left[\frac{\mathrm{J}}{\mathrm{kg\ K}}\right]$
$\dot{m}$	Massflow	$\left[\frac{\mathrm{kg}}{\mathrm{s}}\right]$
U	Thermal transmittance	$\left[\frac{\mathrm{W}}{\mathrm{m}^2\ \mathrm{K}}\right]$
A	Area	$[\mathrm{m}^2]$
E	Effectiveness	$[-]$
P	Electric power	$[\mathrm{W}]$
$\dot{Q}$	Thermal power	$[\mathrm{W}]$
p	Pressure	$[\mathrm{Pa}]$
V	Volume	$[\mathrm{m}^3]$
$\dot{V}$	Volume flow	$\left[\frac{m^3}{s}\right]$
R_{air}	Air gas constant	$\left[\frac{\mathrm{J}}{\mathrm{kg\ K}}\right]$
x	Mass fraction	$\left[\frac{\mathrm{kg}}{\mathrm{kg}}\right]$
d	Thickness	$[\mathrm{m}]$
Ψ	Linear heat transfer coefficient	$\left[\frac{\mathrm{W}}{\mathrm{m\ K}}\right]$
M	Mass	$[\mathrm{Kg}]$
R	Thermal resistance	$\left[\frac{\mathrm{m}^2\ \mathrm{K}}{\mathrm{W}}\right]$
H	Heat transfer coefficient	$\left[\frac{\mathrm{W}}{\mathrm{K}}\right]$

σ	Boltzmann constant	$5.67 \cdot 10^{-8}\ \left[\frac{\mathrm{W}}{\mathrm{K}^4\ \mathrm{m}^2}\right]$
ε	Emissivity of the surface	$[-]$
α	Absorption factor	$[-]$
h	Enthalpy	$\left[\frac{\mathrm{J}}{\mathrm{kg}}\right]$
c	Fluid speed	$\left[\frac{\mathrm{m}}{\mathrm{s}}\right]$
g	Gravity acceleration	$\left[\frac{\mathrm{m}}{\mathrm{s}^2}\right]$
z	Height	$[\mathrm{m}]$
v	Specific volume	$\left[\frac{\mathrm{m}^3}{\mathrm{kg}}\right]$
L	Work	$\left[\frac{\mathrm{m}^2}{\mathrm{s}^2}\right]$
F	Internal losses	$\left[\frac{\mathrm{m}^2}{\mathrm{s}^2}\right]$
η	Efficiency	$[-]$
β	Pressure ratio	$[-]$
n	Number of cycles per second	$\left[\frac{\mathrm{n}}{\mathrm{s}}\right]$
K_p	Proportional gain	$\left[\frac{\mathrm{K}}{\mathrm{K}}\right]$
K_i	Integral gain	$\left[\frac{1}{\mathrm{s}}\right]$
K_B	Back coefficient	$\left[\frac{1}{\mathrm{s}}\right]$
f	Frequency	$[\mathrm{Hz}]$
e	Error	[-]
τ	Time constant	[s]
Q	Thermal energy	[Wh]
E	Electric energy	[Wh]

LIST OF ABBREVIATIONS

iNSPiRe	Infrastructure for Spatial Information in Europe
MVHR	Mechanical Ventilation System with Heat Recovery
m–HP	micro-Heat Pump
PASSYS	Passive Solar Systems and Component Testing
BU	Backup
CARNOT	Conventional And Renewable eNergy systems OpTimization Blockset
NTU	Number of Transfer Units
COP	Coefficient of Performance
$SCOP_{HP}$	Seasonal Coefficient of Performance of the Heat Pump
$SCOP_{SYS}$	Seasonal Coefficient of Performance of the Heating SYStem
PI	Proportional Integrative
LuT	Lookup table
1D	One dimensional
2D	Two dimansional
BCVTB	Building Control Virtual Test Bed
HiL	Hardware in the Loop
TRIAC	TRIode for Alternating Current
LCC	Life Cycle Cost

LIST OF SUBSCRIPTS

in	Internal
ex	External
ins	Insulation
min	Minimum
ext	Extract
amb	Ambient
el	Electric
air	Air
H_2O	Water
CO_2	Carbon Dioxide
sup	Supply
inf	Infiltration
ztz	Zone to Zone
$inters$	Intersection
$mean$	Mean value
$vent$	Ventilation
tr	Transmission
irr	Irradiation
$int\ load$	Internal load
$heat$	Heating System
tb	Thermal Bridge
$conv$	Convective
s	Surface
rad	Radiative
ex	Exchanged
$evap$	Evaporator
$cond$	Condenser
is	Isentropic
m	Mechanic
el	Electric
vol	Volumetric
$meas$	Measured
tr	Test room
cb	Coldbox
amb	Ambient
$diff$	Difference
sim	Simulated

1 INTRODUCTION

1.1 iNSPIRe PROJECT

“The objective of iNSPiRe (Infrastructure for Spatial Information in Europe) is to tackle the problem of high-energy consumption by producing systemic renovation packages that can be applied to residential and tertiary buildings. The renovation packages developed by iNSPiRe aim to reduce the primary energy consumption of a building to lower than 50 $\left[\frac{\mathrm{kWh}}{\mathrm{m^2\ a}}\right]$. The packages need to be suitable to a variety of climates while ensuring optimum comfort for the building users” (iNSPIRe, 2016). After an analysis of building stock across Europe the second stage of iNSPiRe is the development of multifunctional renovation kits that involves innovative envelope technologies, energy generation systems and energy distribution systems. This multifunctional renovation kits will be installed and tested on three case studies, two residential and one office building, in Germany, Spain and Italy.
A decentralised façade-integrated mechanical ventilation system with heat recovery (MVHR) and a micro heat pump is developed by the University of Innsbruck, Unit for Energy Efficient Building, together with the companies SIKO Solar (Jenbach, Austria) and Gumpp & Maier (Binswangen, Germany).

The present work is focused on the optimization of the façade integrated micro-heat pump (m–HP) in combination with mechanical ventilation with heat recovery (MVHR) control. The PASSYS test cell is used in order to test the performance of the mechanical ventilation unit with heat recovery and of the micro-heat pump.

1.1 HEAT PUMP AND HEAT RECOVERY SYSTEM

Figure 1-1 shows the sketch of the heat pump and of the MVHR. The heat pump recovers energy from the exhaust airflow and increases the temperature of the inlet airflow. The heat recovery system preheats the inlet airflow by using the energy of the extract airflow. Condensation can occur inside the heat exchanger when the extract air has high humidity level and/or the ambient air has low temperature. The preheater is present in order to avoid the icing of the condensation inside the heat exchanger. The heat pump compressor is speed controlled. The backup heater placed after the heat pump condenser, works when the heat pump does not deliver enough power to the supply airflow. A more detailed description of the heating system can be found in the chapter 3.

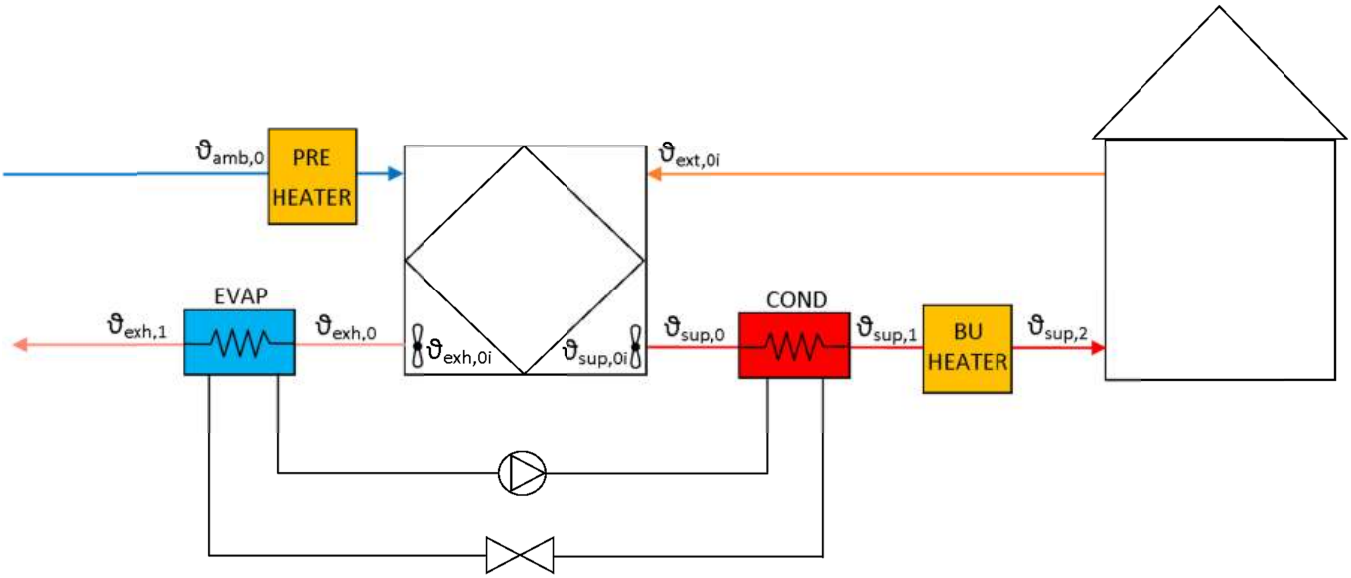

Figure 1-1: Heat pump and MVHR sketch

1.2 BUILDING

The building under study has been identified within the iNSPIRe project as a reference building. "*The demo building in Ludwigsburg, Germany is an example of social housing built in the 1970s, which contains four flats on four stories. During the renovation process a timber frame façade is fitted onto the building. The m–HP with the MVHR is integrated into the prefabricated façade. The prefabricated unit is designed as a compact system for minimal space use. Renovations with minimum intervention are enabled (minimum invasive renovation). A minimal installation effort is desirable for economic reasons. As the whole solution will be façade integrated and prefabricated, construction and installation time can be kept very short*." (Dermentzis, Ochs, Siegele, & Feist, 2014)

Figure 1-2 shows the plan of the flat under study. Each colour represents one zone of the model. The sketch of the air ducts is present in the figure. As it can be seen, the air is extracted from two zones and supplied in other three zones. The designed volume flow is 120 $\left[\frac{\mathrm{m}^3}{\mathrm{h}}\right]$. The whole flat is simulated by using six zones. Moreover, the connections between the zones are considered. The following sections describe the fundamental equations implemented in the model. The CARNOT toolbox (Juelich, 2016) is used for the model implementation.

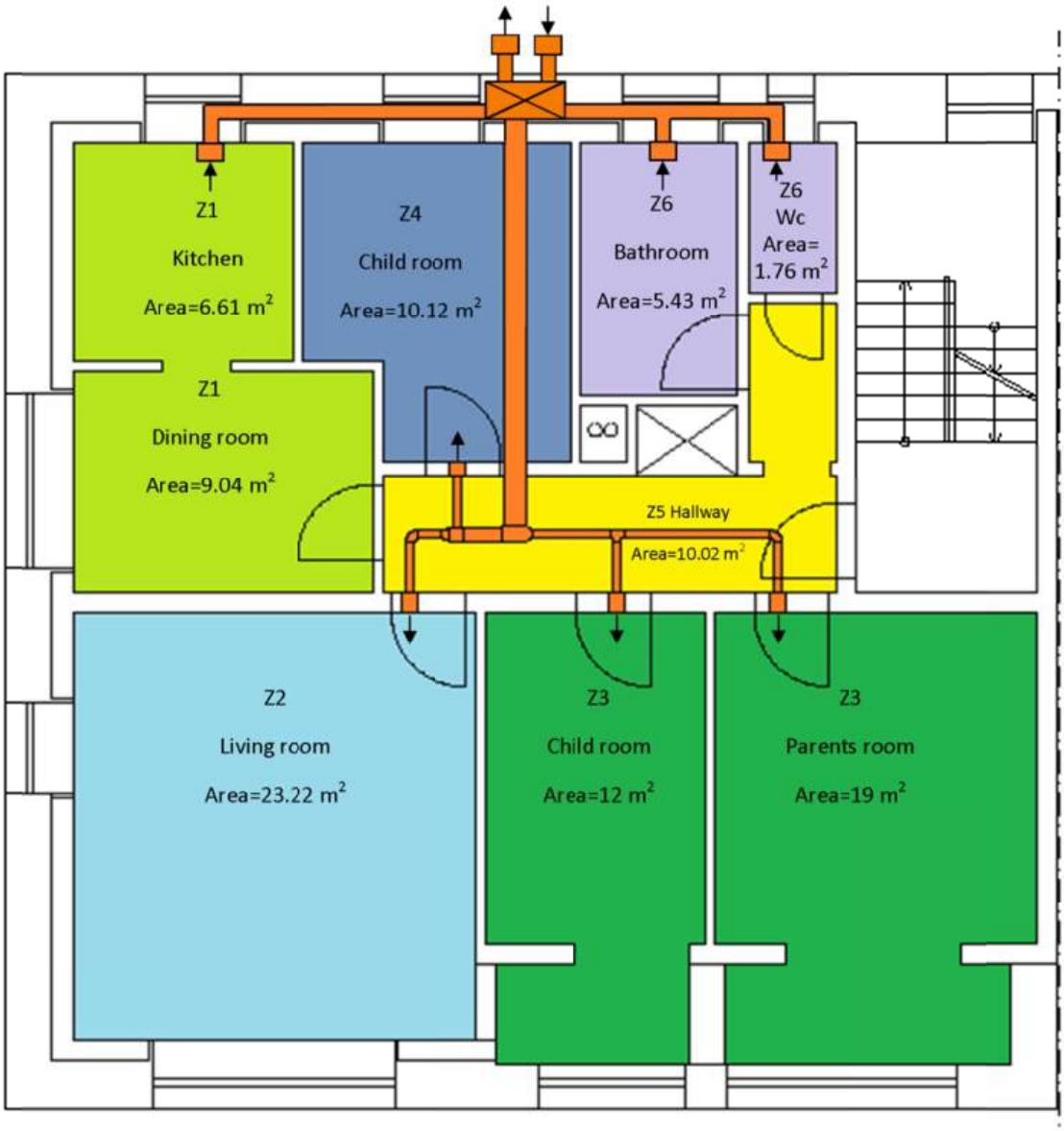

Figure 1-2: Ground floor (iNSPIRe, 2016)

2 BUILDING MODELS

2.1 MATHEMATICAL DESCRIPTION

2.1.1 Transmission Losses

The transmission losses can be described with the Fourier equation (2.1). This is the generic equation and it is valid for a generic material with variable properties λ, ρ, c_v.

$$\begin{cases} \nabla \cdot (\lambda \, \nabla \vartheta) = \rho \, c_v \dfrac{\partial \vartheta}{\partial t} \\ \vartheta(x_0, t) = a(t) \\ \vartheta(x_1, t) = b(t) \\ \vartheta(x, t_0) = c(x) \end{cases} \tag{2.1}$$

Each wall layer has constant properties, and the problem can be studied just in one spatial coordinate. For these reasons, the equation (2.1) can be written as the (2.2):

$$\frac{\partial^2 \vartheta}{\partial x^2} = \frac{\rho \, c_v}{\lambda} \frac{\partial \vartheta}{\partial t} \tag{2.2}$$

From this point, the transmission losses are calculated in different ways within the two models in the chapters 2.2.2 and 2.3.3.

2.1.2 Ventilation Losses

The mechanical ventilation with heat recovery system and the infiltration are described in this section. In the flat under study, the air is extracted from two zones and supplied to three zones, the volume flows are summarized in Table 2-1. In the hallway, the air is neither supplied nor extracted. The air supplied in the zones 2, 3 and 4 pass through the hallway in order to reach the extraction points in the zones 1 and 6. In Figure 1-2, the mechanical ventilation ducts are shown.

Table 2-1: Extract and supply air volume flows

	Zone		Volume flow $\left[\frac{\mathrm{m}^3}{\mathrm{h}}\right]$
Extract air	1	Kitchen	60
	6	Bathroom and WC	60
Supply air	2	Living room	50
	3	Child and parents room	40
	4	Child room	30
-	5	Hallway	0

Ducts

The air ducts losses represent a heat source for the zones 4, 5, 2 and 3, as it can be seen in Figure 1-2. The heat transfer is calculated by using a static formulation. Figure 2-1 represents the duct section, with the insulation layer and the steel layer.

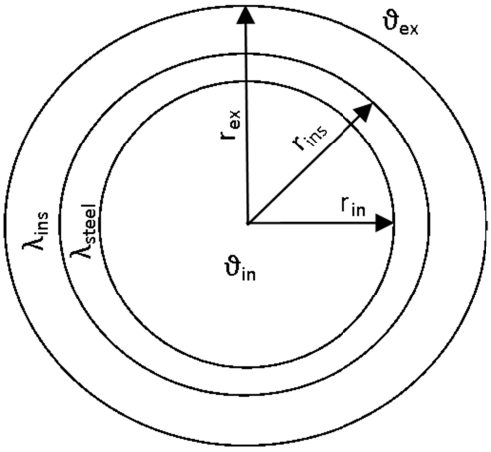

Figure 2-1: Ducts section

The resistance of the ducts is described in the equation (2.3):

$$R_{pipe} = \frac{1}{h_{in} \cdot 2\pi \cdot l \cdot r_{in}} + \frac{1}{2\pi \cdot l \cdot \lambda_{steel}} \cdot \ln\left(\frac{r_{ins}}{r_{in}}\right) + \frac{1}{2\pi \cdot l \cdot \lambda_{ins}} \ln\left(\frac{r_{ex}}{r_{ins}}\right) + \frac{1}{h_{ex} \cdot 2\pi \cdot l \cdot r_{ex}} \qquad (2.3)$$

Where:

- h_{in}, h_{ex} are the internal and external heat transmission coefficient $\left[\frac{W}{m^2\,K}\right]$;
- l is the length of the considered duct $[m]$;
- r_{in}, r_{ins}, r_{ex} are the internal and ezternal insulation radius and the external duct radius $[m]$;
- $\lambda_{ins}, \lambda_{steel}$ is the conductivity coefficient of the insulation and of the steel $\left[\frac{W}{m\,K}\right]$.

The heat transfer is calculated according to the equation (2.4) with the hypothesis of constant ϑ_{in} and ϑ_{ex} for the length l of the duct:

$$\dot{Q}_{pipe} = \frac{1}{R_{pipe}} \cdot (\vartheta_{in} - \vartheta_{ex}) \qquad (2.4)$$

Mechanical Ventilation with Heat Recovery (MVHR)

The mechanical ventilation involves a counter/cross flow heat exchanger. Figure 2-2 shows the sketch of the heat exchanger. The blue arrow represents the ambient air while the red one represents the extract air. The pre-heater operates in case of low ambient air temperature $\vartheta_{amb,0i}$, in order to avoid ice formation in the heat exchanger.

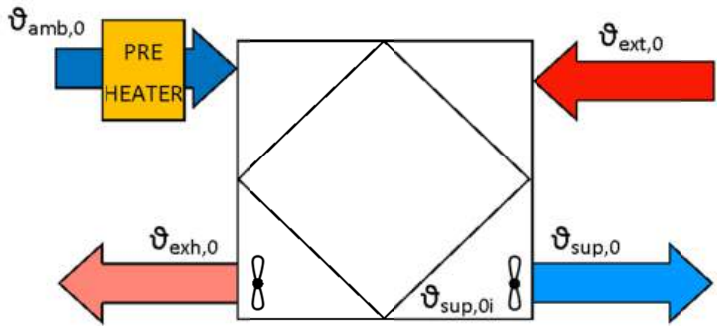

Figure 2-2: Sketch of the heat exchanger

In Simulink, the temperature of the supply airflow is calculated with given heat recovery effectiveness and the inlet air states. The NTU (Number of Transfer Unit) method is used in order to calculate $\vartheta_{sup,0i}$. It is supposed that the two flows have the same heat capacity rate $\dot{C} = \frac{\dot{C}_c}{\dot{C}_h} = 1$, this hypothesis is realistic, in case of balanced system, because the two flows have the same mass flow and almost the same capacity because they are both air flows. The maximum value of heat transfer rate is given by the equation (2.5):

$$\dot{Q}_{max} = \dot{C}_{min} \cdot (\vartheta_{ext,0} - \vartheta_{amb,1}) \tag{2.5}$$

Where: $\dot{C}_{min} = mi\,n\left(\dot{C}_h = \dot{m}_{ext} \cdot c_{p_{ext}}; \dot{C}_c = \dot{m}_{amb} \cdot c_{p_{amb}}\right)$ $\left[\frac{\mathrm{W}}{\mathrm{K}}\right]$

In this case $\dot{C}_h = \dot{C}_c$.

The effectiveness of the heat exchanger is calculated by using the NTU method, for this case it is described by the equation (2.6):

$$E = \frac{NTU}{1 + NTU}; \qquad \mathrm{NTU} = \frac{U \cdot A}{\dot{C}_{min}}; \tag{2.6}$$

The heat transfer effectiveness is the ratio between the exchanged thermal power and the maximum value of heat transfer rate:

$$E = \frac{NTU}{1 + NTU} = \frac{\dot{Q}_{exchanged}}{\dot{Q}_{max}} = \frac{\vartheta_{sup,0i} - \vartheta_{amb,1}}{\vartheta_{ext,0i} - \vartheta_{amb,1}}; \tag{2.7}$$

Where:

- U is the overall heat transfer coefficient $\left[\frac{\mathrm{W}}{\mathrm{m^2\,K}}\right]$;
- A is the heat transfer area $[\mathrm{m^2}]$.

From the equation (2.7) it is possible to define the equation for the $\vartheta_{sup,0i}$ determination:

$$\vartheta_{sup,0i} = \frac{NTU \cdot \vartheta_{ext,0i} + \vartheta_{amb,1}}{1 + NTU} \tag{2.8}$$

$\vartheta_{sup,0}$ is then calculated, with the equation (2.9), by considering the temperature increment caused by the fan.

$$\vartheta_{sup,0} = \vartheta_{sup,0i} + \frac{P_{el}}{\dot{m}_{air} \cdot c_{p_{air}}} \tag{2.9}$$

Where:

- P_{el} is the electric power demand of the fan [W];
- $\dot{m}_{air}$ is the air massflow $\left[\frac{\text{kg}}{\text{s}}\right]$;
- c_p is the specific heat capacity of the air $\left[\frac{\text{J}}{\text{kg K}}\right]$.

Zone balances

Each zone *i* has balances for:

- $\dot{Q}_i = \sum_{j=1}^{n} \dot{Q}_j$ Power balance [W];
- $\dot{m}_{i,air} = \sum_{j=1}^{n} \dot{m}_{j,air}$ Air mass balance $\left[\frac{\text{kg}}{\text{s}}\right]$;
- $\dot{m}_{i,H_2O} = \sum_{j=1}^{n} \dot{m}_{j,H_2O}$ Vapor mass balance $\left[\frac{\text{kg}}{\text{s}}\right]$;
- $\dot{m}_{i,CO_2} = \sum_{j=1}^{n} \dot{m}_{j,CO_2}$ Carbon dioxide mass balance $\left[\frac{\text{kg}}{\text{s}}\right]$.

The simple building model has only one node for each zone instead the complex building model has the convective and the radiative nodes, so the complex model has two power balances while the simple model has only one power balance. The power balances are explained in chapters 2.2 and 2.3.

The air mass balance is used in order to calculate the pressure of the zones with the equation (2.10).

$$p_i = \frac{\int \dot{m}_{i,air}\, dt}{V_i} \cdot R_{air} \cdot \vartheta_i \tag{2.10}$$

Where:

- $\dot{m}_{i,air}$ is the results of the air massflow balance $\left[\frac{\text{kg}}{\text{s}}\right]$;
- V_i is the zone *i* volume $\left[\text{m}^3\right]$;
- $R_{air} = 287$ is the air gas constant $\left[\frac{\text{J}}{\text{kg K}}\right]$;
- ϑ_i is the air temperature [K].

The vapour mass balance is used in order to identify the air absolute humidity by means of the equation (2.11):

$$x_{i,H_2O} = \frac{\int \dot{m}_{i,H_2O}\, dt}{\rho_{i,air} \cdot V_i} \tag{2.11}$$

The carbon dioxide mass balance is used in order to identify the CO_2 concentration in the air by means of equation (2.12):

$$x_{i,CO_2} = \frac{\int \dot{m}_{i,CO_2}\, dt}{\rho_{i,air} \cdot V_i} \tag{2.12}$$

The contributes *j,* involved in these balances, are:

- Air extraction;
- Supply air;
- Infiltration;
- Ventilation zone to zone;
- Ventilation intersection.

a. Air Extraction

The air extraction has no contribute to the zone power balance because a Lagrangian approach is used. On the other hand, the mass of the extract air, calculated as in the equation (2.13), is subtracted to the mass balance of the zone.

$$\dot{m}_{ext,air} = \dot{V}_{ext,i} \cdot \rho_{i,air} \tag{2.13}$$

Where:

- $\dot{V}_{ext,i}$ is the extract volume flow $\left[\frac{\mathrm{m}^3}{\mathrm{s}}\right]$;
- ρ_i is the air density of the zone $\left[\frac{\mathrm{kg}}{\mathrm{m}^3}\right]$.

The extract air has an influence also on the vapour and CO_2 balance of the zone. The vapour and CO_2 flows are calculated by multiplying the air mass flow and the vapour or CO_2 mass fraction as the equations (2.14) and (2.15) show. Then these flows are subtracted from the vapour and CO_2 balances of the zone *i*.

$$\dot{m}_{ext,H_2O} = \dot{m}_{ext,air} \cdot x_{i,H_2O} \tag{2.14}$$

$$\dot{m}_{ext,CO_2} = \dot{m}_{ext,air} \cdot x_{i,CO_2} \tag{2.15}$$

b. Supply air

The air mass flow is calculated as the equation (2.16) shows:

$$\dot{m}_{sup,air} = \dot{V}_{sup,i} \cdot \rho_{sup,air} \tag{2.16}$$

Where:

- $\dot{V}_{sup,i}$ is the inlet volume flow $\left[\frac{\mathrm{m}^3}{\mathrm{s}}\right]$;
- $\rho_{sup,air}$ is the inlet air density $\left[\frac{\mathrm{kg}}{\mathrm{m}^3}\right]$.

In the zones with the supply air, in addition to the air mass, also thermal power needs to be considered. The thermal power is calculated by means of the equation (2.17).

$$\dot{Q}_{sup} = \dot{m}_{sup,air} \cdot c_{p_{sup,air}} \cdot (\vartheta_{sup} - \vartheta_i) \tag{2.17}$$

Where:

- $\dot{m}_{sup,air}$ is the inlet mass flow $\left[\frac{\mathrm{kg}}{\mathrm{s}}\right]$;
- $\mathrm{c_p}_{sup,air}$ is the specific capacity of the air $\left[\frac{\mathrm{J}}{\mathrm{kg\,K}}\right]$;
- ϑ_{sup} is the temperature of the inlet air [°C];
- ϑ_i is the temperature of the zone [°C].

The air, vapour, and CO_2 flows are calculated as already explained for the extract air.

$$\dot{m}_{sup,H_2O} = \dot{m}_{sup,air} \cdot x_{sup,H_2O} \tag{2.18}$$

$$\dot{m}_{sup,CO_2} = \dot{m}_{sup,air} \cdot x_{sup,CO_2} \tag{2.19}$$

Where:

- $\dot{m}_{in,H_2O}$, $\dot{m}_{in,CO_2}$ are the inlet vapour and carbon dioxide mass flow $\left[\frac{\mathrm{kg}}{\mathrm{s}}\right]$;
- x_{in,H_2O}, x_{in,CO_2} are the vapour and carbon dioxide mass fraction $\left[\frac{\mathrm{kg}}{\mathrm{kg}}\right]$;

c. Infiltration and Windows Opening

The infiltration involves the accidental air exchange between the external ambient and the building. In this model, a constant value is taken for the infiltration rate.

The infiltration mass flow depends on many factors (e.g. the pressure difference, the temperature difference, the wind speed and direction etc.), but these factors are disregarded in the model.

It is not possible to know if the air flows from inside to outside or in the opposite direction due to the simplifications introduced in the model, but the same incoming and out coming mass flow are considered. Therefore, the infiltration has no contribute to the air mass balance of the zone. Vice versa, the contribute of the thermal energy is considered, as it is shown in equation (2.20):

$$\dot{Q}_{inf,i} = \dot{V}_{inf,i} \cdot c_{p_{amb,air}} \cdot \rho_{amb,air} \cdot (\vartheta_{amb} - \vartheta_i) \quad (2.20)$$

Where:

- $\dot{V}_{inf,i}$ is the infiltration volume flow $\left[\frac{\mathrm{m}^3}{\mathrm{h}}\right]$;
- $c_{p_{amb,air}}$ is the specific capacity of the ambient air $\left[\frac{\mathrm{J}}{\mathrm{kg\,K}}\right]$;
- $\rho_{amb,air}$ is the density of the ambient air $\left[\frac{\mathrm{kg}}{\mathrm{m}^3}\right]$;
- ϑ_{amb} is the temperature of ambient air [°C].

The vapour and CO_2 mass flows are calculated with the equations (2.21) and (2.32) by considering the same inlet and outlet air mass flow $\dot{m}_{air}$.

$$\dot{m}_{inf,H_2O} = \dot{m}_{air} \cdot (x_{H_2O,amb} - x_{H_2O,i}) \quad (2.21)$$

$$\dot{m}_{inf,CO_2} = \dot{m}_{air} \cdot (x_{CO_2,amb} - x_{CO_2,i}) \quad (2.22)$$

Where:

- $x_{CO_2/H_2O,i}$, $x_{CO_2/H_2O,amb}$ are the CO_2 or H_2O mass fraction of the considered zone and of the ambient air $\left[\frac{\mathrm{kg_{CO_2/H_2O}}}{\mathrm{kg_{air}}}\right]$.

d. Ventilation zone to zone

A constant and known airflow takes place between each zone and the hallway as it is schematized in Figure 2-3.

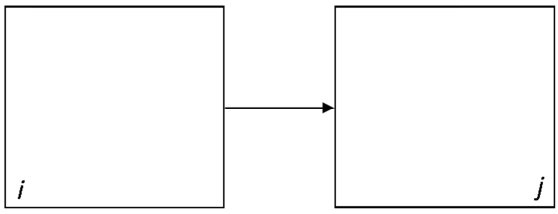

Figure 2-3: Airflow zone to zone

The mass flow from the zone *i* to the zone *j*, is calculated with the equation (2.23).

$$\dot{m}_{ztz,air} = \dot{V}_{ztz,i} \cdot \rho_{i,air} \quad (2.23)$$

Where:

- $\dot{V}_{ztz,i}$ is the volume flow from the zone *i* to the zone *j*;
- $\rho_{i,air}$ is the density of the zone *i*.

Equation (2.24) is used in order to calculate the energy carried by the air from the zone *i* to the zone *j:*

$$\dot{Q}_{ztz} = \dot{m}_{ztz,air} \cdot c_{p_{i,air}} \cdot (\vartheta_i - \vartheta_j) \tag{2.24}$$

The vapour and CO_2 mass flows are calculated by multiplying the mass fractions of the zone *i* for the air mass flow. Then they are subtracted from the zone *i* and added to the zone *j.*

$$\dot{m}_{ztz,H_2O} = \dot{m}_{ztz,air} \cdot x_{H_2O,i} \tag{2.25}$$

$$\dot{m}_{ztz,CO_2} = \dot{m}_{ztz,air} \cdot x_{CO_2,i} \tag{2.26}$$

e. Ventilation intersection

An additional air exchange is considered in order to take into account the doors opening. Since the additional volume flow is taken as a constant value and it is not calculated in function of the pressure, temperature and composition difference between the zones, it is not possible to know in which direction it occurs. For this reason, the same mass flow $\dot{m}_{air}$ incoming and out coming is considered for each intersection, as it is shown in Figure 2-4.

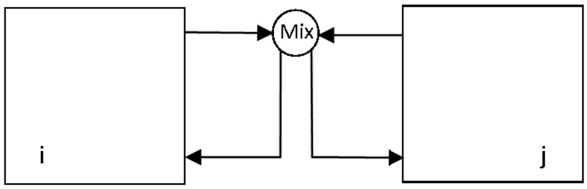

Figure 2-4: Intersection's ventilation

The extra intersection ventilation gives a null air mass flow, but energy contributes to both the involved zones. It is assumed that the air flows from each zone to the intersection and then the two streams are mixed. Actually, the warm airflow takes place in the upper part of the door while the cold airflow takes place in the lower part. The mean values of density, specific heat capacity and temperature are used in the equations. The power to the zone *i* is calculated with the equation (2.27):

$$\dot{Q}_{inters,i} = \dot{V}_{inters} \cdot \mathrm{c_p}_{mean,ij} \cdot \rho_{mean,ij} \cdot (\vartheta_{mean,ij} - \vartheta_i) \tag{2.27}$$

Where:

- $\dot{V}_{inters}$ is the exchanged volume flow $\left[\frac{\mathrm{m}^3}{\mathrm{s}}\right]$;
- $\mathrm{c_p}_{mean,ij}$, $\rho_{mean,ij}$, $\vartheta_{mean,ij}$ are the mean values of specific capacity $\left[\frac{\mathrm{J}}{\mathrm{kg\,K}}\right]$, density $\left[\frac{\mathrm{kg}}{\mathrm{m}^3}\right]$ and temperature $[\mathrm{K}]$;
- ϑ_i is the temperature of the considered zone $[\mathrm{K}]$;.

The vapour and CO_2 mass flows calculation is done with equation (2.28) and (2.29).

$$\dot{m}_{H_2O,i} = \dot{m}_{air} \cdot (x_{H_2O,mean} - x_{CO_2,i}) \tag{2.28}$$

$$\dot{m}_{CO_2,i} = \dot{m}_{air} \cdot (x_{CO_2,mean} - x_{CO_2,i}) \tag{2.29}$$

Where:

- $\dot{m}_{air}$ is the exchanged air mass flow $\left[\frac{\mathrm{kg}}{\mathrm{s}}\right]$;
- $x_{CO_2/H_2O,i}$, $x_{CO_2/H_2O,mean}$ are the CO_2 or H_2O mass fraction of the zone *i* and the mean concentration between the two air flows $\left[\frac{\mathrm{kg}_{\mathrm{CO_2/H_2O}}}{\mathrm{kg}_{\mathrm{air}}}\right]$.

2.1.3 Internal Gains

The internal loads are strictly dependent on the presence and behaviour of the inhabitants, so they are not easy to predict therefore, in the model a constant value it is set. The internal loads involve the sensible heat, the humidity and CO_2 delivered from the inhabitants and the power delivered by the lights and equipment.

2.1.4 Solar Gains

The climate considered in this work is the standard climate of Stuttgart (meteonorm, 2016). The incoming irradiation is distributed between the structures of the zone by means of area-weighted factors.

2.2 SIMPLE BUILDING MODEL

2.2.1 Introduction

The simple model involves just one node for the whole zone. This is a strength simplification, which will be explained in more detail with the results in section 4.3.3 and in the appendix A1. Figure 2-5 shows a simplified scheme of the simple model for one zone. All the powers are summed up in one node and only one capacity is present in order to represent the whole mass of the building (air, furniture, structure). The powers, involved in the balances, are the same already explained in the previous sections. $\dot{Q}_{vent}$ involves the inlet, outlet airflow and the infiltration, while $\dot{Q}_{inters}$ involves the ventilation zone to zone and ventilation intersection.

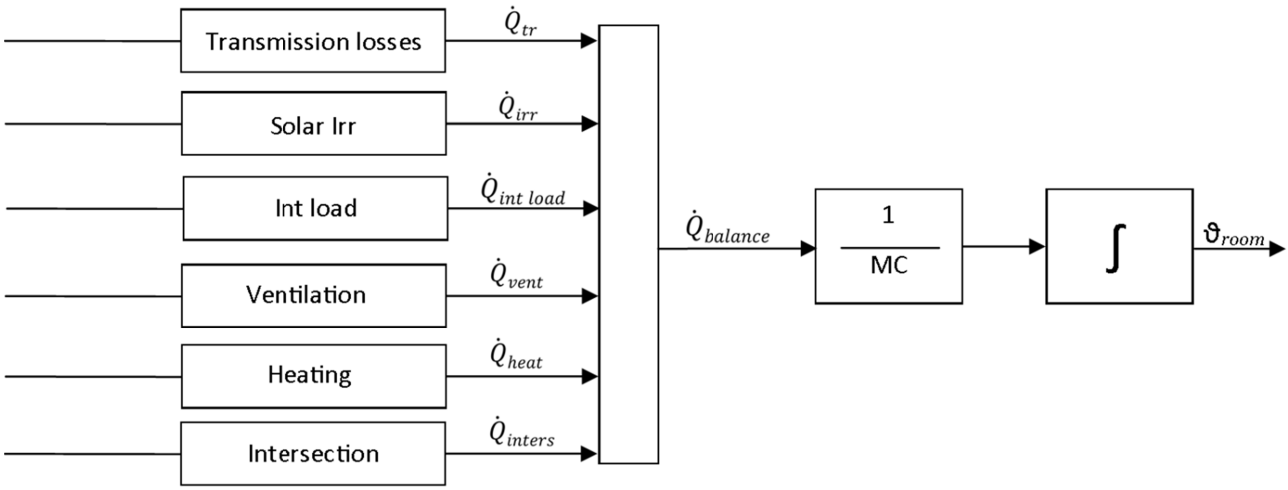

Figure 2-5: Simple model sketch

The equation (2.30) and (2.31) are used for the determination of the temperature of the node:

$$\dot{Q}_{balance} = \dot{Q}_{tr} + \dot{Q}_{irr} + \dot{Q}_{int\ load} + \dot{Q}_{vent} + \dot{Q}_{heat} + \dot{Q}_{inters} \tag{2.30}$$

$$\frac{\dot{Q}_{balance}}{MC} = \frac{d\vartheta}{dt} \tag{2.31}$$

Where:

- MC corresponds to the whole capacity of the zone $\left[\frac{\mathrm{J}}{\mathrm{K}}\right]$;
- $\dot{Q}_{balance}$ corresponds to the node's power balance [W];
- $\frac{d\vartheta}{dt}$ corresponds to the deviation of the zone temperature with respect to time $\left[\frac{\mathrm{K}}{\mathrm{s}}\right]$.

2.2.2 Transmission Losses

A steady state calculation of the transmission losses is implemented in the simple model, so the equation (2.1) becomes:

$$\begin{cases} \frac{\mathrm{d}^2\vartheta}{dx^2} = 0 \\ \vartheta(0) = \vartheta_1 \\ \vartheta(l) = \vartheta_2 \end{cases} \tag{2.32}$$

The solution of this problem is the following:

$$\vartheta(\mathrm{x}) = \frac{\vartheta_1 - \vartheta_2}{d} \cdot x + \vartheta_1 \tag{2.33}$$

The Fourier law is shown in (2.34):

$$\dot{\mathrm{Q}} = -\int \lambda \cdot \frac{d\vartheta}{dx}\, dA \tag{2.34}$$

Therefore, the trend of the power through a plane layer, with area A [m^2] and thickness d [m], is described by the equation (2.35):

$$\dot{\mathrm{Q}}_{12} = \lambda \cdot \frac{A}{d} \cdot (\vartheta_1 - \vartheta_2) \tag{2.35}$$

The equation (2.35) considers only the conductive heat transfer. While the equation (2.36) takes into account also the convective and irradiative heat exchange with the global transmission coefficient U_i for the generic element *i*. The total transmission losses power $\dot{Q}_{tr}$, is given by the sum over all the elements *i* involved in the considered zone.

$$\dot{Q}_{tr} = \sum_{i=1}^{r} U_i \cdot A_i \cdot \Delta\vartheta_i \tag{2.36}$$

The thermal bridges transmission losses are calculated with the (2.37) where the sum takes into account all the thermal bridges *j* involved in the considered zone:

$$\dot{Q}_{tb} = \sum_{j=1}^{n} \Psi_j \cdot l_j \cdot \Delta\vartheta_j \tag{2.37}$$

2.3 COMPLEX BUILDING MODEL

2.3.1 Introduction

Within the complex building model, two nodes are involved in each zone: the radiative node and the convective node. In this way two temperatures are calculated (convective and radiative) and not only one as for the simple model. Figure 2-6 shows the sketch of the two star model. The analogy between electric and thermal circuits is used in order to describe the radiative and convective heat exchanges. The temperature $[\mathrm{K}]$ is the analogous of the voltage $[\mathrm{V}]$, the heat flow $[\mathrm{W}]$ is the analogous of the current $[\mathrm{A}]$ and the thermal resistance $\left[\frac{\mathrm{K}}{\mathrm{W}}\right]$ is analogous to the electric resistance $[\Omega]$ (Davies, 2004). Each surface exchange power with the radiative and the convective node (just one surface is present in figure for sake simplicity). Other gains are present in each node balance. These gains came from the heating system, the solar irradiation, internal loads, etc. The subdivision of these gains between the radiative and the convective nodes depends on many factors (e.g. the source type, the surfaces temperatures, the view factor etc.). For example, the power from a radiative heating system will be mainly added to the radiative node. The convective node has also a capacity that represents the air and the furniture. The radiative node has no capacity, but a transfer function is used in the model in order to avoid algebraic loop. The capacity of the walls and windows are presented in the sketch as C_w. The powers exchanged between the surfaces and the nodes (convective and radiative) are calculated by means of the convective resistance (R_c) and radiative resistance (R_r). In the simple model, these two resistances are joined in one global resistance.

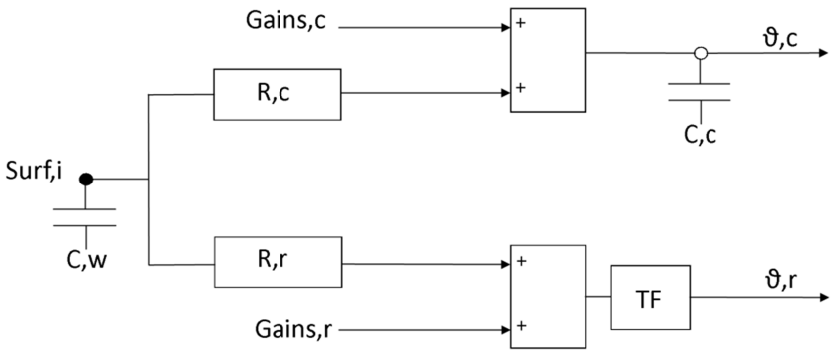

Figure 2-6: Two star model sketch

2.3.1 Convective Node

The equation (2.38) is solved in the convective node:

$$\dot{Q}_{conv} = M \cdot c_p \cdot \frac{d\vartheta_{conv}}{dt} \tag{2.38}$$

The convective temperature is calculated in the model by integration of the convective power balance. The convective power exchanged between the vertical surfaces and the convective node is calculated with the equation (2.39) (Glück, 1990)

$$\dot{Q}_{conv} = 1.6 \cdot \left|\vartheta_{s,i} - \vartheta_{conv}\right|^{0.3} \tag{2.39}$$

2.3.2 Radiative Node

The radiative exchange that takes part between three wall surfaces at different temperatures can be schematised as in Figure 2-7.

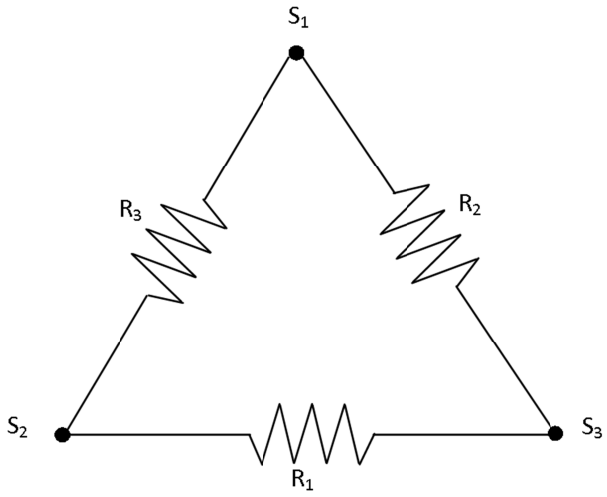

Figure 2-7: Triangle resistance scheme

Since the triangle conductance is equivalent to the star one, the sketch in Figure 2-7 is equivalent to the connection of Figure 2-8.

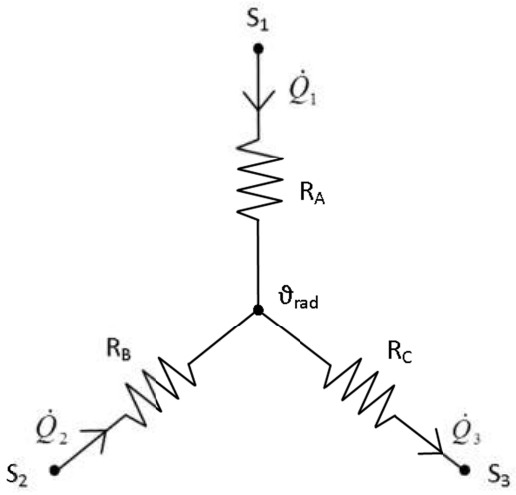

Figure 2-8: Star resistance scheme

The equivalence between the delta and star configuration is written in equations (2.40) and (2.41).

$$R_A = \frac{R_1 \cdot R_3}{R_1 + R_2 + R_3}$$
$$R_B = \frac{R_1 \cdot R_2}{R_1 + R_2 + R_3} \tag{2.40}$$
$$R_C = \frac{R_2 \cdot R_3}{R_1 + R_2 + R_3}$$

$$R_1 = \frac{R_A \cdot R_B + R_B \cdot R_C + R_C \cdot R_A}{R_C}$$
$$R_2 = \frac{R_A \cdot R_B + R_B \cdot R_C + R_C \cdot R_A}{R_A} \tag{2.41}$$
$$R_3 = \frac{R_A \cdot R_B + R_B \cdot R_C + R_C \cdot R_A}{R_C}$$

According to the thermic Ohm law ($\Delta\vartheta = \dot{Q} \cdot r$), it is possible to write the following equations:

$$\vartheta_1 - \vartheta_{rad} = r_1 \cdot \dot{Q}_1 \tag{2.42}$$

$$\vartheta_2 - \vartheta_{rad} = r_2 \cdot \dot{Q}_2 \tag{2.43}$$

$$\vartheta_3 - \vartheta_{rad} = r_3 \cdot \dot{Q}_3 \tag{2.44}$$

$$\dot{Q}_1 + \dot{Q}_2 + \dot{Q}_3 = 0 \tag{2.45}$$

From equations (2.42), (2.43), (2.44) and (2.45) it is possible to determine ϑ_{rad}:

$$\vartheta_{rad} \cdot \left(\frac{1}{r_1} + \frac{1}{r_2} + \frac{1}{r_3}\right) = \frac{\vartheta_1}{r_1} + \frac{\vartheta_2}{r_2} + \frac{\vartheta_3}{r_3} \tag{2.46}$$

$$\vartheta_{rad} = \frac{\frac{\vartheta_1}{r_1} + \frac{\vartheta_2}{r_2} + \frac{\vartheta_3}{r_3}}{\frac{1}{r_1} + \frac{1}{r_2} + \frac{1}{r_3}} \tag{2.47}$$

The star configuration is equivalent to the delta configuration, but the star one has not direct physical significance. ϑ_{rad} is a weighted mean of ϑ_1, ϑ_2 and ϑ_3. In a problem with three surfaces, the delta and star configurations deliver the same results, while with more than three surfaces an error is present, but it is acceptable (Feist, 1994). The power exchanged between each surface and the radiative node is given from the equation (2.48):

$$\dot{Q}_{rad} = \left(T_{s,i}^4 - T_{rad}^4\right) \cdot \sigma \cdot \varepsilon_i \tag{2.48}$$

Two grey plane surfaces can be considered in order to explain the equation (2.48) (Zanchini, 2012):

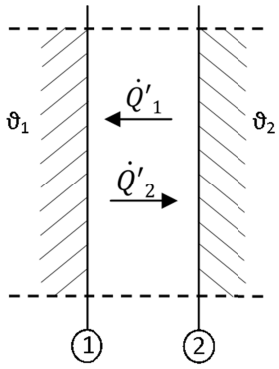

Figure 2-9: Radiative heat transfer between two grey plane surfaces

$\dot{Q}_1{}'$ and $\dot{Q}_2{}'$ are the total radiative powers incident on the grey surfaces 1 with area A_1 and 2 with area A_2. The exchanged power between 1 and 2 is shown in equation (2.49).

$$\dot{Q}_{exchanged} = \dot{Q}_{emitted} - \dot{Q}_{adsorbed} = \dot{Q}_1 - \alpha_1 \cdot \dot{Q}'_1 \tag{2.49}$$

Where:

- $\dot{Q}_{exchanged}$ is the exchanged power [W];
- $\dot{Q}_{emitted}$ is the surface 1 emitted power [W];
- $\dot{Q}_{adsorbed}$ is the surface 1 adsorbed power that correspond to the absorption factor α_1 $[-]$ for the incidence power $\dot{Q}'_1$ $[W]$;
- $\dot{Q}_1 = \sigma_0 \cdot S_1 \cdot T_1^4$ and $\dot{Q}_2 = \sigma_0 \cdot S_2 \cdot T_2^4$ are the emitted power from the surface 1 and 2.

The emitted powers $\dot{Q}_1$ and $\dot{Q}_2$ are different from the total incident powers $\dot{Q}_1{}'$ and $\dot{Q}_2{}'$, because a part of the emitted power is reflected from the other surface.

Q'_1 can be written as in the equation (2.50)

$$\dot{Q}_1' = \left[\dot{Q}_2 + (1 - \alpha_2) \cdot \dot{Q}_2'\right] \tag{2.50}$$

Where:

- $(1 - \alpha_2) \cdot \dot{Q}_2'$ is the power reflected from the surface 2 and incidents on surface 1 $[\mathrm{W}]$;
- $\dot{Q}_2$ is the power emitted from the surface 2 and incidents on surface 1 $[\mathrm{W}]$.

Q_2' can be written as in the equation (2.51):

$$\dot{Q}_2' = \left[\dot{Q}_1 + (1 - \alpha_1) \cdot \dot{Q}_1'\right] \tag{2.51}$$

Where:

- $(1 - \alpha_1) \cdot \dot{Q}_1'$ is the power reflected from the surface 1 and incidents on the surface 2 $[\mathrm{W}]$;
- $\dot{Q}_1$ is the power emitted from the surface 1 and incidents on the surface 2 $[\mathrm{W}]$.

By replacing the before described espressions for each value, the exchanged power becomes:

$$\dot{Q}_{exchanged} = \frac{\sigma_0 \cdot A_2 \cdot (T_1^4 - T_2^4)}{\frac{1}{\alpha_2} + \frac{1}{\alpha_1} - 1} \tag{2.52}$$

The following hypotheses are introduced:

- $\alpha_1 = 1$: the radiative node is a black body;
- $\varepsilon_2 = \alpha_2$ for Kirchhof law.

Therefore, the (2.52) can be written as the (2.53):

$$\dot{Q}_{ex} = \sigma_0 \cdot A_2 \cdot (T_1^4 - T_2^4) \cdot \varepsilon_2 \tag{2.53}$$

2.3.3 Structure Model And Transmission Losses

The CARNOT Blockset includes the structure block where it is possible to change the considered layers number. A simplified structure with a fixed number of layers is used in this work in order to makes it possible to use a discrete solver, necessary for the HiL simulation (see chapter 5). As it is shown in Figure 2-10 the walls are represented by three capacities C_1, C_2 and C_3 and two resistances R_1 and R_2. Furthermore, the external resistances are present: R_{amb}, R_{conv} and R_{rad}.

Where:

- R_{amb} is used in the calculation of the convective and radiative heat exchange between the external surface of the wall and the ambient;
- R_{conv} is used in the calculation of the convective heat exchange between the surface of the wall and the convective node;
- R_{rad} is used in the calculation of the radiative exchange between the wall surface and the radiative node.

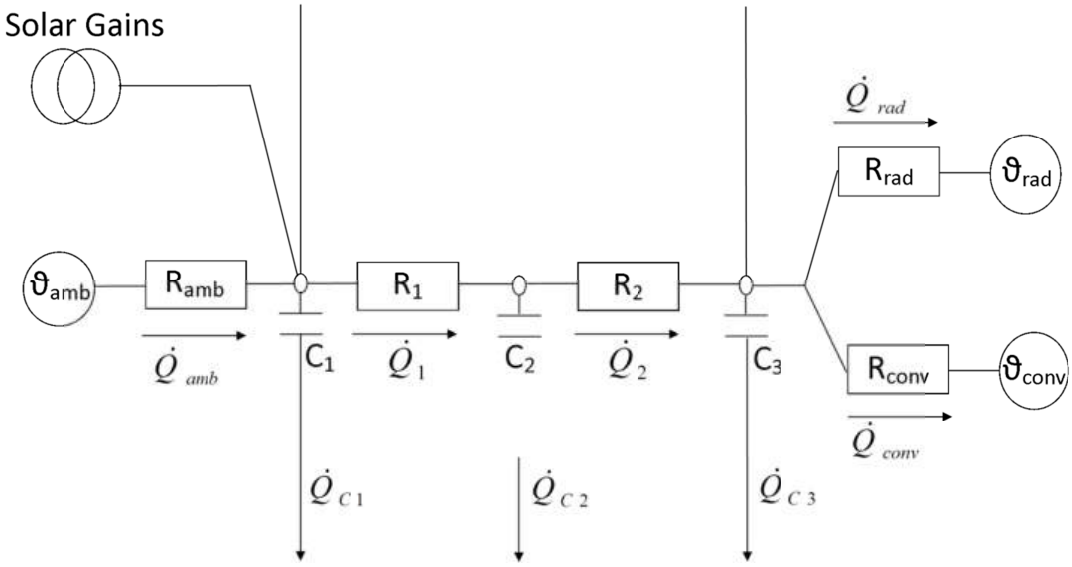

Figure 2-10: Sketch of the walls model

The equations regarding the balance on the node 1 are:

$$\dot{Q}_{amb} = (\vartheta_1 - \vartheta_{amb}) \cdot \frac{1}{R_{amb}} \tag{2.54}$$

$$\dot{Q}_1 = (\vartheta_2 - \vartheta_1) \cdot \frac{1}{R_1} \tag{2.55}$$

$$\dot{Q}_{amb} - \dot{Q}_1 = C_1 \cdot \frac{d\vartheta(x_1)}{dt} \tag{2.56}$$

This model is used for the external walls and ceilings while for the windows and internal walls only two capacities are considered. The relevance of the wall discretization is analysed in the appendix A1.3.

3 HEAT PUMP AND CONTROLLER MODEL

3.1 INTRODUCTION

The micro-heat pump (m-HP) works in combination with the mechanical ventilation with heat recovery system. During the wintertime, the m-HP uses as heating source (evaporator) the exhaust air, and as cooling sink (condenser) the supply air. The extract air (ext,0) goes through a filter (7) and then it flows in the heat exchanger, where it is cooled down by the supply air. The exhaust airflow goes through the fan (9) and trough the evaporator where the airflow is cooled down by the evaporation of the refrigerant (11). The ambient air passes the defroster (5), the filter (6), the heat exchanger (16), the fan (8), the condenser (13) and the backup heater (15). The defroster (5) is necessary to heat up the ambient airflow when its temperature is too low, in order to avoid ice formation in the heat exchanger. The backup heater (15) works in times when the heat source of the m-HP is not high enough to cover the building heat load. Figure 3-1 shows the scheme of the micro-heat pump and of the heat recovery system. The backup heater is composed by a resistance and its maximum power is 600 W.

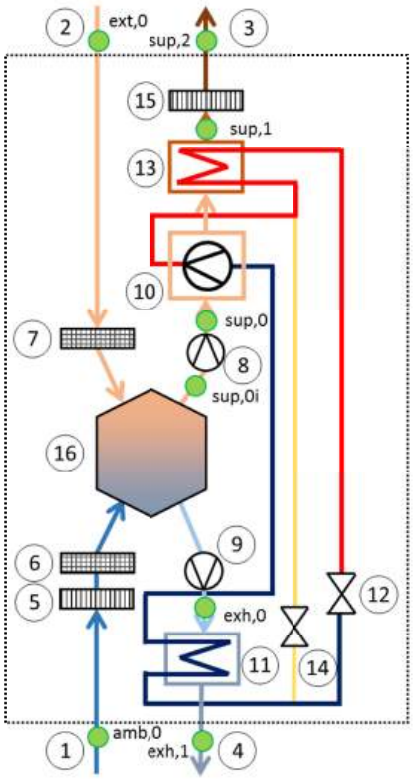

1 Ambient air
2 Extract air
3 Supply air
4 Exhaust air
5 Defroster HRC
6 Filter ambient air
7 Filter extract air
8 Ventilator supply air
9 Ventilator exhaust air
10 Compressor (speed controlled)
11 Evaporator
12 Throttle
13 Condenser
14 Hot gas defrost bypass
15 Supplementary heater
16 Heat exchanger

Figure 3-1: Heat recovery system and micro-heat pump scheme (Siegele, 2015)

An important aspect of the m-HP operation is the ice formation in the evaporator.
As this is not avoidable, de-icing intervals are necessary. The ice presence on the evaporator increases the airflow pressure drop, reduces the heat transfer and can even damage the ventilation unit. The de-icing control of the heat pump is based on the evaporator surface temperature and on the time. If the evaporator temperature is lower than the set point temperature the time counter starts. If the time count reaches a fixed value, and the evaporator temperature is still lower than the set point, the de-icing starts for a fixed time interval. During the de-icing period, the heat pump cycle by-passes the condenser thanks to the by-pass valve (14). When it is activated, the refrigerant gas goes directly to the evaporator where it melts the ice.
The m-HP has a four poles electric motor:

$$rpm = \frac{f \cdot 60}{2} \left[\frac{1}{\text{min}}\right] \tag{3.1}$$

Furthermore, an inverter is present in order to change the input frequency.
The m-HP frequency range is 49 Hz – 150 Hz, where 49 Hz corresponds to the m-HP switched off and 150 Hz corresponds to the maximum m-HP power. The backup heater has a maximum power of 600 [W] and it can be modulated from 0 [W] to 600 [W]. In the whole working range of the backup heater, the m-HP works with the maximum power. The backup heater power is regulated by the same controller used for the m-HP. The frequency is used in order to define the heating system set point power. Actually, the m-HP frequency is modulated, while the backup power is controlled with a TRIAC.

3.2 PHYSICS OF THE HEAT PUMP AND OF THE COMPRESSOR

3.2.1 Ideal Cycle

Figure 3-2 shows the ideal heat pump cycle in the P-h diagram. The main phases are:

- 1-2: The compression of the refrigerant fluid that is drawn as a constant entropy process.
- 2-3: The condense occurs at constant pressure, without pressure drop losses.
- 3-4: The expansion valve realizes the lowering of the pressure with a constant enthalpy process $h_4 = h_3$.
- 4-1: The refrigerant fluid evaporation occurs at constant pressure.

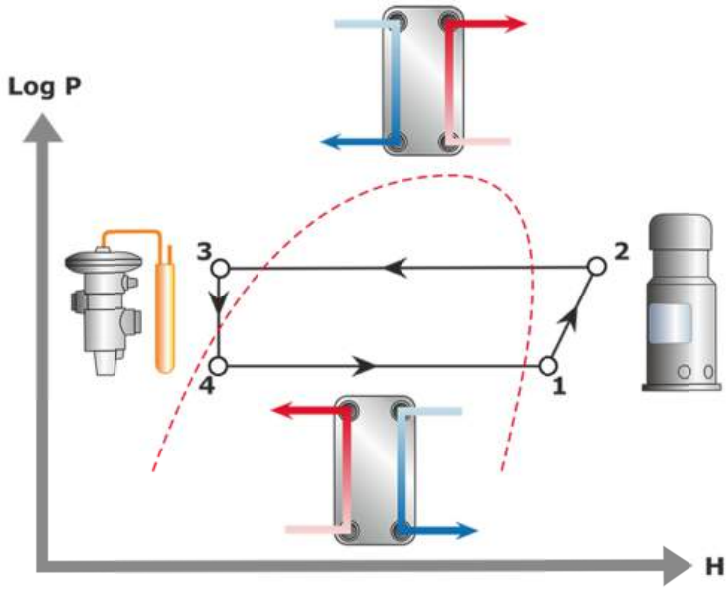

Figure 3-2: Ideal cycle in log(P)-h diagram (SWEP, 2016)

3.2.2 Real Cycle

Figure 3-3 shows the real heat pump cycle in a log(P)-h diagram. In the real cycle, the refrigerant is overheated (temperature difference between the point 1.2 and 1.1), this is necessary in order to ensure that only vapour flows in the compressor, in fact a liquid presence can damage the compressor. Anyway, the level of overheating should be minimized in order to minimize the compressor works and the heat transfer surface of the evaporator. The enthalpy of the point 1 is a function of the evaporator temperature and of the overheating: $h_1 = f(\vartheta_{evap}, \vartheta_{overheat})$.

In a real cycle, the liquid refrigerant is sub-cooled by the condenser (temperature difference between the point 3.1 and 3.2). This is done in order to increase the capacity of the refrigeration process and in order to avoid the formations of gas bubbles in the inlet flow of the expansion valve. The formation of these bubbles can occur if the refrigerant is not sub-cooled because of the pressure losses between the condenser and the expansion valve cause the formation of flash vapour. The presence of these bubbles, disrupt the regulation mechanism of the expansion valve. The enthalpy of the point 3 is a function of the condenser temperature and of the sub-cooling: $h_3 = f(\vartheta_{cond}, \vartheta_{sub})$.

The compression process does not follow the entropy line, this increases the compression works.

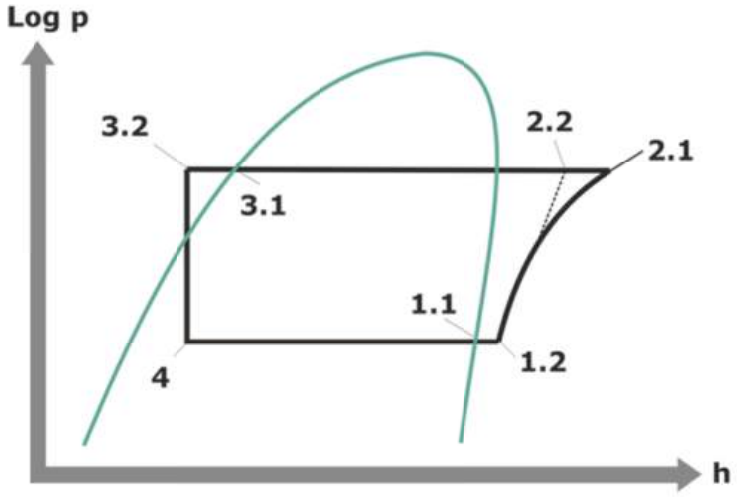

Figure 3-3: Real cycle in log(P)-h diagram (SWEP, 2016)

3.2.3 Coefficient of Performance

When the cycle is used for heating purpose, the useful effect is the thermal power delivered by the condenser to a secondary fluid (Q_1), vice versa when it is used for cooling purposes, the useful effect is the thermal power removed from a secondary fluid from the evaporator (Q_2). The first law of thermodynamics is reported in the equation (3.2):

$$Q_2 + L = Q_1 \tag{3.2}$$

Where L is the compression works. The coefficient of performance COP is defined as the ratio between the useful effect and the work:

$$COP = \frac{Q_1}{L} \tag{3.3}$$

The maximum theoretical efficiency is:

$$COP = \frac{T_1}{T_2 - T_1} \tag{3.4}$$

Where, T_1 is the temperature of the hot fluid and T_2 is the temperature of the cold fluid.

3.2.4 Evaporator

The mean logarithmic temperature of the airflow over the evaporator is written in equation (3.5) (iNSPiRe, 2014) and (Ochs, Dermentzis, Siegele, & Wolfgang, 2014):

$$\Delta T_{evap} = \frac{(\vartheta_{exh,0} - \vartheta_{evap}) - (\vartheta_{exh,1} - \vartheta_{evap})}{\ln\left(\frac{(\vartheta_{exh,0} - \vartheta_{evap})}{(\vartheta_{exh,1} - \vartheta_{evap})}\right)} \tag{3.5}$$

Where ϑ_{evap} is the temperature of the refrigerant fluid in the evaporator.

The power exchanged with the evaporator is given by the equation (3.6):

$$Q_{evap} = UA_{evap} \cdot \Delta T_{evap} = \dot{m} \cdot (h_{exh,0} - h_{exh,1}) \tag{3.6}$$

Where UA_{evap} is the global heat transfer coefficient of the evaporator multiplied for the area of the evaporator.

3.2.5 Condenser

The mean logarithmic temperature of the airflow over the condenser is written in equation (3.7) (iNSPiRe, 2014) and (Ochs, Dermentzis, Siegele, & Wolfgang, 2014):

$$\Delta T_{cond} = \frac{(\vartheta_{sup,1} - \vartheta_{cond}) - (\vartheta_{sup,0} - \vartheta_{cond})}{\ln\left(\frac{(\vartheta_{sup,1} - \vartheta_{cond})}{(\vartheta_{suo,0} - \vartheta_{cond})}\right)} \tag{3.7}$$

Where ϑ_{cond} is the temperature of the refrigerant fluid in the condenser.
The power exchanged with the condenser is given by the equation (3.8):

$$Q_{evap} = UA_{cond} \cdot \Delta T_{cond} = \dot{m} \cdot (h_{sup,1} - h_{sup,0}) \tag{3.8}$$

Where UA_{cond} is the global heat transfer coefficient of the condenser multiplied for the area of the condenser.

3.2.6 Compressor

The mechanical energy equation for a fluid element is:

$$c\ dc + g\ dz + v\ dp + F - \delta L = 0 \tag{3.9}$$

By disregarding dc, dz and R, the compression work can be expressed by the equation (3.10):

$$\delta L = v\ dp \tag{3.10}$$

The subscript *is*, means isentropic. With the integration of δL it is possible to define the isentropic work for a compression process from 1 to 2_{is}:

$$L_{is} = \int_1^{2is} v\,dp = L = \int_1^{2is} \frac{1}{\rho_1}\left[\frac{p_1}{p}\right]^{\frac{1}{\gamma}} dp = \frac{p_1^{\frac{1}{\gamma}}}{\rho_1}\int_1^{2is} p^{-\frac{1}{\gamma}}\,dp = \frac{p_1^{\frac{1}{\gamma}}}{\rho_1}\left[\frac{p^{1-\frac{1}{\gamma}}}{1-\frac{1}{\gamma}}\right]_{p_1}^{p_2} \tag{3.11}$$

For an adiabatic process of an ideal gas $p\,v^{\gamma} = cost = p_1\,v_1^{\gamma}$ with $\gamma = \frac{c_p}{c_v}$.

The real compression process is different from the ideal compressor process because:

- Mechanical friction η_m;
- The real process is not adiabatic so the isentropic efficiency as to be considered $\eta_{is} = \frac{L_{is}}{L_r} = \frac{h_{2.2} - h_{1.2}}{h_{2.1} - h_{1.2}}$. η_{is} depends on the pressure ratio;
- The electric efficiencies of the electric engine and of the inverter have to be considered η_{el};

The energy demand of the compressor for unit of mass flow is:

$$L_{Real} = \frac{L_{is}}{\eta_m \, \eta_{is} \, \eta_{el}} \tag{3.12}$$

The mass flow moved by the compressor is:

$$\dot{m}_{refrigerant} = \eta_{vol} \, \rho_{suction} \, i \, V_{displacement} \, n \tag{3.13}$$

Where:

- $\eta_{\mathrm{vol}} = 1 - V_{clearance} \left(\beta^{\frac{1}{\gamma}} - 1 \right)$ is the volumetric efficiency where $V_{clearance}$ is the clearance volume fraction and β is the pressure ratio between the final pressure and the initial pressure. The volumetric efficiency decreases if the pressure ratio increases.
- i is the number of cycles for each rotation;
- n is the number of rotation per second.

3.3 CONCEPTS OF THE CONTROLLER

3.3.1 Introduction

In this work, a closed loop control is studied where the controlled variable is the temperature of the hallway (Figure 1-2), zone 5. In the complex model, the operative temperature is taken for the control. The controlled temperature is monitored and compared with the reference variable. With the difference of these two variables, the error is calculated. The input of the control system is the error and the output is the frequency that the heating system should reach in order to deliver the optimum supply air temperature. The controller is continuous so the controlled variable can change with discrete values within the controller output range. The hardware controller of the m-HP, consist of a PI control and a lookup table as it is explained in the concept 1. The PI parameter determination is carried out in the chapter 4.

3.3.2 Concept 1

Figure 3-4 shows the closed loop control. The concept 1 of the controller involves a PI controller and a lookup table. In this case, the PI controller delivers the set point for the supply air temperature in function of the error. The input is the error and it is calculated as the

difference between the controlled temperature and the set point temperature. The set point supply air temperature delivered by the PI controller is the input for the lookup table that contains the information about the different heating system working points. The lookup table output is the set point frequency for the heating system. The lookup table of the controller can be one or more dimensional in function of the degree of detail. The differences between a one dimensional and a two dimensional lookup table are described in chapter 4.5.1. Here with the second dimension the dependency of the system by the ambient temperature is introduced. As it is discussed in the chapter 5.1.2 it would be possible to introduce also the dependency from the extract air humidity content. The heating system model is described in chapter 3.5.2.

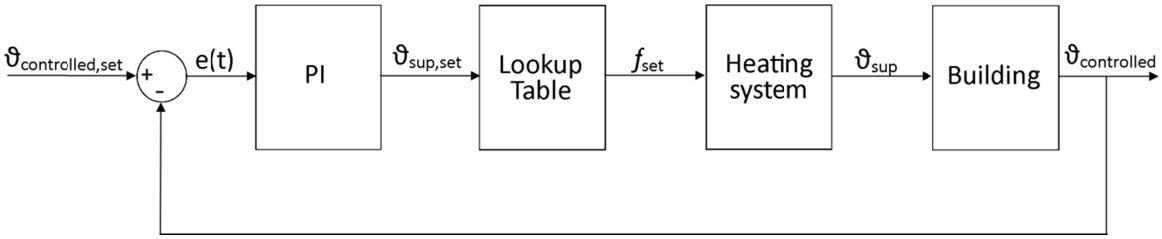

Figure 3-4: PI-LuT controller scheme

3.3.3 Concept 2

The implementation of a second PI controller (Figure 3-5) is another possibility for the set point frequency determination. Here, the first PI controller delivers the set point for the supply temperature in function of the difference between the sensitive temperature and the set point temperature of the zone 5. The second PI controller input is the difference between the set point temperature of the supply air and the real supply air temperature provided by the heating system, and its output is the set point frequency.

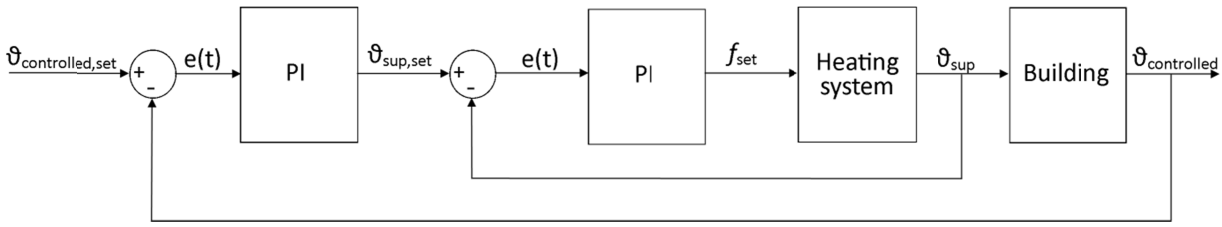

Figure 3-5: PI-PI controller scheme

3.4 MATHEMATICS OF THE PI CONTROLLER

The PI controller schema is shown in Figure 3-6:

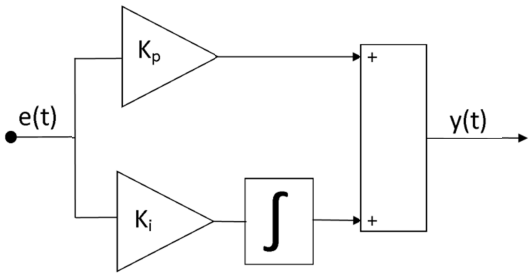

Figure 3-6: PI controller

Equation (3.14) shows the PI controller equation:

$$y(t) = e(t) \cdot K_p + K_i \cdot \int e(t)\, dt \tag{3.14}$$

The proportional part delivers an output proportional to the error as it is shown in the equation (3.15).

$$y_p(t) = K_p \cdot e(t) \tag{3.15}$$

The intensity of the response y_p depends on the error and on the K_p magnitude.

This part of the controller reacts without lags and only if a system deviation is present. With a proportional control, a steady state error cannot be completely balanced because the proportional part delivers a constant output if the error is constant.

With a PI controller the integral part, continues to change the manipulated variable, as long as the error is not zero. The equation (3.16) shows the equation of the integral part.

$$y_i = K_i \cdot \int e(t)\, dt\,; \qquad K_i = \frac{K_p}{T_n}; \tag{3.16}$$

The response of this part of the controller depends on the error and gain magnitude. The lower the integrative time constant T_n is, the faster the manipulated variable response is. A controller with just the integral part is slower with respect to a proportional controller. It is possible to speed up the integral response by reducing the T_n value, but this can cause instability in the system.

The lacks of the integral and proportional part are balanced with a PI controller. The system responds faster to the error thanks to the proportional part while the integral part starts to gain influence with a delay, but it ensure a zero error at every working points.

3.4.1 Steady State Error

In order to reach a null error an integrative part is necessary. With the integrative part, the error can be fully corrected at every working point. In order to understand better this concept, the system of Figure 3-7 is considered.

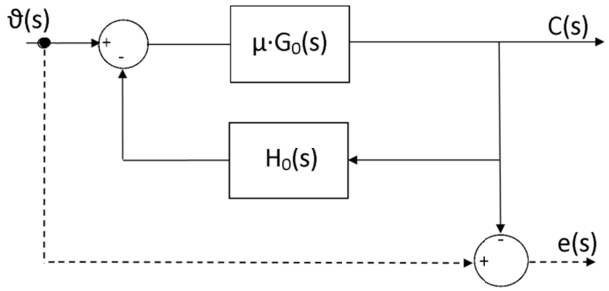

Figure 3-7: Example system according to (Borghetti, 2012)

Here the reference value is ϑ(s), while the output value is $C(s)$. Therefore, the system is producing an error $e(s) = \vartheta(s) - C(s)$. It is possible to write the same system in an open loop with the equivalent transfer function, this is shown in Figure 3-8.

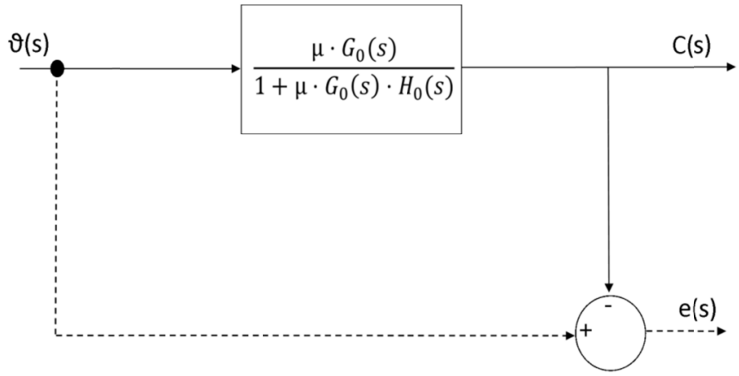

Figure 3-8: Equivalent system

The error of this system is written in equation (3.17):

$$e(s) = \vartheta(s) \cdot \left[1 - \frac{\mu \cdot G_0(s)}{1 + \mu \cdot G_0(s) \cdot H_0(s)}\right] = \frac{\vartheta(s) \cdot \left(1 + \mu \cdot G_0(s) \cdot H_0(s) - \mu \cdot G_0(s)\right)}{1 + \mu \cdot G_0(s) \cdot H_0(s)} \tag{3.17}$$

G_0, H_0 are canoic transfer function:

$$G(s) = \mu \cdot G_0(s) = \mu \cdot \frac{\prod_{l=1}^{m}(1 - \tau_l \cdot s)}{s^g \cdot \prod_{i=1}^{n}(1 - \tau_i \cdot s)} \tag{3.18}$$

Where:

- μ is the transfer function gain;
- g is called type of the transfer function, H_0 has type zero while G_0 may has type higher than zero;
- τ_l, τ_i are time constants where $\tau_l = -\frac{1}{z_i}$ and $\tau_i = -\frac{1}{p_i}$;
- z_i are the zeros of the transfer function;
- p_i are the poles.

By using the final value theorem, it is possible to calculate the final output of the system, represented by the transfer function.

$$\lim_{t \to \infty} g(t) = \lim_{s \to 0} s \cdot G(s) \tag{3.19}$$

With the final value theorem and the expression (3.17) of the error, it is possible to analyse which final error the system delivers in function of the transfer function type. If the transfer function has type zero, its final value with a step input $\frac{1}{s}$ is the gain of the transfer function:

$$\lim_{s\to 0} \frac{1}{s} \cdot s \cdot G(s) = \mu \tag{3.20}$$

By using the final value theorem with $e(s)$ it is possible to deduce the following conclusion:

- If G_0 has type zero the final value of the error will be: $\frac{1}{1+\mu}$. Therefore, the error will never be zero. This is the case of the proportional controller where the integral part is not present. If the system should deliver as less error as possible, a high proportional gain, is necessary. However, this can lead the system to instability conditions.
- If G_0 has type higher than zero, the final value of the error will be zero. This is the case of a PI controller where the integral part ensures a type higher than zero.

The PI parameters are calculated with the study of the dynamic response of the system (see chapter 4.3 and 4.4).

3.4.2 Anti-Windup

The anti-windup is important in order to ensure a fast response of the system when the output is limited, as in the case of ϑ_{sup}. When the output is fixed at the maximum (minimum) value and the error is still increasing (decreasing), the integral output is continuing to grow. Therefore, when the error changes its sign, it is necessary to wait the desaturation of the integrator in order to see a decrement of ϑ_{sup}. In order to reduce this problem the anti-windup is necessary. Different kinds of anti-windup are studied in this work.

Back calculation anti-windup

Figure 3-9 shows the back calculation anti-windup. When the output reaches the maximum (minimum) value, the difference over the saturation block is multiplied for the back coefficient (K_B) and then it is summed up to the integrator input. Since the difference over the saturation block is negative (positive) it is reducing (increasing) the integrator input.

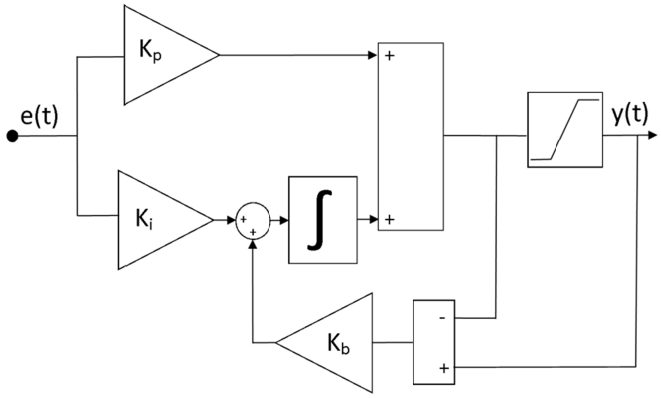

Figure 3-9: Back calculation anti-windup

Conditional integration anti-windup

Another kind of anti-windup is shown in Figure 3-10. Here, when the output reaches its maximum or the minimum value, the input of the integrator is fixed to zero. The minimum and maximum values of the saturation block are particularly important for this kind of anti-windup, as it will be discussed in the section 'Conditional Integration Anti-Windup Sensibility to the Saturation Block Limits'.

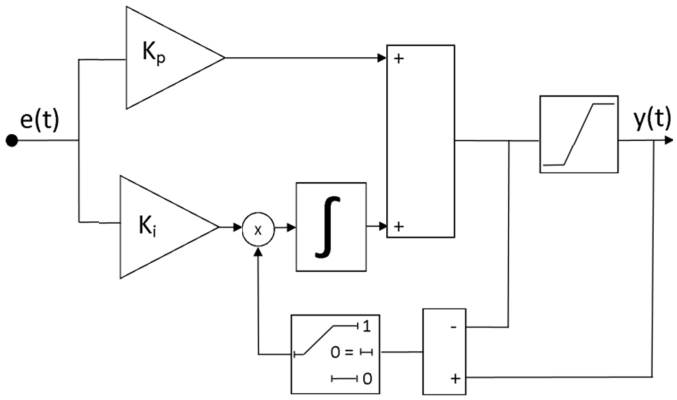

Figure 3-10: Conditional integration anti-windup

Comparison

The following figures show the differences between a control system without anti-windup, with the back calculation and with the conditional integration anti-windup. The output limitation of this system is 90, the proportional gain is 0.5 while the integral gain is 1. In Figure 3-11 it is possible to notice that the input starts to decrease after 100 s and it changes the sign after 200 s while the output decreases only after 420 s. This lag is due to the integral part that continuously increases its output as long as its input is positive.

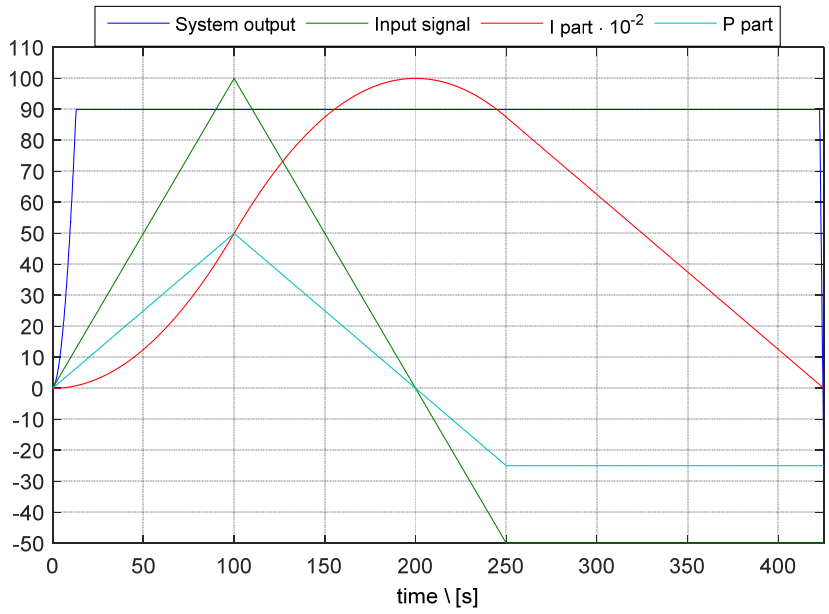

Figure 3-11: Control behaviour without anti-windup

Figure 3-12 shows the idea of the back calculation anti-windup. In this case, the output signals starts to decrease after 200 s (the half respect to the case without anti-windup). In this case, the integral part is able to follow the input behaviour, so there is no delay between the moment in which the input signals becomes negative and the moment in which the output starts to decrease.

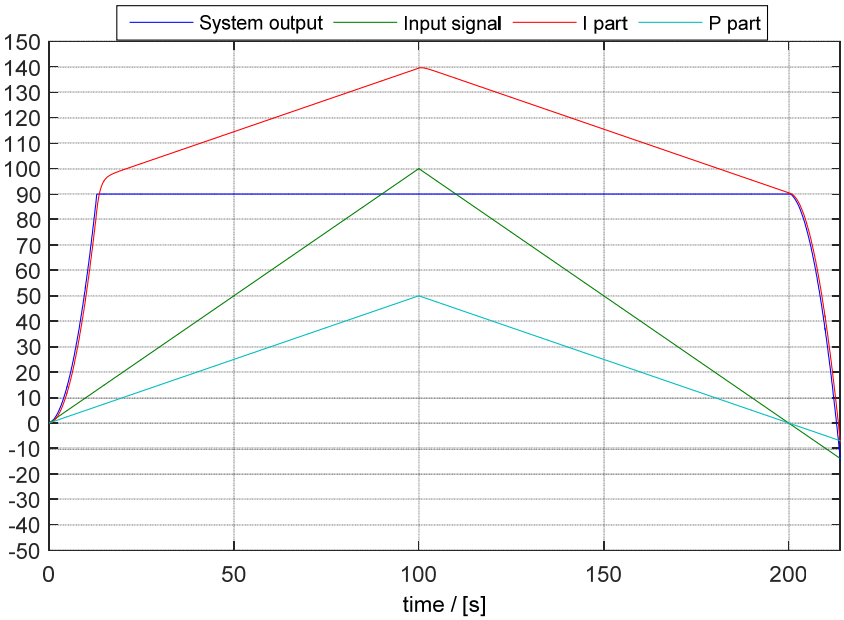

Figure 3-12: Control behaviour with back calculation anti-windup

Figure 3-13 shows the conditional integration anti-windup. When the output is equal to 90 the saturation is working and the integral part is hold. At 190 s, the integral part is not hold because the proportional part is sufficiently decreased. Also with this kind of anti-windup the delay between the period of time in which the input becomes negative and the output starts to decrease is reduced with respect to the case without anti-windup.

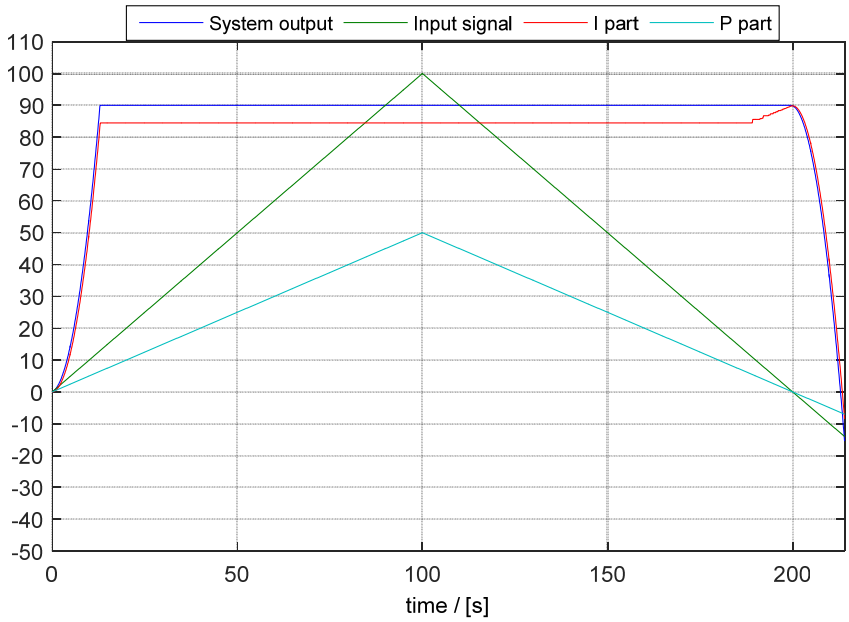

Figure 3-13: Control behaviour with conditional integration anti-windup

Conditional Integration Anti-Windup Sensibility to the Limits of the Saturation Block

With the conditional integration anti-windup, the lower and higher limit values of the saturation block are critical values. By considering a practical case is easier to understand why the maximum and minimum saturation block values are important. If the controller starts with a null initial value for the integral part, only the proportional part is activated until the output of the controller is higher than the lower limit of the saturation. The system needs an error higher than the ratio between the lower limit of the saturation block and the proportional gain before that the integration part starts to count and gain influence on the output. This means that if the lower limits of the saturation block is $20°C$ and the proportional gain is $35\left[\frac{\mathrm{K}}{\mathrm{K}}\right]$, the system needs an error of $0.571\ [\mathrm{K}]$ before that the integrator is enabled to count and to gain influence on the controller output. If the lower limit of the saturation block is $10°\mathrm{C}$, the system needs an error of $0.285\ [\mathrm{K}]$. If the maximum and minimum values of the saturation block change, also the operative interval of the lookup table of the controller has to be changed according to the maximum and minimum value of the saturation. Figure 3-14 shows the comparison between the results of the same model with the same boundary conditions but with different lower value of the saturation block. The case 1 shows the results when the lower temperature limit of the controller is $10°\mathrm{C}$ while the case 2 shows the results when the lower temperature limit of the controller is $20°\mathrm{C}$. The initial error for both cases is $0.4\ [\mathrm{K}]$. As before described, the case 2 needs an error of $0.571[\mathrm{K}]$ in order to enable the system frequency to increase. The frequency starts immediately to increase in the case 1 because from the first instant the system has already an error higher than $0.285\ [\mathrm{K}]$.

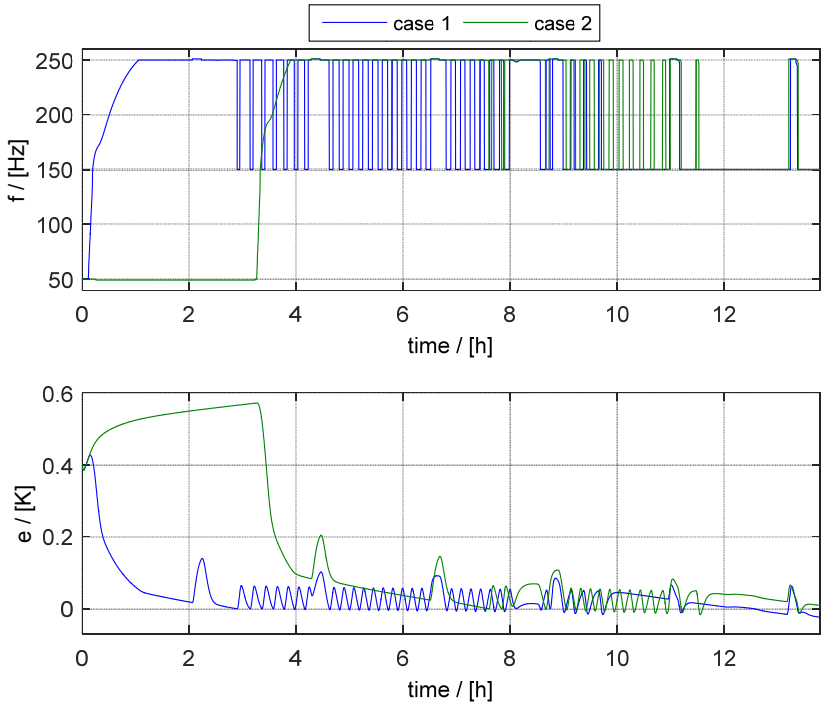

Figure 3-14: Comparison between a controller with a lower saturation limit of 10 °C (case 1) and a lower saturation limit of 20 °C (case 2).

3.5 SIMULINK IMPLEMENTATION

3.5.1 Controller

The controller model, developed in Simulink, involves a PI controller and a lookup table. The sensitive temperature is taken from the zone 5 and a transfer function is used in order to obtain the controlled signal that is subtracted from the set point temperature. The transfer function represents the measurement chain delay and it has a time constant of 2 s. In Simulink, it is possible to choose between the three types of anti-windup as before mentioned. The output of the PI controller is the input for the lookup table. Figure 3-15 shows the Simulink controller. By changing the variable `HP.a_w` it is possible to switch between the different types of anti-windup. The PI with conditional integration anti-windup 1 and with back calculation anti-windup are explained in section 3.4.2. The PI with conditional integration anti-windup 2 is slightly different because it holds the integrative part only when the system reaches the saturation maximum value and not when the saturation regards the lower limit. With the variable `HP.LuT` and the switch, it is possible to use a 2D lookup table or a 1D lookup table or a second PI controller. The differences between these three cases are explained in chapter 3.4.2.

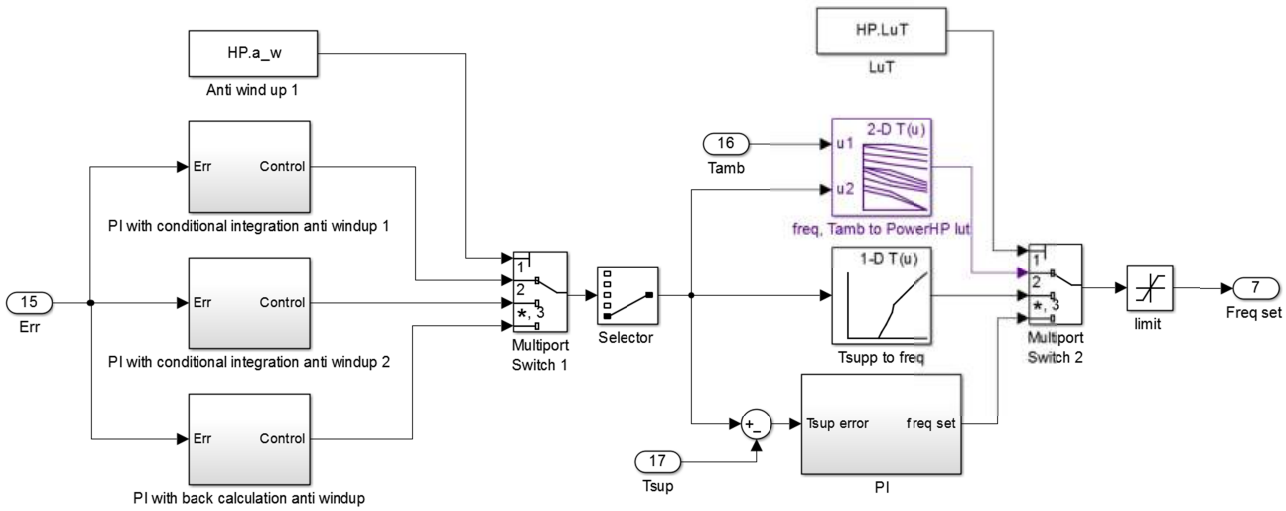

Figure 3-15: Simulink implementation of the controller

The PI controller output is limited between 20 °C and 45.9 °C. The lookup tables use a linear interpolation. The 1D lookup table points are shown in Table 3-1. This lookup table does not extrapolate its output.

Table 3-1: 1D lookup table

		f_{set}
$\vartheta_{sup,set}$	20.0	49.0
	23. 7	50.0
	25.3	70.0
	27.3	90.0
	28.8	110.0
	30.3	130.0
	30.8	150.0
	34.5	175.0
	38.3	200.0
	42.1	225.0
	45,9	250.0

The 2D lookup table points are shown in Table 3-2. In this case, the outputs are extrapolated when the ambient temperature is higher than 5 °C or lower than -4 °C. The extrapolation is linear. The accuracy of this extrapolation has to be validated by measuring further working points of the m-HP.

Table 3-2: 2D Lookup table

		$\vartheta_{amb,0}$ / [°C]		
		-4	0	5
$\vartheta_{sup,set}$ / [°C]	20.0	0	0.0	0.0
	23.7	74.4	50.0	0.0
	25.3	94.1	70.0	0.0
	27.3	119.4	90.0	68.1
	28.8	150.9	110.0	80.1
	30.3	161.2	130.0	94.3
	30.8	164.0	150.0	101.7
	34.5	189.0	175.0	157.1
	38.3	214.0	200.0	182.1
	42.1	239.0	225.0	207.1
	45.9	250.0	250.0	232.1

The measured points are determined with constant volume flow and $\vartheta_{ext,0}$ and with dry extract air. It would be possible to extend the lookup tables by measuring more working points for examples with different volume flow, with different degree of absolute humidity and temperature of the extract air.

3.5.2 Heat Pump Model

Introduction

Figure 3-16 shows the sketch of the m-HP and backup heater model.

The Simulink m-HP model uses a lookup table. Its inputs are the set point frequency set by the controller and the ambient temperature and its output is the power provided by the m-HP in this condition. After the lookup table, a transfer function is present, which is necessary to slow down the system response and makes the heat pump behaviour more realistic. The backup heater model involves another lookup table, which delivers in function of the system frequency, the backup power. The backup heater has a linear behaviour, i.e. its power is proportional to the input frequency. The powers of the m-HP and of the backup heater are then summed up and the supply temperature is calculated with equation (3.21):

$$\vartheta_{sup,2} = \vartheta_{sup,0} + \frac{\dot{Q}}{\dot{V}_{air} \cdot \frac{\rho}{c_p}} \tag{3.21}$$

Where:

- $\dot{Q}$ is the power delivered by the heating system [W];
- $\vartheta_{sup,0}$ is the air temperature of the supply air flow after the MVHR [°C];
- $\dot{V}_{air}$ is the volume flow of the mechanical ventilation system $\left[\frac{\mathrm{m}^3}{\mathrm{s}}\right]$;

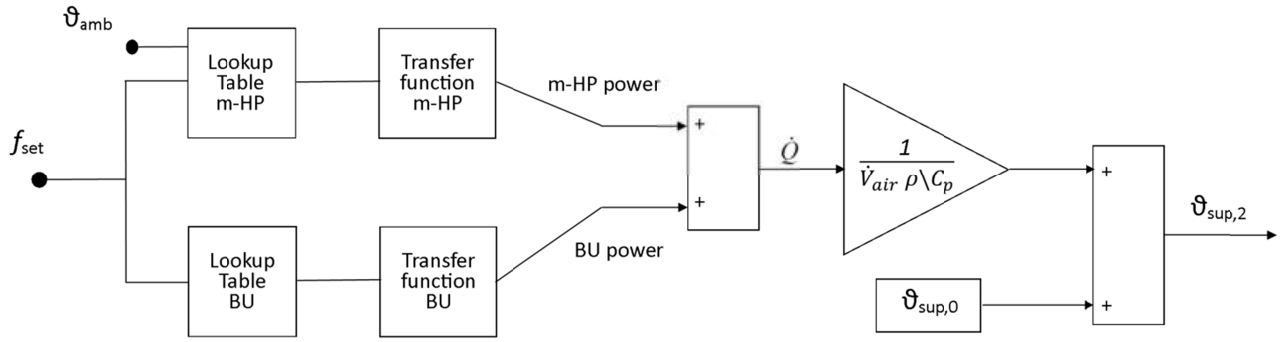

Figure 3-16: Sketch of the m-HP and backup heater

Micro Heat Pump model

Figure 3-18 shows the m-HP model. The frequency is normally limited between 49 Hz and 250 Hz, but when the minimum runtime test is activated (see section 3.5.2, minimum runtime) it is limited between 50 Hz and 250 Hz. This test forces the heat pump to work for at least the prefixed time, even if meanwhile the system frequency is decreased to the minimum level.

The frequency and ϑ_{amb}, are the two inputs of the lookup table. ϑ_{amb} corresponds to $\vartheta_{amb,0}$ with limited lower value, because of the pre-heater contribute. Its output is the power delivered by the m-HP, with a fixed frequency, in function of ϑ_{amb}, the m-HP supplies different thermal power because its performance changes with the working point.

A switch controlled by the de-icing test is present, after the lookup table. When the heat pump is in the de-icing period, it delivers a zero power to the system. The dynamic behaviour of the m-HP is modelled by using two transfer functions with two different time constants. In function of `test 2` the transfer function is selected by means of the `switch 3`. Two different time constants are necessary because the switching off and switching on dynamic behaviours are different. The system takes more time when it is switching on compared to when it is switching off, this effect is mainly due to the following aspects:

- The thermal losses accelerate the temperature decreasing during the switching off period;
- Another hypothesis is the following: After a period in which the heat pump is switched off, the refrigerant fluid is all in a liquid form in the evaporator because there is no valve for the refrigerant receiver. Therefore the evaporation of that liquid with resulting heat production takes time.

Figure 3-17 shows the switching on and off heat pump behaviour. As it can be observed, the heat pump needs 63 min to reach the maximum supply temperature, while it needs only 3 min to decrease the supply air temperature when it is switched off.

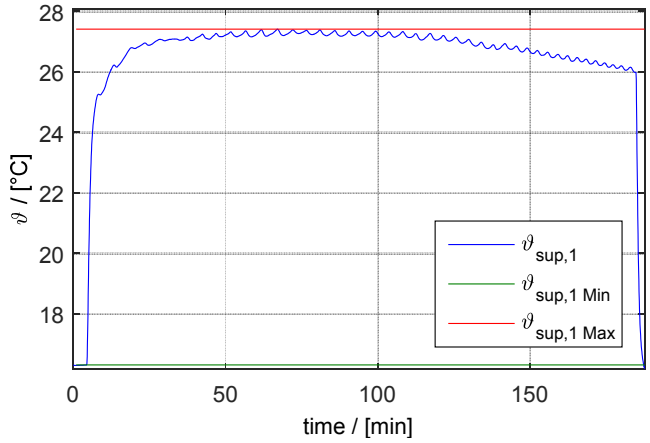

Figure 3-17: Heat pump on off behaviour (measured)

The `test 2` is true when the heat pump is in the de-icing period and it is switched on or when it is switched off.

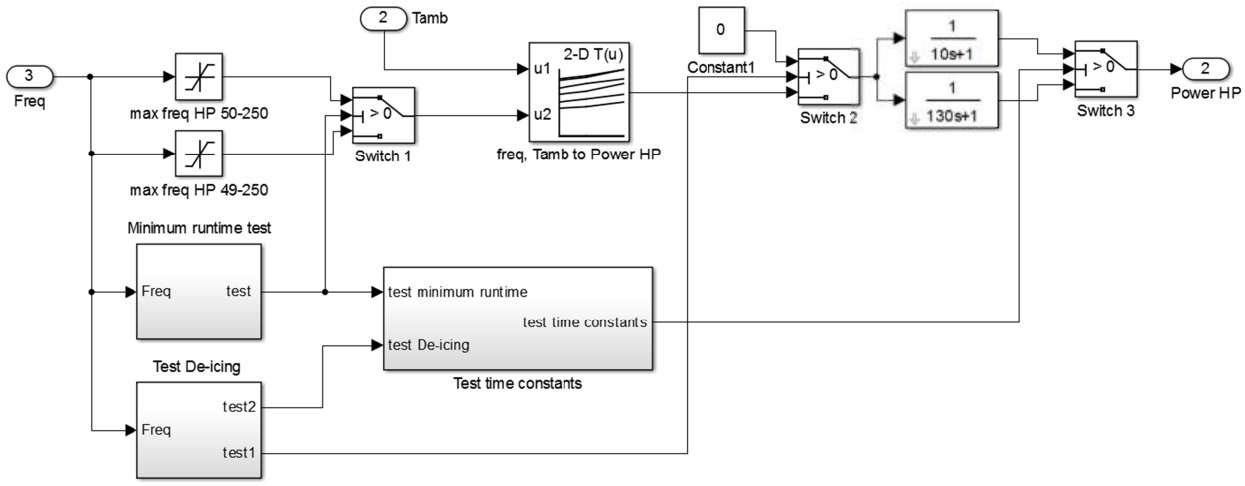

Figure 3-18: m-HP Simulink model

Figure 3-19 shows the logic scheme of the heat pump time constants control that involves the minimum runtime and the de-icing tests. These are explained in the following chapters. The flow diagram of Figure 3-19 has as input the de-icing count, the minimum runtime count and the system frequency and delivers as output the HP time constant (τ_1 for switching off behaviour and τ_2 for switching on behaviour). The explanations about the minimum runtime count and the de-icing count, are reported in the following two sections. When the minimum runtime count is higher than zero, the HP must stay in operation until it reaches the value zero. When the de-icing count is higher than `HP.t2`, the HP is doing the de-icing. The flow diagram test description is the following: when the minimum runtime test is true, or when the HP is not in the de-icing period or the system frequency is higher or equal to 50 Hz the test is true and the heat pump time constant is τ_1 otherwise it is false and the heat pump time constant is τ_2. When the heat pump is switched on the time constant is τ_1 while when the heat pump is switched off or it is in the de-icing period the time constant is τ_2.

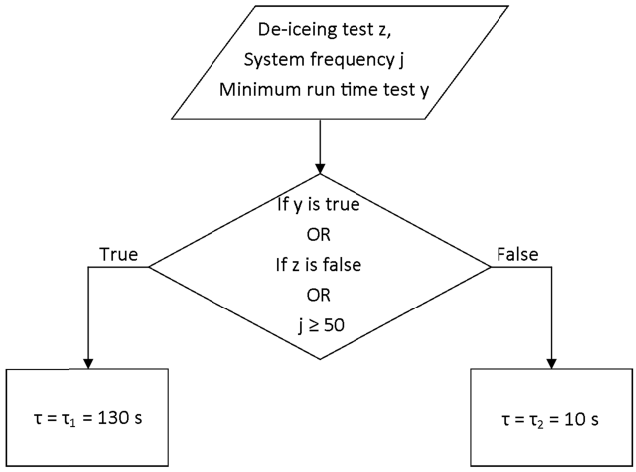

Figure 3-19: Flow diagram of the time constant control

De-icing test

The de-icing behaviour is predicted in Simulink model by a logic test, based on the time and the power delivered by the system. Figure 3-20 shows the implementation of the de-icing test in Simulink. The output of the integrator grows linearly with the time. When this signal is equal to the de-icing interval (e.g. 2 hours plus 10 minutes) the integrator's output is reset to zero. The `test 3` is true from the point of time in which the output of the integrator is equal to `HP.t2` (e.g. 2 hours) to the point of time in which it falls down (e.g. 2 hours plus 10 minutes). The `test 6` is true when both the `test 3` and 4 are true, so when the system is switched on and it is in the de-icing period. The `test 2` is true when the `test 6` or the `test 5` is true. The model cannot predict exactly the de-icing period because the refrigerant cycle is not modelled, i.e. the refrigerant temperature is not available.

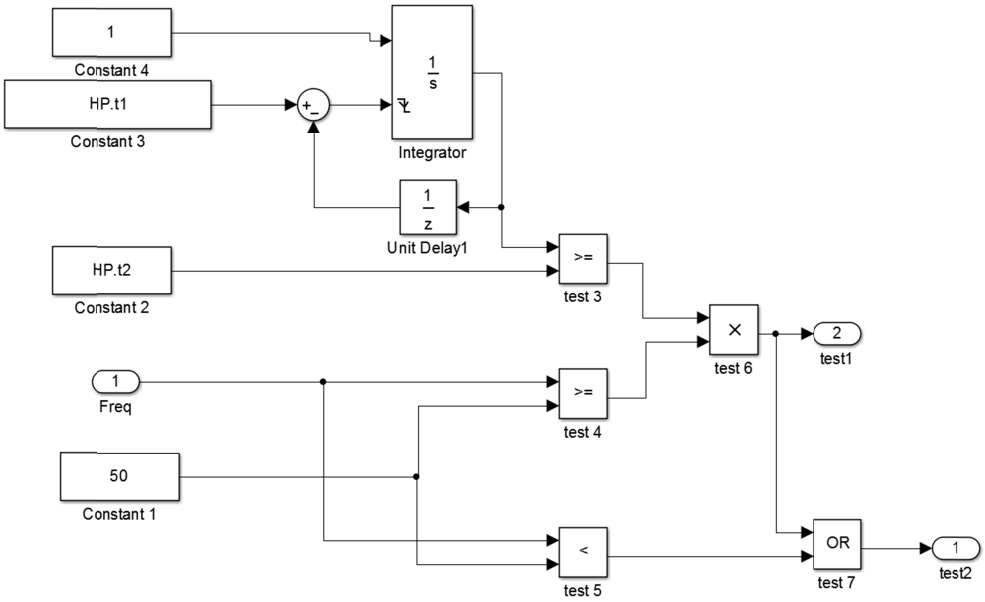

Figure 3-20: De-icing Simulink model

Figure 3-21 shows how the test 1 of the de-icing controls the heat pump power (see Figure 3-18)

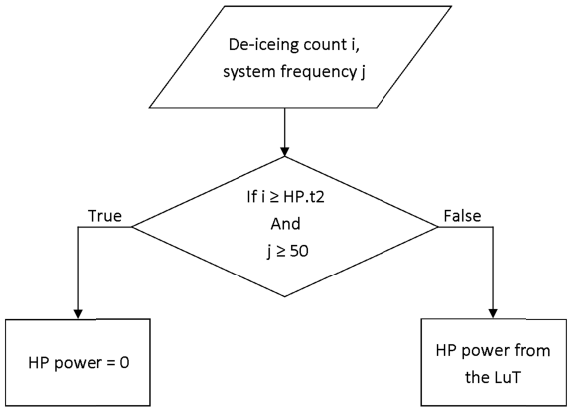

Figure 3-21: Flow diagram of the de-icing control

Minimum runtime

The m-HP minimum runtime is implemented in the model. Therefore, it is possible to change the minimum time for which the m-HP should run when it is switched on. Figure 3-22 shows the Simulink model implemented in order to set the minimum runtime. The `logical operator` is true when the integrator count is higher than zero or the system frequency is increasing. When this test is true, the `integrator` input is `1` otherwise it is `0`. If the integrator input is one, the integrator counts as long as its output is lower than `HP.ton`, than it is reset to zero. When the heat pump is switched on the count starts and as long as it does not reach the `HP.ton` value, the heat pump cannot be switched off. If during this period the frequency is reduced to values lower than 50 Hz, the heat pump is obligated to work as long as the minimum runtime is fulfilled.

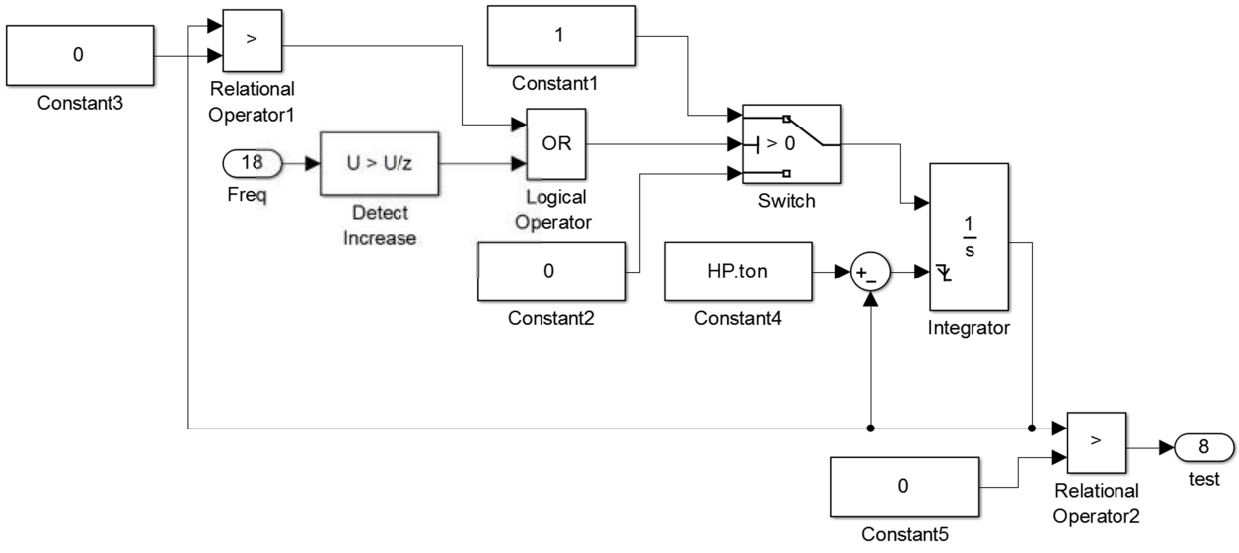

Figure 3-22: Minimum runtime test

Figure 3-23 shows the flow diagram of the minimum runtime test and how it controls the minimum frequency of the heat pump (see Figure 3-18).

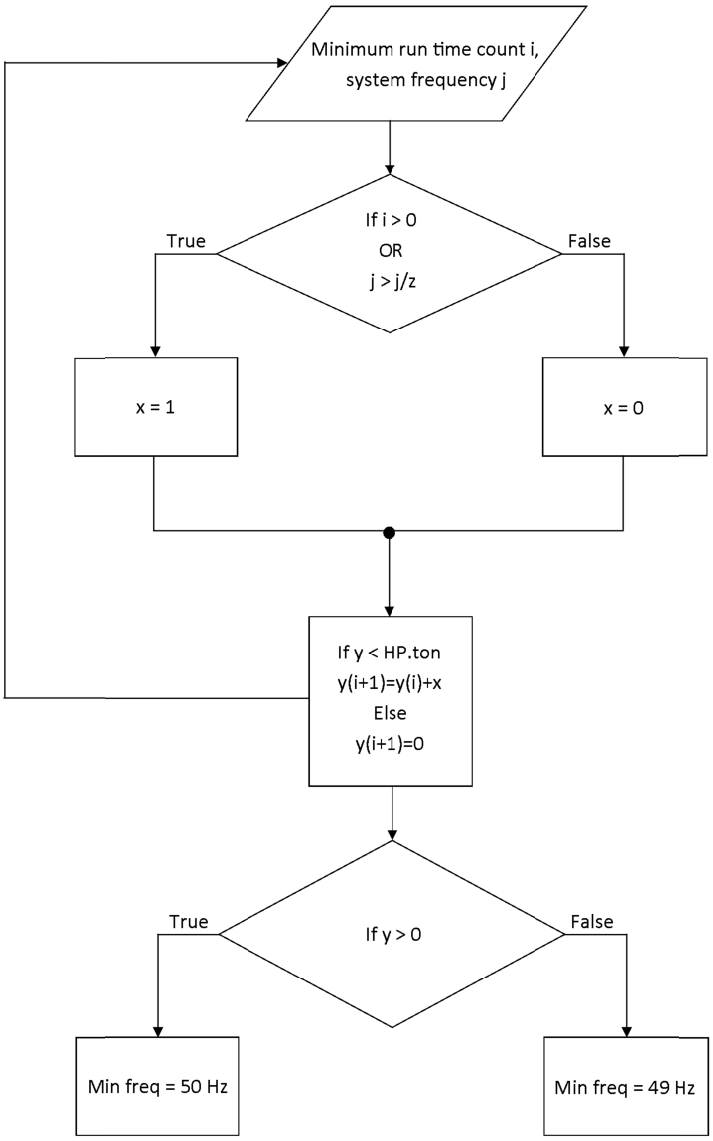

Figure 3-23: Flow diagram of the minimum runtime

Figure 3-24 shows an example of the minimum runtime operating principles. The first subplot shows the input frequency, the second subplot shows the integrator output and the third subplot shows the minimum runtime test. The minimum runtime here considered is 5 min. The input frequency has a step at time 0, in fact the count starts immediately. Then the input frequency decreases to 0 Hz after 3 min while the minimum runtime test remains true until 5 min. The third and fourth frequency steps are longer than the minimum runtime. Here it can be seen that the heat pump can be switched off when the input frequency becomes 0 Hz, if it worked for a period longer than the minimum runtime.

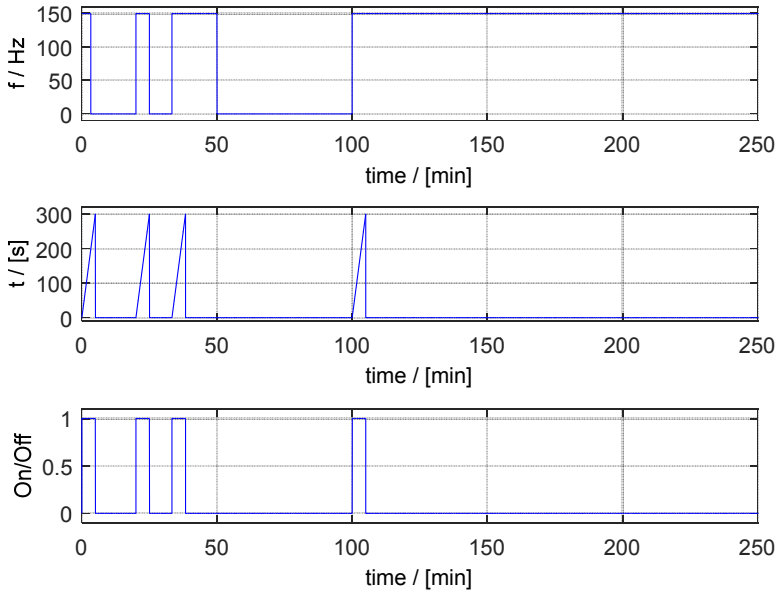

Figure 3-24: Example of the minimum runtime test

Backup heater model

Figure 3-25 shows the backup heater model. The controlled temperature (`T room`) is subtracted from the set point temperature of the backup. The backup heater starts when the controlled temperature is lower than the backup set point temperature. The relay block is necessary to reduce the number of On/Off backup cycles. The input frequency is rescaled in order to fit only the backup heater range and then a lookup table is present, which delivers the backup heater power as a function of the frequency. The output of the `product 1` is the backup heater power. The transfer function is necessary to slow down the system and to obtain more realistic dynamic behaviour. `Test BU` is an output of the backup heater model and it is used in the system frequency determination (see the next section).

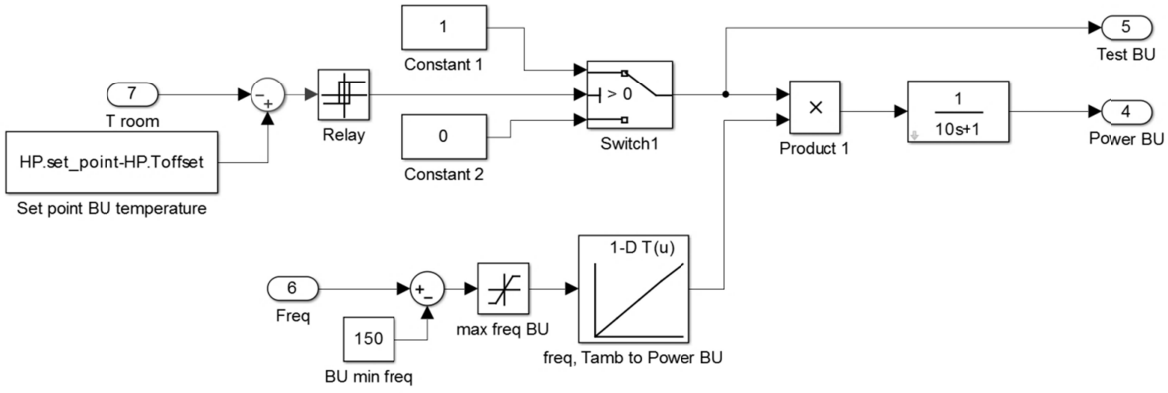

Figure 3-25: Backup Simulink model

System Frequency determination

The system frequency is different from the set point frequency set by the controller because of the de-icing, the backup heater set point and the minimum runtime. For these reasons, another block is developed in order to plot the real frequency and it is shown in Figure 3-26. The `input 8` is the frequency set by the controller and the `input 9` is the de-icing test as before explained. When the two-dimensional lookup table is chosen in the controller and the ambient temperature is lower or higher than the measured values, its output can be outside the real frequency interval. In this case, the `saturation 1` block limits the system frequency into the real interval. The `test 4` is true when the heat pump is doing the de-icing and the system has a set point frequency lower or equal to 150 Hz in these conditions the `switch 2` sets the frequency to 151 Hz. If the heat pump is in the de-icing period and the system has a set point frequency higher than 150 Hz, the `test 2` is true and the `switch 1` sets the frequency to 251 Hz. The `switch 3` takes 150 Hz as frequency if the set point frequency is higher than 150 Hz, otherwise it takes the frequency set from the `switch 1`. If the backup is switched on (`BU test`) the `switch 4` takes the frequency from the `switch 1` (so if there is the de-icing, the frequency is 251 Hz otherwise it is the set point frequency from the controller). If the backup is switched off, but the set point frequency is higher than 150 Hz (i.e. when the controlled temperature is higher than the backup set point temperature) the system frequency is fixed to 150 Hz. If the backup is switched off, but the frequency is lower than 150 Hz then the set point frequency from the controller is taken. The `switch 5` considers the minimum runtime test: if it is true the minimum frequency is limited to 50 Hz otherwise it is limited to 49 Hz.

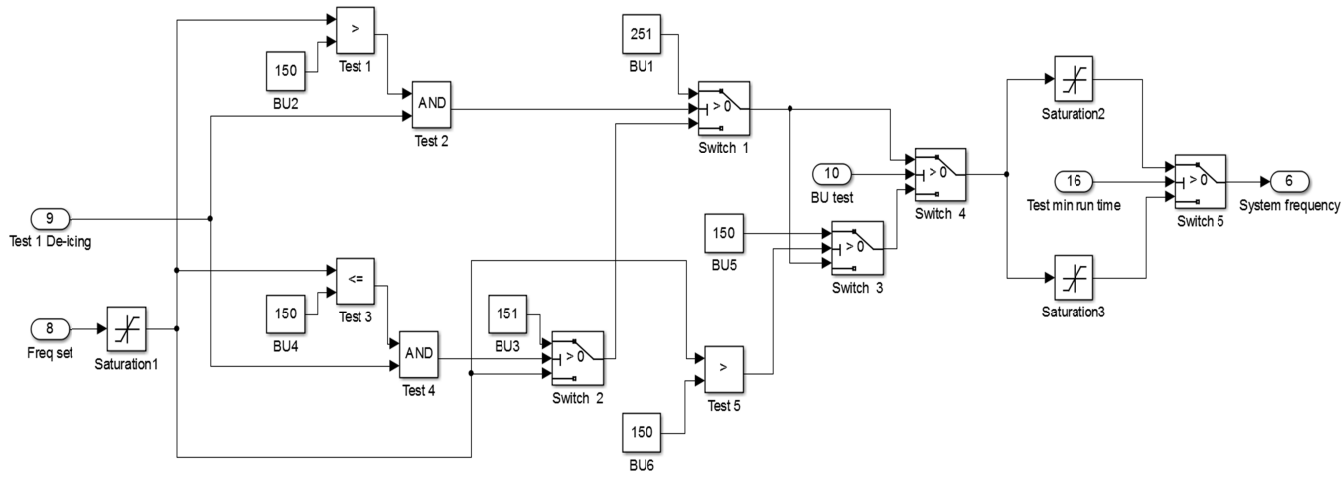

Figure 3-26: System frequency determination

Figure 3-27 shows the flow diagram of the system frequency determination. The set point frequency is set by the controller. The `de-icing test 1` is explained in the chapter 3.5.2, De-icing test. The `test BU` is explained in the chapter 3.5.2, Anti-windup heater model. The `minimum runtime test` is explained in the chapter 3.5.2, Minimum runtime.

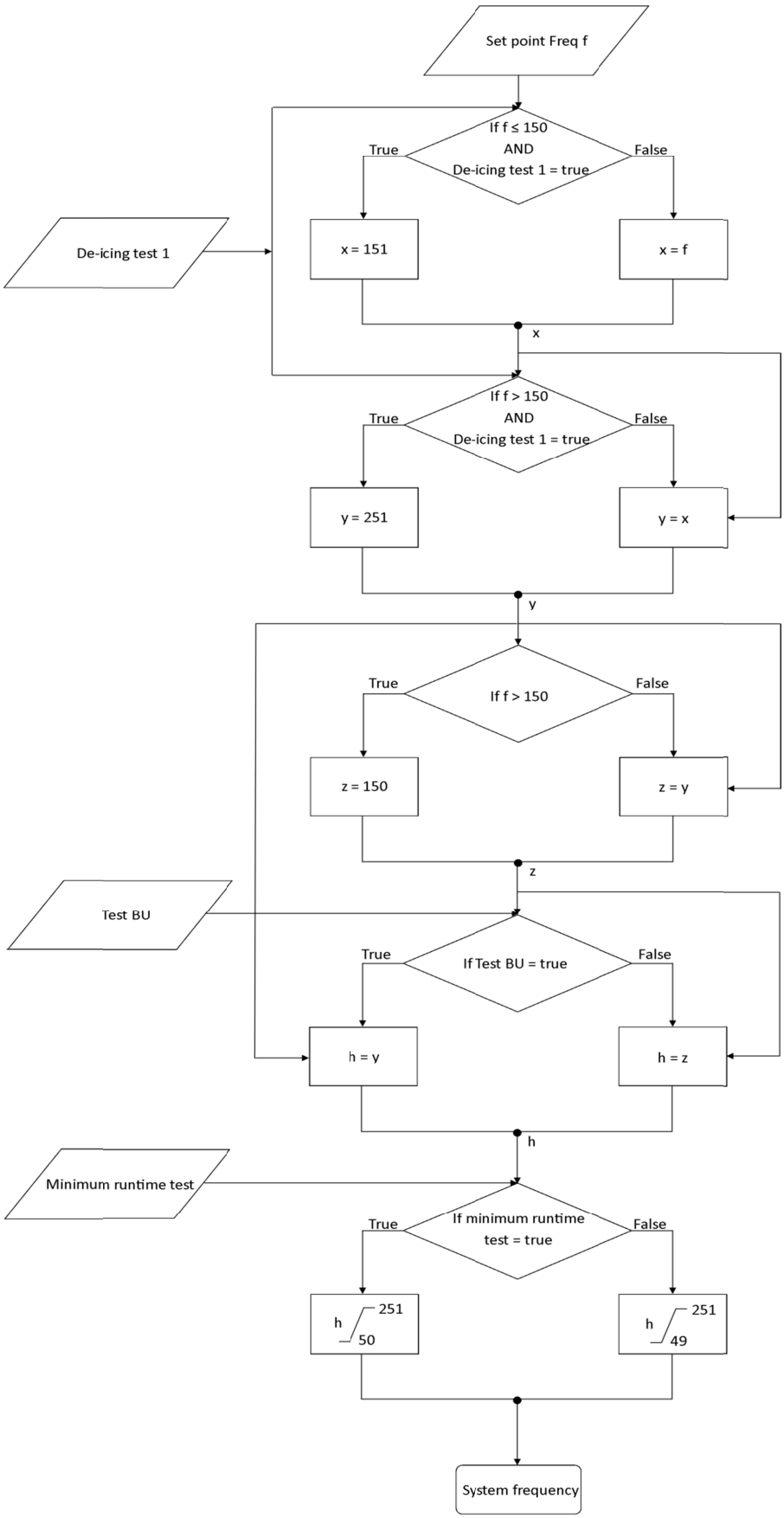

Figure 3-27: Frequency determination flow diagram

Analysis of the Efficiency

Figure 3-28 shows the heating system power calculation. The set point frequency is limited by the saturation block, between 50 Hz and 150 Hz. The COP (Coefficient of Performance) of the m-HP is calculated with a two dimensional lookup table as a function of the ambient temperature and of the frequency. The m-HP electric power demand is given by the m-HP thermal power divided by the COP. During the de-icing period, the m-HP changes its energy consumption. For this reason, another lookup table is present and it delivers the de-icing electric power demand as a function of the ambient temperature. The `switch 6` takes the power required by the HP during the de-icing of for the normal behaviour as a function of the `test 1 De-icing`. The two lookup tables use measured values. The backup heater is an electric resistance, so its energy demand is equal to the thermal energy provided to the airflow (`BU power`). Furthermore, the consumptions of the pre heater and of the fan are considered with (`El_power_vent`). All the powers are added and from this sum, the heating system power demand is determined. The energy demand is determined by the integration of the total power.

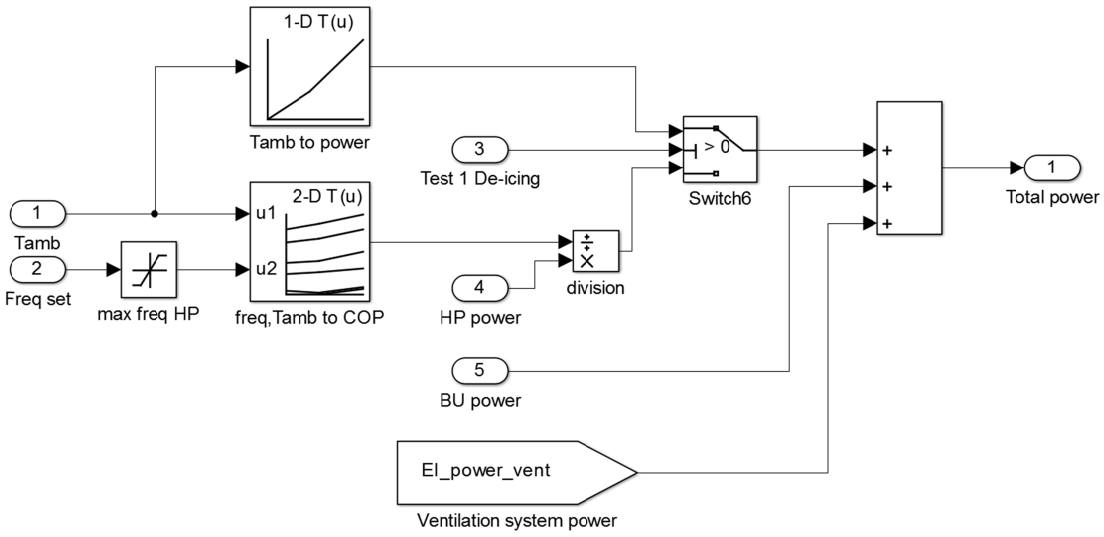

Figure 3-28: Total power calculation

4 SYSTEM PARAMETERS DETERMINATION AND OPTIMIZATION

4.1 INTRODUCTION

The studied system (building and heating system) can store energy, i.e. the state of the system can change only gradually. The controlled variable responds with delay to manipulated variable changes. Therefore, the new steady state of the controlled variable is reached after a finite time. The parameters tuning is done in order to achieve the desired control response for the studied system (SAMSON, 2003). Response velocity, few oscillations, stability and small overshoot are the goals for a good controller, but these requirements may conflict with one another. An incorrect gains determination can lead the system to the instability. When the system becomes instable, its output diverges and it is limited only by a saturation or mechanical breakage (Wikipedia, 2016). This can happen with too high gains.

A linear system is stable if for each limited input, it has a limited output over a time interval $[t_0,\infty)$ for all the initial condition. With the transfer function analysis of the system, it is possible to understand if the system is instable. The equation (4.1) shows a generic transfer function:

$$G(s) = \mu \cdot \frac{\prod_{l=1}^{m}(1-\tau_l \cdot s)}{s^g \cdot \prod_{i=1}^{n}(1-\tau_i \cdot s)} \qquad \tau_l = -\frac{1}{z_i} \qquad \tau_i = -\frac{1}{p_j} \tag{4.1}$$

z_i are the zeros and p_j are the poles of the transfer function, they can be real or complex. The system is stable, if all the poles of the closed loop transfer function have a negative real part. In this section is studied the Laplace transform of a simple linear system for a little variation governed by the following equations:

$$\Delta\dot{Q}_1 = H \cdot \Delta\vartheta_{ext} - H \cdot \Delta\vartheta_{room} \tag{4.2}$$

$$\Delta\dot{Q}_2 = \dot{m}_{supply\ air} \cdot c_{P,air} \cdot \left(\Delta\vartheta_{supply} - \Delta\vartheta_{room}\right) \tag{4.3}$$

$$C_{room} \cdot s \cdot \Delta\vartheta_{room} = -H \cdot \Delta\vartheta_{room} + H \cdot \Delta\vartheta_{ext} + \dot{m}_{supply\ air} \cdot c_{P,air} \cdot \left(\Delta\vartheta_{supply} - \Delta\vartheta_{room}\right) \tag{4.4}$$

Since this system is linear, the superposition principle can be used. It is possible to analyse the system by considering only $\Delta\vartheta_{supply}$ and $\Delta\vartheta_{room}$. So in this scheme ϑ_{ext} is considered as a constant.

The following equation is obtained, by solving the equation (4.4) for $\Delta\vartheta_{room}$:

$$\Delta\vartheta_{room} = \Delta\vartheta_{supply} \cdot \left[\frac{\dot{m}_{supply\ air} \cdot c_{P,air}}{H + \dot{m}_{supply\ air} \cdot c_{P,air} + s \cdot C_{room}}\right] \tag{4.5}$$

The transfer function of this system is:

$$\left[\frac{\dot{m}_{supply\ air} \cdot c_{P,air}}{H + \dot{m}_{supply\ air} \cdot c_{P,air} + s \cdot C_{room}}\right] \tag{4.6}$$

With the transfer function poles analysis, it is possible to know if the system is stable. In this case there are no zeros and just one pole:

$$H + \dot{m}_{supply\ air} \cdot c_{P,air} + s \cdot C_{room} = 0$$
$$s = -\frac{H + \dot{m}_{supply\ air} \cdot c_{P,air}}{C_{room}} \tag{4.7}$$

Because all the values inside the (4.7) are positive, the pole is always negative, so the simple analysed system is always stable for each limited $\Delta\vartheta_{supply}$.

Now the same system is studied with the PI control without saturation in order to keep the system linear. The Laplace transform of the PI controller for a little variation is governed by the following equation:

$$(\Delta\vartheta_{set} - \Delta\vartheta_{room}) \cdot \left(K_p + \frac{K_i}{s}\right) = \Delta\vartheta_{supply} \tag{4.8}$$

Figure 4-1 shows the scheme of the described example:

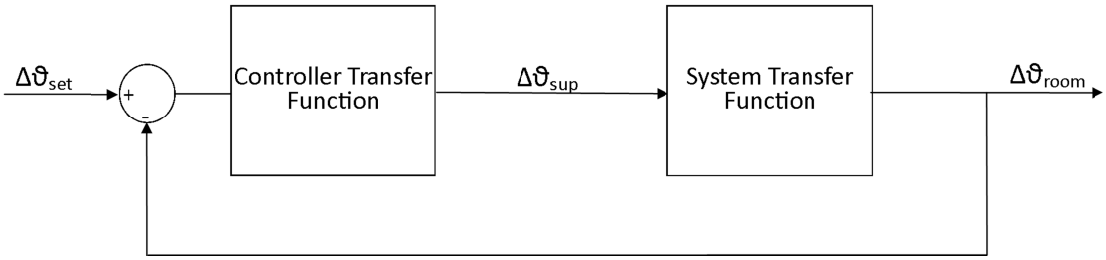

Figure 4-1: System scheme

This system can be represented by an equivalent transfer function with an open loop configuration:

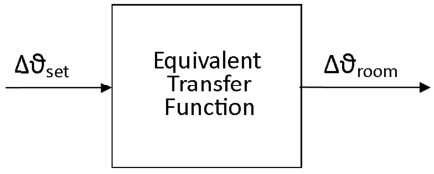

Figure 4-2: Equivalent scheme

The equivalent transfer function is the following:

$$\Delta\vartheta_{\mathrm{room}} = \Delta\vartheta_{set} \cdot \frac{\left(K_p + \frac{K_i}{s}\right) \cdot \left(\frac{\dot{m}_{supply\ air} \cdot c_{P,air}}{H + \dot{m}_{supply\ air} \cdot c_{P,air} + s \cdot C_{room}}\right)}{1 + \left(K_p + \frac{K_i}{s}\right) \cdot \left(\frac{\dot{m}_{supply\ air} \cdot c_{P,air}}{H + \dot{m}_{supply\ air} \cdot c_{P,air} + s \cdot C_{room}}\right)} \tag{4.9}$$

By simplifying the equation (4.9), the equation (4.10) is obtained:

$$\Delta\vartheta_{\mathrm{room}} = \Delta\vartheta_{set} \cdot \frac{\left(K_p + \frac{K_i}{s}\right) \cdot \left(\frac{\dot{m}_{supply\ air} \cdot c_{P,air}}{H + \dot{m}_{supply\ air} \cdot c_{P,air} + s \cdot C_{room}}\right)}{1 + \left(K_p + \frac{K_i}{s}\right) \cdot \left(\frac{\dot{m}_{supply\ air} \cdot c_{P,air}}{H + \dot{m}_{supply\ air} \cdot c_{P,air} + s \cdot C_{room}}\right)} \tag{4.10}$$

With the following parameters the equation (4.10) can be simplified in the equation (4.11).

- $a = \frac{H}{\dot{m}_{supply\ air} \cdot c_{P,air}}$;
- $b = \frac{C_{room}}{\dot{m}_{supply\ air} \cdot c_{P,air}}$.

$$\Delta\vartheta_{\mathrm{room}} = \frac{s \cdot K_p + K_i}{s^2 \cdot b + s \cdot (K_p + a + 1) + K_i} \tag{4.11}$$

The poles of the transfer function are written in the (4.12):

$$s^2 \cdot b + s \cdot (K_p + a + 1) + K_i = 0$$

$$s_1 = \frac{-(K_p + a + 1) + \sqrt{(K_p + a + 1)^2 - 4 \cdot b \cdot K_i}}{2 \cdot b} \tag{4.12}$$

$$s_2 = \frac{-(K_p + a + 1) - \sqrt{(K_p + a + 1)^2 - 4 \cdot b \cdot K_i}}{2 \cdot b}$$

A, b, K_i, K_p have always positive values so s_2 is always negative.

s_1 is negative only if: $-(K_p + a + 1) < -\sqrt{(K_p + a + 1)^2 - 4 \cdot b \cdot K_i}$

Since the values are all positive it is possible to square it, then is easier to notice that:

$(K_p + a + 1)^2 > (K_p + a + 1)^2 - 4 \cdot b \cdot K_i$ is always true.

Therefore this simple system is always stable for every value of A, b, K_i, K_p.

The system can become instable by considering also the heat pump transfer function. The Figure 4-3 shows the sketch of the system.

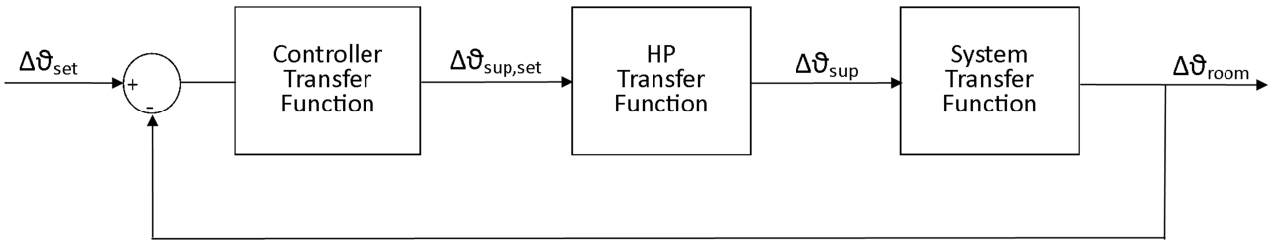

Figure 4-3: Simplified system 2

The heat pump transfer function is $\frac{1}{1+T_H \cdot s}$ where T_H is the time constant of the heat pump. The transfer function of the whole system in an open loop configuration is shown in the equation (4.13).

$$\Delta\vartheta_{room} = \Delta\vartheta_{set} \cdot \left[\frac{K_p \cdot s + K_i}{s \cdot (T_H \cdot s + 1) \cdot (1 + a + b \cdot s) + \left(K_p \cdot s + K_i\right)}\right] \tag{4.13}$$

All the changes in the root sign can be determined by the application of the Routh-Hurwitz method (Bhattacharya, 2013) to the transfer function denominator:

$$s^3 \cdot (T_H \cdot b) + s^2 \cdot (T_H + b + a \cdot T_H) + s \cdot \left(K_p + 1 + a\right) + K_i$$

The Table 4-1 shows the results of the Routh method application.

Table 4-1: Routh-Hurwitz method

$T_H \cdot b$	$K_p + 1 + a$
$T_H + b + a \cdot T_H$	K_i
$\frac{(T_H \cdot b \cdot K_i) - [\left(K_p + 1 + a\right) \cdot (T_H + b + a \cdot T_H)]}{-(a \cdot T_H + T_H + b)}$	0

According to Routh if all the elements of the first column are positive, the denominator roots are all negative. This is the desired case because it means that the system is stable. The element in the third row of the first column is the only one that can be negative, so the following inequality should be satisfied:

$$(T_H \cdot b \cdot K_i) < [\left(K_p + 1 + a\right) \cdot (T_H + b + a \cdot T_H)] \tag{4.14}$$

In this case, K_i and K_p cannot be choosen freely but they has to satisfied (4.14) in order to ensure a stable control.

4.2 DETERMINATION OF THE SYSTEM CHARACTERISTICS

Experiments have been carried out in the PASSYS test cell, in order to characterize m-HP behaviour in different working points. Five tests at the frequency of 50 Hz, 90 Hz, 110 Hz, 130 Hz, and 150 Hz are done for three different ambient temperatures $\vartheta_{amb,0}$ $(-4\,°\mathrm{C}, 0\,°\mathrm{C}, 5\,°\mathrm{C})$. The PASSYS test cell is preconditioned with fixed values for the test room and for the coldbox, until steady state conditions for the ventilation unit are reached, for each $\vartheta_{amb,0}$. Then in each test, the m-HP is operated for the duration of three hours at the fixed frequency

During the runtime, it is possible to observe three main phases:

- The first one is represented by the air flow heating;
- The second one is a steady state phase;
- The third one involves the reduction of $\vartheta_{sup,1}$.

Figure 4-4 shows the main measured quantities during the test at 150 Hz with $\vartheta_{amb,0} = 5\ °C$. In this figure the before described phases are highlighted with different colours. $\vartheta_{sup,1}$ and $\vartheta_{sup,2}$ are almost the same because the backup heater is switched off. $\vartheta_{sup,0}$ is slightly higher than $\vartheta_{sup,0i}$, this is caused by the fan losses. $\vartheta_{sup,0}$ and $\vartheta_{sup,0i}$ increase after the step due to the compressor losses and the heat delivered from the m-HP. For this reason, in order to calculate the right value of the thermal power delivered by the heat pump to the air flow ($\dot{Q}_{HP}$), it is important to take the value of $\vartheta_{sup,0}$ in the ventilation unit steady state with the heat pump switched off.

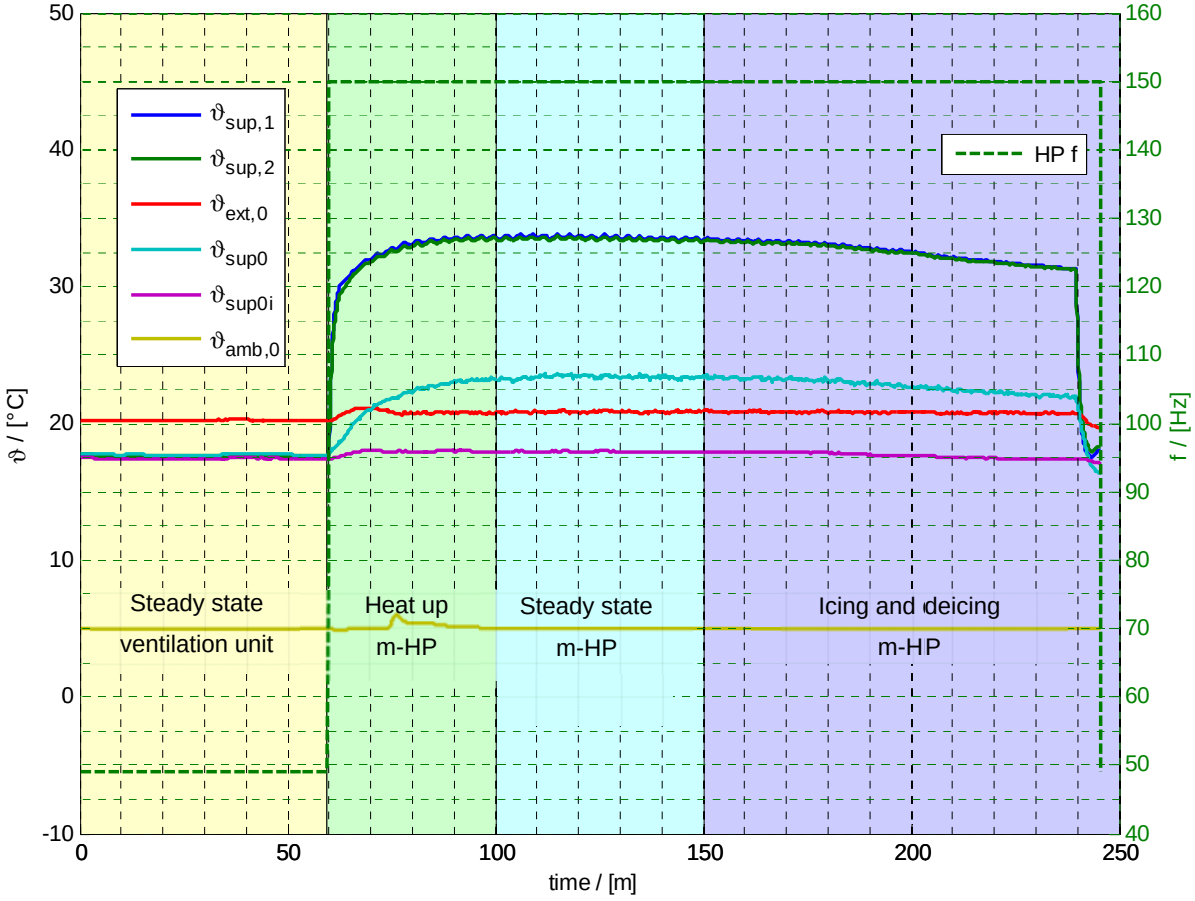

Figure 4-4: Heat pump behaviour with $f = 150\ Hz$, $\vartheta_{amb,0} = 5\ °C$, $\vartheta_{ext,0} = 20\ °C$

Figure 4-5, Figure 4-6 and Figure 4-7 show the supply air temperature for each frequency with $\vartheta_{amb,0} = 5\,°C, 0\,°C, -4\,°C$ and $\vartheta_{ext,0} = 20\,°C$.

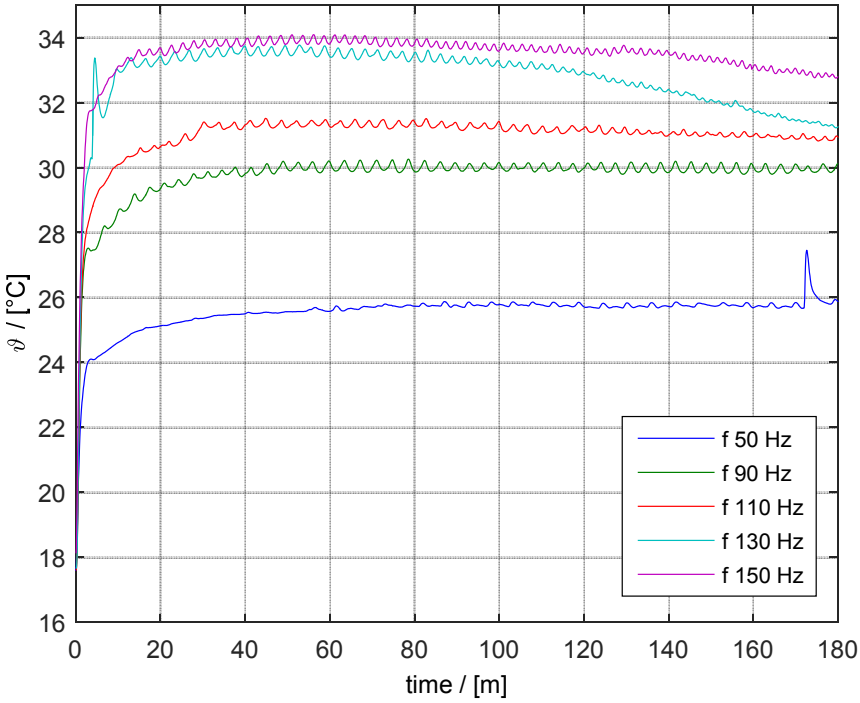

Figure 4-5: Supply air temperatures of the test with $\vartheta_{amb,0} = 5$ °C and $\vartheta_{ext,0} = 20$ °C

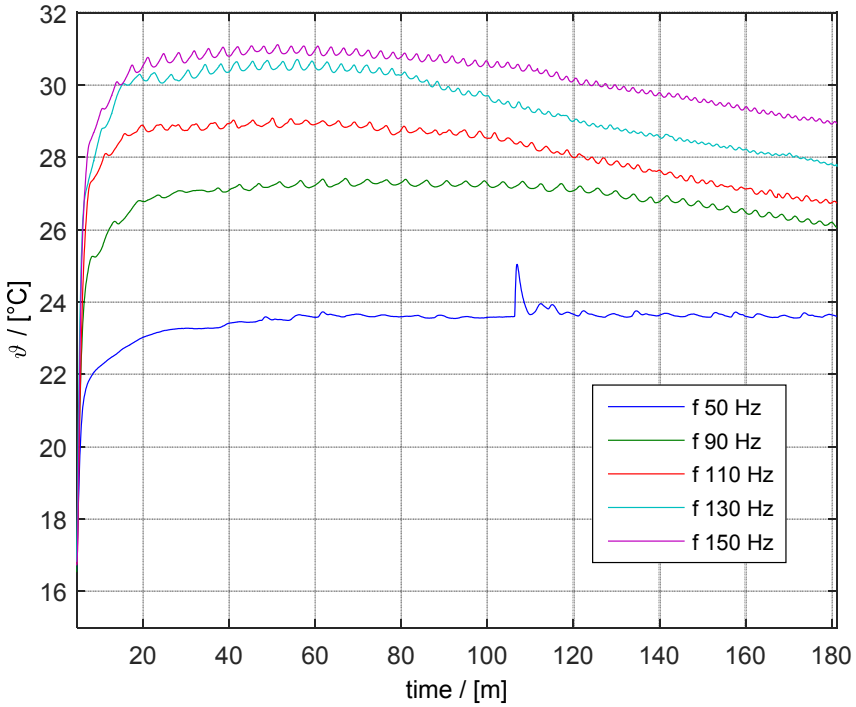

Figure 4-6: Supply air temperatures of the test with $\vartheta_{amb,0} = 0$ °C and $\vartheta_{ext,0} = 20$ °C

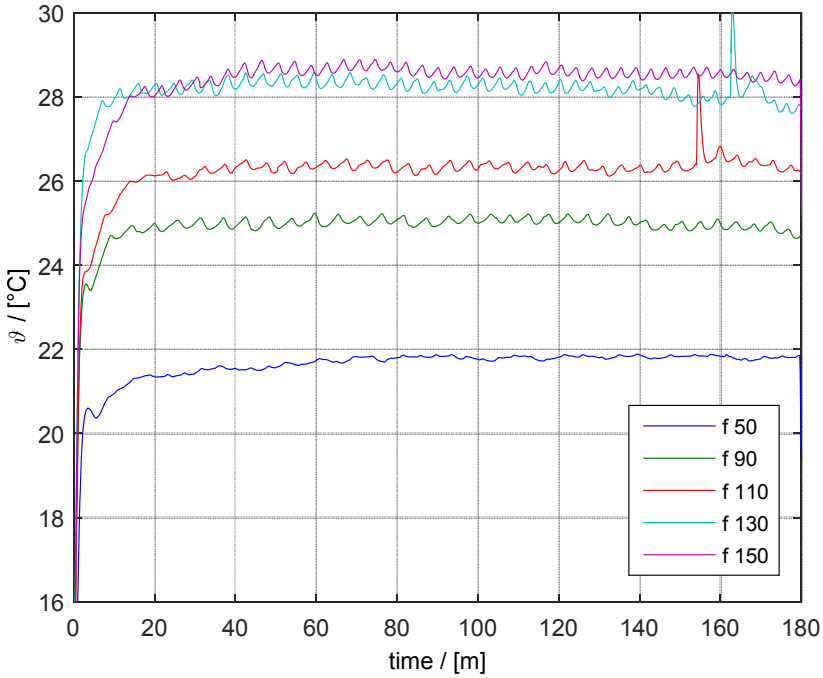

Figure 4-7 Supply air temperatures of the test with $\vartheta_{amb,0} = -4\ °C$ and $\vartheta_{ext,0} = 20\ °C$

Figure 4-8 shows a summary of the measured $\vartheta_{sup,1}$ for each test. As it can be observed, $\vartheta_{sup,1}$ do not grow linearly with the frequency. This is due to the performance reduction with the increasing of the frequency. This behaviour can be noticed also in Figure 4-10 and in Figure 4-11, where the COP and the thermal power are shown. The reduction of performance with the frequency increment can be explained by the increment of the mass flow (see equation (3.13)). If the mass flow increases, also the thermal power exchanged in the condenser increases (see equation (3.20)). UA_{cond} value is constant and the air volume flow is constant, so ΔT_{cond} increases because ϑ_{cond} increases. In the evaporator, the temperature decreases in order to ensure a higher thermal power due to the higher mass flow. Since ϑ_{cond} increases and ϑ_{evap} decreases, the pressure ratio over the compressor increases and with it the compressor work.

At fixed frequency, the delivered thermal power increases with $\vartheta_{amb,0}$. By increasing the temperature of the evaporator, the density of the vapour before the compressor increases so the mass flow moved by the compressor decreases (see equation (3.13)), the pressure ratio decreases and the isentropic efficiency of the compressor decreases. All these factors lead to a higher supply air temperature and thermal power delivered by the heat pump. The m-HP performance decreases, if the frequency increases and $\vartheta_{amb,0}$ decreases.

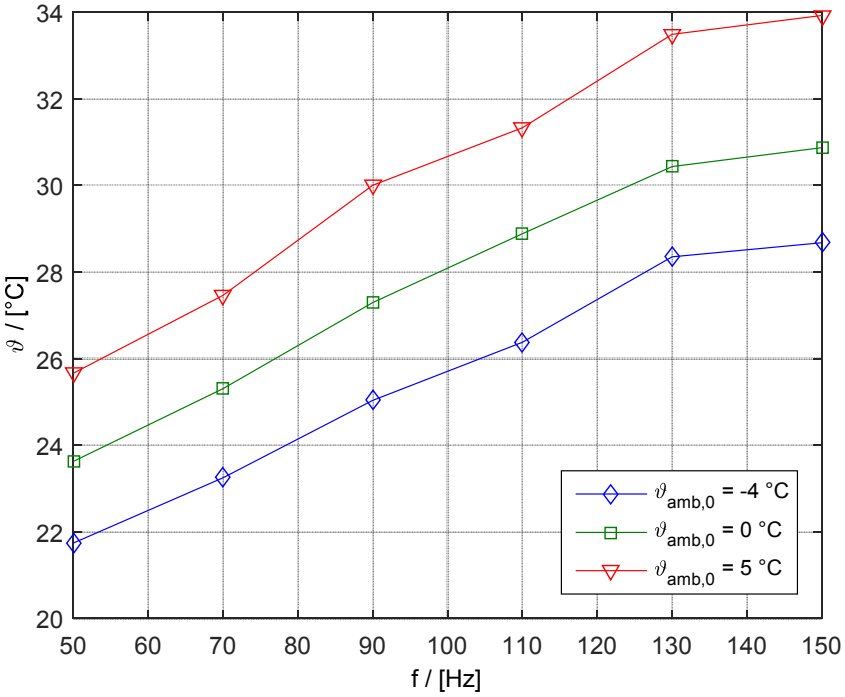

Figure 4-8: Supply air temperatures for each $\vartheta_{amb,0}$ for each frequency

$\vartheta_{sup,1}$, $\dot{V}_{air}$, electric power required by the heat pump P, $\vartheta_{ext,0}$ and $\vartheta_{amb,0}$ are measured. With these values, it is possible to calculate the COP and the power delivered to the air flow. The mean value of ten minutes, after one hour from the step, is taken in order to define $\vartheta_{sup,1}$, and P. $\vartheta_{sup,0}$ is defined again by taking the mean value of ten minutes in the ventilation unit steady state measurements. The $\dot{Q}_{HP}$ is calculated for each time step *i* as it is shown in the equation (4.15):

$$\dot{Q}_{HP} = \dot{V}_{air} \cdot \rho_{air} \cdot c_p \cdot \left(\vartheta_{sup,1} - \vartheta_{sup,0}\right) \tag{4.15}$$

Where:

- $\dot{V}_{air}$ is the air volume flow measured with a calibrated orifice $\left[\frac{\mathrm{m}^3}{\mathrm{s}}\right]$;
- ρ_{air} is the air density considerated as a constant 1.2 $\left[\frac{\mathrm{kg}}{\mathrm{m}^3}\right]$;
- c_p is the specific heat of the air 1000 $\left[\frac{\mathrm{J}}{\mathrm{kg\ K}}\right]$;
- $\vartheta_{sup,1}$ is the supply air temperature after the m-HP condenser [°C];
- $\vartheta_{sup,0}$ is the supply air temperature before the m-HP compressor, measured in the ventilation unit steady state conditions [°C].

A characteristic value for the thermal power delivered by the m-HP ($\dot{Q}_{HP,m}$) and its electric demand P_m, are determined in each test in the same way of $\vartheta_{sup,1}$.

Finally, the COP is calculated as shown in equation (4.16):

$$COP = \frac{\dot{Q}_{HP,m}}{P_m} \tag{4.16}$$

Figure 4-9 shows the electric power consumption of the heat pump for each test.

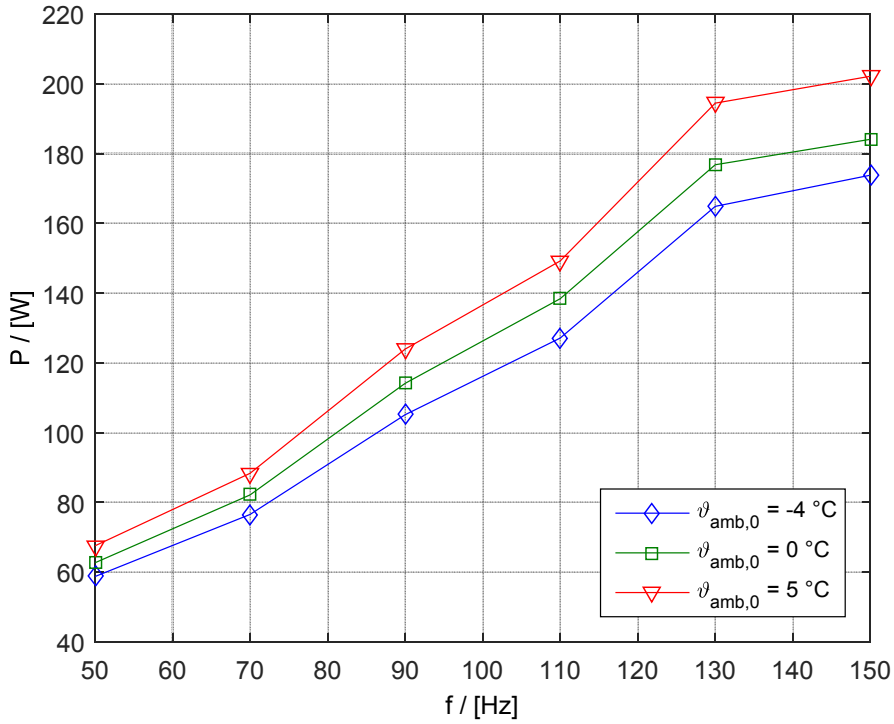

Figure 4-9 : Electric power required by the HP for each $\vartheta_{amb,0}$, as a function of the frequency

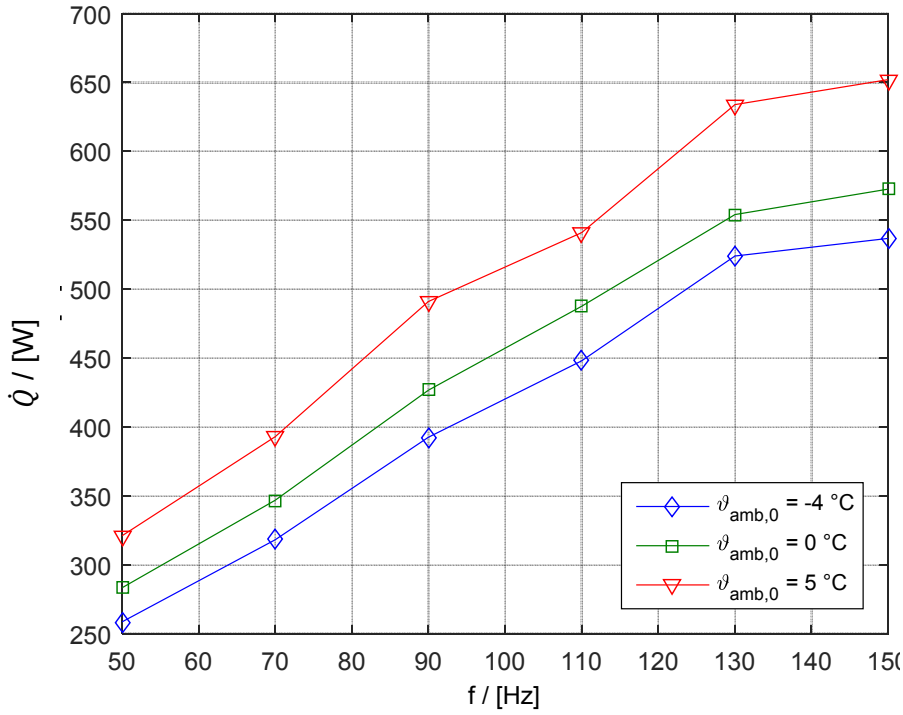

Figure 4-10: Thermal power delivered for each $\vartheta_{amb,0}$ as a function of the frequency

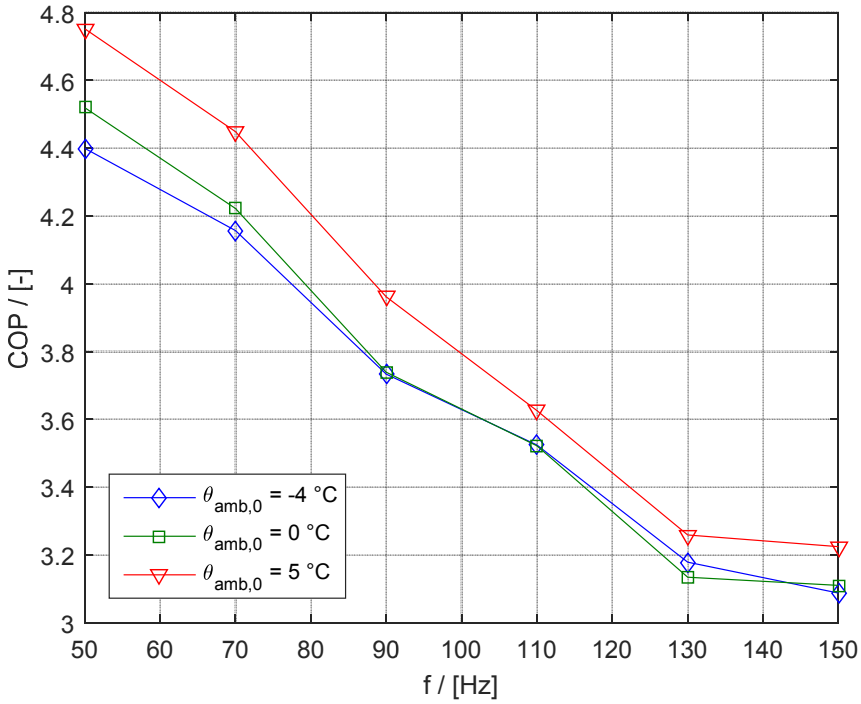

Figure 4-11: COP for each $\vartheta_{amb,0}$ for each frequency

4.3 PARAMETER DETRMINATION

The parameter determination can be done in many ways. In this work, the dynamic system response in an open loop configuration is analysed and the parameters are determined by using the Chien, Hrones and Reswick method (J. A. , J. B. , & Kun Li , 1952). The Figure 4-12 shows the system studied in this chapter, in particular the red encircled part is employed in the study of the open loop dynamic behaviour.

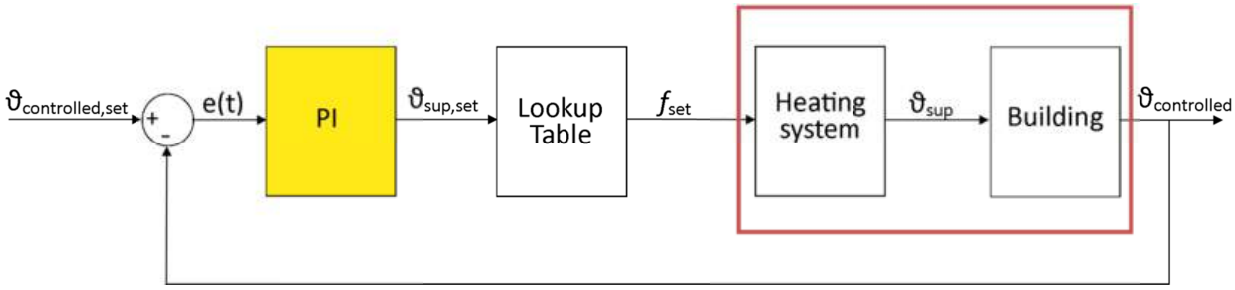

Figure 4-12: Studied system

The dynamic behaviours of the simple and complex building models are studied by applying an input step to the system at the steady state. The system response is determined by keeping as constant all the boundary conditions and by introducing a disturbance in the supply air temperature. The important points that characterize the system are:

- ϑ_i, ϑ_f initial and final value of the controlled variable (sensitive temperature of the hallway);

- $\vartheta_{sup,f}$, $\vartheta_{sup,i}$ initial and final value of the manipulated variable (supply air temperature). These values are measured in the PASSYS test cell;
- τ_u, τ_g the delays. $\tau_u = t_2 - t_1$ is called dead time and it is the time interval between the moment in which the disturbance is introduced and the moment in which the system starts to respond. $\tau_g = t_3 - t_2$ is the time for the response to occur.

The magnitude of the disturbance is expressed in per cent:

$$K_s = \frac{\vartheta_f - \vartheta_i}{\frac{\vartheta_{sup,f} - \vartheta_{sup,i}}{\vartheta_{sup,max} - \vartheta_{sup,min}}} \tag{4.17}$$

The Chien, Hrones and Reswick method uses these variables to calculate the system parameter. Two formulation set are present in the used method, one allows 20% of overshoot and another one without overshoot. The last one is used because it guarantees a more robust control. The equations (4.18) and (4.19) show the two formulations without overshoot. The formulation (4.18) is for disturbed system while the (4.19) is for the regular behaviour. The formulation (4.18) has higher K_p and lower T_n with respect to the (4.19) this means that the controller reacts faster. The (4.20) shows the PI controller equation.

$$K_p = \frac{0.6}{K_s} \cdot \frac{T_g}{T_u} \qquad T_n = 4 \cdot T_u \tag{4.18}$$

$$K_p = \frac{0.35}{K_s} \cdot \frac{T_g}{T_u} \qquad T_n = 1.2 \cdot T_g \tag{4.19}$$

$$y_{PI}(t) = K_p \cdot \left(e(t) + \frac{1}{T_n} \cdot \int e(t)\, dt \right) \tag{4.20}$$

4.3.1 Simple Model Parameter

For the simple building model, the parameters are calculated by using a HiL simulation. The Simulink model is coupled with the PASSYS test cell, the whole system is operated until the steady state is reached. Than the m-HP power level is changed from the minimum to the maximum. This HiL simulation cannot be run until the new steady state is reached, because the m-HP needs de-icing after two or three hours of operation. Therefore, another simulation is done in Simulink with a step source for the supply air temperature in order to simulate the whole period from the moment in which the disturbance is introduced to the moment in which the new steady state is reached. Figure 4-13 shows the whole system response until the new steady state is reached. Where:

- $\vartheta_{5,Sim}$ is the zone 5 temperature from Simulink;
- $\vartheta_{5,HIL}$ is the zone 5 temperature from the HiL simulation;
- $Tangent$ is the tangent line to the first part of the system response;
- $\vartheta_{5,bs}$ is the zone 5 temperature of the steady state before the step;
- $\vartheta_{5,as}$ is the zone 5 temperature of the steady state after the step.

Figure 4-14 shows the zone five temperatures from the HiL and Simulink simulation. The incline of the HiL results changes after two hours because of the ice formation.

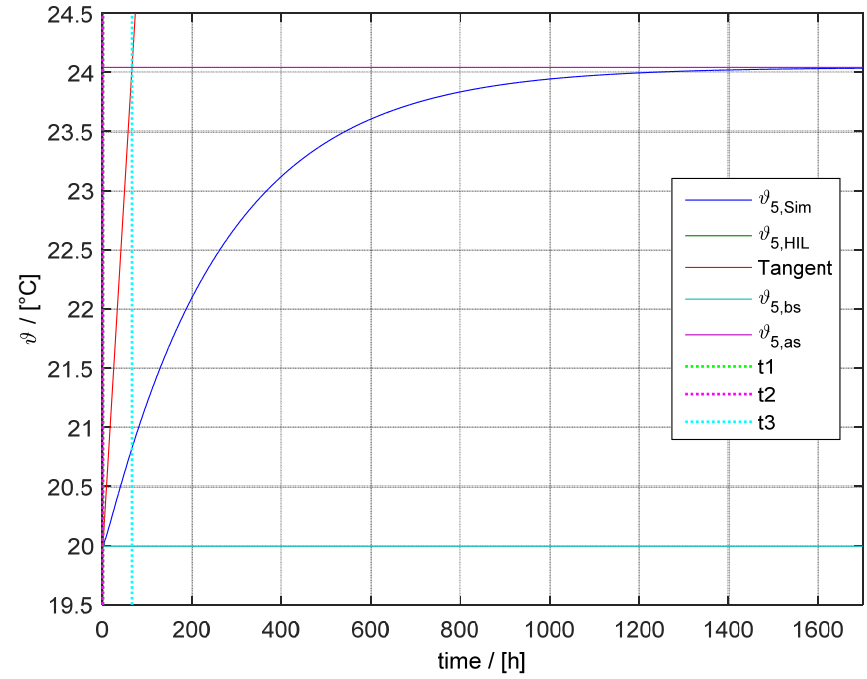

Figure 4-13: Simple model step

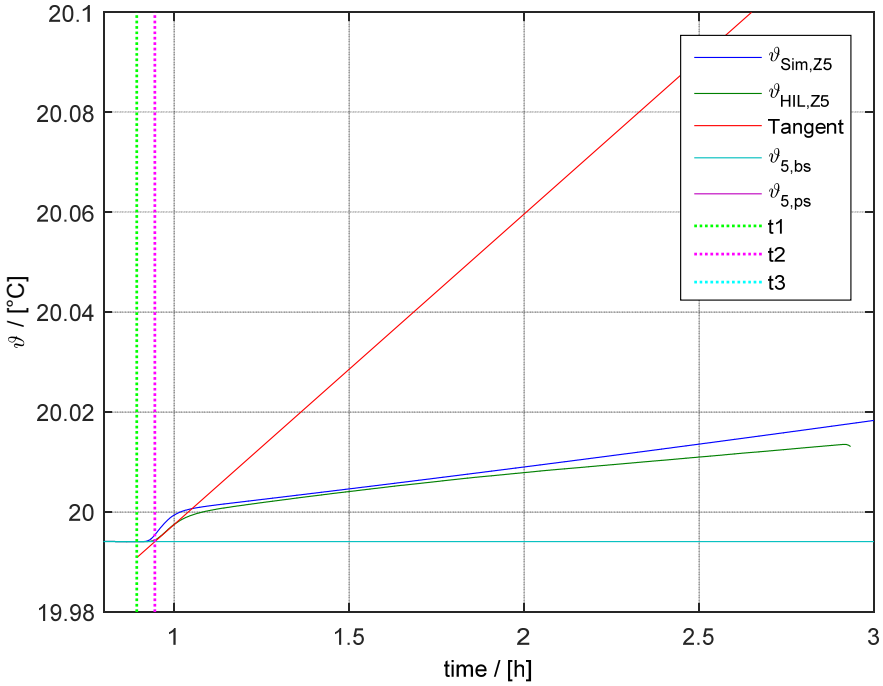

Figure 4-14: Zoom of the step

The data of the problem are:

$$\vartheta_f = 24.0\ [°C] \qquad \tau_u = 186.5\ [s]$$

$$\vartheta_i = 20.0\ [°C] \qquad \tau_g = 234411.4\ [s]$$

$$\vartheta_{sup,2} = 31.6\ [°C] \qquad \vartheta_{sup,min} = 24.3\ [°C]$$

$$\vartheta_{sup,1} = 24.3\ [°C] \qquad \vartheta_{sup,max} = 47.9\ [°C]$$

The parameters resulting from the formulation (4.18) are:

$$K_p = 59.3\ \left[\frac{K}{K}\right] \qquad T_n = 12.4\ [min]$$

The parameters resulting from the formulation (4.19) are:

$$K_p = 34.6\ \left[\frac{K}{K}\right] \qquad T_n = 4688.2\ [min]$$

4.3.2 Complex Model Parameter

Figure 4-15 shows the dynamic behaviour of the complex model. In this figure the whole period is plotted. In Figure 4-16 the tangent line, t_1, t_2 and t_3 can be seen.

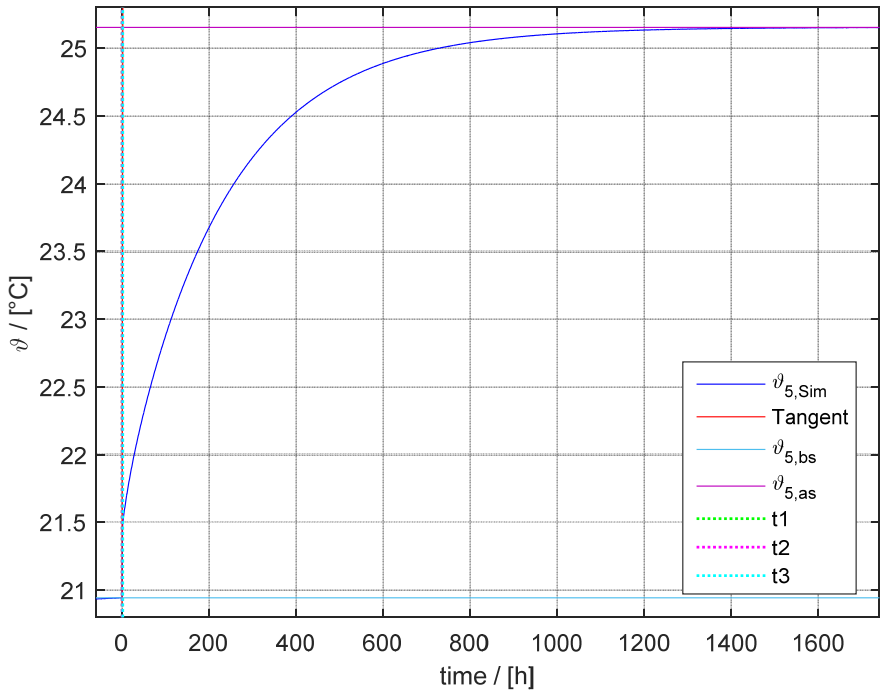

Figure 4-15: Complex model step

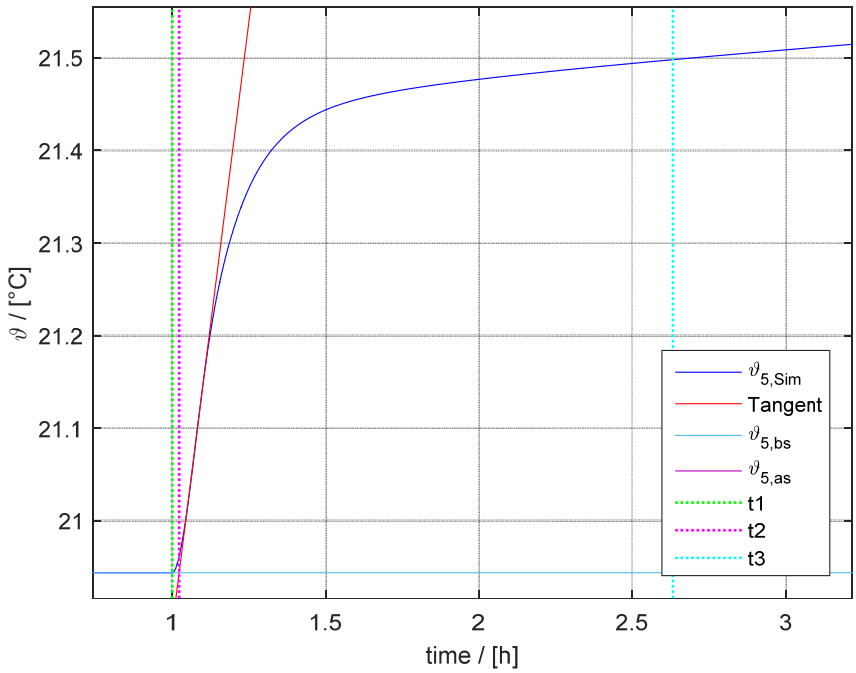

Figure 4-16: Zoom of the step

The data of the problem are:

$$\vartheta_f = 25.1\ [°C] \qquad \tau_u = 73.8\ [s]$$

$$\vartheta_i = 21.0\ [°C] \qquad \tau_g = 12058.2\ [s]$$

$$\vartheta_{sup,2} = 31.6\ [°C] \qquad \vartheta_{sup,min} = 24.3\ [°C]$$

$$\vartheta_{sup,1} = 24.3\ [°C] \qquad \vartheta_{sup,max} = 49.9\ [°C]$$

The parameters resulting from the formulation (4.18) are:

$$K_p = 7.6\ \left[\frac{K}{K}\right] \qquad T_n = 4.9\ [min]$$

4.3.3 Comparison of the Complex and Simple Model Dynamic Behaviours

Figure 4-17 shows the step response of the simple and complex model, where:

- ϑ_S is the temperature of the zone 5 from the simple building model;
- $\vartheta_{C,s}$ is the sensitive temperature of the zone 5 from the complex building model;
- $\vartheta_{C,c}$ is the convective temperature of the zone 5 from the complex building model;
- $\vartheta_{C,r}$ is the radiative temperature of the zone 5 from the complex building model.

Figure 4-17 clearly shows that the dynamic responses are different. This is due to the simplifications present in the simple building model. In the complex model, two nodes are present and the walls have their own structure and capacity. The convective temperature depends on the air capacity while the radiative temperature is influenced by the walls capacity, so its temperature change slowly with respect to the convective temperature. In the

simple model, only one capacity is present this makes the dynamic response slower compared to the complex.

The steady state temperature of the simple model (Figure 4-17) is shifted 0.25 °C in order to easily compare the dynamic behaviours. This steady state temperature difference is due to the simplified thermal transmittances used within the simple model.

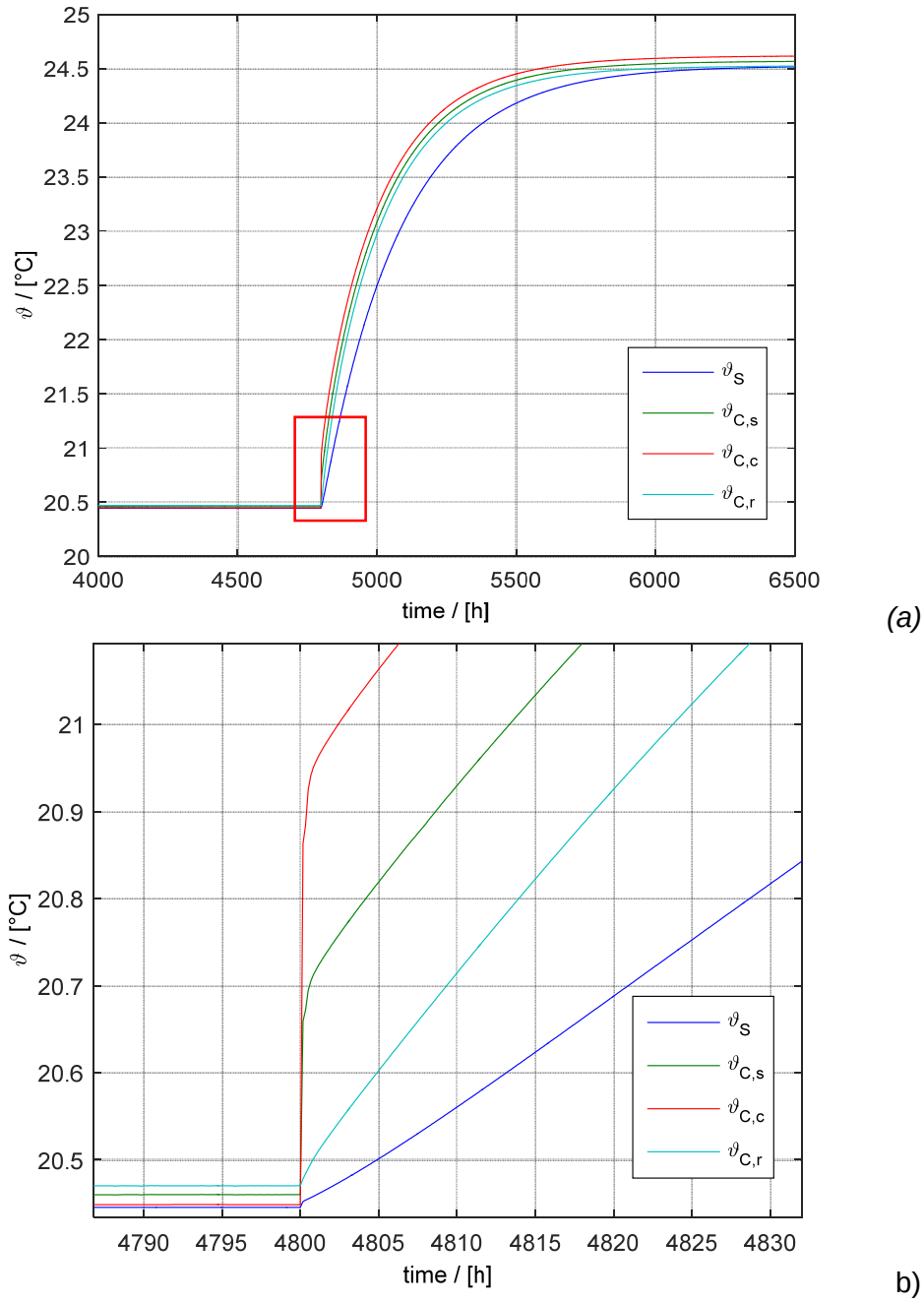

Figure 4-17: (a) Comparison of the complex and simple model dynamic behaviour. (b) zoom of the plot

The dynamic behaviour difference can be analysed by using the results of the step in the simple and complex building models reported in Figure 4-17. $K_i = \frac{1}{T_n}$ can be obtained with the integration of the error, by considering an ideal integrative controller with the equation (4.21)

$$K_i = \frac{\vartheta_{sup}(t_{end})}{\int_0^{t_{end}} e(t)\, dt} \tag{4.21}$$

The results for the simple and complex building models are the following:

$$K_{i,simple} = 4.58 \cdot 10^{-4} \left[\frac{1}{min}\right] \qquad T_{n,simple} = 2183.9\ [min]$$

$$K_{i,complex} = 6.33 \cdot 10^{-4} \left[\frac{1}{min}\right] \qquad T_{n,complex} = 1581.1\ [min]$$

Figure 4-18 shows the supply air temperature that the ideal integrative controller with the before mentioned K_i would deliver with the controlled temperatures behaviour reported in the second subplot.

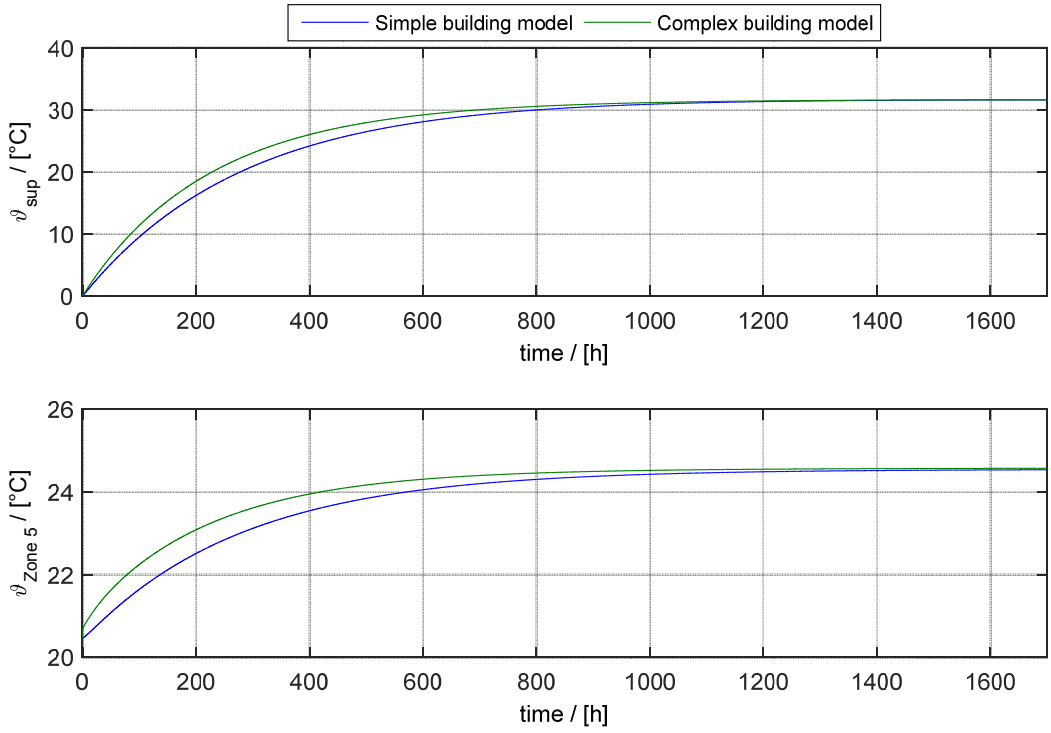

Figure 4-18: Ideal integrative controller and controlled temperature behaviours for the simple and complex building model

The dynamic behaviour of the simple building model is not accurate enough to be used for the controller simulation and parameter determination. The parameters determined with the simple model can be instable in a real system because the simple model is too slow responding. For these reasons the complex model is used in the following work.

4.3.4 Parameter Optimization

Introduction

Simulations with different PI parameters are carried out in order to find the proportional and integral gains with which the controller response is optimized. The factors considered in the optimization are:

- Reaction Speed;
- Energy demand;
- Controlled temperature behaviour;
- Number of On/Off cycles;
- Heating system performance ($SCOP_{HP}$ and $SCOP_{SYS}$).

The analysed cases are:

- Case1: $K_p = 59.3 \left[\frac{K}{K}\right]$; $T_n = 12.4$ [min];
- Case 2: $K_p = 34.6 \left[\frac{K}{K}\right]$; $T_n = 4688.2$ [min];
- Case 3: $K_p = 7.6 \left[\frac{K}{K}\right]$; $T_n = 4.9$ [min];
- Case 4: $K_p = 4.5 \left[\frac{K}{K}\right]$; $T_n = 241.2$ [min];
- Case 5: $K_p = 35 \left[\frac{K}{K}\right]$; $T_n = 10$ [min].

Reaction speed

Figure 4-19 shows the supply air temperatures for each case, where: Figure 4-19 underlines that the parameter involved in the cases 2 and 4 are too slow responding.

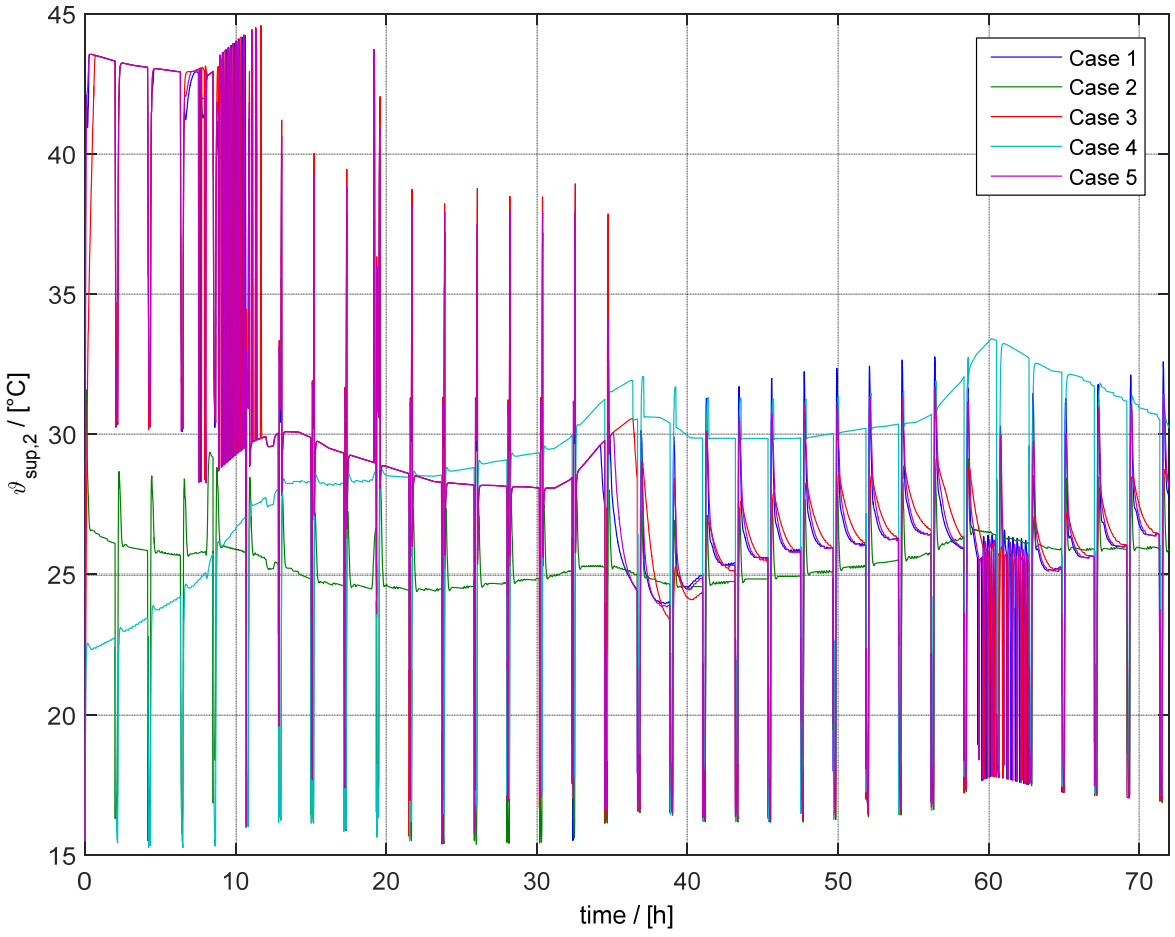

Figure 4-19: Supply air temperature for each test

- Case 1:

The case 1 is the fastest between the considered cases. The system reaches the maximum frequency after few seconds, but since the proportional gain is high, the proportional part rapidly decrease with the error and after four minutes there is a decrement of the system frequency due to the reduction of the proportional output but it reaches again the maximum frequency after sixteen minutes thanks to the integral contribute. Figure 4-20 shows the comparison of the first minutes of simulation between the cases 1, 3 and 5. Here the before described behaviour can be observed.

- Case 2:

The proportional gain is higher with respect to the case 4 and in fact the system has higher supply air temperature in the first period. As the error decreases, the proportional output decreases its influence on the controller output. In the same time, the integral time constant is too high, so the integral part is slowly gaining influence on the controller output. The system dares not reach the maximum power within these 3 days of simulation.

- Case 3:

The case 3 is slower than the case 1. The system reaches here the maximum supply air temperature after 39 minutes.

- Case 4:

In this test, the heating system never reaches the maximum power within the analysed period. Thanks to the anti-windup the system is suddenly switched on but when the system is not anymore below the saturation limit the PI parameters are responsible for the controller behaviour. It can be seen along the considered period that T_n is too high and the integral part needs long time in order to gain influence and the proportional gain is not high enough to ensure a fast control.

- Case 5:

The case 5 is slightly slower than the case 1 but faster than the case 3. The system reaches here the maximum supply air temperature after 15 minutes.

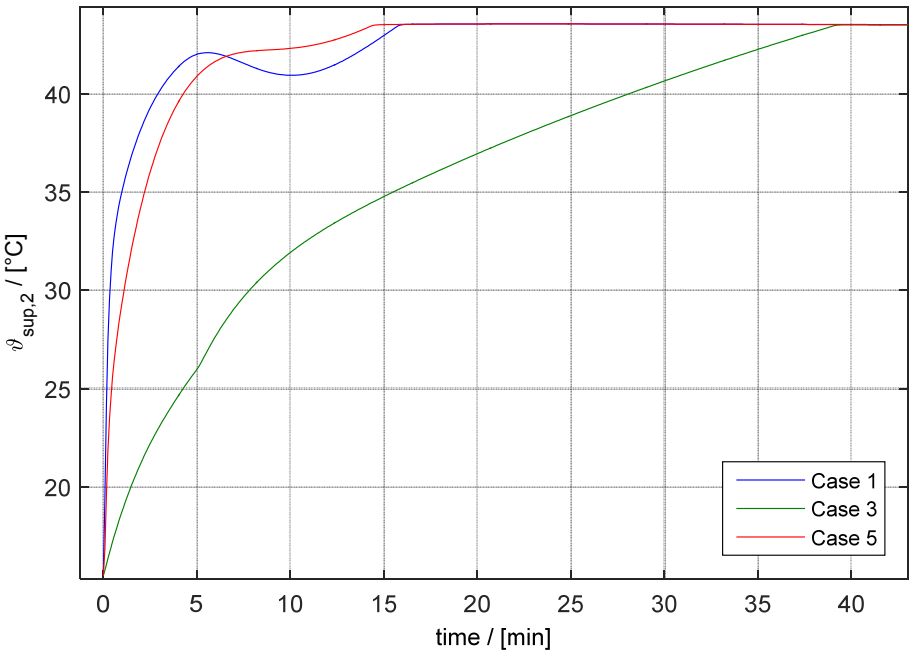

Figure 4-20: Zoom of the first period of the Figure 4-19

Figure 4-21 shows the sensitive temperature of the zone 5 for each case.

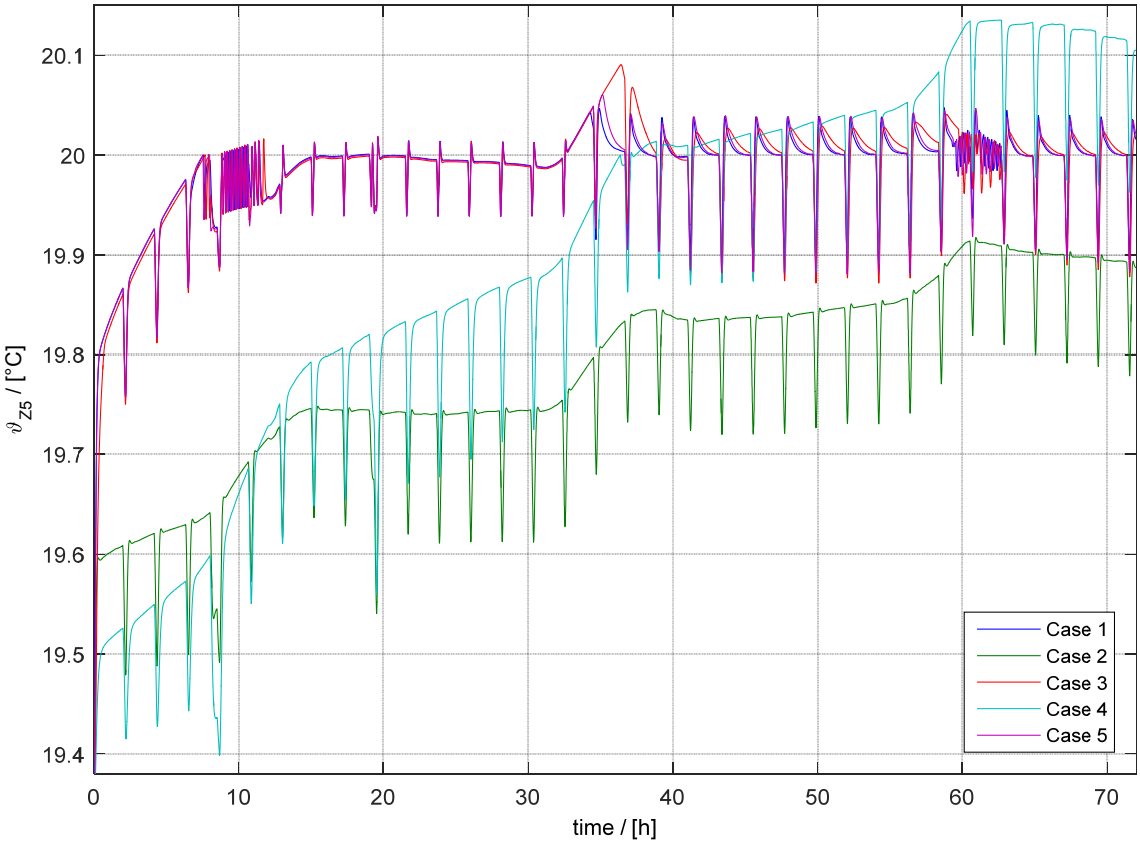

Figure 4-21: Temperatures of the zone 5 for each test

The parameters of the case 5 are the most suitable for the considered case as regard to the reaction speed.

Energy Demand and System Performance

The energy demand together with the controlled temperature, are important factors for the determination of the parameter. $SCOP_{HP}$ (seasonal coefficient of performance of the heat pump) and $SCOP_{SYS}$ (seasonal coefficient of performance of the system) are used for the analysis of the heating system performance, see equation (4.22) and (4.23).

$$SCOP_{HP} = \frac{Q_{HP}}{E_{HP}} \tag{4.22}$$

$$SCOP_{SYS} = \frac{Q_{HP} + Q_{BU}}{E_{HP} + E_{BU}} \tag{4.23}$$

Where:

- Q_{HP} is the thermal energy provided by the heat pump;
- E_{HP} is the electric energy demand of the heat pump;
- Q_{BU} is the thermal energy provided by the backup heater;
- E_{BU} is the electric energy demand of the backup heater.

Only the cases 1, 3 and 5 are analysed because the cases 2 and 4 are not suitable for the studied system. Table 4-2 shows the energy demand of the heat pump, the energy demand of the backup heater (equal to the thermal energy provided by the backup heater to the system), the thermal energy provided by the heat pump to the system, the total energy demand, the $SCOP_{HP}$ and the $SCOP_{SYS}$. The energy demands of the fans and pre heater are equal in every case because the fans power is taken as a constant and the pre-heater energy demand depends on the ambient temperature that is the same for every case. The power of the fan is taken as 54 W, so the energy required by the fan is 473 $\left[\frac{\text{kWh}}{\text{a}}\right]$ for the whole year. If the ambient temperature is lower than -6 °C the pre-heater is switched on in order to avoid ice formation inside the heat exchanger. The pre-heater energy demand is 13.17 $\left[\frac{\text{kWh}}{\text{a}}\right]$, with the considered weather. Case 1 is the fastest reacting system, so it uses more backup heater respect to the cases 3 and 5. The three cases have similar total energy demand.

Table 4-2: Energy demands, $SCOP_{HP}$ and $SCOP_{SYS}$

	HP energy demand $\left[\frac{\text{kWh}}{\text{a}}\right]$	BU energy demand $\left[\frac{\text{kWh}}{\text{a}}\right]$	HP thermal energy $\left[\frac{\text{kWh}}{\text{a}}\right]$	Energy demand tot $\left[\frac{\text{kWh}}{\text{a}}\right]$	$SCOP_{HP}$ [−]	$SCOP_{SYS}$ [−]
Case 1	353.89	100.15	1138.57	940.05	3.22	2.73
Case 3	349.44	90.63	1105.80	926.09	3.17	2.72
Case 5	348.07	95.27	1121.90	929.35	3.22	2.75

Controlled Temperature Behaviour

The numbers of hours in which the controlled temperature falls below 19.9 °C and in which it is higher than 20.1 °C are calculated for January and February. Only these two months are considered because in other periods it is possible that the overheating is caused by high ambient temperature.

Table 4-3 shows for each case:

- The number of underheating hours and the per cent value;
- The number of overheating hours and the per cent value;
- The minimum temperature reached in the considered period;
- The maximum temperature reached in the considered period.

Case 3 is the slowest reacting system between the three considered cases, for this reason, according to Table 4-3, it has the highest number of overheating and underheating hours, the highest maximum temperature and the lowest minimum temperature.

Table 4-3: Over and under heating comparison for January and February (1416 [h])

	Under heating		Over heating		Min temp	Max temp
	[h]	[%]	[h]	[%]	[°C]	[°C]
Case 1	1.70	0.120	13.10	0.935	19.89	20.15
Case 3	18.23	1.29	2.00	0.141	19.85	20.13
Case 5	11.27	0.796	5.90	0.417	19.88	20.14

On/Off Cycles

An important factor is the number of compressor On/Off cycle which has effects on the life time and on the LCC (Life Cycle Cost). This depends mainly on the correct dimensioning of the m-HP with respect to the energy demand of the building and on the minimum runtime. When the heat pump is at the minimum power level, the system cannot regulate its power anymore and if the energy demand decreases, the only one way to regulate the power is doing On/Off cycles. The On/Off behaviour decreases the heating system performances and reduces the service life of the components. The number of yearly On/Off cycles is calculated by means of Simulink simulation with a minimum runtime of 15 [min] for all the three cases:

Table 4-4: Number of On/Off cycles

	Number of yearly On/Off $\left[\frac{n}{a}\right]$
Case 1	3855
Case 3	2315
Case 5	3345

Since the test 3 is the slowest reacting, it has the minimum number of yearly On/Off cycles. The number of On/Off cycles can be reduced by increasing the minimum runtime period (chapter 4.3.5).

Conclusion

The parameters of the case 5 are the best solution for the studied system. These parameters make the control system enough fast responding and stable and they ensure that the controlled temperature lies inside an acceptable range of temperature.

4.3.5 Minimum Runtime Optimization

The number of On/Off cycles can be changed by modifying the minimum runtime. Six yearly simulations are carried out for the case 5 with different values of minimum runtime (5 [min], 15 [min], 30 [min], 45 [min], 60 [min] and 90 [min]). By changing this factor, also the energy demand and the temperature profile change. Table 4-5 shows the results of yearly simulations carried out with different minimum runtimes. Table 4-6 shows the hours of over and under heating and the maximum and minimum temperatures reached by the controlled temperature over a period of two months (January and February). By reading these two tables together, it is possible to observe that by increasing the minimum runtime, the performances of the system are increasing, but the temperature of the zone 5 is less controlled.

Table 4-5: Energy demands, $SCOP_{HP}$ and $SCOP_{SYS}$

Min. runtime	HP energy demand $\left[\frac{\text{kWh}}{\text{a}}\right]$	BU energy demand $\left[\frac{\text{kWh}}{\text{a}}\right]$	HP thermal energy $\left[\frac{\text{kWh}}{\text{a}}\right]$	Energy demand tot $\left[\frac{\text{kWh}}{\text{a}}\right]$	Number of yearly On/Off $\left[\frac{\text{n}}{\text{a}}\right]$	$SCOP_{HP}$ $[-]$	$SCOP_{\text{SYS}}$ $[-]$
5	351.44	96.30	1098.41	933.76	5328	3.13	2.67
15	348.07	95.27	1121.90	929.35	3345	3.22	2.75
30	344.32	94.46	1140.91	924.80	2138	3.31	2.82
60	344.53	93.88	1156.98	924.43	1213	3.36	2.85
90	342.83	93.53	1165.94	922.37	860	3.40	2.89
120	342.89	93.39	1171.86	922.30	670	3.42	2.90

Table 4-6: Over and under heating comparison for January and February (1416 [h])

Min. runtime	Under heating		Over heating		Min temp	Max temp
	[h]	[%]	[h]	[%]	[°C]	[°C]
5	11.87	0.838	0	0	19.88	20.07
15	11.27	0.796	5.90	0.417	19.88	20.14
30	10.53	0.744	25.37	1.79	19.88	20.17
60	11.00	0.780	49.00	3.46	19.88	20.18
90	10.87	0.767	59.00	4.17	19.88	20.20
120	10.70	0.756	64.07	4.53	19.88	20.21

In the case of high minimum runtime, the heating system is kept switched on even if the controller output would give signal to switch it off because the controlled temperature reached or passed the set point temperature this causes the over-heating periods. At the end of the minimum runtime period, the error is negative because the controlled temperature is higher than the set point temperature and the output of the controller reached the lower limits of the saturation block. When the minimum runtime period finishes, the heat pump is immediately switched off. The system with the minimum runtime of five minutes is able to keep the controlled temperature always next to the set point temperature because the system is free to react in a fast way to error changes.

4.4 DETERMINATION AND OPTIMIZATION OF THE HEAT PUMP PARAMETERS

The same method already explained is now used for the determination of the heat pump parameter. Figure 4-22 shows the system studied in this chapter. The goal is the determination of the highlighted PI controller parameter. The heating system (encircled part of Figure 4-24) is studied in an open loop configuration with the set point frequency as input, and as output the supply air temperature. The dynamic behaviour of the open loop system is studied, in order to define the parameter with the Chien, Hrones and Reswick formulation. The input is a step of the frequency from 49 Hz to 90 Hz and the output is the supply air temperature. From the dynamic characterization of the system output, it is possible to use the Chien, Hrones and Reswick for the parameter determination.

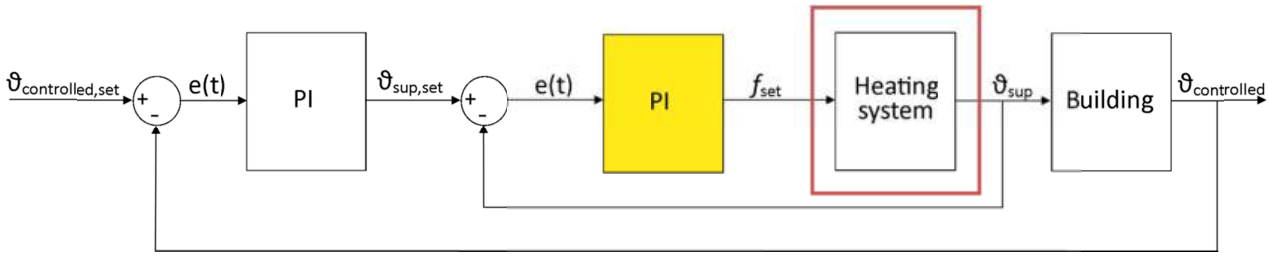

Figure 4-22: Studied system

Figure 4-23 and Figure 4-24 show the step of the heat pump supply air temperature with the step of the frequency from 49 Hz to 90 Hz as input. On the right side the zoom of the first step part is reported. The first green dotted line represents the moment in which the frequency is changed, the second green dotted line represents the moment in which the supply air temperature starts to increase and the last green dotted line represents the moment in which the tangent line reaches the maximum supply temperature value. From these times the system time constants can be calculated.

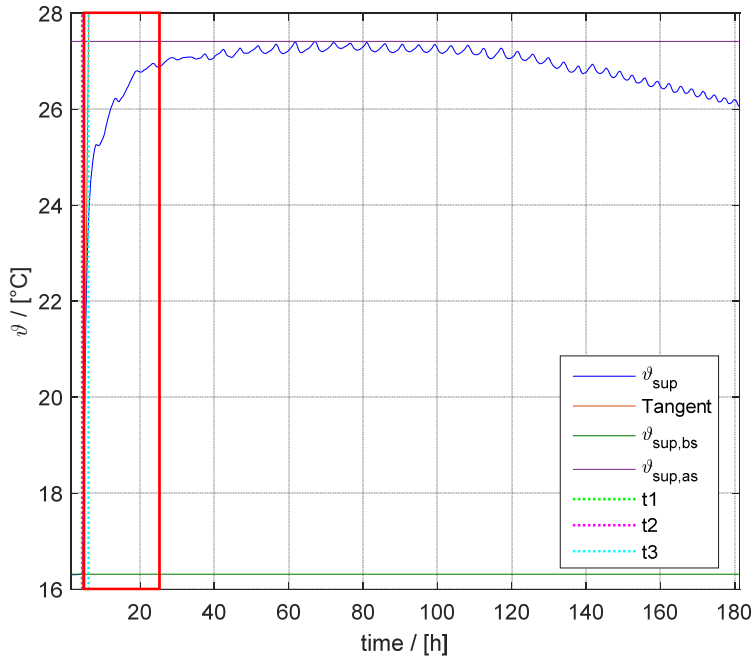

Figure 4-23: Heat pump dynamic behaviour

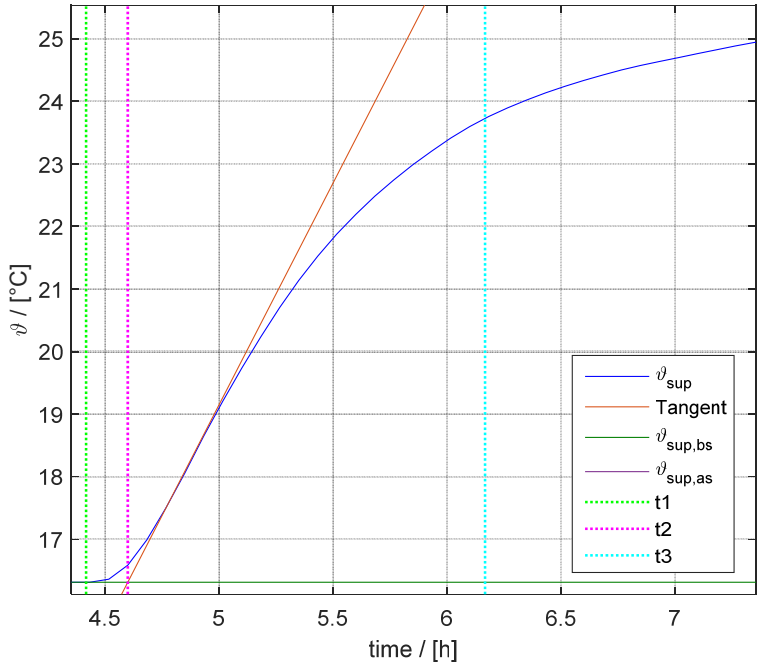

Figure 4-24: Zoom of the previous figure

The data of the problem are:

$$\vartheta_{sup,f} = 27.4\ [°C] \qquad \tau_u = 11.0\ [s]$$
$$\vartheta_{sup,i} = 16.3\ [°C] \qquad \tau_g = 94.0\ [s]$$
$$f_i = 49\ [Hz] \qquad f_{min} = 49\ [Hz]$$
$$f_f = 90\ [Hz] \qquad f_{max} = 150\ [Hz]$$

Where:

- $\vartheta_{sup,f}$ is the supply air temperature at the steady state after the step;
- $\vartheta_{sup,i}$ is the supply air temperature at the steady state before the step;
- f_i is the system frequency before the step;
- f_f is the system frequency after the step;
- $\tau_{u,}\ \tau_g$ are the delays. $\tau_u = t_2 - t_1$ is called dead time and it is the time interval between the moment in which the disturbance is introduced and the moment in which the system starts to respond. $\tau_g = t_3 - t_2$ is the time for the response to occur.
- f_{min} is the system minimum frequency;
- f_{max} is the system maximum frequency.

The parameters resulting from the formulation (4.18) are:

$$K_p = 0.188\ \left[\frac{K}{K}\right] \qquad T_n = 0.733\ [min]$$

Different PI parameters are considered in order to optimize the control:

- Case 1: $K_p = 0.188\ \left[\frac{K}{K}\right] \qquad T_n = 0.733\ [min]$;
- Case 2: $K_p = 0.054\ \left[\frac{K}{K}\right] \qquad T_n = 0.09\ [min]$;
- Case 3: $K_p = 0.733\ \left[\frac{K}{K}\right] \qquad T_n = 0.188\ [min]$;

Figure 4-25 shows the comparison between the different cases. The two subplots show the frequency and the controlled temperature error.

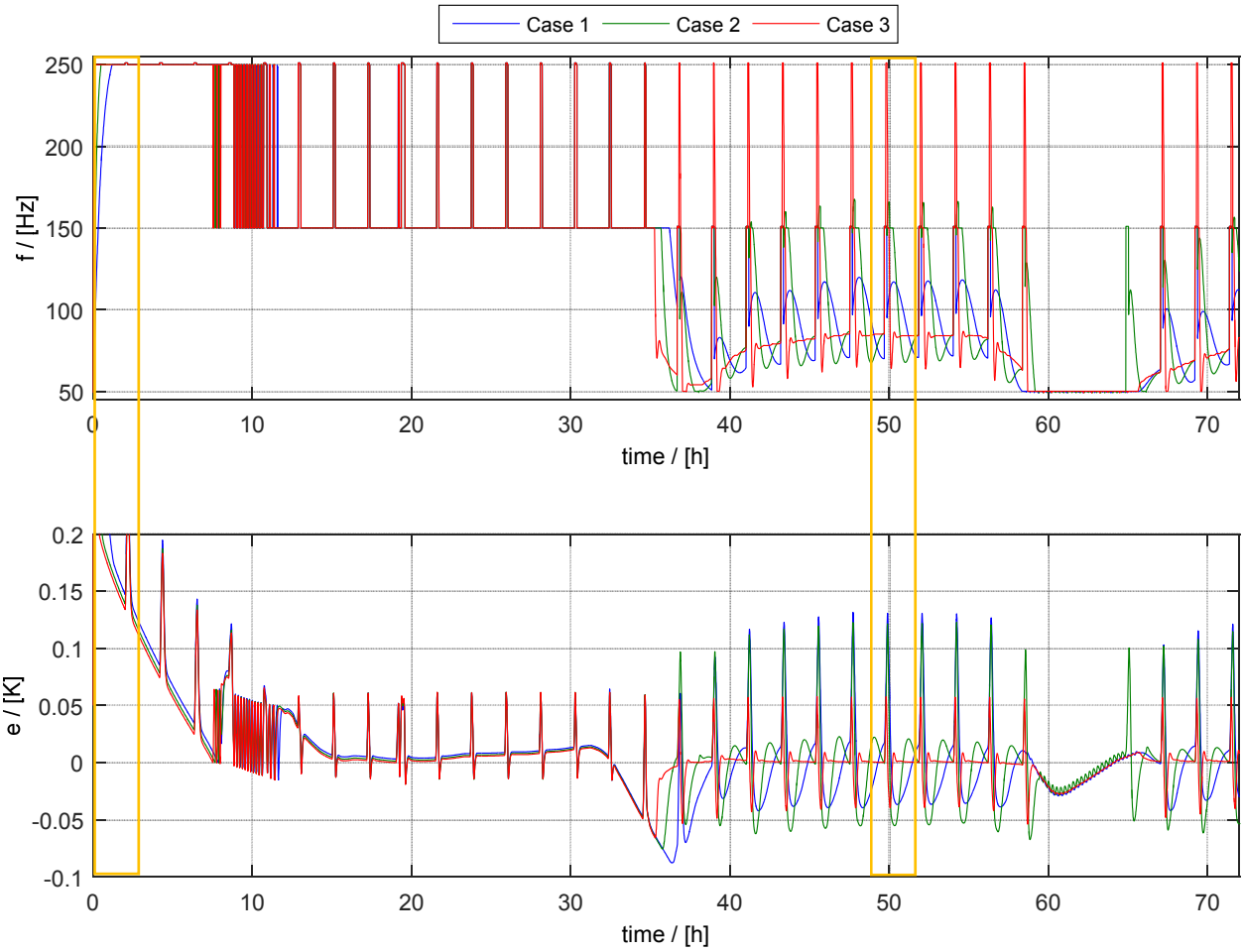

Figure 4-25: Comparison between the behaviour of different PI parameters

Two zooms are reported in order to highlight two important aspects: the delay with which the system reaches the maximum frequency (Figure 4-26) and the use of the backup heater after or while the de-icing period (Figure 4-27).

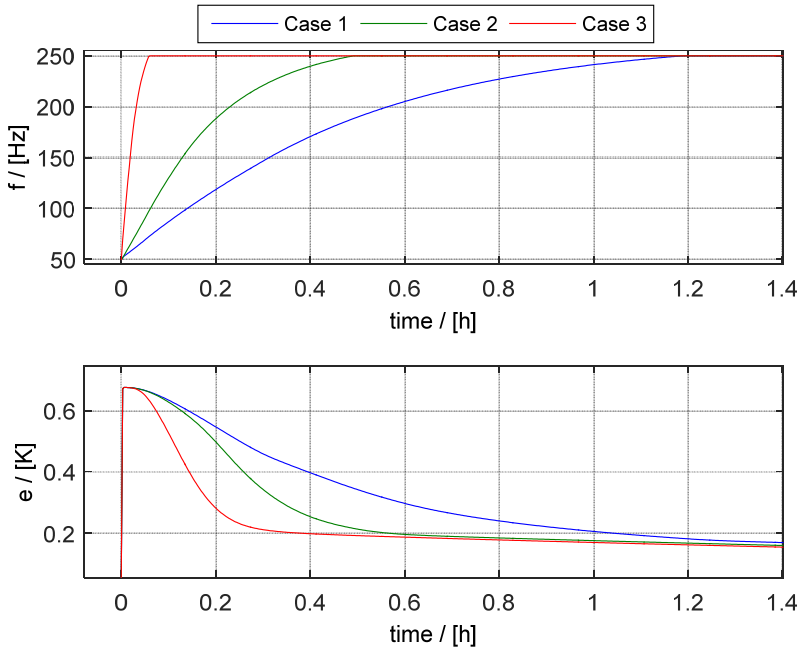

Figure 4-26: Zoom of Figure 4-25 (from 0 to 1.4 hours)

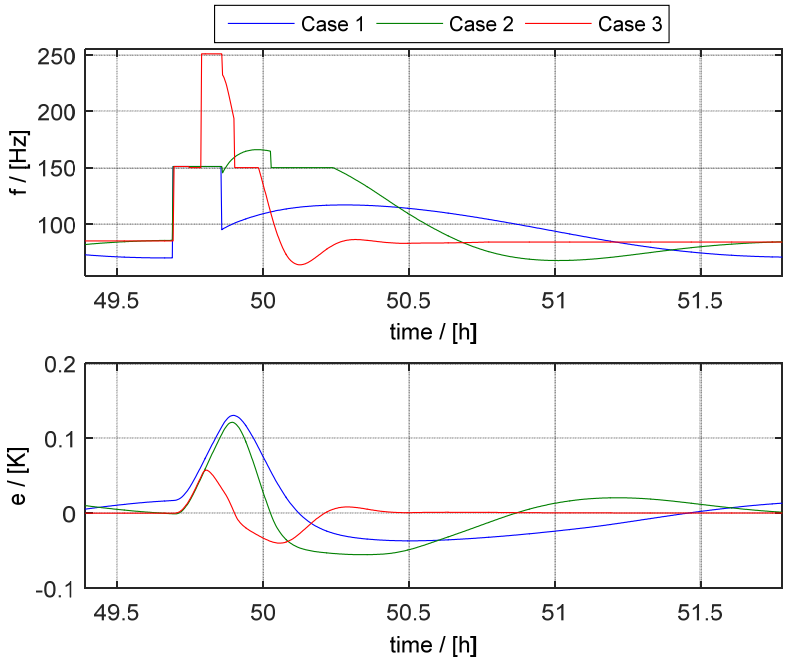

Figure 4-27: Zoom of Figure 4-25 (from 49.4 to 51.7 hours)

Figure 4-28 shows the energy demand of the heat pump and of the backup heater over the three considered days. The total energy demands are listed in Table 4-7.

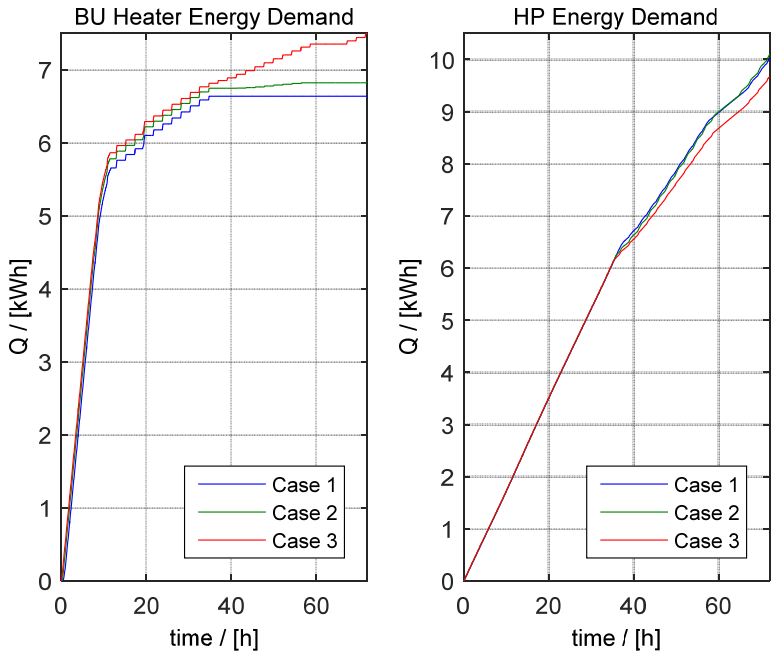

Figure 4-28: Comparison between the energy demands of the backup heater and heat pump

Table 4-7: Total energy demand

Cases	Energy demand tot [kWh]
1	16.67
2	16.93
3	17.17

By considering the energy demand and the speed of the response, the optimal PI parameters are determined.

Case 3 has the highest reaction speed, but it has also the highest energy demand. Case 1 is the slowest responding system but it has also the lowest energy demand. Within the cases 1 and 2 the backup heater is used less than in cases 3.

Case 2 represents a good compromise between energy demand and reaction speed, but if the system has to react fast to rapid air temperature variation (e.g. windows opening) the parameter of the case 3 should be taken.

4.5 COMPARISON OF DIFFERENT CONTROLLER TYPES

4.5.1 1D vs. 2D Lookup Table

The input of the lookup table is the set point for the supply air temperature and its output is the system frequency. The lookup table uses the measured system working points in order to find the correct system frequency in function of the supply air temperature fixed by the PI controller. The description of the lookup table determination is given in chapter 4.2.

Since the lookup table used in the controller does not contain information about all the working points an error is introduced. The lookup table implemented in the hardware controller contains measured data for $\vartheta_{amb,0} = 0\,°C$. When $\vartheta_{amb,0}$ is not $0\,°C$, an error is introduced because the performance of the system changes with the boundary conditions. Figure 4-29 shows in the x-axis the supply air temperature of set point and in the y-axis the set point frequency. The line for $\vartheta_{amb,0} = 0\,°C$ represents the behaviour of the lookup table implemented in the controller. The other lines represent the controller behaviour in case of two-dimensional lookup table where the inputs are the ambient temperature and the set point for the temperature of the supply air and the output is the set point frequency. By considering a $\vartheta_{sup,set}$ equal to $30\,°C$, with the lookup table for $\vartheta_{amb,0} = 0\,°C$ the set point frequency would be 125.7 Hz for every ambient temperature. Actually, the set point frequency with the fixed $\vartheta_{sup,set}$ should change with the ambient temperature from 91.3 Hz for $\vartheta_{amb,0} = 5\,°C$ to 159,0 Hz for $\vartheta_{amb,0} = -4\,°C$. This difference is balanced by a growing error for lower ambient temperature and decreasing error for higher ambient temperature.

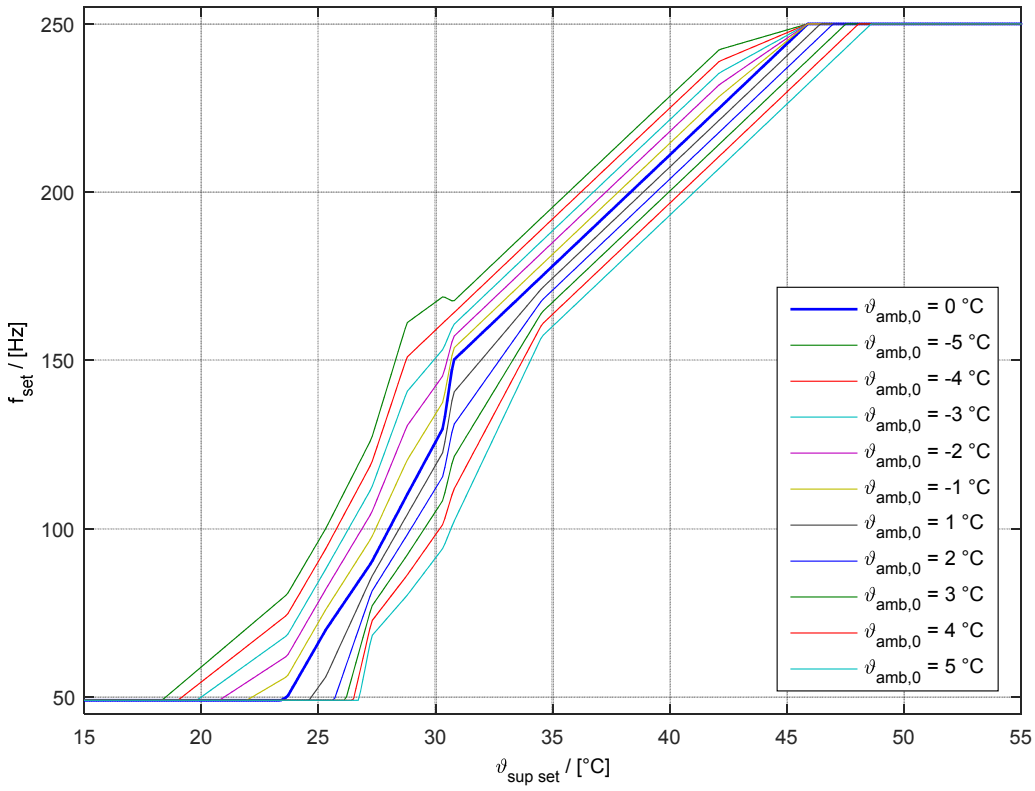

Figure 4-29: Controller's lookup table comparison

The differences between a controller with 1D and 2D lookup table can be better explained by means of Simulink simulations. The boundary conditions are described in chapter 5.4. In one simulation, a two-dimensional lookup table is used while in the other one, a one-dimensional lookup table is used.

Figure 4-30 shows the Simulink results:

- the first subplot shows the supply air temperature $\vartheta_{sup,2}$;
- the second subplot shows the difference between the sensitive temperature of the zone 5 (hallway) and the set point temperature (20 °C);
- the third subplot shows the system frequency;
- the last subplot shows the ambient temperature.

The differences between the two control systems are insignificant.

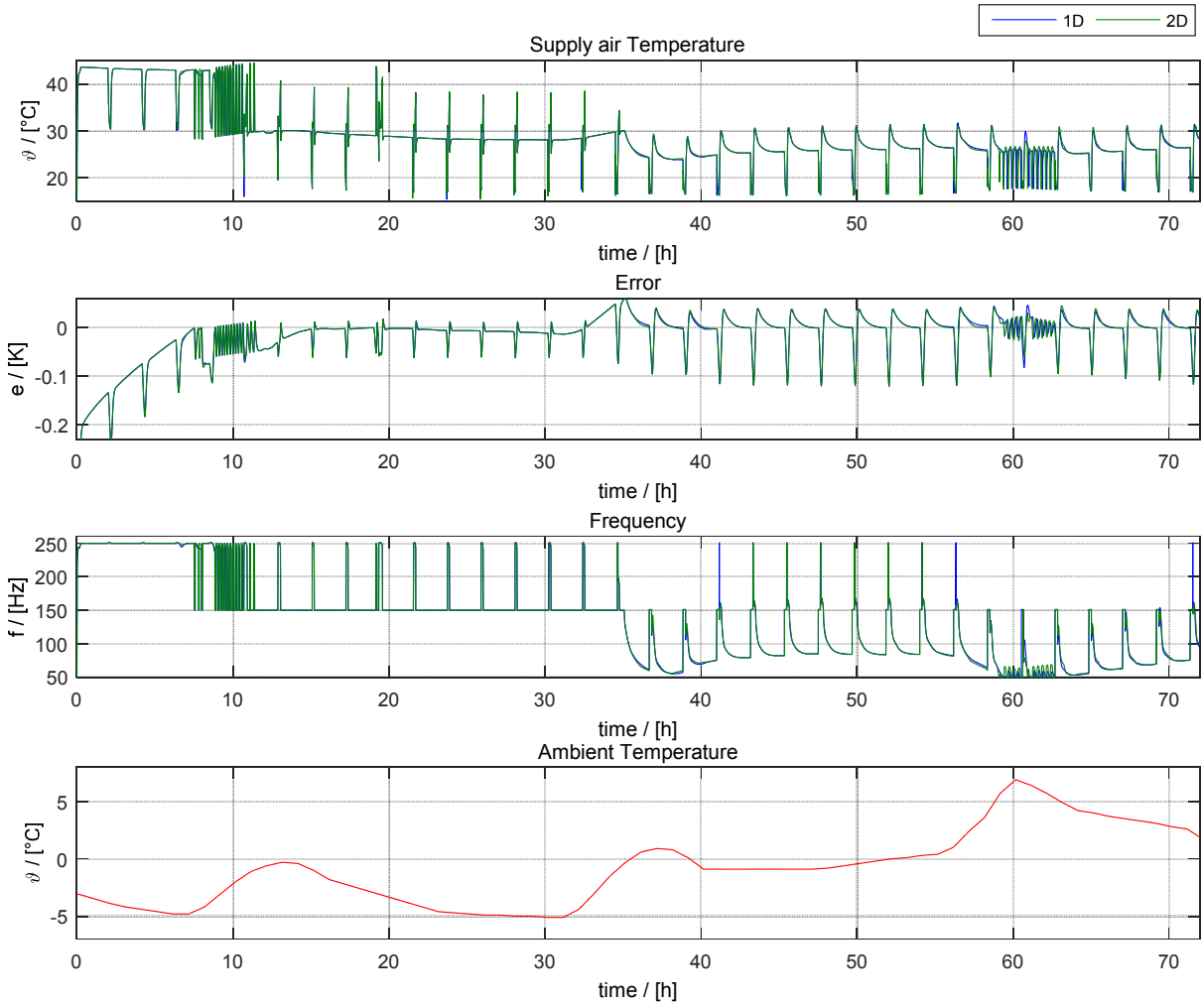

Figure 4-30: Comparison of controllers with one and two dimensional lookup table

Figure 4-31 is a zoom of the previous figure. $\vartheta_{amb,0}$ is below 0 °C in the period around the hour 7, so the two dimensional lookup table delivers higher set point frequency and higher $\vartheta_{sup,2}$ than the one dimensional lookup table. Therefore, in the 1D case the error is higher and the response slower than in the 2D case. The opposite happens when the ambient temperature is higher than 8 C. In the case of Figure 4-31, the 1D case reaches a null error 11.7 min after the 2D case, so it can be calculated that the difference in this application is acceptable.

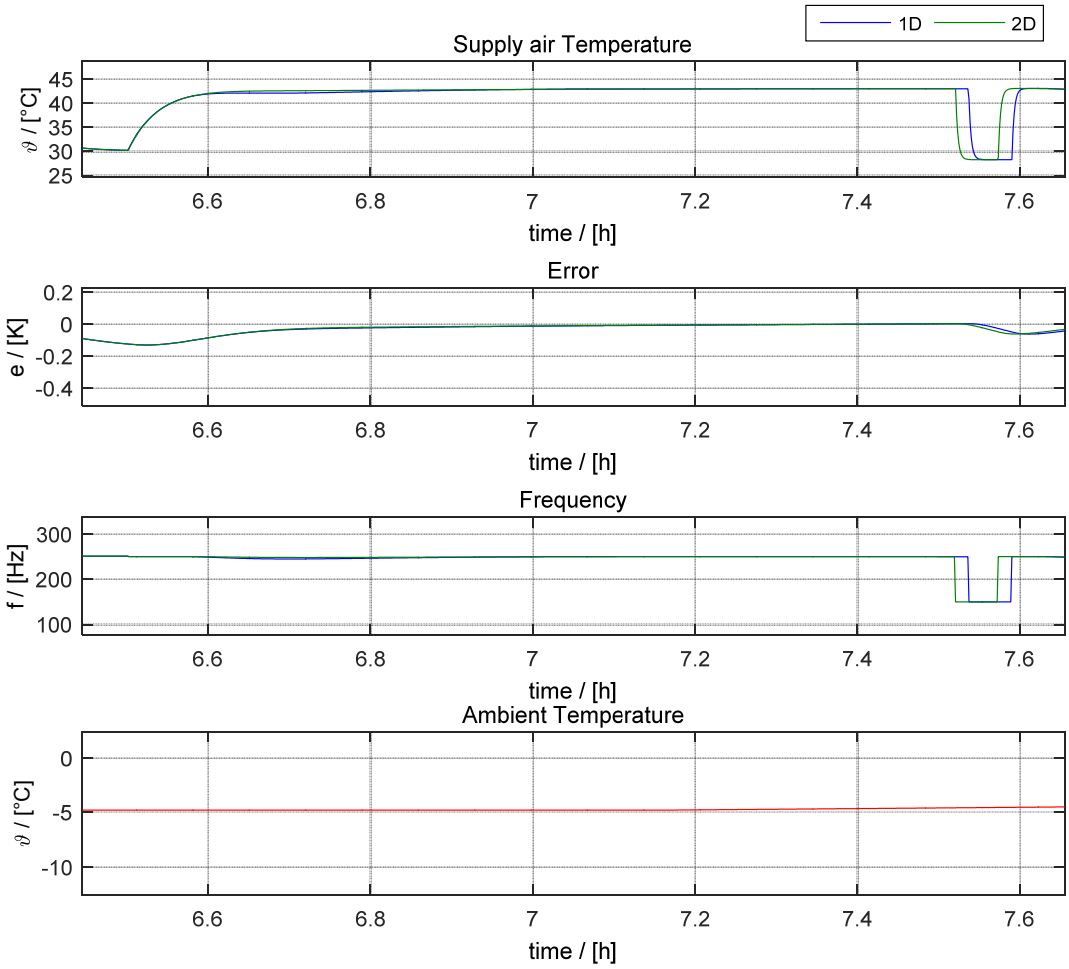

Figure 4-31: Zoom of Figure 4-30

The results of two yearly simulations with the one-dimensional and two-dimensional lookup tables (1D LuT and 2D LuT) are presented in Table 4-8 and Table 4-9. Here the yearly energy demands, the number of On/Off cycles the $SCOP_{HP}$ and $SCOP_{SYS}$ are reported in order to analyse the differences between the usage of the one and two dimensional lookup tables. It can be seen that the main reported parameters are mostly the same. The controller with the two-dimensional lookup tables has a slightly higher number of On/Off cycles with respect to the one-dimensional lookup tables because the 2D LuT reacts slightly faster than the 1D LuT.

Table 4-8: Energy demands, $SCOP_{HP}$ and $SCOP_{SYS}$

	HP energy demand $\left[\frac{\text{kWh}}{\text{a}}\right]$	BU energy demand $\left[\frac{\text{kWh}}{\text{a}}\right]$	HP thermal energy $\left[\frac{\text{kWh}}{\text{a}}\right]$	Energy demand tot $\left[\frac{\text{kWh}}{\text{a}}\right]$	$SCOP_{HP}$ $[-]$	$SCOP_{SYS}$ $[-]$	Number of yearly On/Off $\left[\frac{n}{a}\right]$
LuT 1D	348.07	95.27	1121.90	929.35	3.22	2.75	3345
LuT 2D	345.22	95.45	1099.40	926.69	3.18	2.71	2859

Table 4-9 shows the number of underheating and overheating hours and the maximum and minimum temperatures reached by the controlled temperature in the considered period (January and February).

Table 4-9: Over and under heating comparison for January and February (1416 [h])

	Under heating		Over heating		Min temp	Max temp
	[h]	[%]	[h]	[%]	[°C]	[°C]
LuT 1D	11.27	0.796	5.90	0.417	19.88	20.14
LuT 2D	11.8667	0.83804	0.2	0.014124	19.8776	20.1096

From these results, it is possible to conclude that in the considered case, a two dimensional lookup table and a one dimensional lookup table controller have almost the same performances.

4.5.2 Analysis of the Controller Lookup Table Accuracy

A test is carried out in order to understand how the results change with the accuracy of the controller lookup table. Table 4-10 shows the points of the one-dimensional and two-dimensional lookup table for the most accurate considered case.

Table 4-10: Case 1

		1D	2D		
		$\vartheta_{amb,0}$ / [°C]	$\vartheta_{amb,0}$ / [°C]		
		0	-4	0	5
$\vartheta_{sup,set}$	10.0	49.0	0	0.0	0.0
	23. 7	50.0	74.4	50.0	0.0
	25.3	70.0	94.1	70.0	0.0
	27.3	90.0	119.4	90.0	68.1
	28.8	110.0	150.9	110.0	80.1
	30.3	130.0	161.2	130.0	94.3
	30.8	150.0	164.0	150.0	101.7
	34.5	175.0	189.0	175.0	157.1
	38.3	200.0	214.0	200.0	182.1
	42.1	225.0	239.0	225.0	207.1
	45,9	250.0	250.0	250.0	232.1

Table 4-11 shows the second analysed case where four points are considered.

Table 4-11: Case 2

		1D	2D		
		$\vartheta_{amb,0}$ / [°C]	$\vartheta_{amb,0}$ / [°C]		
		0	-4	0	5
$\vartheta_{sup,set}$	10.0	49.0	0	0.0	0.0
	23. 7	50.0	74.4	50.0	0.0
	28.8	110.0	150.9	110.0	80.1
	34.5	175.0	189.0	175.0	157.1
	45,9	250.0	250.0	250.0	232.1

Table 4-12 shows the third considered case. Here, only three measured points are considered.

Table 4-12: Case 3

		1D	2D		
		$\vartheta_{amb,0}$ / [°C]	$\vartheta_{amb,0}$ / [°C]		
		0	-4	0	5
$\vartheta_{sup,set}$	10.0	49.0	0	0.0	0.0
	23. 7	50.0	74.4	50.0	0.0
	30.3	130.0	161.2	130.0	94.3
	45,9	250.0	250.0	250.0	232.1

Table 4-13 shows the fourth considered case in which only the first and the last working points are considered.

Table 4-13: Case 4

		1D	2D		
		$\vartheta_{amb,0}$ / [°C]	$\vartheta_{amb,0}$ / [°C]		
		0	-4	0	5
$\vartheta_{sup,set}$	10.0	49.0	0	0.0	0.0
	23. 7	50.0	74.4	50.0	0.0
	45,9	250.0	250.0	250.0	232.1

Figure 4-32 shows the data involved in the two-dimensional lookup table for $\vartheta_{\mathrm{amb},0} = -4°\mathrm{C}$ in each considered case.

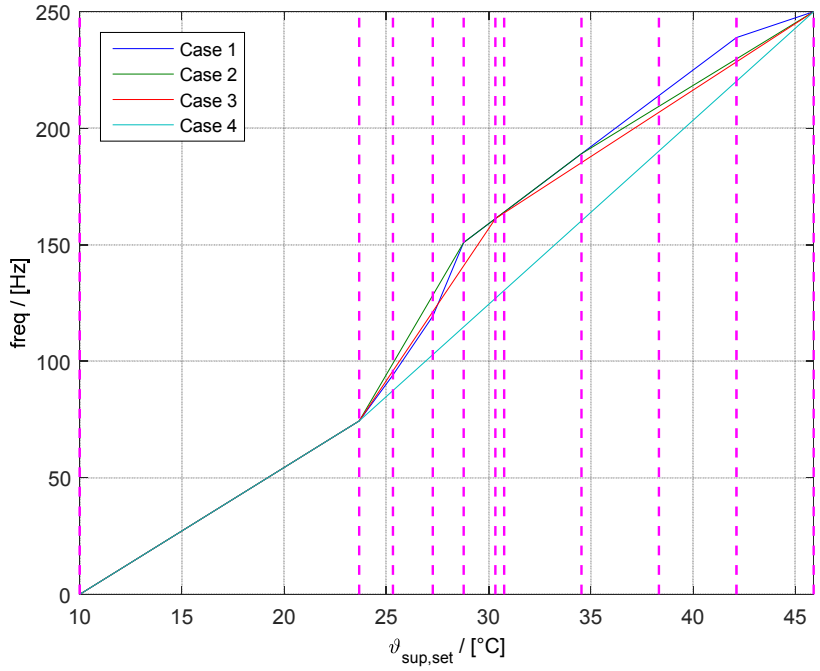

Figure 4-32: Data of the lookup tables for $\vartheta_{amb,0} = -4°C$

Figure 4-33 shows the data involved in the two-dimensional lookup table for $\vartheta_{\mathrm{amb},0} = -0°\mathrm{C}$ and in the one-dimensional lookup table, in each considered case.

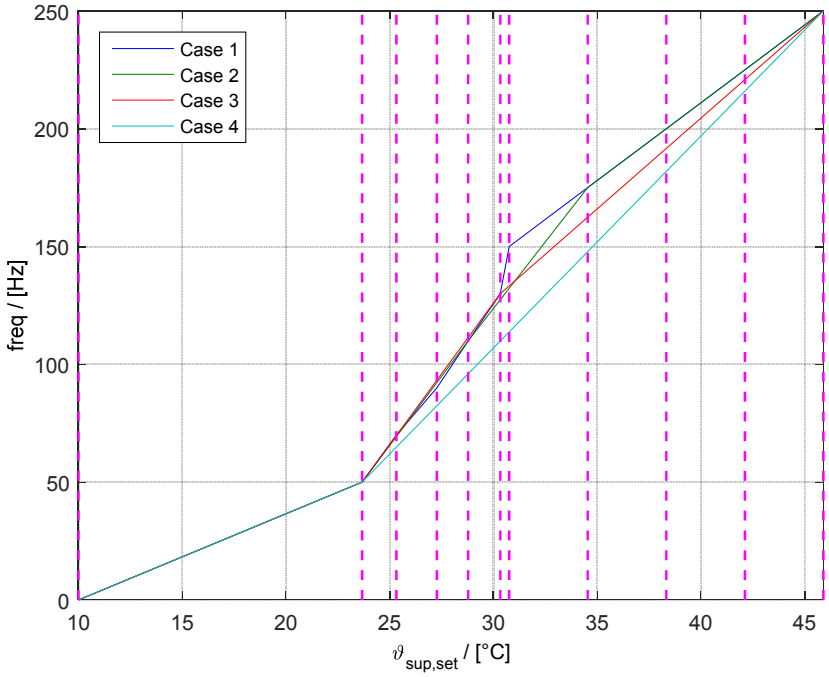

Figure 4-33: Data of the lookup tables for $\vartheta_{amb,0} = 0°C$

Figure 4-34 shows the data involved in the two-dimensional lookup table for $\vartheta_{\mathrm{amb},0} = 5°\mathrm{C}$.

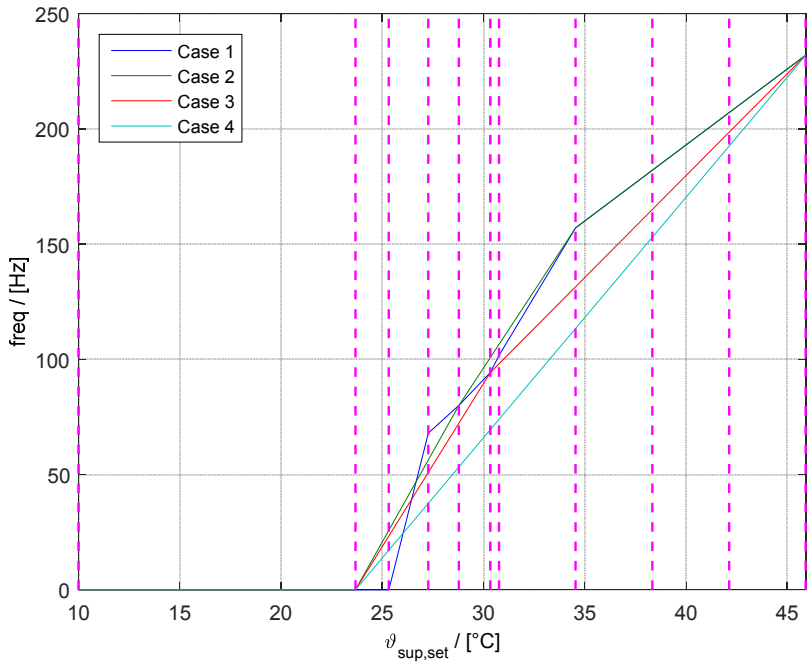

Figure 4-34: Data of the lookup tables for $\vartheta_{amb,0} = 5°C$

Figure 4-35 shows the comparison between the different cases with the one dimensional lookup table. The selected time interval shows the de-icing period that determines an error increment and the consequent system reaction. The results for the two dimensional lookup table are not shown because they are similar to the results already reported in Figure 4-35. It is possible to notice that the case 1 is slightly faster than the other cases. The case 1 rapidly decreases its frequency at the hour 44.65. This behaviour is due to the non-linear measured data between the set point supply temperature of 30.3 °C and 30.8 °C.

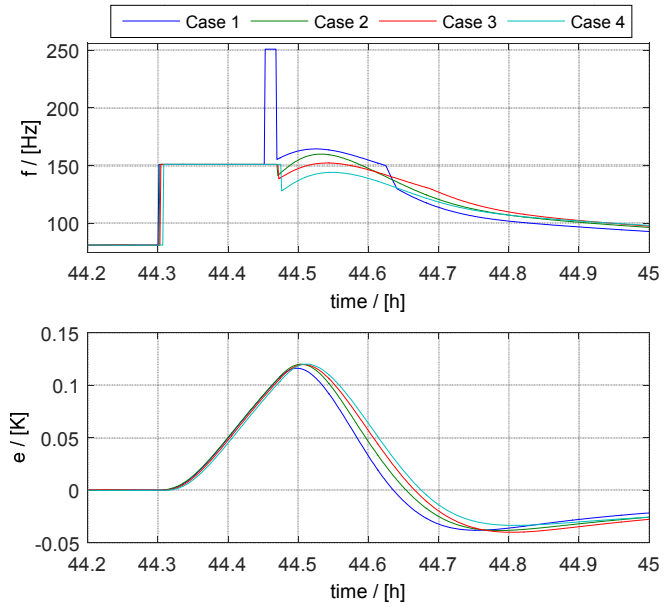

Figure 4-35: Comparison between the different cases which one dimensional lookup table

With these results, it is possible to conclude that the controller can properly works with a lookup table that involve only few working points.

4.5.3 PI-PI Controller vs. PI-Lookup Table

In this section the comparison between the concept 1 (chapter 3.3.2) and 2 (chapter 3.3.3) of the controller is analysed.

Figure 4-36 shows the comparison between the three kind of analysed controllers:

- PI-1D lookup table;
- PI-2D lookup table;
- PI-PI controller.

The system frequency and the error have the same trend with the 1D and 2D lookup tables. The system with the PI-PI controller uses more backup than the controller with the lookup table in order to correct the temperature error, but the PI-PI controller takes the error closer to zero than the controller with the lookup table.

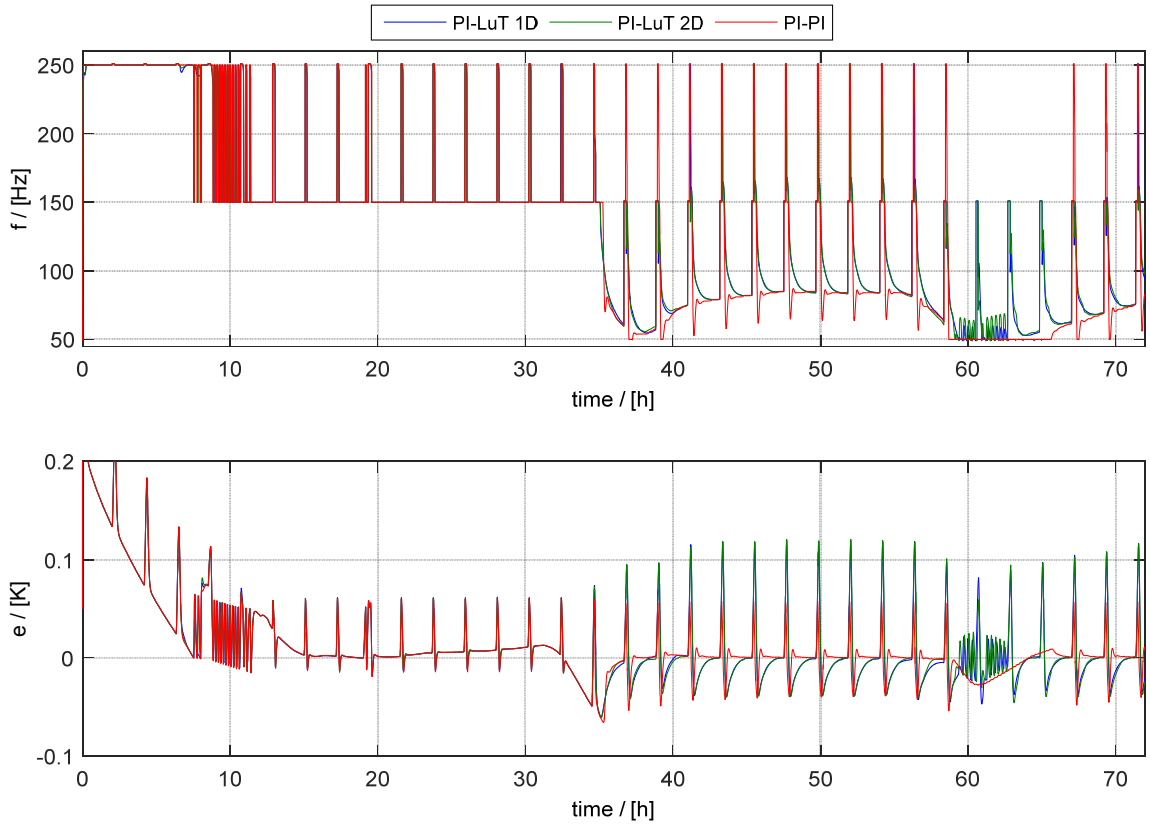

Figure 4-36: Comparison between the three different kinds of controllers

Figure 4-37 shows the zooms of the first part of the simulation and Figure 4-38 shows the zoom over the de-icing period. It can be seen that the PI-PI controller and the PI-LuT controller decrease the error with almost the same speed. From Figure 4-38 can be observed that the PI-PI controller is able to keep the error closer to zero with respect to the PI-LuT controller by reducing the over and under heating periods. The PI-PI controller leads to use more backup heater than the PI-LuT controller.

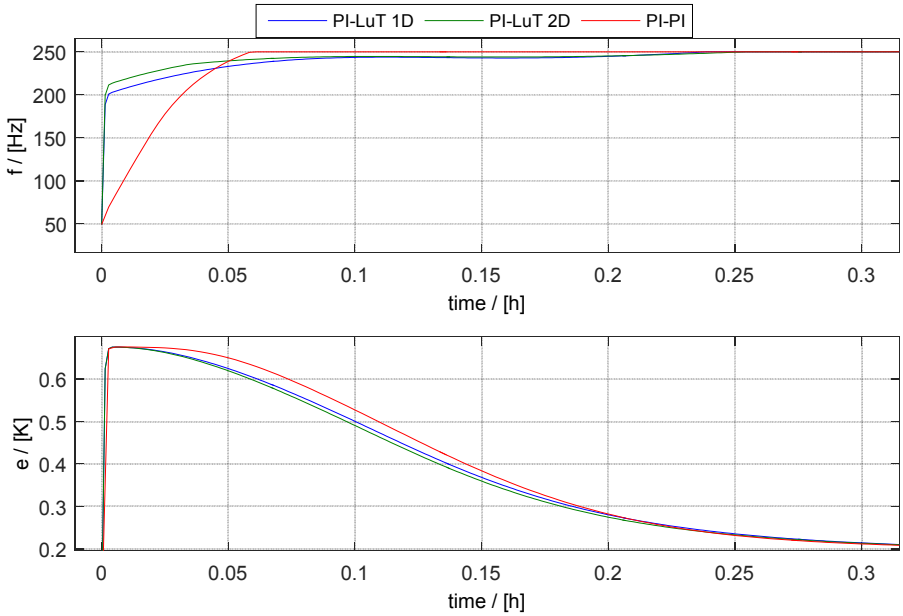

Figure 4-37: Zoom of the Figure 4-36

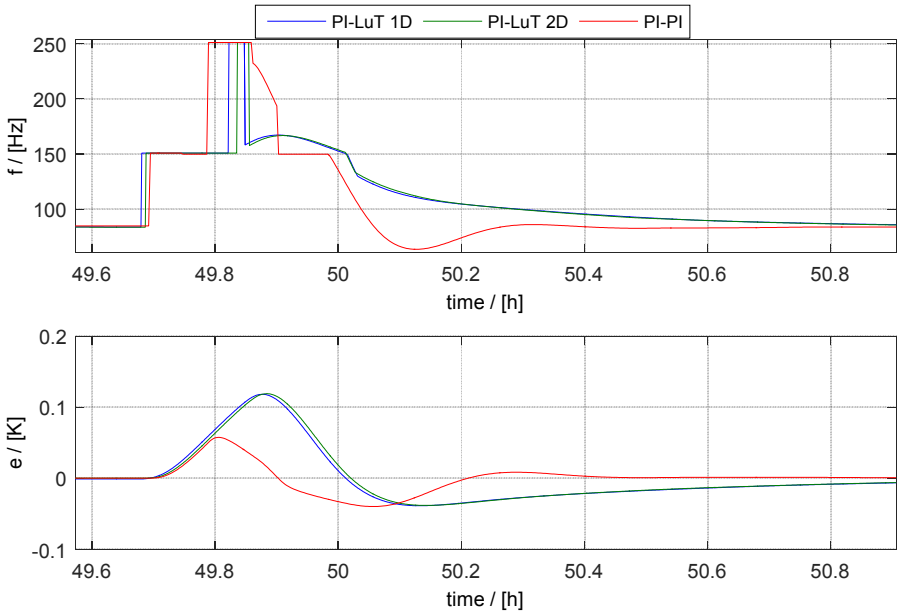

Figure 4-38: Zoom of the Figure 4-36

Figure 4-39 shows the comparison of the backup heater and of the heat pump energy demands for the three cases. The backup heater energy demand is higher for the PI-PI controller but it features lower HP energy demand.

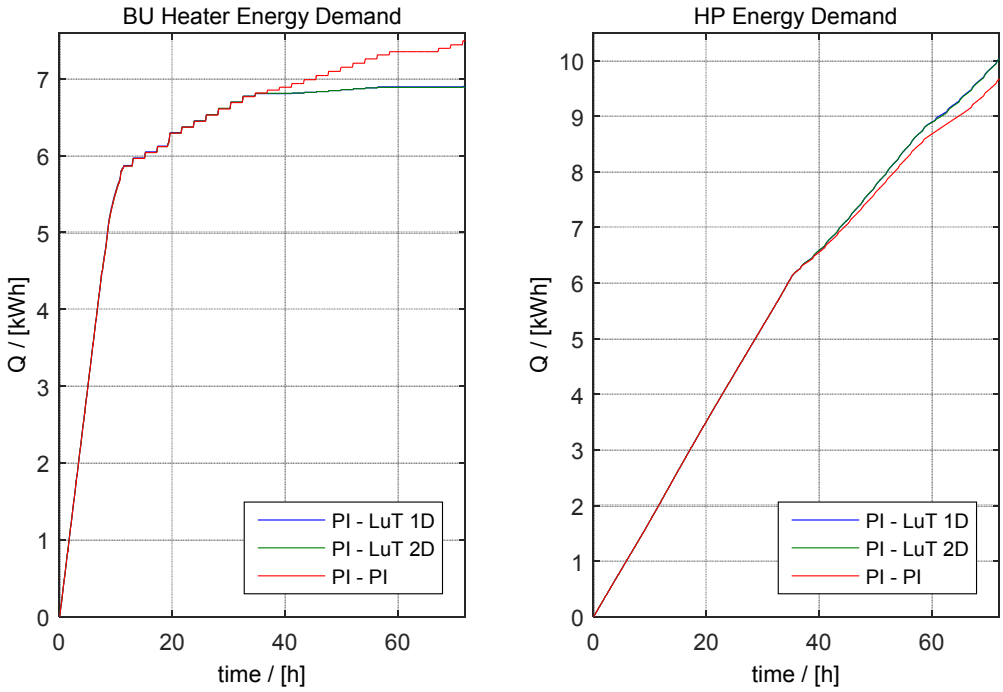

Figure 4-39: Comparison of the BU heater energy demand and of the HP energy demand for the three considered cases.

Table 4-14 shows the comparison between the total energy demand for the three considered cases. As it can be seen the PI-PI controller has slightly higher energy demand compared to the PI-LuT controller.

Table 4-14: Total energy demand of the three cases over the considered period

	Energy demand tot [kWh]
PI-LuT 1D	16.95
PI-LuT 2D	16.93
PI-PI	17.17

The PI-PI controller enables the system to ensure a smaller error with respect to the cases with the LuT but it requires a second temperature sensor and leads to higher energy demand. The controller PI-LuT is easier to implement with respect to the PI-PI controller because it requires only one sensor while the PI-PI controller needs two sensors (one for the controlled temperature and one for the supply air temperature). The feasibility of a PI-PI controller should be tested in a real system where the noise of the signals can create problem in the control. From these results, it is possible to conclude that the controller PI-LuT ensures a good quality control and it is simpler to implement compared to the PI-PI controller.

5 HiL HARDWARE IN THE LOOP SIMULATION

5.1 INTRODUCTION

Within this work HiL Hardware in the Loop simulations are used in order to test the m-HP. The HiL simulation involves the PASSYS test cell, the heat pump and the Simulink building model. Thus, HiL simulation provides a virtual building for the heat pump controller validation and verification. During the HiL simulation, the extract and supply air behaviour are reproduced in the hardware (PASSYS test cell) and their behaviours are controlled by means of Simulink simulation, where the building model is implemented. With an appropriate building model, the dynamic of the studied building can be reproduced inside the PASSYS test cell, so the heat pump can be tested as it works in a real building (SaLüH!, 2016). The data exchange between the PASSYS test cell and the Simulink model is done with a co-simulation. In the co-simulation more than two simulators are coupled to exchange data. In this specific case, the actors are Simulink and the PASSYS test cell. BCVTB (Building Control Virtual Test Bed) is the software environment used in order to conduct the HiL (Wetter, 2010). It synchronizes the exchanged data and allows the user to follow the system evolutions by means of a graphic interface. For the HiL simulations, a discrete solver is used within this work. This is necessary for the data exchange between the different actors that happens every fixed time step.

5.2 PASSYS TEST CELL

Figure 5-1 shows the sketch of the PASSYS (Passive Solar Systems and Component Testing) test cells with which the m-HP is tested. The PASSYS test cell has three rooms:

- the service room is used in order to access to the test room. The temperature of the service room is controlled in order to avoid temperature fluctuation in the test room when the door is opened.
- the test room, where the conditions of the extract air of the simulated building are reproduced;
- the coldbox, where the conditions of the ambient air are reproduced.

The mechanical ventilation system with heat recovery and heat pump is integrated inside the test façade.

The measurement system is described in (Siegele, 2015). A high power heater and cooler allow to control the test room temperature. Humidifier devices in the test room enable to control the vapour content. The cold box air temperature can be controlled by means of a second heating and cooling system. Therefore, the temperature and humidity conditions of the extract air and the temperature of the ambient air can be reproduced inside the test room and

coldbox in order to simulate the boundary conditions with which the test façade has to be tested.

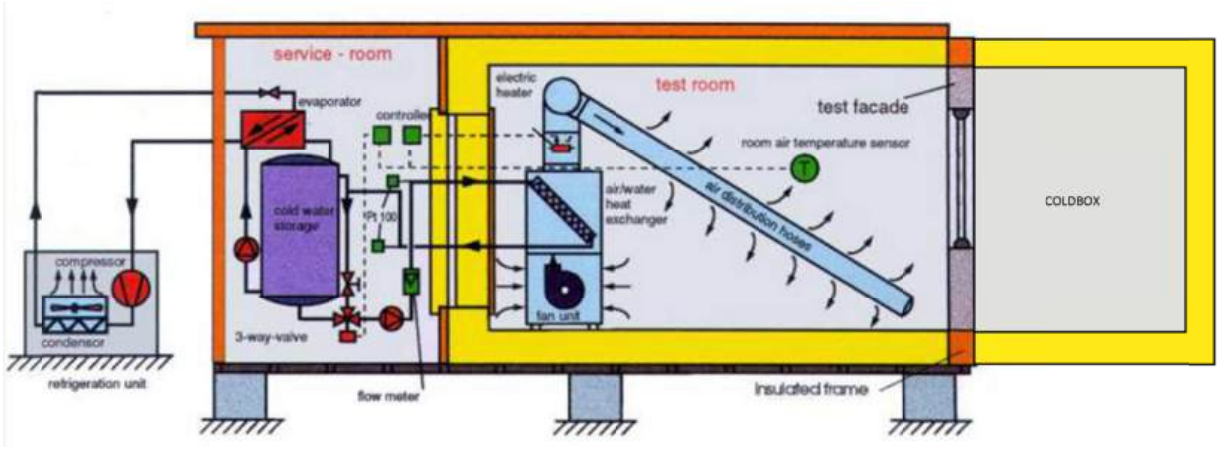

Figure 5-1: PASSYS test cell sketch according to (Commisssion of the European Communities, 1990), modified

5.3 DESCRIPTION OF THE SCENARIOS

5.3.1 Scenario 1

Figure 5-2 shows the data exchange between the actors. In this scenario, the measured $\vartheta_{sup,1}$ and the system frequency are taken from the PASSYS test cell and sent to Simulink. These measured values are used in the simulation and $\vartheta_{sup,2}$ is calculated with equation (5.1). Simultaneously, $\vartheta_{amb,0}$, $\vartheta_{ext,0}$ and $\vartheta_{Zone\ 5}$ (sensitive temperature of the zone 5 which corresponds to the hallway temperature) are taken from Simulink and sent to the PASSYS test cell. Inside the PASSYS test cell, the test room temperature is kept at $\vartheta_{ext,0}$ and the coldbox temperature is kept at $\vartheta_{amb,0}$. The hardware controller of the heat pump receives the sensitive temperature of zone 5 ($\vartheta_{Zone\ 5}$) and it controls the heat pump power based on the difference between the controlled temperature and the set point temperature.

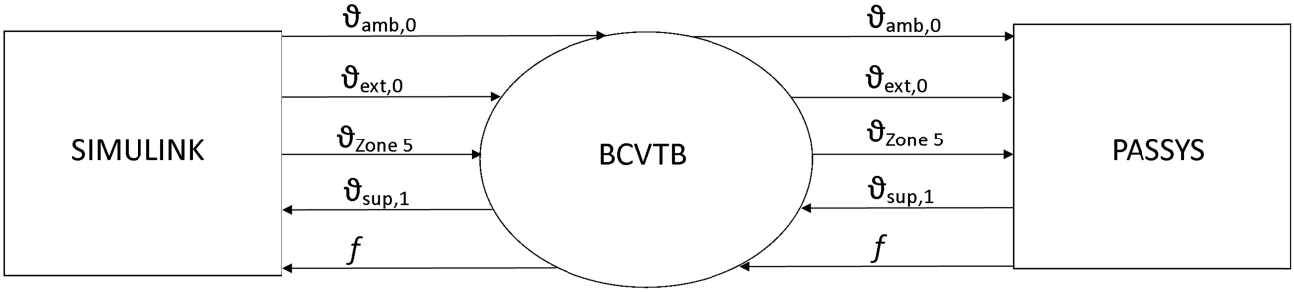

Figure 5-2: Data exchange sketch

$\vartheta_{sup,2}$ is calculated in Simulink by means of the equation (5.1).

$$\vartheta_{sup,2} = \vartheta_{sup,1} + \frac{f}{100} \cdot P_{max,BU} \cdot C \qquad (5.1)$$

Where:

- $\vartheta_{sup,1}$ is measured in the test façade and used in Simulink $[°C]$;
- f is the system frequency set by the m-HP hardware controller and then reduced in order to match only the backup heater range $[Hz]$;
- $P_{max,BU}$ is the maximum power of the backup heater 600 W;
- $C = \frac{1}{\dot{V} \cdot \rho \cdot c_p} = 0.025 \left[\frac{K}{W}\right]$ is a constant where $\dot{V}$ is the air volume flow of 0.0333 $\left[\frac{m^3}{s}\right]$, ρ is the air density taken as 1.22 $\left[\frac{kg}{m^3}\right]$ and c_p is the heat capacity taken as 1000 $\left[\frac{J}{kg\,K}\right]$.

Here, a small error is introduced because a constant volume flow and constants airflow properties are considered instead of the real values. Moreover, the supply air temperature $\vartheta_{sup,1}$ is measured in the real airflow, and it is introduced in the Simulink model where the inlet airflow has different characteristics, so the power introduced in the model is different from the real heat pump power.

Within this scenario, the heat pump controller is implemented with the conditional integration anti-windup.

5.3.2 Scenario 2

The data exchange and the supply air temperature $\vartheta_{sup,2}$ calculation are as explained in the chapter 5.3.1. The difference between scenario 1 and 2 is the type of implemented anti-windup. In the scenario 1 the conditional integration anti-windup is used while here the back calculation anti-windup is implemented.

5.3.3 Scenario 3

This scenario is carried out with the same settings of the previous two scenarios but with the backup heater switched off in order to avoid the problem with the measurement of $\vartheta_{sup,1}$ explained with the Figure 5-25. The backup heater power is taken into account in the HiL simulation such power is calculated in the model by means of the frequency set by the hardware controller and by means of the measured $\vartheta_{sup,1}$.

5.3.4 Scenario 4

The real volume flow is not perfectly constant because change of pressure losses happens during the operation time (i.e. the pressure losses variation can be caused by the icing and de-icing cycles in the evaporator) and because of the temperatures variation along the ducts. Therefore, the measured volume flow $\dot{V}_{air_m}$ is involved in the Simulink model used in this

scenario in order to calculate the power provided by the heat pump to the airflow. The data exchange between the PASSYS test cell and the Simulink model is shown in Figure 5-3. The only one difference between the earlier described scenarios, is the volume flow.

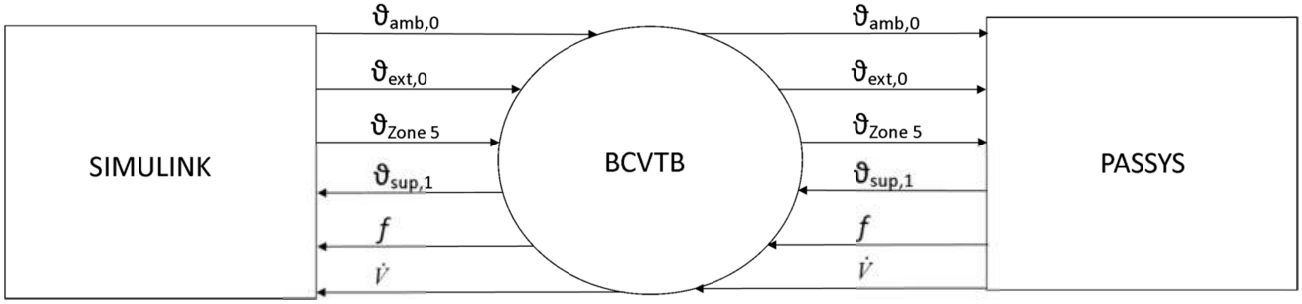

Figure 5-3: Data exchange sketch

In this scenario the inlet air density ρ_{air} and the specific heat capacity $c_{p_{air}}$ are calculated as a function of the measured supply air temperature $\vartheta_{sup,1}$, of the ambient air absolute humidity and of the ambient air pressure by means of the correspondent Carnot blocks. The heat pump power is calculated by means of the equation (5.2).

$$\dot{Q}_{HP} = \rho_{air} \cdot \dot{V}_{air_m} \cdot c_{p_{air}} \cdot \left(\vartheta_{sup,1} - \vartheta_{sup,0}\right) \tag{5.2}$$

Then, the heat pump power is added to the backup heater power calculated as it is shown in the equation (5.3).

$$\dot{Q}_{BU} = \frac{f}{100} \cdot P_{max,BU} \tag{5.3}$$

Where:

- f is the system frequency set by the hardware controller, than rescaled in order to consider only the backup heater range [Hz];
- $P_{max,BU}$ is the maximum power of the back up heater [W].

The Simulink model uses a fixed inlet air volume flow of 120 $\left[\frac{\mathrm{m}^3}{\mathrm{h}}\right]$ for the inlet air, so the heating system power is converted in supply air temperature by using a volume flow of 120 $\left[\frac{\mathrm{m}^3}{\mathrm{h}}\right]$ by means of the equation (5.4).

$$\vartheta_{sup,2} = \frac{\dot{Q}_{BU} + \dot{Q}_{\mu HP}}{\rho_{air} \cdot c_{p_{air}} \cdot \dot{V}_{air_c}} + \vartheta_{ext,0} \tag{5.4}$$

Where: ρ_{air}, $c_{p_{air}}$ and $\vartheta_{ext,0}$ are the same involved in the equation (5.2) while $\dot{V}_{air_c}$ is a constant value. In this scenario, the power delivered by the heating system in the PASSYS test cell is exactly the same of the power introduced in the Simulink model.

5.3.5 Scenario 5

In this scenario, the heat pump behaviour with high relative humidity in the extract air is analysed. The relative humidity value of the extract air is taken from Simulink and sent to the

PASSYS test cell where it is used in order to reproduce the simulated humidity condition inside the test room. Figure 5-4 shows the data exchange between the Simulink building model and the PASSYS test cell during this scenario.

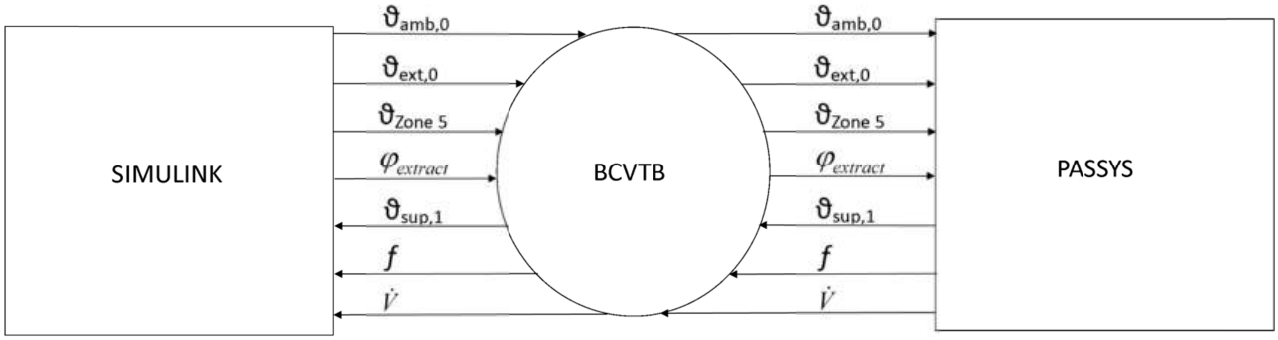

Figure 5-4: Data exchange sketch

The calculation of the supply air temperature inside the building model is done with equations (5.2), (5.3) and (5.4).

The internal loads block contains also the moisture sources profiles taken from (Leonardi, 2016) where they are determined by calibration and validation with measured value. The results of the model of (Leonardi, 2016) are taken as reference case. The model used in this work has no humidity buffer implemented in the structures while the reference model has the humidity buffer. In order to reduce the humidity peaks, a reduction factor for the moisture is introduced in each zone. The value of this factor is determined by comparing the humidity trends of the reference model and of the model used in this work. This factor is used to reduce $\dot{m}_{i,H_2O}$ in the equation (2.2).

Figure 5-5 shows the comparison between the relative humidity trends of the reference model (ref) and of the used model (HiL) for the period involved in the HiL simulation. Zone 6 (bathroom) and 1 (kitchen) have higher peaks with respect to the other zones. The peaks amplitude are similar between the HiL case and the reference case, this is due to the introduced capacities. The trend of the HiL profile changes along the time according to the ambient humidity variations, while the reference case trend is almost constant. This effect is due to the humidity buffer of the structures that are modelled in the reference case but not in the HiL case.

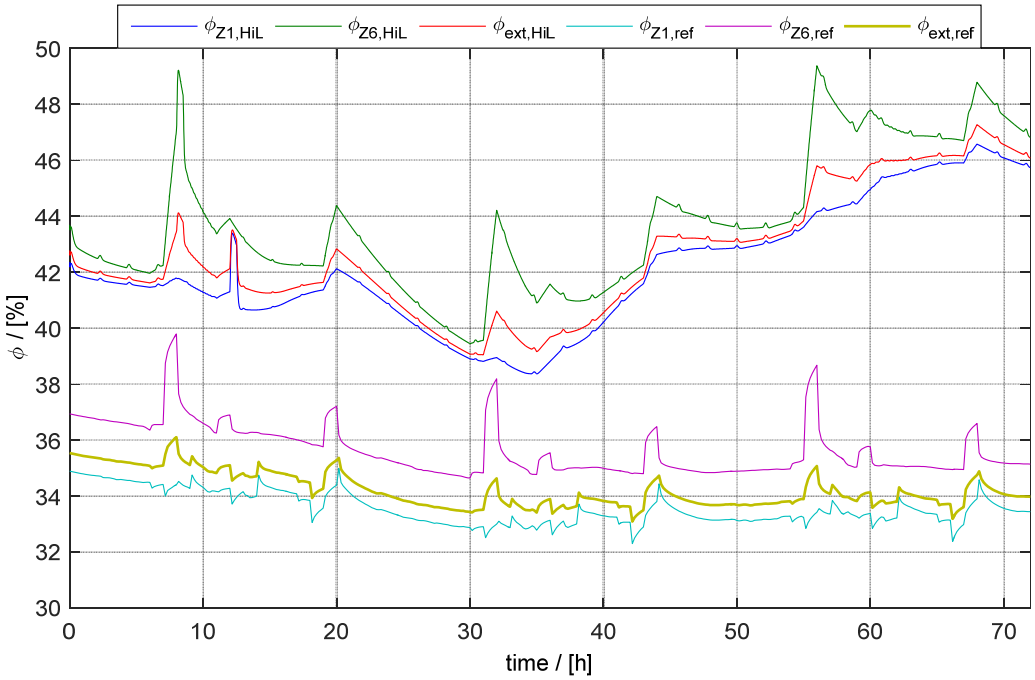

Figure 5-5: Comparison of the relative humidity trends

Figure 5-6 shows the temperature profiles measured during the scenario 1 with dry air. The extract airflow is exposed to risk of condensation. As it has a temperature around 20°C before the heat exchanger and its temperature decreases rapidly in the heat exchanger. $\vartheta_{exh,1}$ is the temperature measured after the heat pump evaporator, it increases quickly during the de-icing periods.

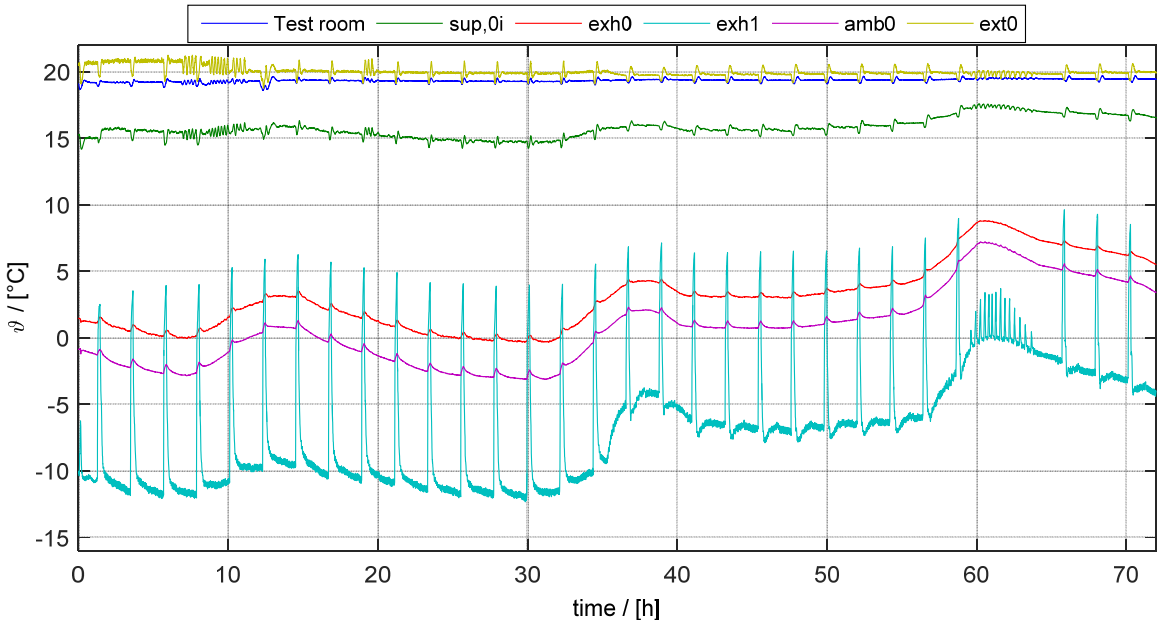

Figure 5-6: Temperature profiles for dry air in the heat exchanger

Figure 5-7 shows the psychrometric diagram with two highlighted areas that represent humidity and the temperatures range in which the condensation takes place in the heat exchanger with an extract air temperature of 20 C. When $\vartheta_{exh,0}$ is 0 °C (blue area), the condensation takes place for a relative humidity range of the extract airflow between 25% and

100%. When $\vartheta_{exh,0}$ is 8.9 °C (red area), the condensation takes place for a relative humidity range between 48% and 100%.

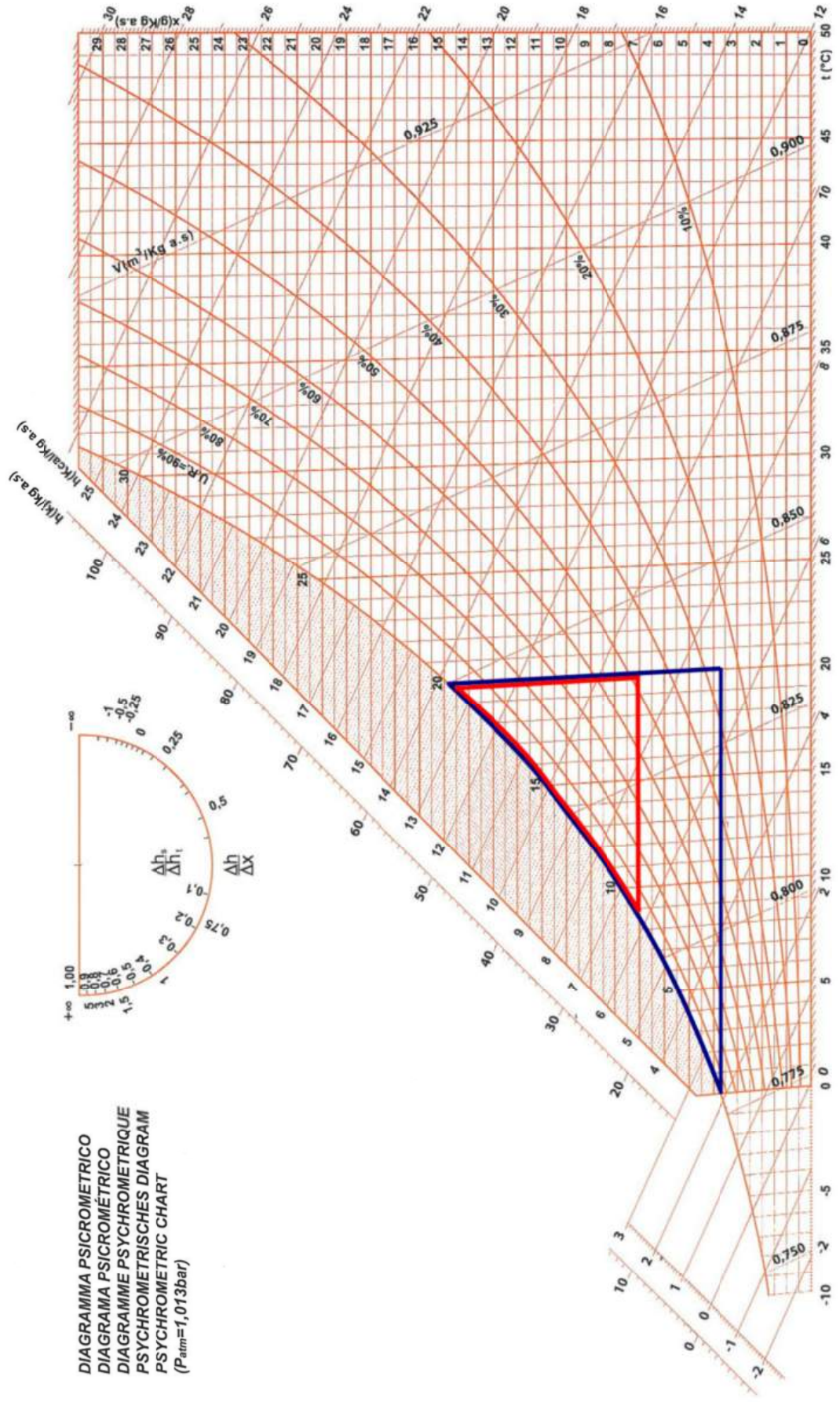

Figure 5-7: Condensation zones (Enerclima, 2016)

In the supply airflow, condensation does not take place because this airflow is heated up through the heat exchanger and subsequently by the heat pump and backup heater. In previous study (Siegele, 2015), is demonstrated that $\dot{Q}_{MVHR}$ is almost constant with respect to extract air relative humidity variation. The equation (5.5) shows the definition of $\dot{Q}_{MVHR}$.

$$\dot{Q}_{MVHR} = \left(h_{sup,0i} - h_{amb,0}\right) \cdot \dot{m}_{sup} = UA_{HRC} \cdot \Delta\vartheta_{log} \tag{5.5}$$

$$\Delta\vartheta_{log} = \frac{\left(\vartheta_{ext,0i} - \vartheta_{sup,0i}\right) - \left(\vartheta_{exh,0i} - \vartheta_{amb,1}\right)}{\ln\left(\frac{\left(\vartheta_{ext,0i} - \vartheta_{sup,0i}\right)}{\left(\vartheta_{exh,0i} - \vartheta_{amb,1}\right)}\right)} \tag{5.6}$$

Where:

- $h_{sup,0i}$ is the enthalpy of supply air after the heat exchanger $\left[\frac{\mathrm{J}}{\mathrm{kg}}\right]$;
- $h_{amb,0}$ is the enthalpy of ambient air before the heat exchanger $\left[\frac{\mathrm{J}}{\mathrm{kg}}\right]$;
- $\dot{m}_{sup}$ is the supply air massflow $\left[\frac{kg}{s}\right]$;
- UA_{HRC} is the heat transfer coefficient of the heat exchanger $\left[\frac{\mathrm{W}}{\mathrm{K}}\right]$;
- $\Delta\vartheta_{log}$ is the logarithmic temperature difference $[\mathrm{K}]$.

In the before mentioned work, the trend of the exhaust air enthalpy with respect to the extract air relative humidity and the ambient temperature is reported. By increasing the extract air relative humidity, the exhaust air enthalpy is increasing.
If condensation takes place in the heat exchanger, the temperature of the exhaust airflow before the evaporator $\vartheta_{exh,0i}$ is higher than in the case without condensation i.e. the heat pump evaporator can work at higher temperature and it has higher power available, so the performance of the system can be increased.

5.4 BOUNDARY AND INITIAL CONDITIONS

5.4.1 Initial Conditions

The model needs the initial values for the convective and radiative nodes of each zone and the initial temperature values of each structure layer. A pre-simulation is done in order to define realistic initial conditions. The pre-simulation is a Simulink simulation of the 14 days preceding the HiL simulation period. In this simulation the heat pump and controller model are used. The initial values calculated by means of the pre-simulation are used in all the scenarios. The set point temperature for the heating system, during the pre-simulation is 19.4 °C. Figure 5-8 shows the sensitive temperatures of each zone. After 14 days without the heating system, the temperatures are lower than 20 °C.

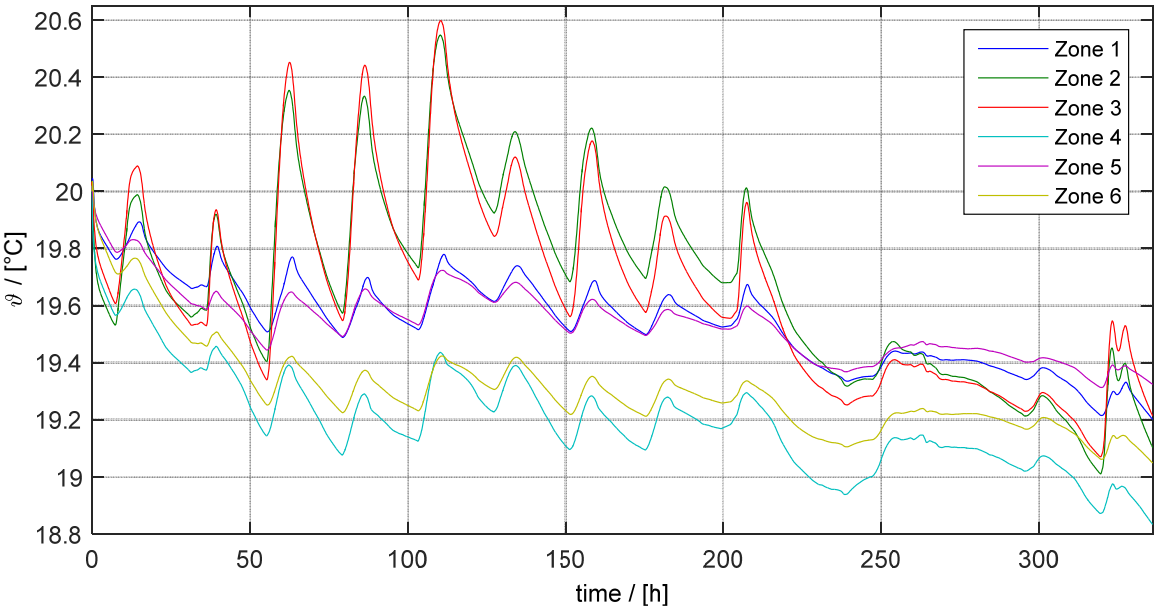

Figure 5-8: Sensitive temperatures of each zone during the pre-simulation

Figure 5-9 shows the ambient temperature, the downstairs and the upstairs neighbour temperature as well as the staircase temperature, and the supply air temperature.

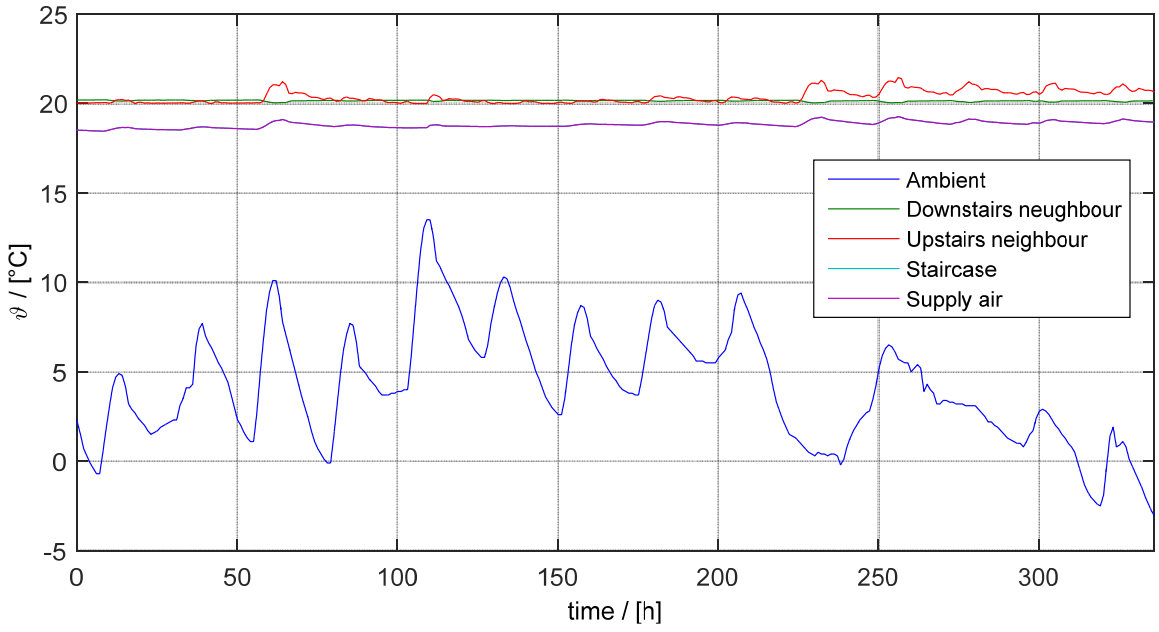

Figure 5-9: Temperatures of the boundary conditions and of the supply air

The temperatures of each structure layer are calculated and saved during the pre-simulation. Therefore, the HiL simulation starts with realistic walls, ceilings and windows temperatures.

5.4.2 Boundary and Operative Conditions

The main boundary and operative conditions for the scenario are:

- Ambient temperature;
- Windows and doors opening;
- Internal loads.

The ambient temperature and the boundary temperatures are shown in Figure 5-10. The climate is the standard climate of Stuttgart. The chosen period is suitable for the intention of the HiL simulation because:

- It involves one day of low temperature where the m-HP and the backup are working toghether;
- In the period between hour 40 and 50 only the m-HP works, thanks to the temperate climate;
- A temperature peak is present at the hour 60. This is important in order to study the on/off behaviour.

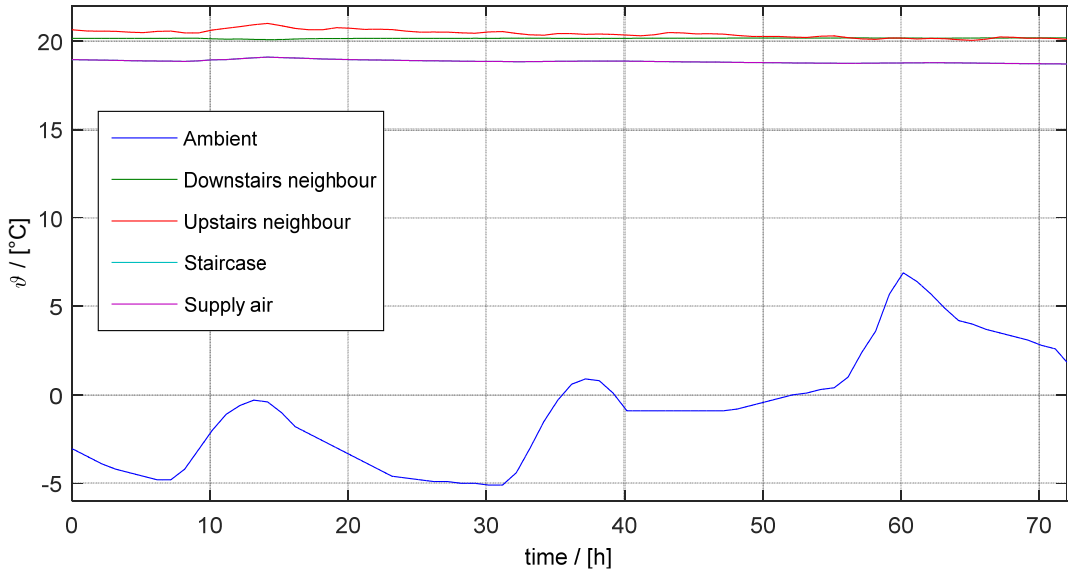

Figure 5-10: HiL boundary temperatures

Figure 5-11 shows the solar irradiation for each zone.

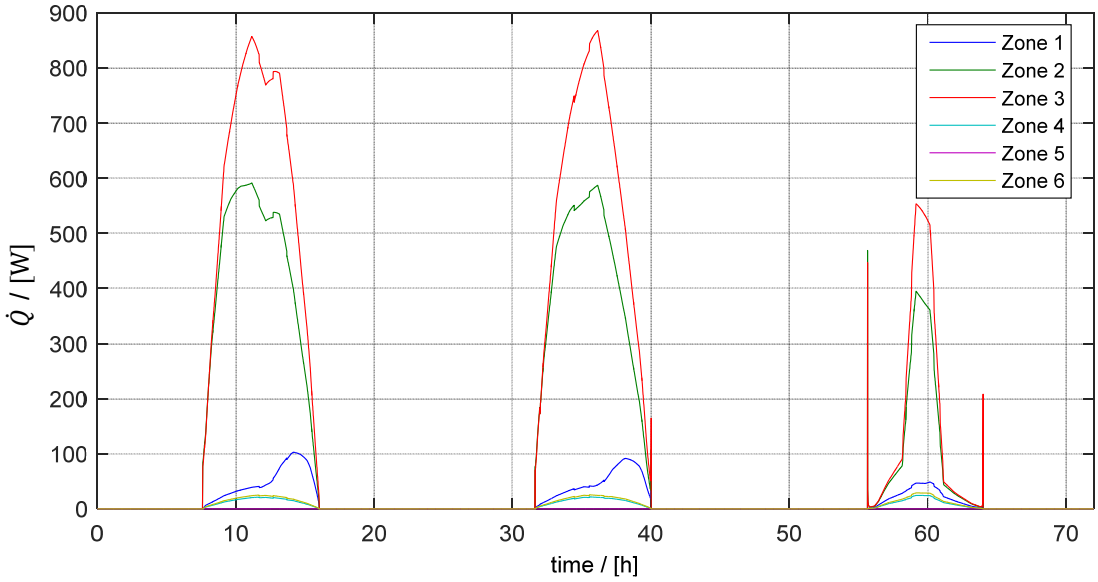

Figure 5-11: Solar irradiation

The windows opening is used in order to test the controller with a disturbance.

A windows opening profile is considered in the model. Figure 5-12 shows the infiltration and the windows opening trend. A constant factor of $0.07\ \left[\frac{m^3}{h}\right]$ is taken for the infiltration, and it is ten times higher when the windows are open. As the infiltration regards the whole volume of the flat, also the zone 5 has the infiltration losses. The opening lasts 30 minutes and the windows are opened in the morning for the zones 3, 4 and 6, at midday in the zone 1 and in the evening for the zone 2.

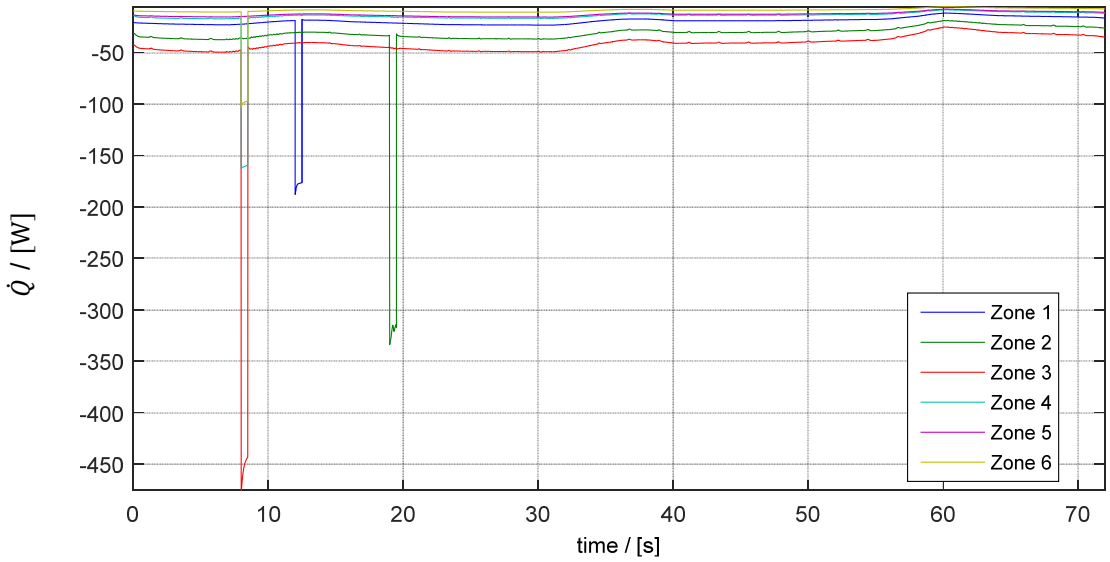

Figure 5-12: Infilatration and windows opening

The internal loads are constant in the whole period, which is not realistic, but allows better comprehension of the controller response to the windows opening disturbance. Table 5-1 shows the internal loads value for each zone.

Table 5-1: Internal loads value

Zone	Internal loads value [W]
1	47.62
2	71.87
3	96.88
4	32.34
5	30.49
6	21.88

5.4.3 Controller Settings

The hardware controller uses the following settings in all the scenarios:

- $K_p = 35\ \left[\frac{\mathrm{K}}{\mathrm{K}}\right]$ proportional gain;
- $K_i = \frac{35}{10 \cdot 60} = 0.05833\ \left[\frac{1}{\mathrm{s}}\right]$ integral gain;
- Set point temperature for the backup heater: $\vartheta_{set,BU} = 20\ °\mathrm{C}$;
- Minimum runtime: 15 min;
- In the first scenario is used the conditional integration anti-windup while in the others scenarios the back calculation anti-windup is used.

5.5 TEST ROOM AND COLDBOX TEMPERATURES ERROR

5.5.1 Test Room Temperature Error

Due to the limited heating and cooling system of the PASSYS test cell, within a short time range it cannot be ensure that the test room temperature coincides with the extract air set point temperature. Especially when the heat pump or the backup heater change their power. A power balance over the test room (Figure 5-13) is done in order to understand the magnitude of the committed error.

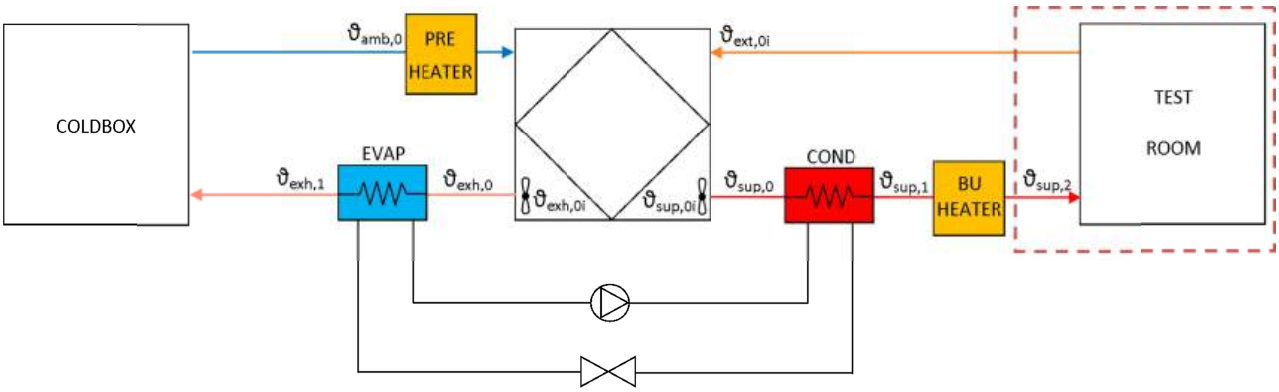

Figure 5-13: Power test room balance

The supply air temperature measured in the PASSYS test cell and used in Simulink is taken for the inlet airflow $\vartheta_{sup,2}$. The set point temperature $\vartheta_{ext,set\ point}$ and the real test room temperature $\vartheta_{ext,measured}$ are considered in order to calculate $\dot{Q}_{set\ point}$ and $\dot{Q}_{meas}$. The measured extract air volume flow $\dot{V}_{meas,ext}$ is used in the powers calculation. The air density ρ and specific heat capacity c_p are calculated in Simulink by using the measured test room temperature and relative humidity.

$$\dot{Q}_{set\ point,tr} = \dot{V}_{meas,ext} \cdot \rho \cdot c_p \cdot \left(\vartheta_{sup,2} - \vartheta_{ext,set\ point}\right) \tag{5.7}$$

$$\dot{Q}_{meas,tr} = \dot{V}_{meas,ext} \cdot \rho \cdot c_p \cdot \left(\vartheta_{sup,2} - \vartheta_{ext,measured}\right) \tag{5.8}$$

The power difference is given by the equation (5.9):

$$\dot{Q}_{diff,tr} = \dot{Q}_{set\ point,tr} - \dot{Q}_{meas,tr} = \dot{V}_{meas,ext} \cdot \rho \cdot c_p \cdot \left(\vartheta_{ext,measured} - \vartheta_{ext,set\ point}\right) \tag{5.9}$$

The energy can be obtained by integration of the powers over the HiL period:

$$Q_{set\ point,tr} = \int \dot{Q}_{set\ point,tr}\, dt \tag{5.10}$$

$$Q_{meas,tr} = \int \dot{Q}_{meas,tr}\, dt \tag{5.11}$$

$$Q_{diff,tr} = Q_{set\ point,tr} - Q_{meas,tr} \tag{5.12}$$

The supply air temperature considered in these balances is measured in the PASSYS test cell and it corresponds to the supply air temperature that the heating system can provide under the specified conditions (extract and ambient air temperature). The supply air temperature that would occur with the set point extract temperature would be slightly different from the measured one. This aspect is disregarded in the previous balances.

5.5.2 Coldbox Temperature Error

The ambient temperature is reproduced in the coldbox. As already explained for the test room, also here an error cannot be completely avoided. This error is caused by the possible deviation between the set point temperature and the real coldbox temperature. In order to evaluate this deviation, a energy balance is carried out including the heat pump condenser and backup heater.

The equations (5.13), (5.14) and (5.15) are used in order to evaluate the deviations of the heating system power caused by the coldbox temperature deviation. The supply air temperature used in the equations (5.13) and (5.14) is the measured supply air temperature during the HiL simulation. $\vartheta_{sup,0}$ is the temperature of the airflow before the heat pump condenser. This is calculated with the Simulink model of the heat exchanger by using as input the set point coldbox temperature in order to obtain $\vartheta_{sup,0_{set\ point}}$ and the measured cold box temperature in order to obtain $\vartheta_{sup,0_{measured}}$. The volume flow $\dot{V}_{meas,sup}$ is measured during the HiL simulation after the backup heater so the air density ρ and specific heat capacity c_p are calculated by using as input $\vartheta_{sup,1}$, the ambient pressure and the ambient absolute humidity. The ambient air is always heated up through which the heat exchanger and the heating system so the absolute humidity is constant.

$$\dot{Q}_{set\ point,cb} = \dot{V}_{meas,sup} \cdot \rho \cdot c_p \cdot \left(\vartheta_{sup,2} - \vartheta_{sup,0_{set\ point}}\right) \tag{5.13}$$

$$\dot{Q}_{meas,cb} = \dot{V}_{meas,sup} \cdot \rho \cdot c_p \cdot \left(\vartheta_{sup,2} - \vartheta_{sup,0_{measured}}\right) \tag{5.14}$$

$$Q_{diff,cb} = Q_{set\ point,cb} - Q_{meas,cb} = \dot{V}_{meas,sup} \cdot \rho \cdot c_p \cdot (\vartheta_{sup,0_{measured}} - \vartheta_{sup,0_{set\ point}}) \tag{5.15}$$

The energy can be obtained by integration of the powers over the HiL period:

$$Q_{set\ point,cb} = \int \dot{Q}_{set\ point,cb}\, dt \tag{5.16}$$

$$Q_{meas,cb} = \int \dot{Q}_{meas,cb}\, dt \tag{5.17}$$

$$Q_{diff,tr} = Q_{set\ point,cb} - Q_{meas,cb} \tag{5.18}$$

The supply air temperature $\vartheta_{sup,2}$ used in the equations (5.13) and (5.14) is taken from the HiL simulation. This temperature would be slightly different if the cold box temperature was equal to the set point temperature. This aspect is disregarded in the balances.

5.5.3 Total Error

The committed error over the test room temperature is calculated by disregarding the coldbox temperature error and the error over the coldbox temperature is calculated by disregarding the test room temperature error. By using the superimposition principle it is possible to add the two balances in order to calculate the overall error. The balance involved in the total error calculation is shown in Figure 5-14.

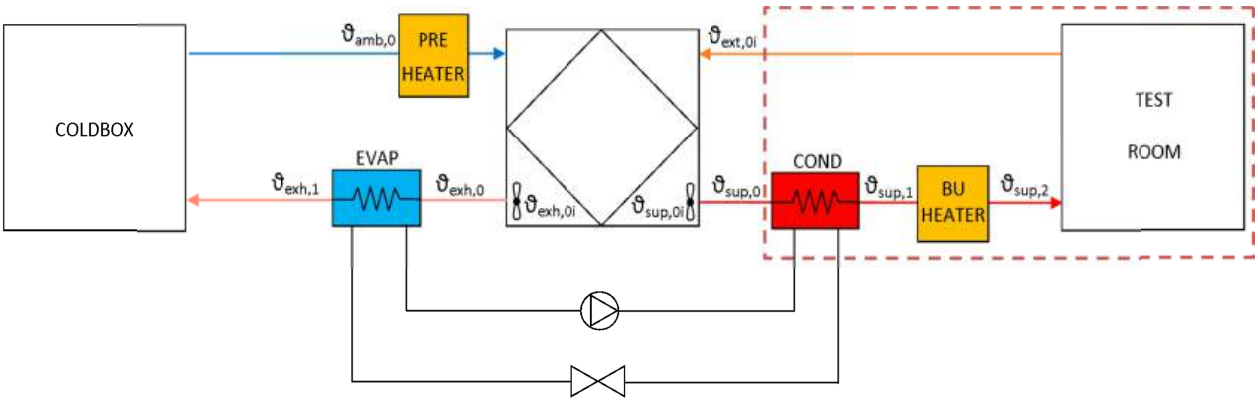

Figure 5-14: Energy Balance

The equations (5.19), (5.20) and (5.21) are involved in the total error determinations.

$$\dot{Q}_{set\ point} = \dot{Q}_{set\ point,cb} - \dot{Q}_{set\ point,tr} \tag{5.19}$$

$$\dot{Q}_{meas} = \dot{Q}_{meas,cb} - \dot{Q}_{meas,tr} \tag{5.20}$$

$$\dot{Q}_{diff} = \dot{Q}_{set\ point} - \dot{Q}_{meas} \tag{5.21}$$

The energy can be obtained by integration of the powers over the HiL period:

$$Q_{set\ point} = \int \dot{Q}_{set\ point}\, dt \tag{5.22}$$

$$Q_{meas} = \int \dot{Q}_{meas}\, dt \tag{5.23}$$

$$Q_{diff} = Q_{set\ point} - Q_{meas} \tag{5.24}$$

5.6 HEAT PUMP POWER DEVIATION

The power introduced in the Simulink building model can be different from the real power produced by the heating system and delivered to the real airflow that takes place within the MVHR inside the PASSYS test cell, so the deviation between these two powers is calculated. This problem is present only within the scenarios 1, 2 and 3.

The real heat pump power is calculated with the equation (5.25), by using:

- the measured volume flow $\dot{V}_{meas}$ $\left[\frac{\mathrm{m}^3}{\mathrm{s}}\right]$;
- the measured supply air temperature $\vartheta_{sup1,meas}$ [°C];
- the simulated density $\rho_{sim}(\vartheta_{sup1,meas}, x_{amb}, p_{amb})$ $\left[\frac{\mathrm{kg}}{\mathrm{m}^3}\right]$;
- the simulated specific heat capacity $c_{p,sim}(\vartheta_{sup1,meas}, x_{amb}, p_{amb})$ $\left[\frac{\mathrm{J}}{\mathrm{kg\,K}}\right]$;
- the simulated supply air temperature after the heat exchanger $\vartheta_{sup0,sim}$ [°C];
- the frequency set by the hardware controller f [Hz].

$$\dot{Q}_{Real} = (\vartheta_{sup1,meas} - \vartheta_{sup0,sim}) \cdot \dot{V}_{meas} \cdot \rho_{sim} \cdot c_{p,sim} \cdot + \frac{f}{100} \cdot P_{max,BU} \qquad (5.25)$$

The power used within the building model during the HiL simulation is calculated by using the equation (5.26).

$$\dot{Q}_{HiL} = (\vartheta_{sup2,HiL} - \vartheta_{sup0,sim}) \cdot \dot{m}_{HiL} \cdot c_{p,sim} \qquad (5.26)$$

Where:

- $\vartheta_{sup2,HiL}$ is the supply air temperature of the air flow used in the building model during the HiL simulation [°C].
- $\dot{m}_{HiL}$ is the air massflow used in the building model during the HiL simulation $\left[\frac{kg}{s}\right]$;

By knowing $\dot{Q}_{Real}$ and $\dot{Q}_{HiL}$ the deviation can be analysed.

5.7 SCENARIO 1

5.7.1 Test Room Temperature Error

Figure 5-15 shows the comparison between the measured test room temperature (blue) and the test room set point temperature (magenta) that corresponds to the extract air temperature, measured in the scenario 1. As it can be observed, the test room temperature has some oscillations when the backup heater or the heat pump change quickly their power. This can happen when the heat pump and the backup heater are doing on/off cycles or when the heat pump is doing the de-icing.

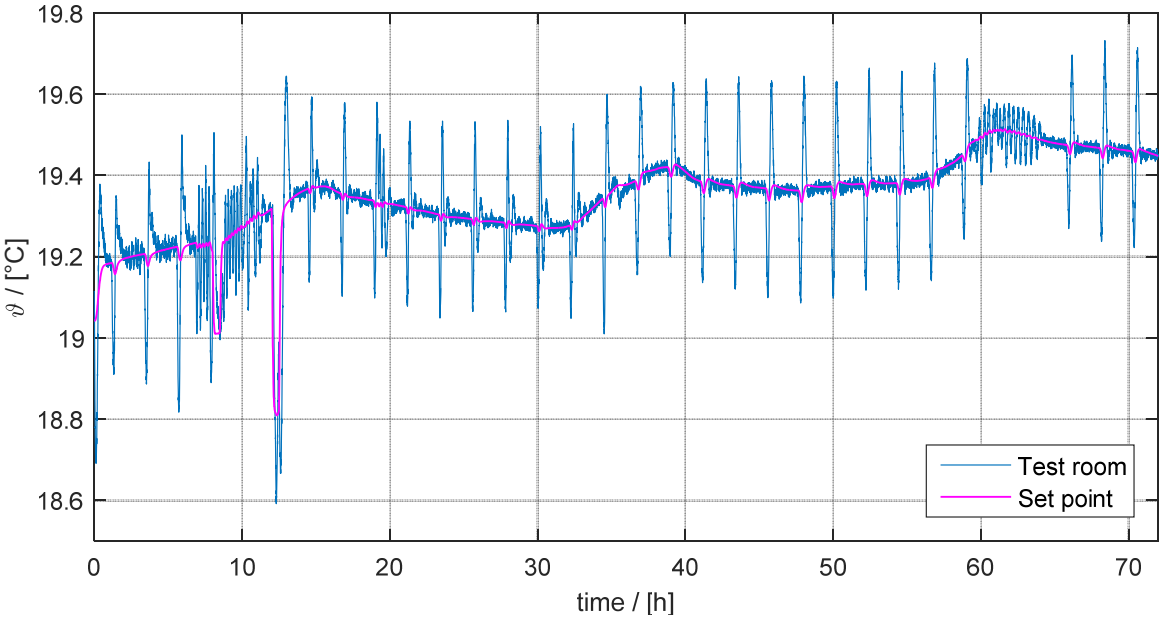

Figure 5-15: Comparison of the measured and set point temperature of the test room (scenario 1)

Table 5-2 shows the maximum, mean and minimum value of $\dot{Q}_{diff,tr}$ and $\dot{Q}_{set\ point,tr}$ calculated according to equations (5.7), (5.8) and (5.9).

These powers are calculated by doing a balance over the test room, the set point power ($\dot{Q}_{set\ point,tr}$) uses the set point temperature of the extract air while the measured power ($\dot{Q}_{meas,tr}$) uses the measured temperature of the extract air. $\dot{Q}_{diff,tr}$ is the difference between the set point and the measured power.

The mean value of $\dot{Q}_{diff,tr}$ and $\dot{Q}_{set\ point,tr}$ are calculated by considering the absolute values.

Table 5-2: Maximum, mean and minimum value of $\dot{Q}_{diff,tr}$ and $\dot{Q}_{set\ point,tr}$ for the balance over the test room (scenario 1)

	$\dot{Q}_{diff,tr}$ [W]	$\dot{Q}_{set\ point,tr}$ [W]
Max	15.0	818.5
Mean	1.47	298.1
Min	-17.8	-135.5

The energy can be obtained by integration of the powers over the considered period, as it is shown in the equations (5.10), (5.11) and (5.12), and these values are listed in Table 5-3.

Table 5-3: Energy values of the balance over the test room (scenario 1)

	Q_{tr} [Wh]
$Q_{set\ point,tr}$	20958.5
$Q_{mea,tr}$	20960.0
$Q_{diff,tr}$	-1.5

The balance already explained in section 5.5.1 is now applied to the most critical point around the hour 12.5. Figure 5-16 shows the zoom of the Figure 5-15 around the hour 12.5.

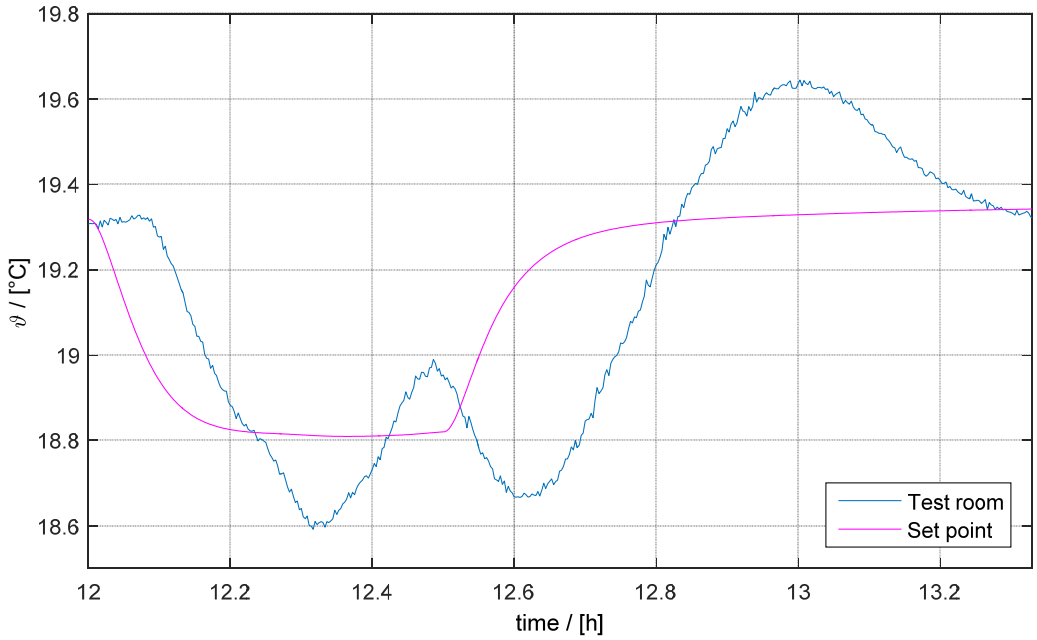

Figure 5-16: Zoom of Figure 5-15

With the equations (5.7), (5.8) and (5.9) the power differences are calculated and the results are listed in the Table 5-4. The mean value of $\dot{Q}_{diff,tr}$ and $\dot{Q}_{set\ point,tr}$ are calculated by considering the absolute values.

Table 5-4: Maximum, mean and minimum value of $\dot{Q}_{diff,tr}$ and $\dot{Q}_{set\ point,tr}$ for a section of period of the scenario 1

	$\dot{Q}_{diff,tr}$ [W]	$\dot{Q}_{set\ point,tr}$ [W]
Max	10.8	725.7
Mean	6.0	328.7
Min	-17.8	-70.1

The energy values can be obtained by integration of the powers, as shown in the equations (5.10), (5.11) and (5.12), and these values are listed in Table 5-5.

Table 5-5: Energy values of the balance over the test room for a section of period of the scenario 1

	Q_{tr} [Wh]
$Q_{set\ point,tr}$	431.02
$Q_{meas,tr}$	430.91
$Q_{diff,tr}$	0.11

From these results, it is possible to conclude that the temperatures deviations which occur in the test room are not significant in the considered case.

5.7.1 Coldbox Temperature Error

Figure 5-17 shows the measured and the set point coldbox temperatures. As it can be seen, the trends are almost coincident. This aspect is underlined in Figure 5-18 where a zoom of Figure 5-17 is reported.

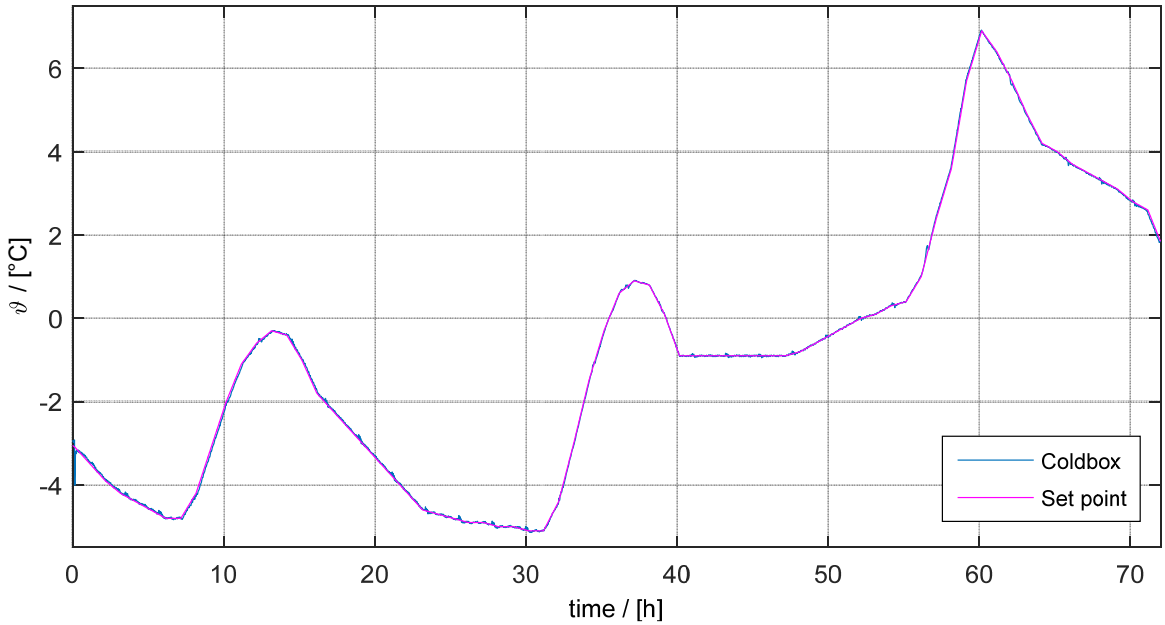

Figure 5-17: Comparison of the measured and set point temperature of the Coldbox for the scenario 1

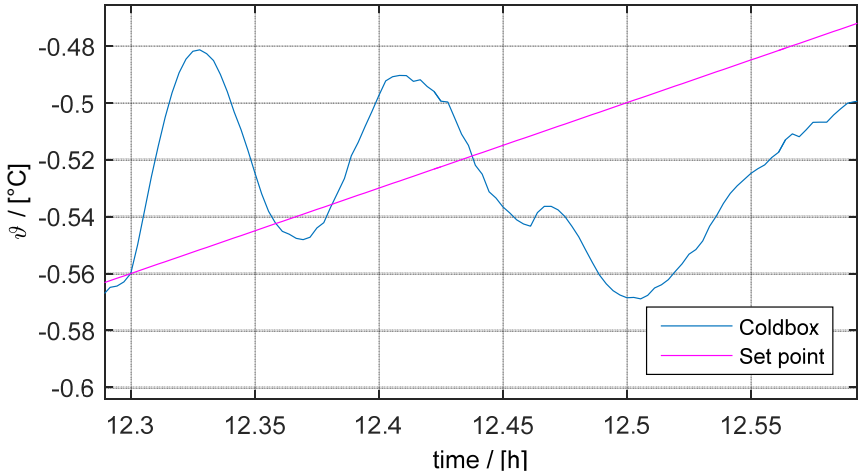

Figure 5-18: zoom of the Figure 5-17

$\dot{Q}_{set\ point,cb}$, $\dot{Q}_{meas,cb}$ and $\dot{Q}_{diff,cb}$ are calculated by means of the equations (5.13), (5.14) and (5.15). These powers are calculated by doing a balance over the heat pump condenser and backup heater, the set point power $\dot{Q}_{set\ point,cb}$ is calculated by using the set point temperature of the supply air after the heat exchanger, the measured power $\dot{Q}_{meas,cb}$ is calculated by using the temperature of the supply air after the heat exchanger that occurs with the measured coldbox temperature. Table 5-6 shows the maximum, mean and minimum values of $\dot{Q}_{diff,cb}$ and $\dot{Q}_{set\ point,cb}$. The mean value of $\dot{Q}_{diff,cb}$ is calculated by considering the absolute values of $\dot{Q}_{diffcb}$.

Table 5-6: Maximum, mean and minimum value of $\dot{Q}_{diff,cb}$ and $\dot{Q}_{set\ point,cb}$ for the balance over the coldbox (scenario 1)

	$\dot{Q}_{diff,cb}$ [W]	$\dot{Q}_{set\ point,cb}$ [W]
Max	1.52	1142.7
Mean	0.142	468.14
Min	-0.911	0

The energy values can be obtained by integration of the powers, as it is shown in the equations (5.16), (5.17) and (5.18), and these values are listed in Table 5-7.

Table 5-7: Energy values of the balance over the coldbox (scenario 1)

	$Q_{diff,cb}$ [Wh]
$Q_{set\ point,cb}$	33706.0
$Q_{meas,cb}$	33707.0
$Q_{diff,cb}$	-1

From these results, it is possible to conclude that the coldbox temperature deviations are not significant in the considered case.

5.7.2 Total error

$\dot{Q}_{set\ point}$, $\dot{Q}_{meas}$ and $\dot{Q}_{diff}$ are calculated by means of the equations (5.19), (5.20) and (5.21). By using the superposition principle, the errors calculated from the balances over the coldbox and over the test room can be summed up in order to define the total error.

The maximum, minimum and mean value of $\dot{Q}_{diff}$ and of $\dot{Q}_{set\ point}$ are shown in Table 5-8. The mean value of $\dot{Q}_{diff}$ is calculated by considering the absolute values.

Table 5-8: Maximum, mean and minimum value of $\dot{Q}_{diff}$ and $\dot{Q}_{set\ point}$ for the scenario 1

	$\dot{Q}_{diff}$ [W]	$\dot{Q}_{set\ point}$ [W]
Max	17.5	366.3
Mean	1.58	177.1
Min	-15.0	58.2

The energy values can be obtained by integration of the powers, as it is shown in the equations (5.22), (5.23) and (5.24) and these values are listed in Table 5-9.

Table 5-9: Energy values calculated from the whole balance for the scenario 1

	Q_{diff} [Wh]
$Q_{set\ point}$	12747.6
Q_{meas}	12747.0
Q_{diff}	0.6

The overall error calculated during the three day of the HiL simulations is minor compared with the involved powers, so the set point temperatures are reproduced with high accuracy inside the cold box and the test room.

5.7.3 Power deviation

In this scenario is present a deviation between the power delivered by the heat pump inside the PASSYS test cell and the power introduced in the building model. This deviation is caused by the usage of the measured supply air temperature inside the building model. In fact, the measured supply air temperature occurs in a defined airflow in the PASSYS test cell while the airflow introduced in the model has different characteristics (i.e. the building model uses a

constant air volume flow while the volume flow that occurs within the PASSYS is not constant and the simulated air density is not equal to the real one).

The powers calculated with the equations (5.25) and (5.26) are reported in Figure 5-19.

The mean power values and the relative deviation are reported in Table 5-10.

Table 5-10: HiL and real power comparison for the scenario 1

	$\dot{Q}$ [W]
HiL	509.8 (7.6%)
Real	473.7

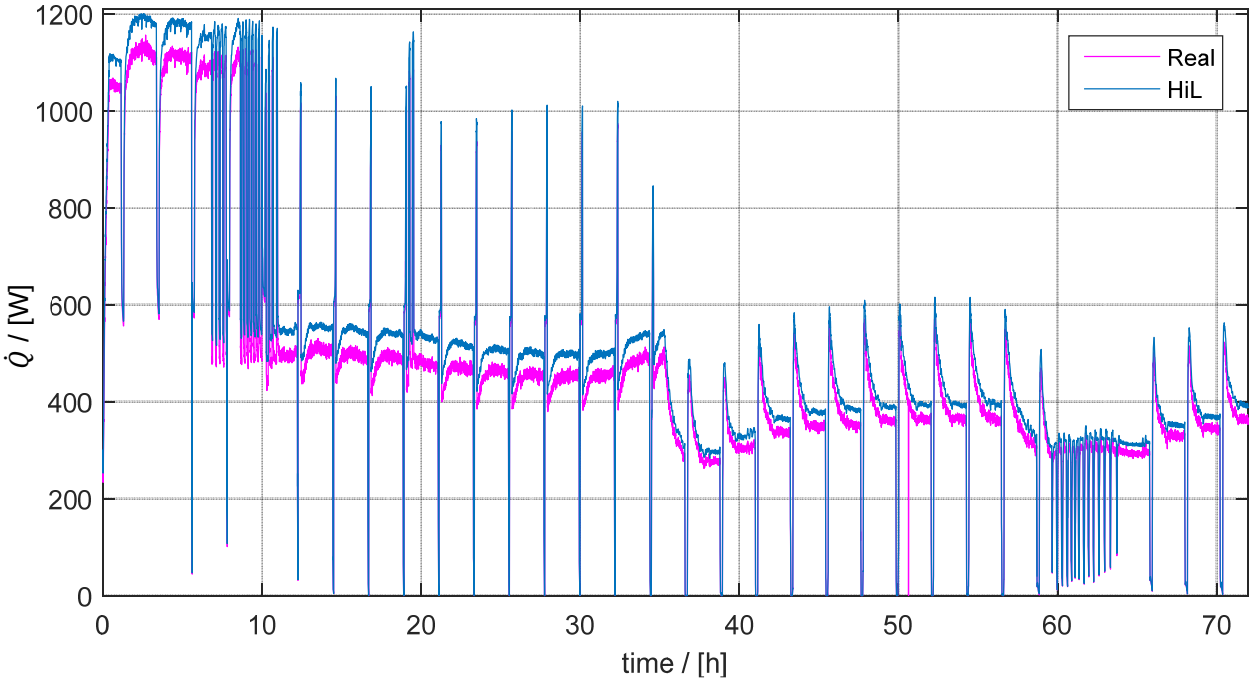

Figure 5-19: HiL simulation and real heating system powers for the scenario 1

The deviation decreases with the power because with high supply air temperature the error over the Simulink mass flow calculation is higher.

5.7.1 Results of the Scenario 1

Comparison of the HiL and Simulink simulation

In this section, the results obtained from the HiL simulation are compared with the results obtained from the Simulink model of the heat pump and of the controller. In order to make the results comparable, the same assumptions over the supply air mass flow calculation are taken in the Simulink model.

Figure 5-20 shows the frequency and the controlled temperature error trends of:

- the HiL simulation (where the heat pump is controlled by the hardware controller)
- the Simulink simulation, where the heat pump and controller models are used.

When the frequency is equal to 251 Hz or 151 Hz the heat pump is doing the de-icing. Within the first 7 hours, the heat pump and the backup heater are both working with the maximum power, then the windows opening disturbance is simulated. Here the backup heater has some on/off cycles because the controlled temperature reaches the set point value and because of the disturbance. Until the hour 34, the heat pump works with the maximum power and the backup heater is switched on only when the heat pump is in the de-icing period. In the period after 35 hours, only the heat pump is working. Since the error increases during the de-icing period, the set point frequency can becomes higher than 150 Hz, so the backup heater is switched on and the set point frequency becomes 251 Hz. In the hour 60, the heat pump is doing on/off cycles, in this simulation the minimum runtime of the heat pump is 15 min.

The Simulink model cannot recognize that the heat pump is working at the minimum level and the evaporator temperature is not low enough for the de-icing, so it is doing the de-icing also in this period where the hardware controller does not require the de-icing. Moreover, the Simulink frequency cannot match exactly the de-icing timing. Even if the heat pump is working all the simulation time with the full power, the real de-icing timing are different from the timing set in the simulation (e.g. after the de-icing the evaporator temperature takes time to decrease so the next de-icing cycle will take place later than 2 hours). This effect is not avoidable with this model because the physical model of the refrigerant cycle is not implemented.

The hardware controller variables can change with an accuracy of 0.05, while in Simulink the accuracy is $eps = 2.2204 \cdot 10^{-16}$. From the hour 10 to 34, the backup heater is switched off even if the error is not zero. This is due to the error accuracy, in fact the hardware controller is able to read the error with round off number. In Simulink this effect is reproduced by means of a relay block (Figure 3-25).

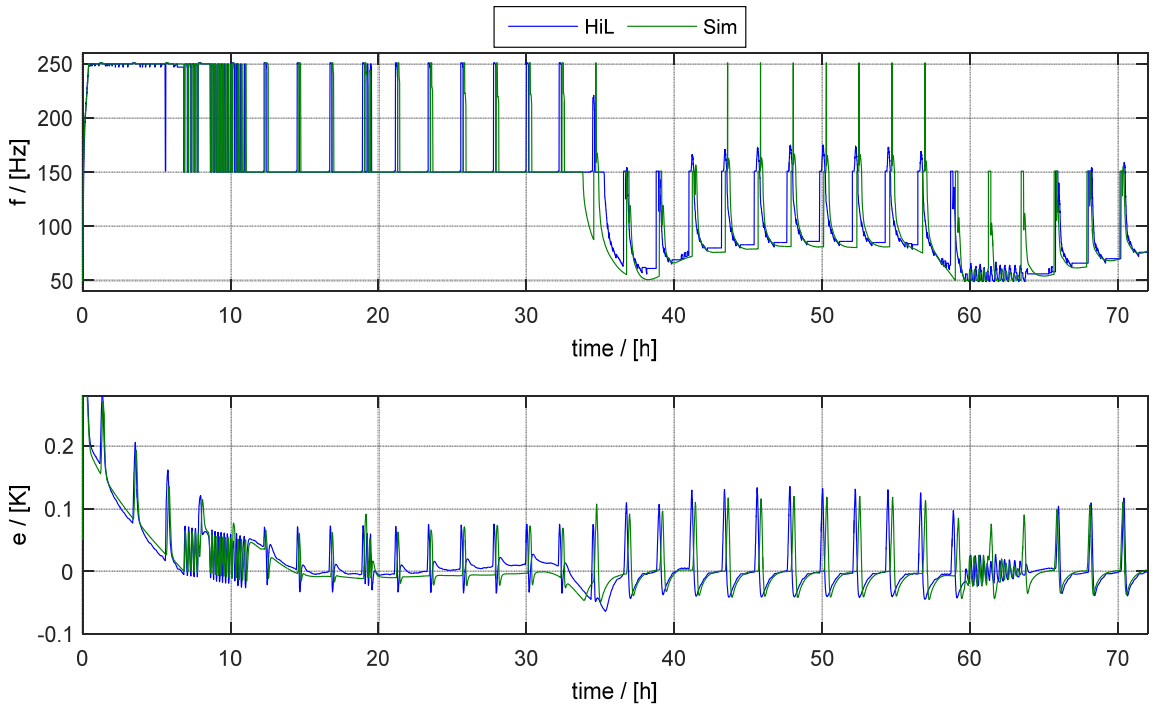

Figure 5-20: Comparison of frequency and error between HiL simulation and Simulink simulation

Figure 5-21 shows in the first subplot, the comparison between the controlled temperature in the HiL and Simulink simulations and in the second subplot the comparison of the supply air temperatures. In the first 1.5 hours the supply air temperature of the HiL is lower than the Simulink one, this can be caused by non-steady state conditions in the beginning of the HiL experiment. From the hour 1.5 to the hour 10, the HiL supply temperature is higher than the Simulink temperature. This is caused by a measurement error in the $\vartheta_{sup,1}$ as discussed with Figure 5-16. Around the hour 19 the controlled temperature decreases because of the windows opening, for this reason the backup heater does some on/off cycles.

In the hour 37.5 the ambient temperature has a peak, so the controlled temperature increase and the supply air temperature decrease. In the period between the hours 40 and 55 the backup heater is not necessary thanks to the higher ambient temperatures respect to the previous period and because the error is already reduced. In the hours 60 the ambient temperature has a peak, so the building energy demand decreases and the heat pump is not anymore able to reduce its power. In this period the heat pump works with on/off cycles.

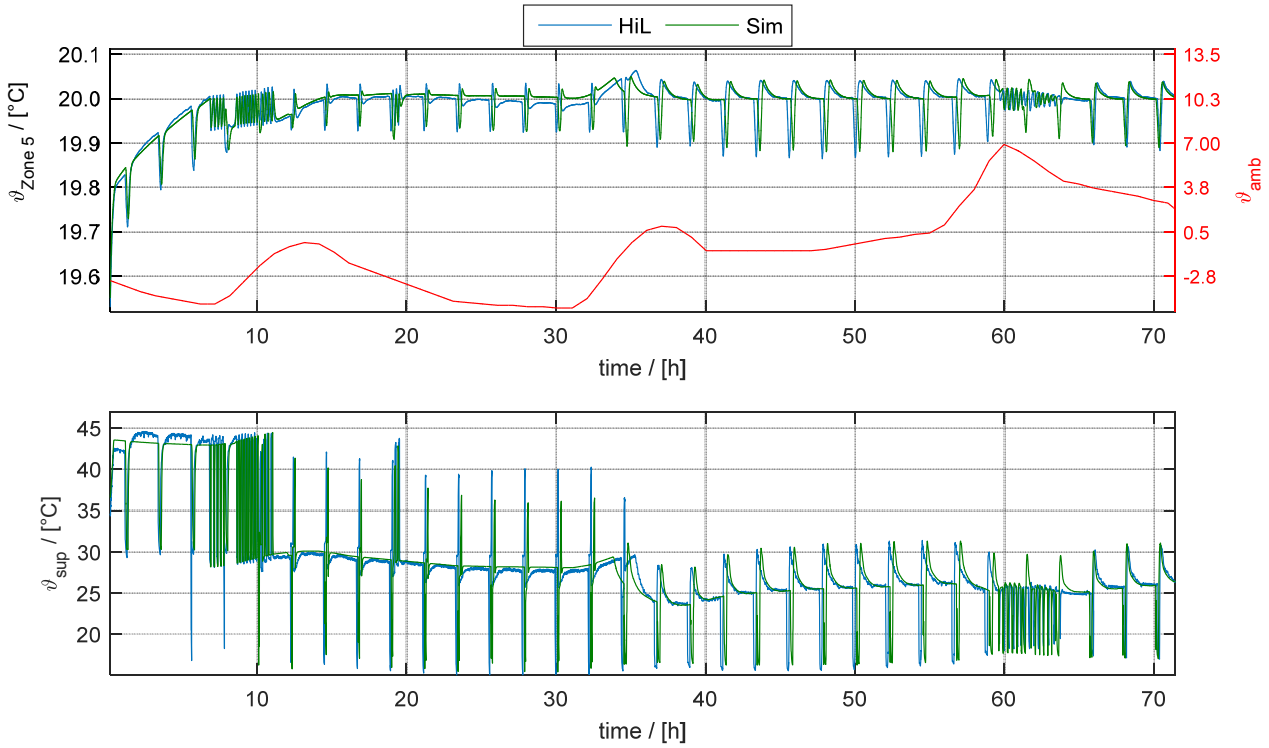

Figure 5-21: Comparison of the controlled and supply air temperatures between HiL simulation and Simulink simulation

Controller behaviour

The HiL and Simulink frequencies are not constant in the first hours, but they have some steps caused by the anti-windup. When the controller output reaches the maximum saturation limit, the integrator part is hold. When the error decreases, the integral gain is again free to change its value. Figure 5-22 shows the Simulink controller parameters, the first plot shows the supply air temperature set point, the second subplot shows the temperature difference over the controller saturation block, the third subplot shows the proportional gain and the last subplot shows the integral gain. The already described anti-windup behaviour is illustrated here. When the temperature difference over the controller saturation block is different from zero, the integrator gain is hold and the supply air temperature set point has its maximum value. Than the proportional gain decreases with the error and with the controller output, so the integrator is again free to increase its value.

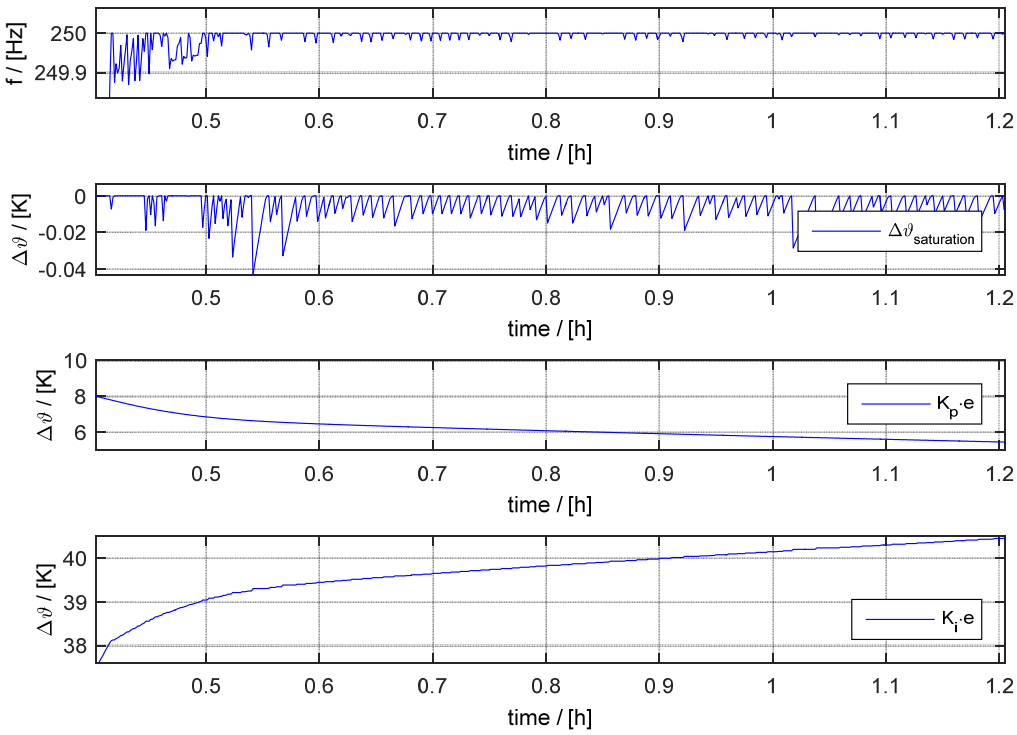

Figure 5-22: Simulink controller parameters

5.8 SCENARIO 2

5.8.1 Test Room, Coldbox and Total Temperatures Error

These analysis are carried out in APPENDIX 2.1.

5.8.2 Comparison of HiL and Simulink Simulation

In this section, the results obtained from the HiL simulation are compared with the results obtained from the Simulink model of the heat pump and of the controller. In order to make the results comparable, the same mistake over the supply air mass flow calculation is taken in the Simulink model.

Figure 5-23 shows the frequency and the controlled temperature error trends of:

- the HiL simulation (where the heat pump is controlled by the hardware controller)
- the Simulink simulation, where the heat pump and controller models are used.

The Simulink and HiL trend comparison is quite good. It can be seen that in the first period both system are working with the maximum power but the error decreases faster within the HiL simulation respect to the Simulink simulation.

This is due to the higher supply air temperature measured in the HiL simulation with respect to the supply air temperature delivered by the heat pump model within the Simulink simulation. This problem is explained with Figure 5-25.

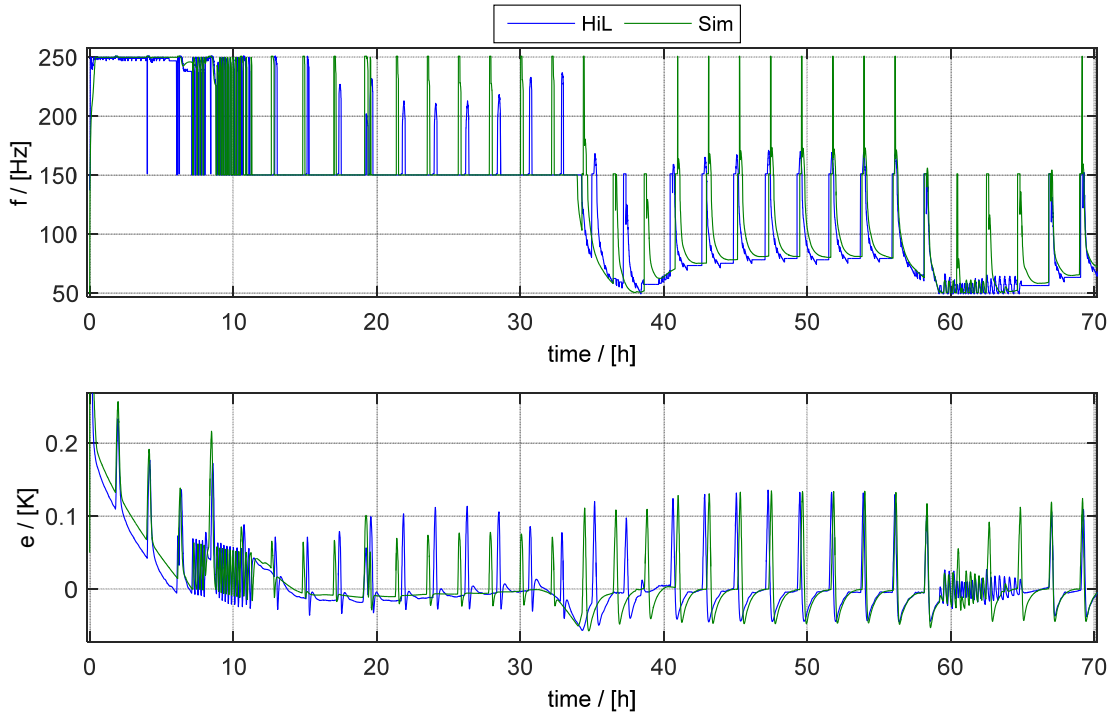

Figure 5-23: Comparison of frequency and error between HiL simulation and Simulink simulation

Figure 5-24 shows in the first subplot the sensitive temperature of the zone 5 for the HiL and Simulink simulation and the ambient temperature trend. In the second subplot are present the supply air temperatures of the HiL and Simulink simulation.

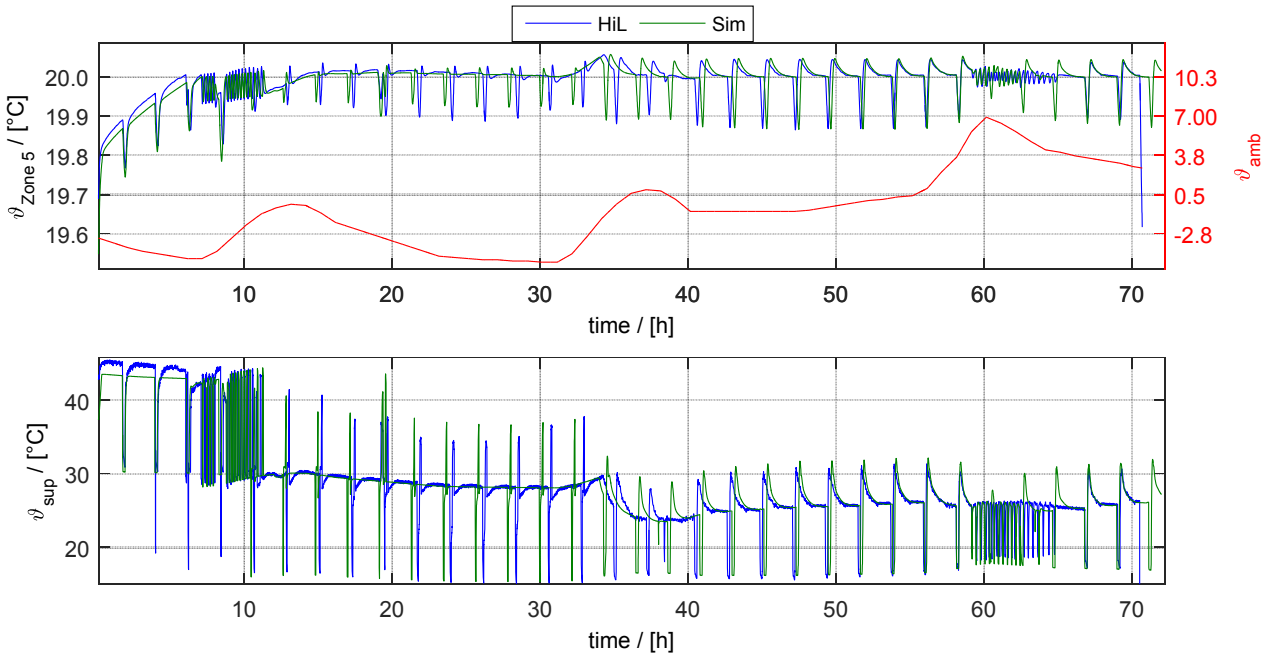

Figure 5-24: Comparison of controlled and the supply air temperatures between HiL simulation and Simulink simulation

5.8.3 Measurement error

The test shown in Figure 5-25 is carried out in order to understand the $\vartheta_{sup,1}$ measurement deviation. The heat pump is switched on with the maximum power and than also the backup heater is switched on with the maximum power. $\vartheta_{sup,1}$ and $\vartheta_{sup,2}$ have the same value as long as the backup heater is switched off. When the backup heater is switched on both $\vartheta_{sup,1}$ and $\vartheta_{sup,2}$ increase while only $\vartheta_{sup,2}$ should increase. This difference is due to an error in the measurement of the $\vartheta_{sup,1}$. The temperature sensor is not protected from the irradiation hence when the backup heater is switched on, the measured temperature is higher than the real temperature.

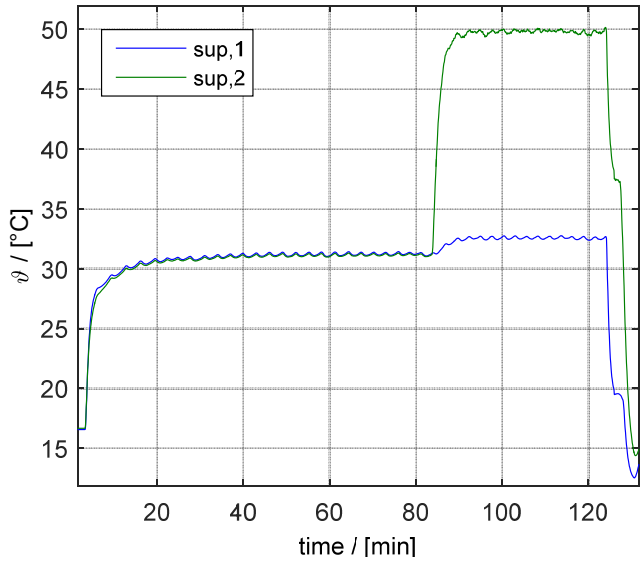

Figure 5-25: Test over $\vartheta_{sup,1}$ and $\vartheta_{sup,2}$

5.8.4 Controller behaviour

Figure 5-26 shows the Simulink controller parameters: the first subplot shows the set point of the supply air temperature, the second subplot shows the temperature difference over the controller saturation block, the third subplot shows the proportional gain and the last subplot shows the integral gain. With the back calculation anti-windup, the integral gain is always free to change even if the system is in saturation. Since the back calculation anti-windup is used in this scenario, the problems explained in the chapters 3.4.2 and 5.7 are here not present.

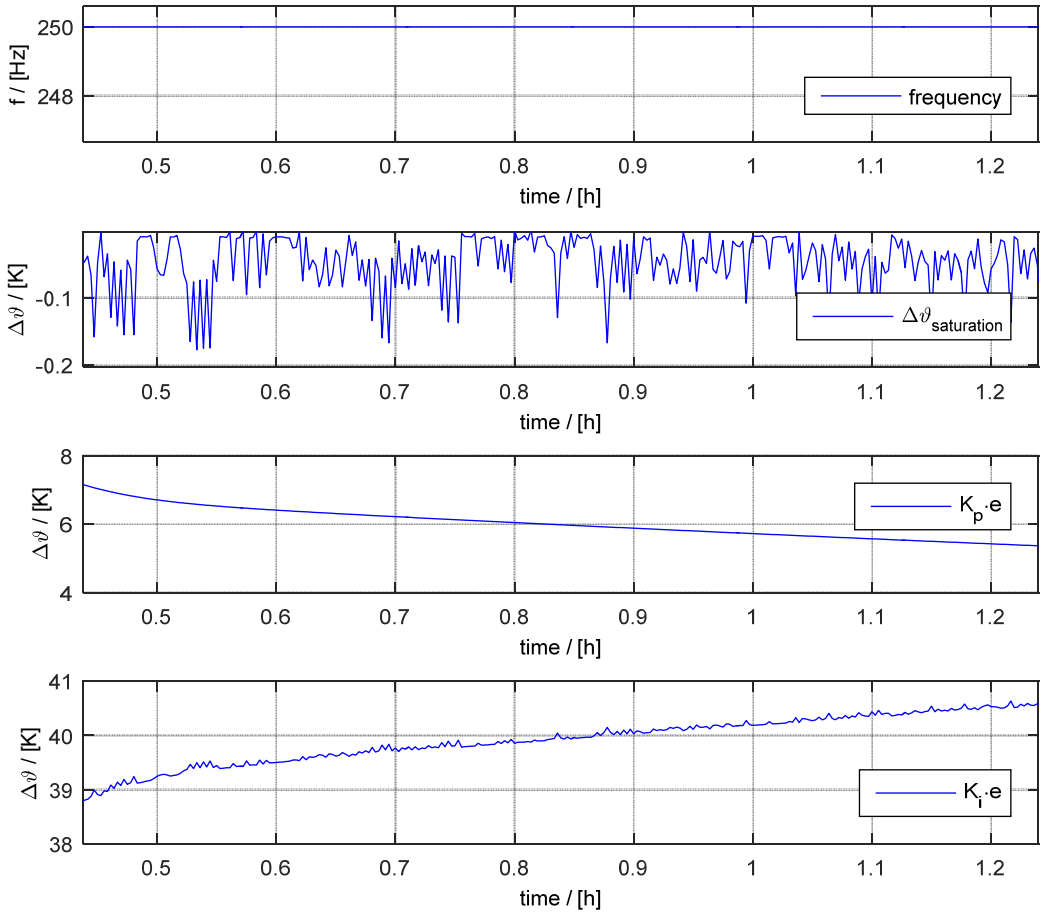

Figure 5-26: Simulink controller parameters

5.9 SCENARIO 3

5.9.1 Test Room, Coldbox and Total Temperatures Error

The analysis of these deviations are not done in this scenario because the boundary conditions are the same of the scenarios 1 and 2 and for these cases the error analysis has been already discussed.

5.9.1 Power deviation

The calculation of the supply airflow characteristics is done as in the scenarios 1 and 2 so the power deviation is again the same already explained.

Comparison of the Supply Air Temperature Between the Scenarios 1, 2 and 3

The trend of the results is the same already explained in the previous scenarios so only the main difference is here reported. Figure 5-27 shows the comparison between the measured $\vartheta_{sup,1}$ within the scenarios 1, 2 and 3. The selected period is the periods in which the backup heater is in operation. The scenarios 1 and 2 have higher supply air temperature with respect to the scenario 3. From the hour 7 the backup heater does on/off cycles, while the heat pump

is still working with the maximum power. Theoretically, $\vartheta_{sup,1}$ should not be affected by any variation of the backup heater power, but in the scenario 1 and 2 can be seen that $\vartheta_{sup,1}$ is changing if the backup heater power changes.

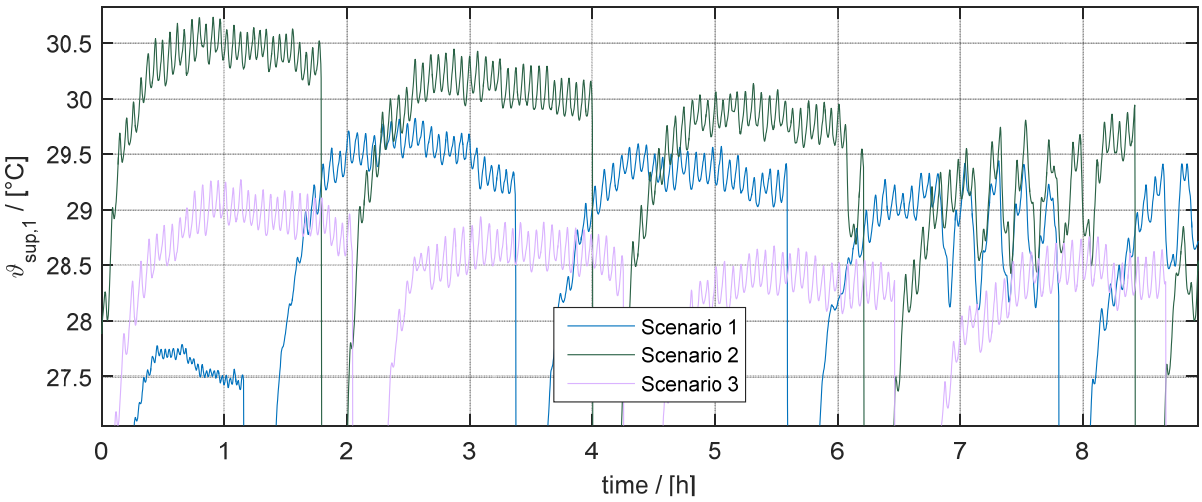

Figure 5-27: Comparison between the measured $\vartheta_{sup,1}$ of the scenarios 1,2 and 3

5.10 SCENARIO 4

5.10.1 Test Room, Coldbox and Total Temperatures Error

These analysis are carried out in APPENDIX 2.2.

5.10.1 Power deviation

Within this scenario the power delivered by the heating system in the PASSYS test cell is exactly the same of the power introduced in the Simulink building model during the HiL simulation. The powers are coincident because the temperature difference of the supply airflow caused by the heating system is calculated with the equation (5.4) where $\vartheta_{sup,2}$ is calculated by dividing the real heating system power for the simulated supply air mass flow and specific heat capacity. Anyway, an analysis can be done over the deviation of the mass flow.

Figure 5-28 shows the comparison between the mass flow introduced in the building model and the real mass flow that occurs inside the MVHR system of the PASSYS. The mass flow introduced in the building model is calculated by considering a constant volume flow of $120\ \left[\frac{\mathrm{m}^3}{\mathrm{h}}\right]$ and an air density simulated in function of $\vartheta_{sup,1}$, absolute humidity of the ambient temperature and in function of the ambient pressure. The real mass flow is calculated by considering the same density and the measured supply air volume flow. The reported values are mediated every three minutes. As it can be seen, the trends are similar.

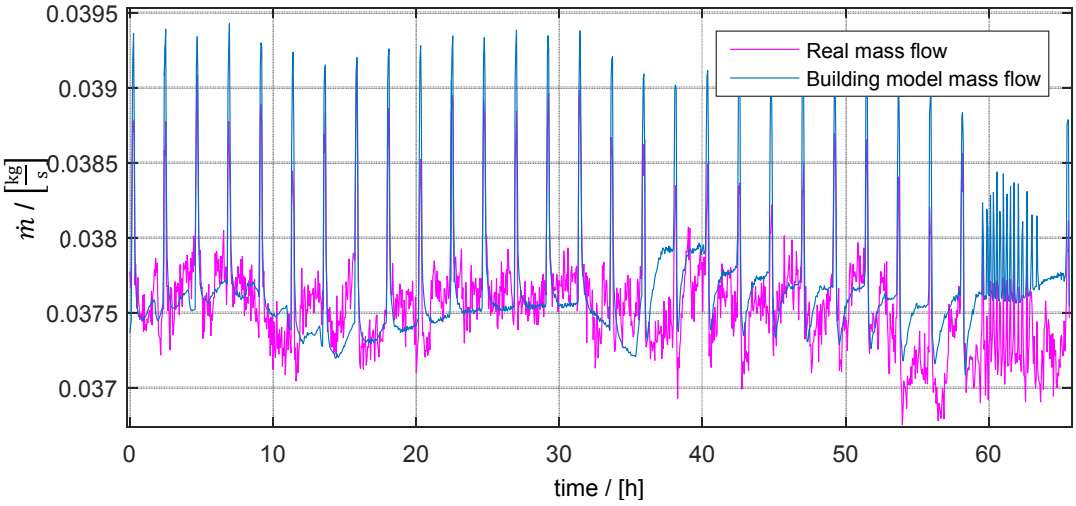

Figure 5-28: Comparison of the mass flow for PASSYS test cell and building model

Table 5-11 shows the comparison between the mean values (over the considered period) of the real mass flow and of the mass flow introduced in the Simulink model. As it can be seen, these values are almost the same.

Table 5-11: Mean values of the mass flows

	Mass flow $\left[\frac{kg}{s}\right]$
Real mass flow	0.0376
Simulink model mass flow	0.0377

Since the powers and the mass flows have close trend in the Simulink model and in the PASSYS test cell, also the supply air temperatures should be close.

5.10.2 Comparison of the HiL and Simulink simulation

The results collected from the HiL simulation are compared with the results obtained by using the Simulink model of the heating system and of the controller.

Figure 5-29 shows the comparison between HiL and Simulink results of the frequency and of the error (difference between set point temperature and controlled temperature). As it can be seen, the Simulink trend and the HiL trend are similar. The different usage of the backup heater during the de-icing between the HiL and Simulink simulation that can be noticed in the period from hour 42 to hour 58 cannot be explained without the analysis of more detailed data of the Hardware controller, but it has a minor influence.

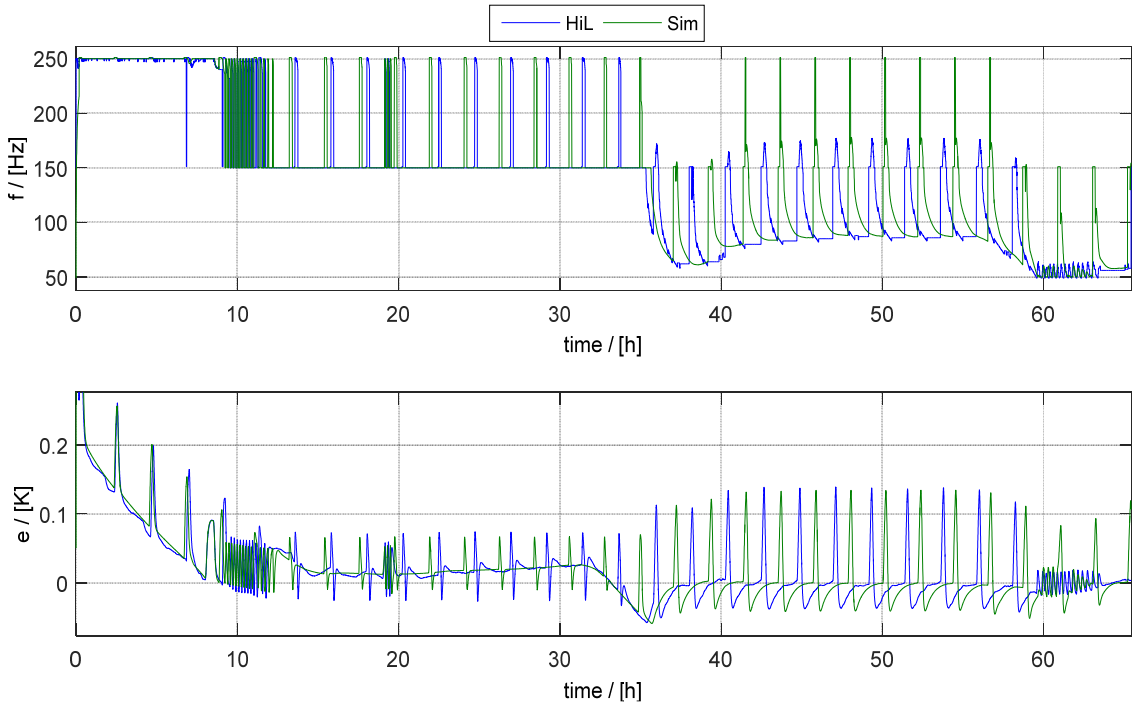

Figure 5-29: Comparison of frequency and error between HiL simulation and Simulink simulation

Figure 5-30 shows the comparison of the controlled and supply air temperatures between HiL simulation and Simulink simulation.

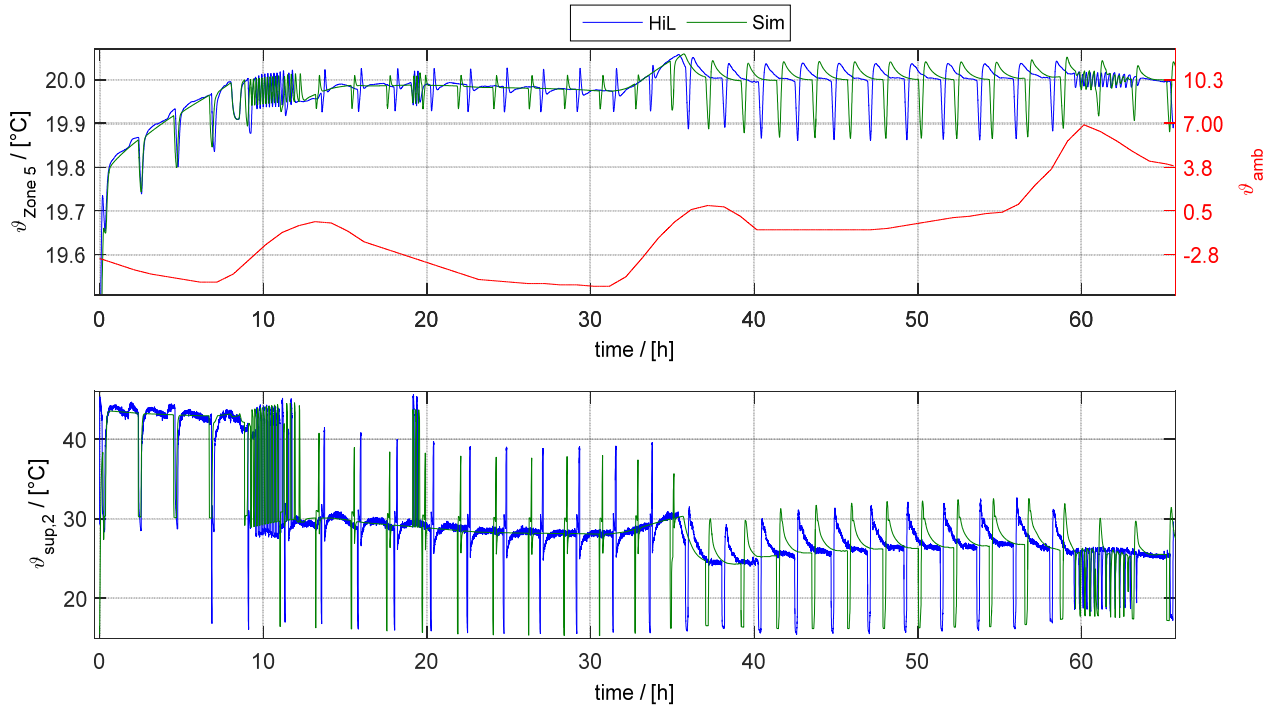

Figure 5-30: Comparison of the controlled and supply air temperatures between HiL simulation and Simulink simulation

Figure 5-31 shows the first hours of simulation, as it can be seen the Simulink and HiL simulations deliver close results. In the first instant the supply air temperatures are different because the integrator of the Simulink controller starts from zero while the integrator of the hardware controller cannot be reset to zero. The controlled temperature reaches the set point values almost in the same moment within the HiL and Simulink simulation and the supply air temperature has almost no deviation. It can be noticed that in the HiL simulation the de-icing interval are slightly longer than in the Simulink simulation this is due to the temperature-time control of the de-icing that is actually implemented while in the Simulink model only a time control is implemented.

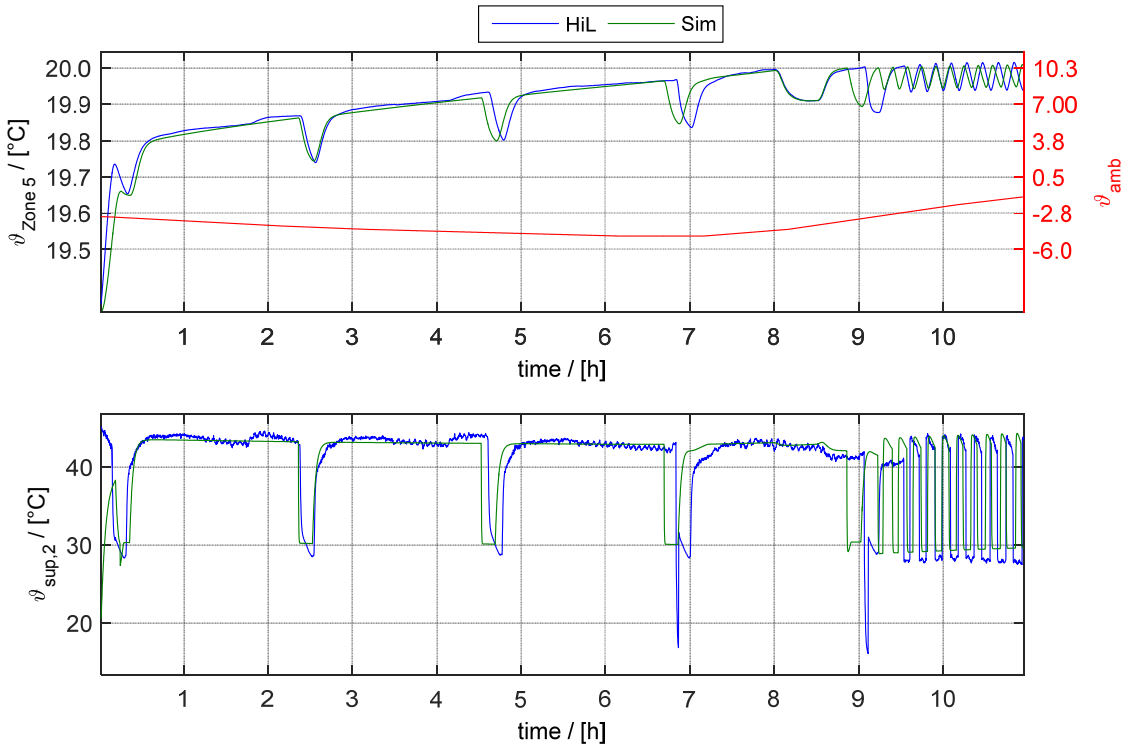

Figure 5-31: Zoom of the first hours of Figure 5-30

Figure 5-32 shows the comparison of the de-icing period around the hour 22. As it can be seen, the controlled temperature trend and the supply air trend over the de-icing period are similar.

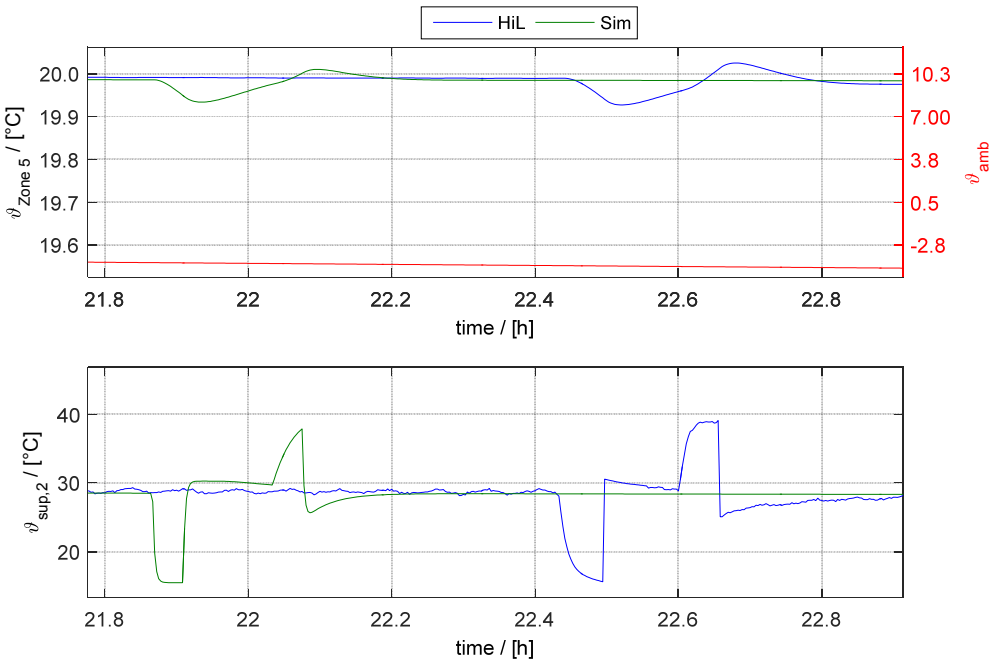

Figure 5-32: Zoom of the de-icing period of Figure 5-30

Figure 5-33 shows the period around the hour 59 where the heat pump does on/off cycles after the de-icing. Here can be noticed that both the hardware controller (used within the HiL simulation) and the Simulink controller model start the on/off cycles period almost in the same time.

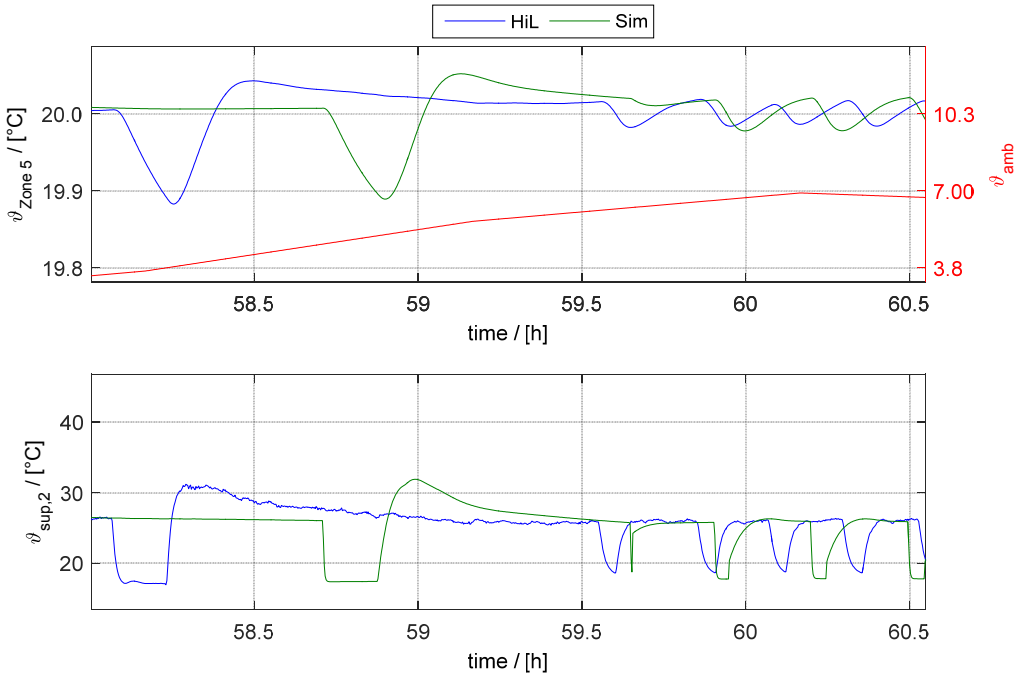

Figure 5-33: Zoom of last hours of Figure 5-30

From these results, it is possible to say that the heat pump controller model is able to simulate with quite high accuracy the real heat pump behaviour with the boundary conditions used in this scenario.

5.10.3 Analysis of the Energy Demand Calculation Accuracy

The energy demand calculation is explained in chapter 3.5.2. The comparison between the electric power measured during the HiL simulation and the electric power simulated with Simulink is reported in Figure 5-34. After the de-icing period, the electric power in Simulink falls to zero because during the de-icing the heat pump power is kept equal to zero and when the de-icing is finished, the power delivered by the heat pump increases but not immediately thanks to the time constant. This problem can be clearly seen in Figure 5-35. This aspect can be improved within the Simulink model.

The electric power simulated in Simulink is lower than the measured electric power because in Simulink the additional heater used in order to avoid the icing of the condensate created during the de-icing period is not considered. As it can be seen in Figure 5-35 when the de-icing period starts, the electric power increases because the compression work increases. When the de-icing period finishes the electric power demand is still higher with respect to the normal behaviour demand, this is due to the additional heater that is in operation for a time period longer than the de-icing period.

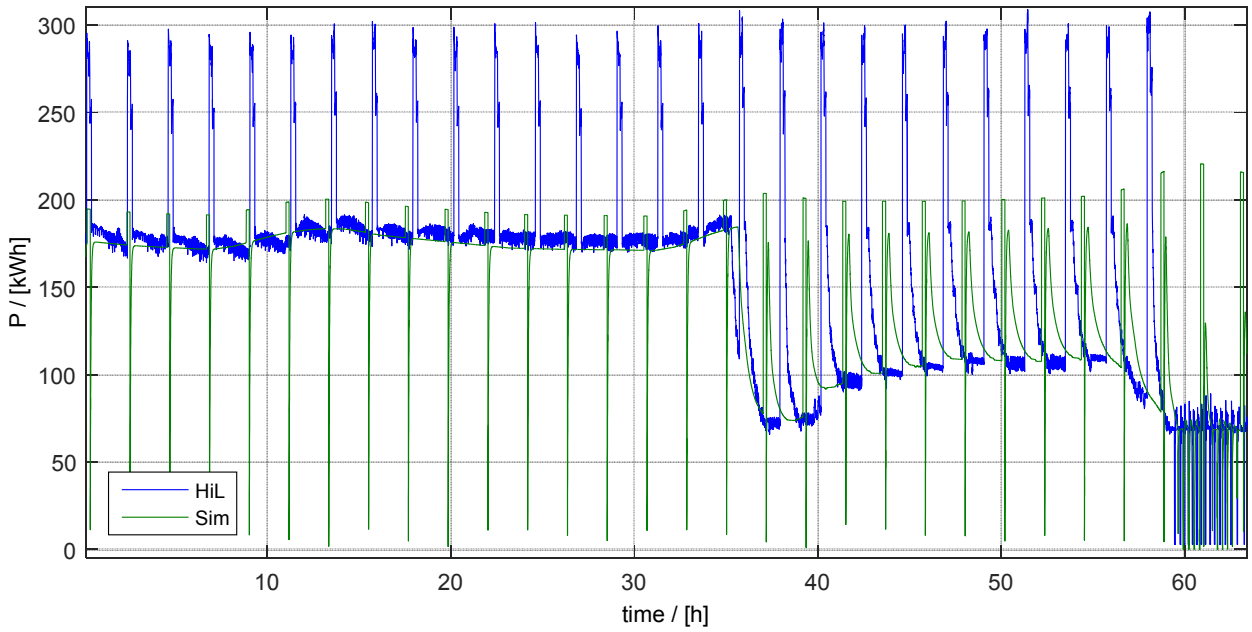

Figure 5-34: HiL and Simulink simulation electric power comparison

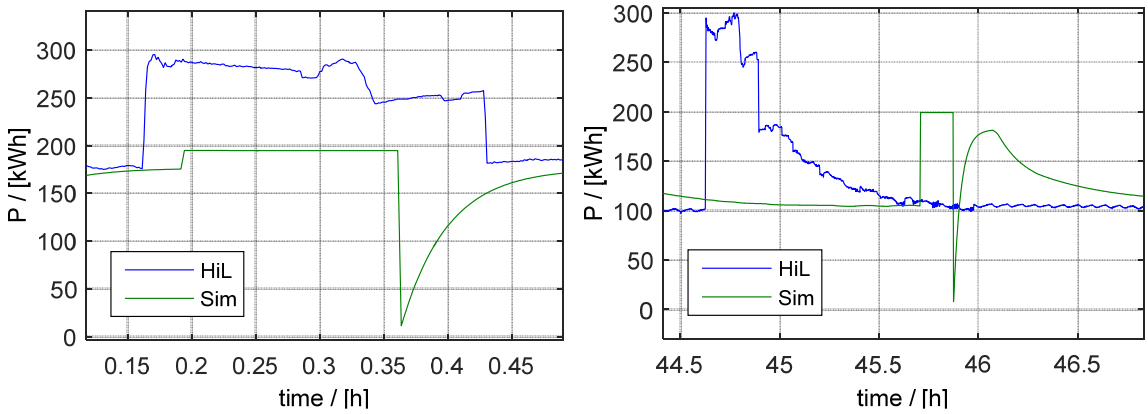

Figure 5-35: Zoom of two de-icing period of Figure 5-34

5.1 SCENARIO 5

5.1.1 Humidity Error

Within this scenario, the extract air humidity is used as input for the PASSYS test cell. The deviation between the extract air humidity and the test room humidity is reported in Figure 5-36. As it can be seen, the humidity inside the test room is always following the set point trend except for the highest peak around the hour 8 where the measured humidity is in delay with respect to the set point trend.

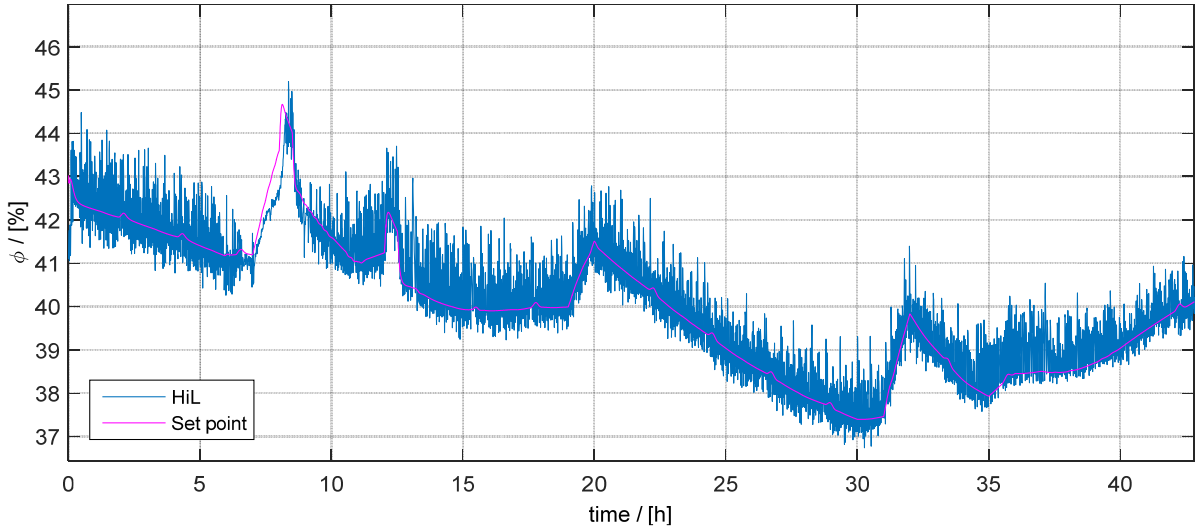

Figure 5-36: Comparison of the set point and test room relative humidity

5.1.2 Comparison of the Scenarios 4 and 5

In this section the comparison between the scenarios 4 and 5 is presented. Figure 5-37 shows the controlled temperature and the supply air temperature of the scenarios 4 and 5. As it can be observed, the scenario 5 has higher supply air temperature and for this reason, the controlled temperature increases faster compared to the scenario 4. Within the period from the hour 12 to 35, the controlled temperature is higher in the scenario 5 with respect to the scenario 4.

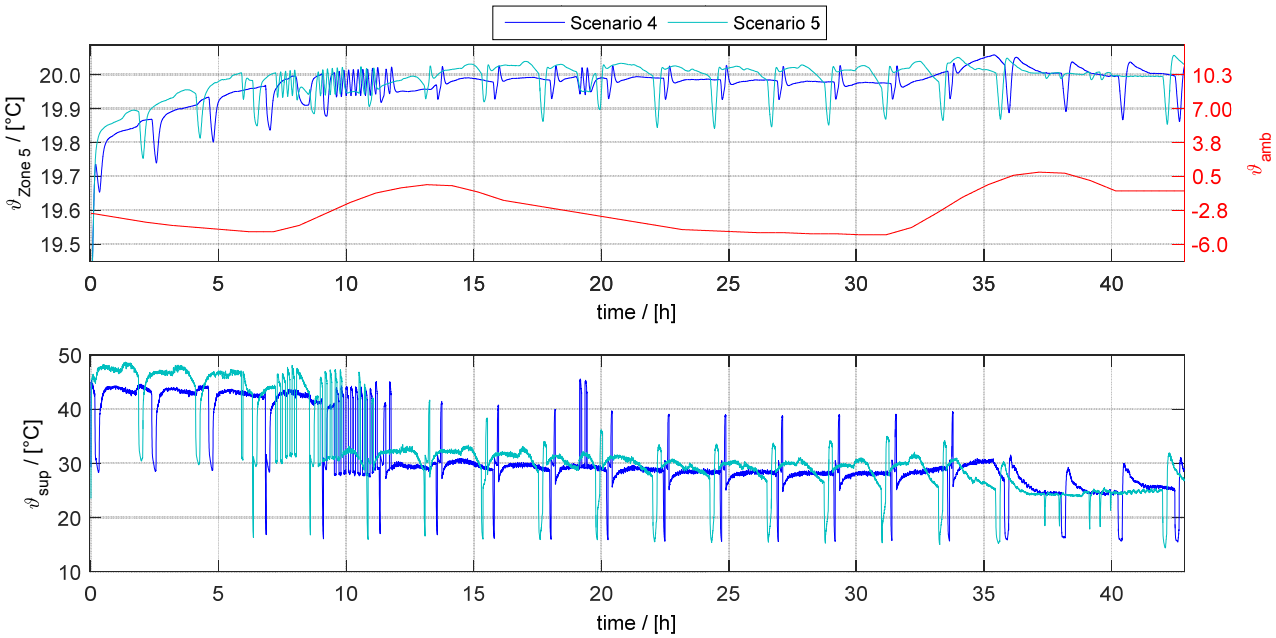

Figure 5-37: Comparison of the controlled temperature and supply air temperature

Figure 5-38 shows the comparison of the thermal power delivered by the heat pump and of the system frequency. Within the scenario 5, the heat pump delivers higher power. With higher humidity content, more condensate is created within the heat exchanger so the exhaust air has higher temperature. This means that the evaporator has higher power available and that the condenser is able to deliver higher thermal power to the supply airflow. In the previous scenarios, the extract air had a relative humidity around 20-25%, so even with low temperature it produces only a few amount of condensate.

In the period from the hour 16 to the hour 34, after the de-icing the system starts with the frequency of 150 Hz in the scenario 4 and 5. Within the scenario 5, the heat pump is able to deliver more power, so it quickly reaches the set point temperature than the controller lowers the set point frequency, while within the scenario 4 the system is kept to 150 Hz during the whole period. This effect cannot be simulated with the Simulink controller and heat pump model because the implemented lookup tables do not contain information regarding the heat pump behaviour with different level of relative humidity in the extract air. This aspect can be examined more into detail in further work.

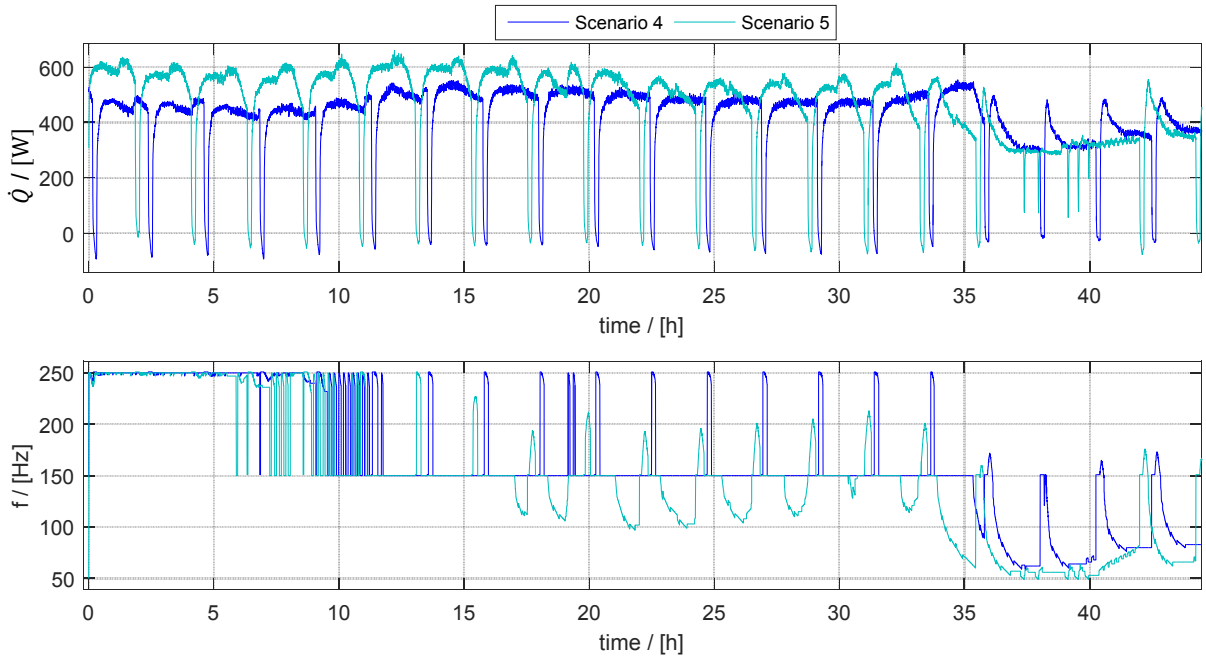

Figure 5-38: Comparison of the thermal power delivered by the heat pump and of the frequency between the scenarios 4 and 5.

Figure 5-39 shows the electric power demand of the heat pump for the scenarios 4 and 5. As it can be observed, the electric demand follows the frequency trend, so the power required by the heat pump with dry extract air (scenario 4) has different trend compared to the power required within the scenario 5.

The implemented Simulink model cannot predict the electric power required by the heat pump when the extract air has high level of relative humidity because the lookup table involved in the model does not contain enough information about the heat pump behaviour in these conditions.

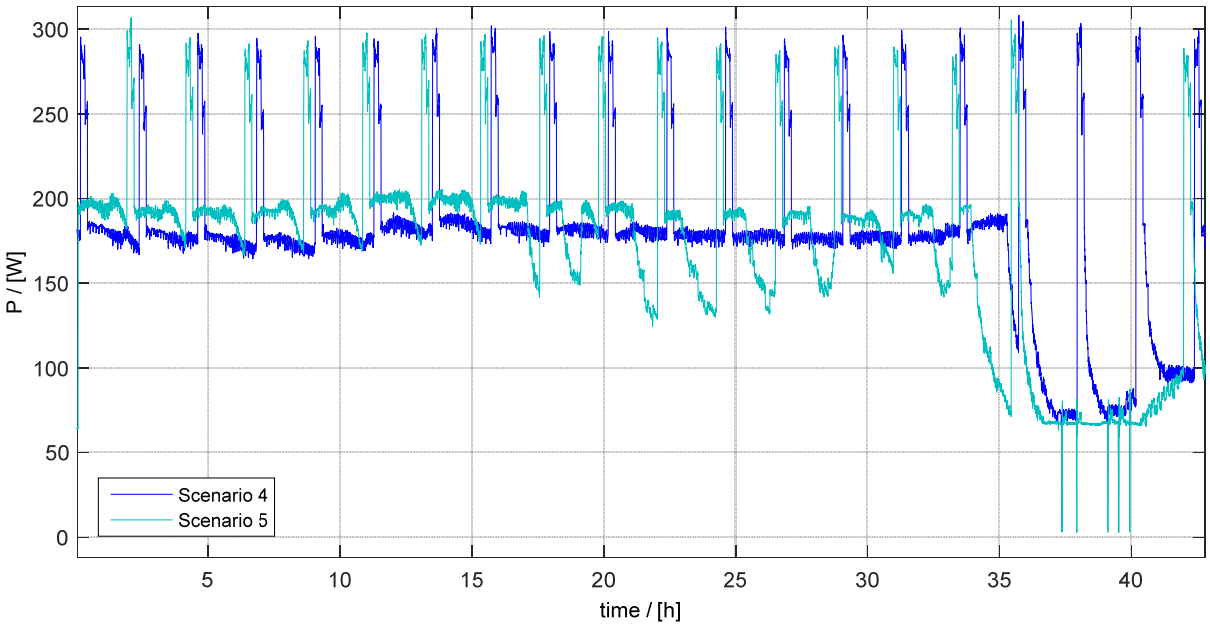

Figure 5-39: Electric power required by the heat pump

The energy demands of the heat pump for the scenarios 4 and 5, over the considered period of time, are listed in tables Table 5-12.

Table 5-12: Energy demand of the heat pump over the considered period for the scenario 4 and 5

	E / [kWh]
Scenario 4	7.65
Scenario 5	7.46

6 CONCLUSIONS AND OUTLOOK

The system controls parameters are determined by studying the open loop dynamic system response to an input disturbance. The Chien, Hrones and Reswick formulations are used in the determination of the proportional integrative control parameter. These formulations are defined for fast responding systems while the building is slow responding, so the PI parameter delivered from the Chien, Hrones and Reswick formulations are modified in order to ensure a good control. The hallway temperature is the controlled variable for the controller. Further investigations can be done in order to examine the case in which the extract air temperature is the controlled variable or the case in which the controlled variable is a floating temperature.

An optimization of the minimum runtime is carried out by running yearly simulations with different minimum runtimes and by comparing the number of on/off cycles, the number of under and over-heating hours, the $SCOP_{SYS}$ and the $SCOP_{HP}$.

The heating system and controller models are developed in this work. Both are based on the lookup tables of the studied system performances. By changing the data of the involved system with other data, it is possible to simulate other systems with the same model. From the comparison between the HiL and Simulink simulation the controller and heating system model are validated.

The performances of the heat pump with different ambient temperatures and fixed room temperature are determined by means of measurement within the PASSYS test cell and used in the lookup tables involved in the Simulink model. Other measurement can be done in order to have a more detailed performances map that involves also different extract air temperatures and humidity levels. Anyway, the ice formation on the evaporator cannot be predicted. The determination of the performances map is time consuming. In order to reduce the time required by this phase, automatic algorithms can be developed. With dry extract air, the accuracy of the results is not strictly dependent on the considered number of measured points.

The simple building model is implemented within this work and then compared with an already calibrated and validated complex model. The simple model is low time consuming and for the whole flat delivers energy demand with low deviations with respect to the complex building model results. Therefore, it can be used in order to estimate the results before to use the complex model. However, the simple model cannot be used when the air temperature fluctuations within the zones are studied. The simple model temperatures, change slowly because its calculation involves the whole zone capacity while the convective node temperature of the complex model responds quickly to the convective power balance

variations. For this reason, the complex model is used in the HiL simulations where the convective temperatures variations are essential in order to test the controller behaviour.

Hardware controller problems have been detected thanks to the HiL simulations. In the first scenario the limits of the conditional integration anti-windup are highlighted. In the fourth scenario, the error on the supply air temperature is reduced. This error is caused by the constant air volume flow implemented in the building model and the non-constant volume flow that actually occurs. Further model improvement can be done in order to ensure a variables volume flow.

The deviation of the test room and coldbox temperatures are studied and from the power balances can be seen that this deviations are not relevant with respect to the system power. The accuracy of the coldbox and test room temperatures is important in order to assure the accuracy of the HiL simulations.

In the last scenario, the heat pump behaviour with different air humidity level of the extract air is analysed. The condensation occurs inside the heat exchanger with high humidity level of the extract air. In this case, the temperature difference of the extract air over the heat exchanger is reduced and a higher power is available in the exhaust airflow for the heat pump evaporator. After the de-icing, the heat pump power is higher than in the cases without condensation. HiL can be used to study systems with high nonlinearities, like the ice formation on the evaporator.

APPENDIX 1: COMPARISON OF SIMPLE AND COMPLEX BUILDING MODEL

APPENDIX 1.1: INTRODUCTION

Within this work, both complex (chapter 2.3) and simple (chapter 2.2) building models are used. The complex model is based on the CARNOT toolbox and has been developed by (Siegele, 2013) and then calibrated and validated by means of comparation with measured data for the existing building (Leonardi, 2016). A simplified model has been developed within this work. A comparison between the yearly results of the simple and complex building models is done in order to test the accuracy of the simple model. This comparison is carried out by considering the same boundary conditions, building properties and heating system in both models. The heating system used in the comparison is based on ideal radiators. In the following section the building energy balances are analysed.

APPENDIX 1.2: HEATING DEMAND

Figure A1-1 shows the monthly heating demand differences for each zone for each month. These values are calculated for each zone *i* and for each month *j*, by doing the differences between the monthly energy demand of the complex and the simple model as it is shown in the equation (A1.1).

$$Q_{i,j} = Q_{i,j_{COMPLEX}} - Q_{i,j_{SIMPLE}} \qquad (A1.1)$$

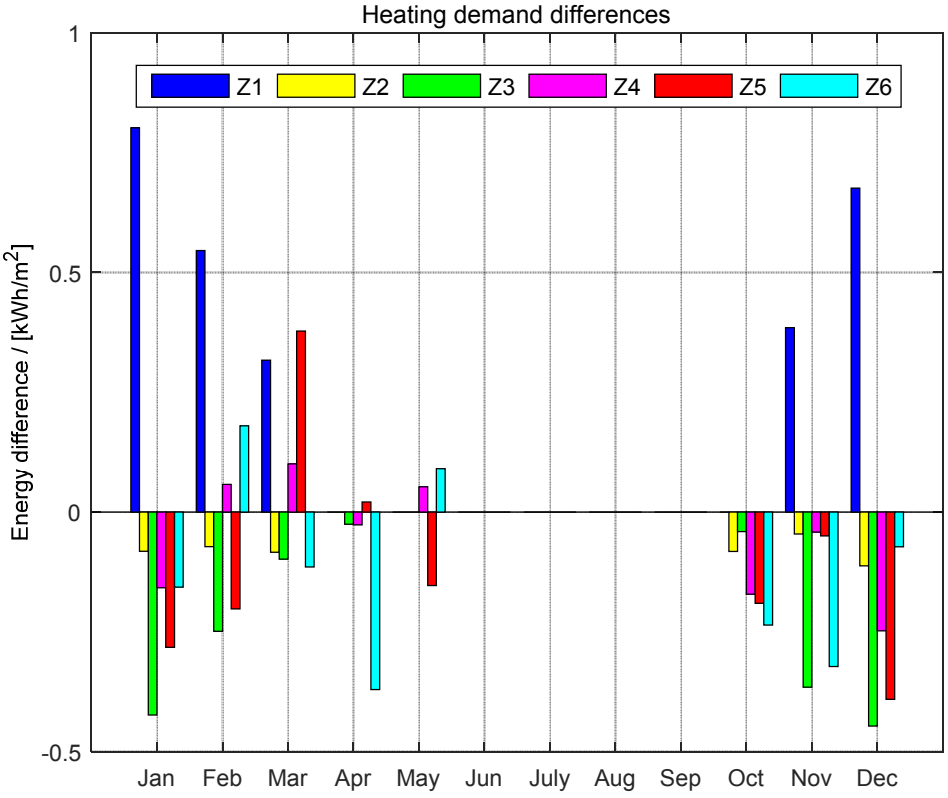

Figure A1-1: Monthly heating demand differences for each zone

The yearly differences for each zone and the total yearly difference for the whole flat are shown in Table A1-1. The zone coupling is probably not perfect in the simple model due to the required simplifications, but the yearly balance for the whole flat delivers good results. The deviation of the simple model is less than 3% with respect to the yearly energy demand of the complex model $\left(14.0\ \left[\frac{\mathrm{kWh}}{\mathrm{m^2\ a}}\right]\right)$.

Table A1-1: Yearly energy demand differences

	Yearly heating demand Complex model	Yearly heating demand simple model	Yearly heating demand differences
Zone 1 $\left[\frac{\mathrm{kWh}}{\mathrm{m^2\ A}}\right]$	9.42	6.69	2.73
Zone 2 $\left[\frac{\mathrm{kWh}}{\mathrm{m^2\ a}}\right]$	7.64	8.11	-0.47
Zone 3 $\left[\frac{\mathrm{kWh}}{\mathrm{m^2\ a}}\right]$	13.0	14.6	-1.65
Zone 4 $\left[\frac{\mathrm{kWh}}{\mathrm{m^2\ a}}\right]$	25.5	25.9	-0.44
Zone 5 $\left[\frac{\mathrm{kWh}}{\mathrm{m^2\ a}}\right]$	15.1	15.9	-0.86
Zone 6 $\left[\frac{\mathrm{kWh}}{\mathrm{m^2\ a}}\right]$	31.4	32.4	-1,.00
Total $\left[\frac{\mathrm{kWh}}{\mathrm{m^2\ a}}\right]$	**14.0**	**14.5**	**-0.42**

Table A1-2 shows the monthly heating demands for the whole flat. As it can be observed, the differences for the whole flat are small. In April, May and October, the relative deviations are high but the absolute values are small.

The simple model is useful because it takes few minutes to run a yearly simulation, so it can be used in order to estimate the results before to runtime-consuming simulation with a complex model.

Table A1-2: Monthly balances over the whole flat

	Monthly heating demand complex $\left[\frac{kWh}{m^2\ a}\right]$	Monthly heating demand simple $\left[\frac{kWh}{m^2\ a}\right]$	Monthly heating demand differences $\left[\frac{kWh}{m^2\ a}\right]$	% Deviation
Jan	3.79	3.88	**-0.0862**	2.27
Feb	2.93	2.94	**-0.0122**	0.416
Mar	1.68	1.64	**+0.0391**	2.33
Apr	0.117	0.153	**-0.0359**	30
May	0.0184	0.0217	**-0.0033**	17.93
Jun	0	0	**0**	
July	0	0	**0**	
Aug	0	0	**0**	
Sept	0	0	**0**	
Oct	0.118	0.206	**-0.0876**	74.3
Nov	1.97	2.07	**-0.101**	5.13
Dec	3.40	3.54	**-0.135**	3.97

APPENDIX 1.3: STRUCTURES MODEL

The complex model has been modified within this work. In particular, the structure block has been changed with a simplified structure with a fixed number of layers. The number of layers and the subdivision of the wall layers are important factors in matter of accuracy. In this section, the temperature profiles inside the wall with different wall subdivisions are analysed and compared. The wall properties are reported in Table A1-3. The layers 1 and 7 are the external and internal plaster, the layer 6 is the brick layer and the layers 2, 3, 4 and 5 are insulation layers.

Table A1-3: Wall properties from the external to the internal layer

	Layers						
	1	2	3	4	5	6	7
d [m]	0.035	0.3	0.015	0.06	0.06	0.24	0.01
$\lambda \left[\frac{W}{m^2 K}\right]$	0.08	0.049	0.2	0.04	0.06	0.7	1
$R \left[\frac{m^2 K}{W}\right]$	0.438	6.122	0.0750	1.50	1.00	0.343	0.01
$c \left[\frac{J}{kg K}\right]$	2500	753.6	1700	600	1000	900	900
$\rho \left[\frac{kg}{m^3}\right]$	300	93.2	650	50	50	1400	1400
Capacity $\left[\frac{J}{m^2 K}\right]$	26250	21071	16575	1800	3000	302400	12600

Figure A1-2 shows the different kinds of analysed wall subdivision. The blue layers correspond to insulation materials, the red layer corresponds to the brick and the pink layers correspond to the plaster. In the cases 1, 2 and 3 the wall is subdivided in two layers with three capacities, while in the case 4 the wall is divided in 7 layers with 8 capacities. Over the considered cases, the total wall capacity (383700 $\left[\frac{J}{m^2 K}\right]$) and the total wall resistance (9.488 $\left[\frac{m^2 K}{W}\right]$) are constant.

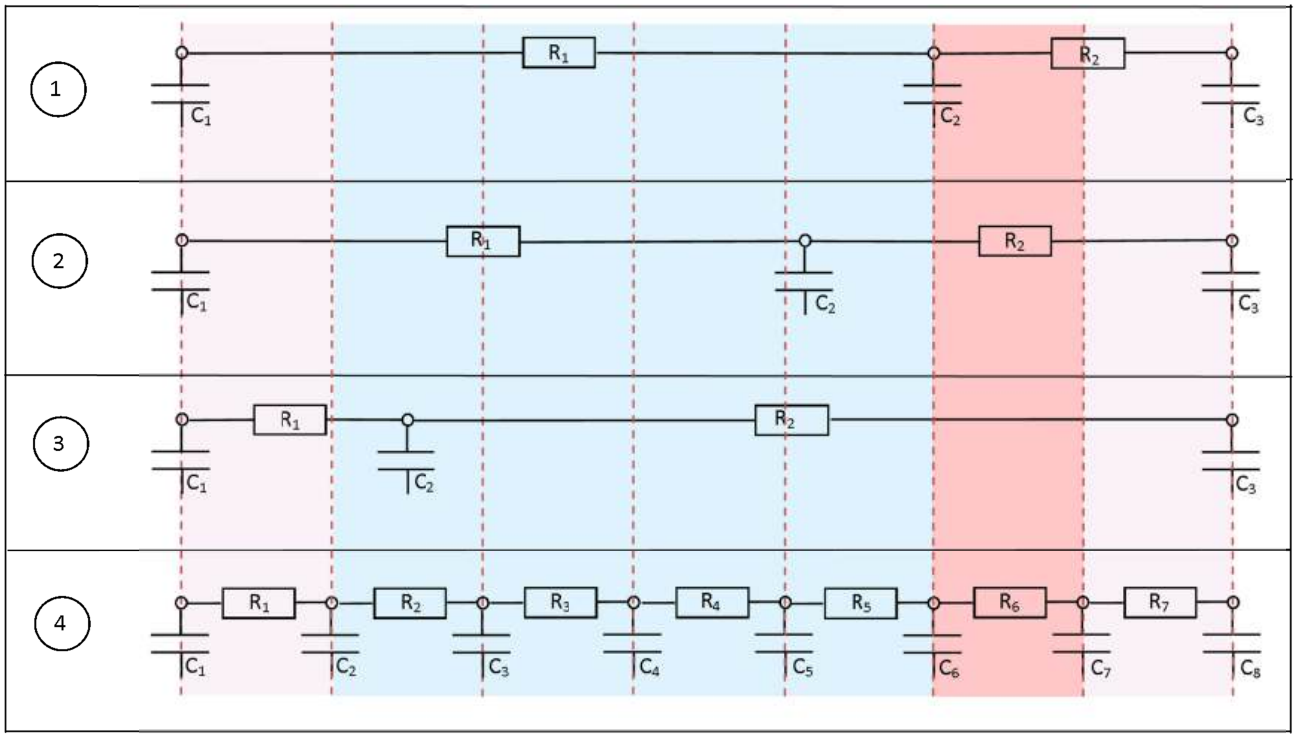

Figure A1-2: Wall subdivisions for the four analysed cases

Table A1-4 shows the capacities and resistances values for each case. Since the case 4 involves the higher number of layers, it is the most accurate between the considered cases. The accuracy of the results can be increased by considering more wall layers.

Table A1-4: Capacities and resistance values for each case

Cases	*Capacities* $\left[\frac{J}{m^2 K}\right]$	*Resistances* $\left[\frac{m^2 K}{W}\right]$	*Layers position* $[m]$
1	$C1 = 34348$ $C2 = 191850$ $C3 = 157500$	$R1 = 9.135$ $R2 = 0.353$	*d1=0.47* *d2=0.25*
2	$C1 = 32337$ $C2 = 191850$ $C3 = 159510$	$R1 = 8.251$ $R2 = 1.237$	*d1=0.423* *d2=0.297*
3	$C1 = 18393$ $C2 = 191850$ $C3 = 173460$	$R1 = 3.499$ $R2 = 5.989$	*d1=0.185* *d2=0.5350*
4	$C1 = 13125$ $C2 = 23660$ $C3 = 18823$ $C4 = 9188$ $C5 = 2400$ $C6 = 152700$ $C7 = 157500$ $C8 = 6300$	$R1 = 0.438$ $R2 = 6.122$ $R3 = 0.0750$ $R4 = 1.50$ $R5 = 1.00$ $R6 = 0.343$ $R7 = 0.01$	*d1=0.035* *d2=0.30* *d3=0.015* *d4=0.060* *d5=0.060* *d6=0.240* *d7=0.010*

The different wall discretization are tested by using an external temperature with a step and a constant internal temperature. These boundary conditions are shown in Figure A1-3. The wall model is used in the two star model so two internal temperature are present ($\vartheta_{radiative}$ and $\vartheta_{convective}$).

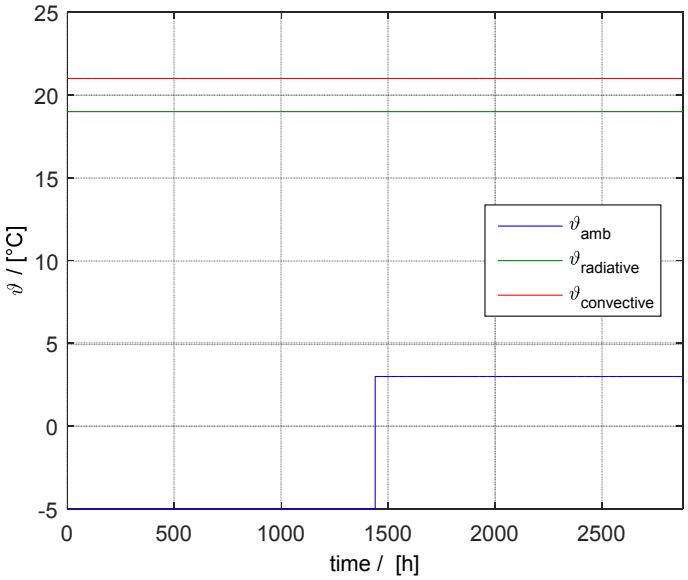

Figure A1-3: Boundary conditions

Figure A1-4 shows the temperature profiles in the wall for each case before the step. The wall is at the steady state so each model has the same heat losses. In fact, the internal and external surface temperatures are the same for each model, but the temperature profiles are different. As it can be seen in Figure A1-4 the case 1 has the best agreement with the case 4. The wall layers are represented by the magenta dotted lines.

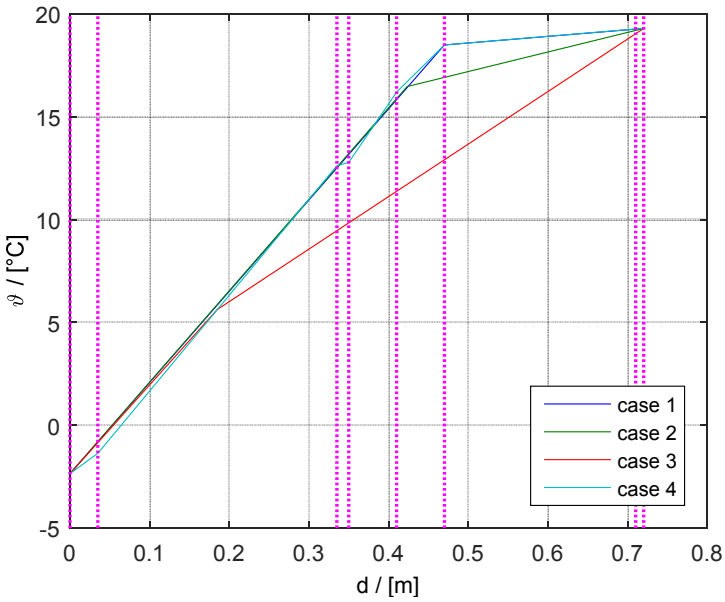

Figure A1-4: Temperature profiles in the wall before the step

Figure A1-5 shows the temperature profile for each case after 5.83 hours from the step. Since the wall is not in the steady state, the heat losses are not the same in each case in fact the external surface temperatures are not equal.

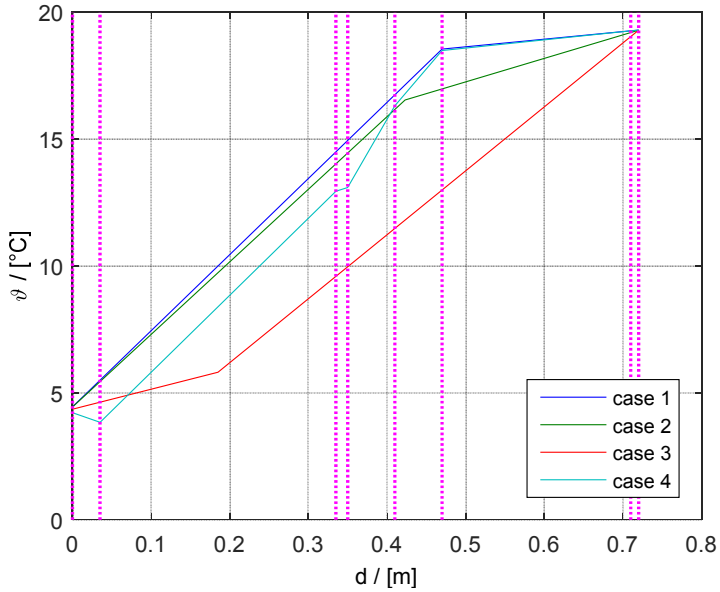

Figure A1-5: Temperature profiles in the wall after 5.83 hours from the step

The temperature profiles after 60 days from the step are shown in Figure A1-6, where new steady state conditions are reached.

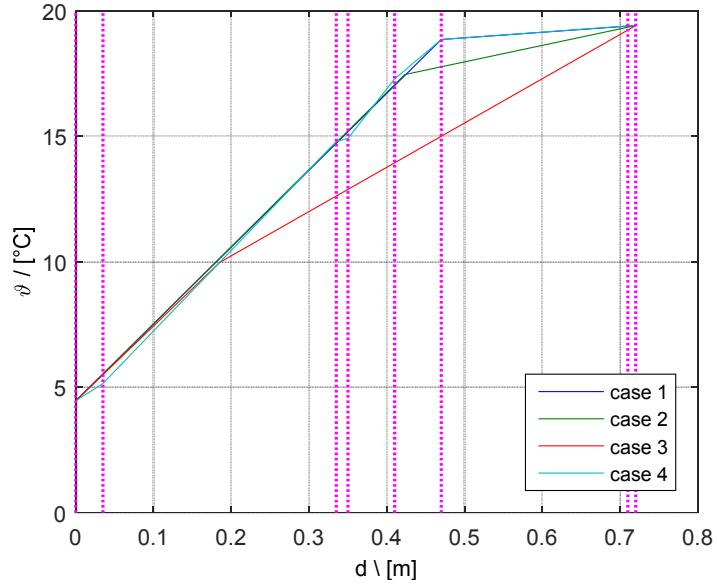

Figure A1-6: Temperature profiles after 60 days from the step (new steady state is reached)

The case 1 has the better agreement with the more accurate case 4 in each time step.

Figure A1-7 shows the different dynamic behaviour of the four cases. As for the temperature profiles, again the case 1 has the best agreement with the case 4. The heat losses in the steady state are the same for each case, while the dynamic behaviours are different as it can

be seen in Figure A1-7. The dynamic behaviour depends on where the capacities are placed and which values are given to the resistances. In the case 1, all the insulation is considered in the resistance R1 while in the case 2 and 3 a part of insulation is included in the resistance R2. For this reason, the cases 2 and 3 have slower response with respect to the cases 1 and 4.

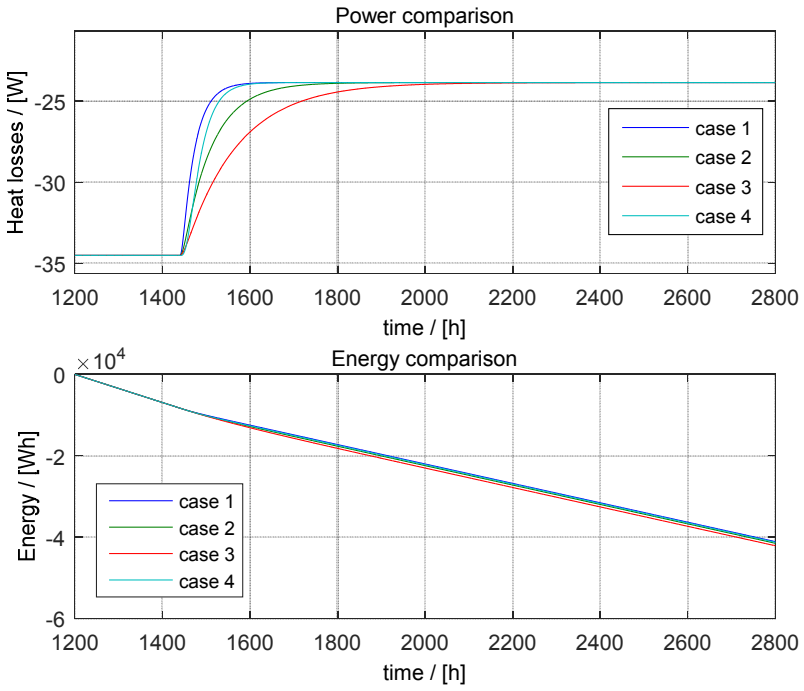

Figure A1-7: Heat losses (power and energy) through the studied wall

After this analysis, it is possible to conclude that the discretization used in the case 1 is the most suitable for the dynamic simulation.

APPENDIX 2: ERROR ANALYSIS OF THE HIL SIMULATIONS

APPENDIX 2.1: SCENARIO 2

APPENDIX 2.1.1: Test Room Temperature error

Figure A2-1 shows the comparison between the test room temperature (blue) and the test room set point temperature (magenta) that corresponds to the extract air temperature, measured in the scenario 1. As it can be observed, the test room temperature has some oscillations when the backup heater or the heat pump change quickly their power. This can happen when the heat pump and the backup heater are doing on/off cycles or when the heat pump in the de-icing period.

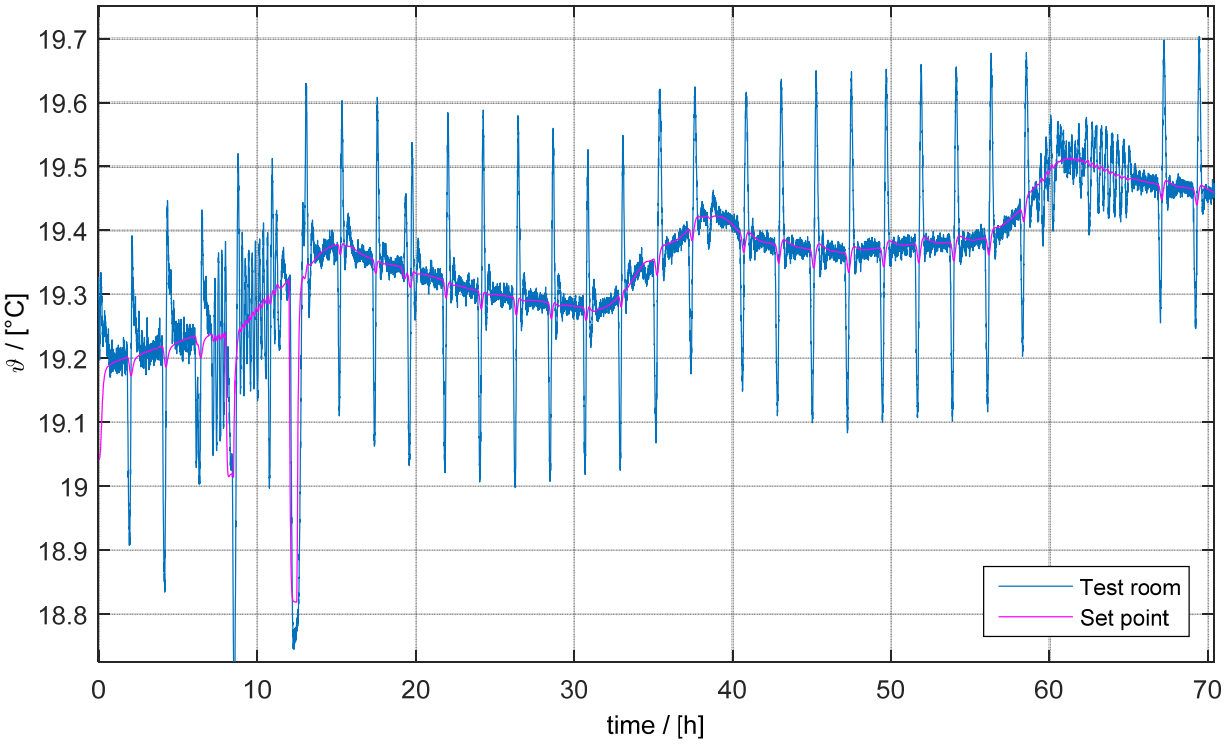

Figure A2-1: Comparison of the measured and set point temperature of the test room (scenario 2)

Table A2-1 shows the maximum, mean and minimum value of $\dot{Q}_{diff,tr}$ and $\dot{Q}_{set\ point,tr}$ calculated according to the equations (5.7), (5.8) and (5.9). The mean value of $\dot{Q}_{diff,tr}$ and $\dot{Q}_{set\ point,tr}$ are calculated by considering the absolute values.

Table A2-1: Maximum, mean and minimum value of $\dot{Q}_{diff,tr}$ and $\dot{Q}_{set\ point,tr}$ for the balance over the test room (scenario 2)

	$\dot{Q}_{diff,tr}$ [W]	$\dot{Q}_{set\ point,tr}$ [W]
Max	10.74	865.91
Mean	1.49	310.43
Min	-15.48	-136.17

The energy can be obtained by integration of the powers over the considered period, as it is shown in the equations (5.10), (5.11) and (5.12), and these values are listed in Table A2-2.

Table A2-2: Energy values of the balance over the test room (scenario 2)

	Q_{tr} [Wh]
$Q_{set\ point,tr}$	21381.1
$Q_{mea,tr}$	21380.9
$Q_{diff,tr}$	0.20

The balance already explained in section 5.5.1 is now applied to the most critical point around the hour 12.5. Figure A2-2 shows the zoom of the Figure A2-1 around the hour 12.5.

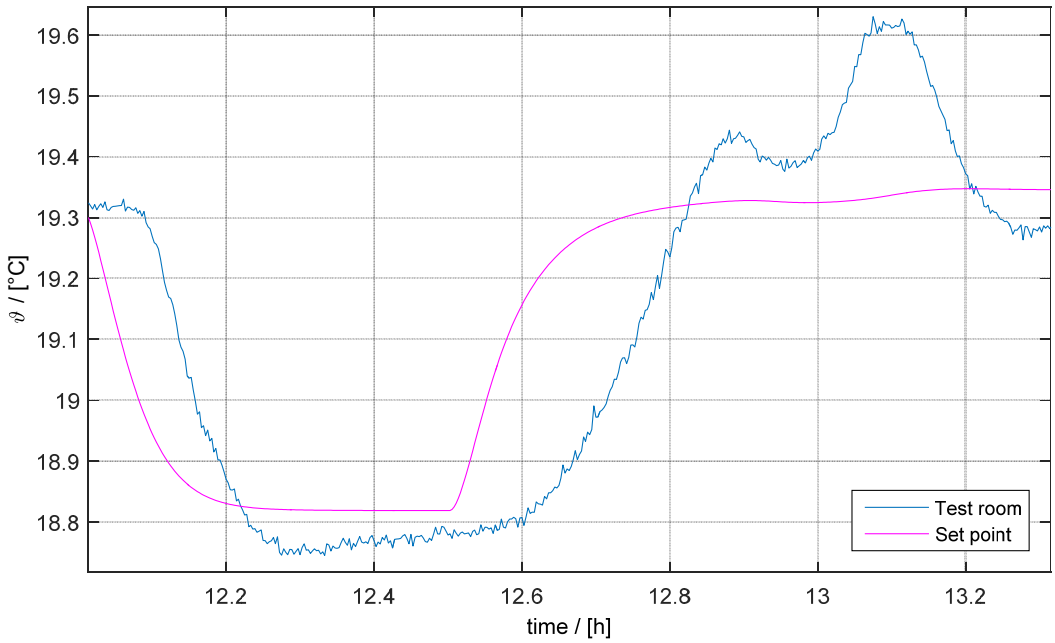

Figure A2-2: Zoom of Figure 5-15

With the equations (5.7), (5.8) and (5.9) the power differences are calculated and the results are shown in the Table A2-3. The mean value of $\dot{Q}_{diff,tr}$ and $\dot{Q}_{set\ point,tr}$ are calculated by considering the absolute values.

Table A2-3: Maximum, mean and minimum value of $\dot{Q}_{diff,tr}$ and $\dot{Q}_{set\ point,tr}$ for a section of period of the scenario 2

	$\dot{Q}_{diff,tr}$ [W]	$\dot{Q}_{set\ point,tr}$ [W]
Max	10.73	720.16
Mean	4.49	341.00
Min	-12.48	-86.50

The energy values can be obtained by integration of the powers, as shown in the equations (5.10), (5.11) and (5.12), and these values are listed in Table A2-4.

Table A2-4: Energy values of the balance over the test room for a section of period of the scenario 2

	Q_{tr} [Wh]
$Q_{set\ point,tr}$	443.79
$Q_{meas,tr}$	444.10
$Q_{diff,tr}$	-0.31

From these results, it is possible to conclude that the temperature deviations, occur in the test room are not significant in the considered case.

APPENDIX 2.1.2: Coldbox Temperature Error

Figure A2-3 shows the measured and the set point coldbox temperatures.

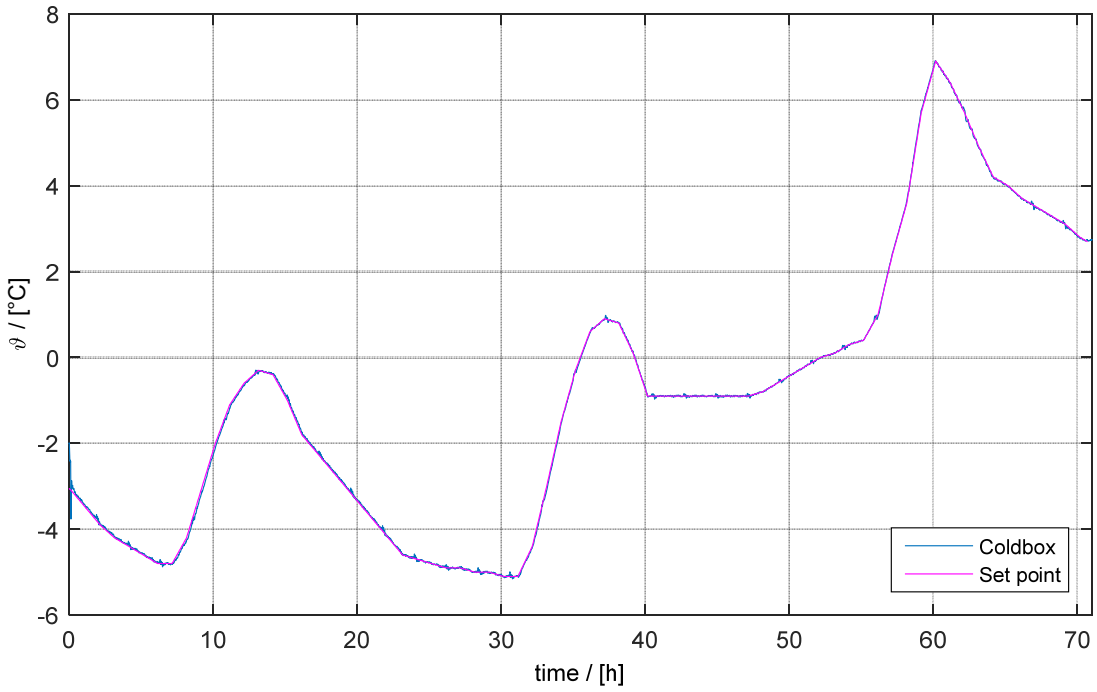

Figure A2-3: Comparison of the measured and set point temperature of the Coldbox for the scenario 2

Table A2-5 shows the maximum, mean and minimum values of $\dot{Q}_{diff,cb}$ and $\dot{Q}_{set\ point,cb}$. The mean value of $\dot{Q}_{diff,cb}$ is calculated by considering the absolute values.

Table A2-5: Maximum, mean and minimum value of $\dot{Q}_{diff,cb}$ and $\dot{Q}_{set\ point,cb}$ for the balance over the coldbox (scenario 2)

	$\dot{Q}_{diff,cb}$ [W]	$\dot{Q}_{set\ point,cb}$ [W]
Max	0.962	1159.7
Mean	0.122	473.4
Min	-0.980	0

The energy values can be obtained by integration of the powers, as it is shown in the equations (5.16), (5.17) and (5.18), and these values are listed in Table A2-6.

Table A2-6: Energy values of the balance over the coldbox (scenario 2)

	$Q_{diff,cb}$ [Wh]
$Q_{set\ point,cb}$	33479.4
$Q_{meas,cb}$	33479.7
$Q_{diff,cb}$	-0.30

From these results, it is possible to conclude that the coldbox temperatures deviations are not significant in the considered case.

APPENDIX 2.1.3: Total Error

$\dot{Q}_{set\ point}$, $\dot{Q}_{meas}$ and $\dot{Q}_{diff}$ are calculated by means of the equations (5.19), (5.20) and (5.21). The maximum, minimum and mean value of $\dot{Q}_{diff}$ and of $\dot{Q}_{set\ point}$ are shown in Table A2-7. The mean value of $\dot{Q}_{diff}$ is calculated by considering the absolute values.

Table A2-7: Maximum, mean and minimum value of $\dot{Q}_{diff}$ and $\dot{Q}_{set\ point}$ for the scenario 2

	$\dot{Q}_{diff}$ [W]	$\dot{Q}_{set\ point}$ [W]
Max	15.49	328.51
Mean	1.50	171.95
Min	-10.99	58.48

The energy values can be obtained by integration of the powers, as it is shown in the equations (5.22), (5.23) and (5.24) and these values are listed in Table A2-8.

Table A2-8: Energy values calculated from the whole balance for the scenario 2

	Q_{diff} [Wh]
$Q_{set\ point}$	12110.5
Q_{meas}	12111.2
Q_{diff}	-0.70

The overall error calculated during the three day of the HiL simulations is minor compared with the involved powers, so the set point temperatures are reproduced with high accuracy inside the coldbox and the test room.

APPENDIX 2.1.4: Power Deviation

The comparison between the real power produced by the heating system in the PASSYS test cell and the power used in the Simulink model during the HiL simulation is shown in Figure A2-4. The powers are calculated with the equations (5.25) and (5.26).

The mean power values and the relative deviation are reported in Table A2-9.

Table A2-9: HiL and real power comparison for the scenario 2

	$\dot{Q}$ [W]
HiL	507.2 (7.4%)
Real	472.4

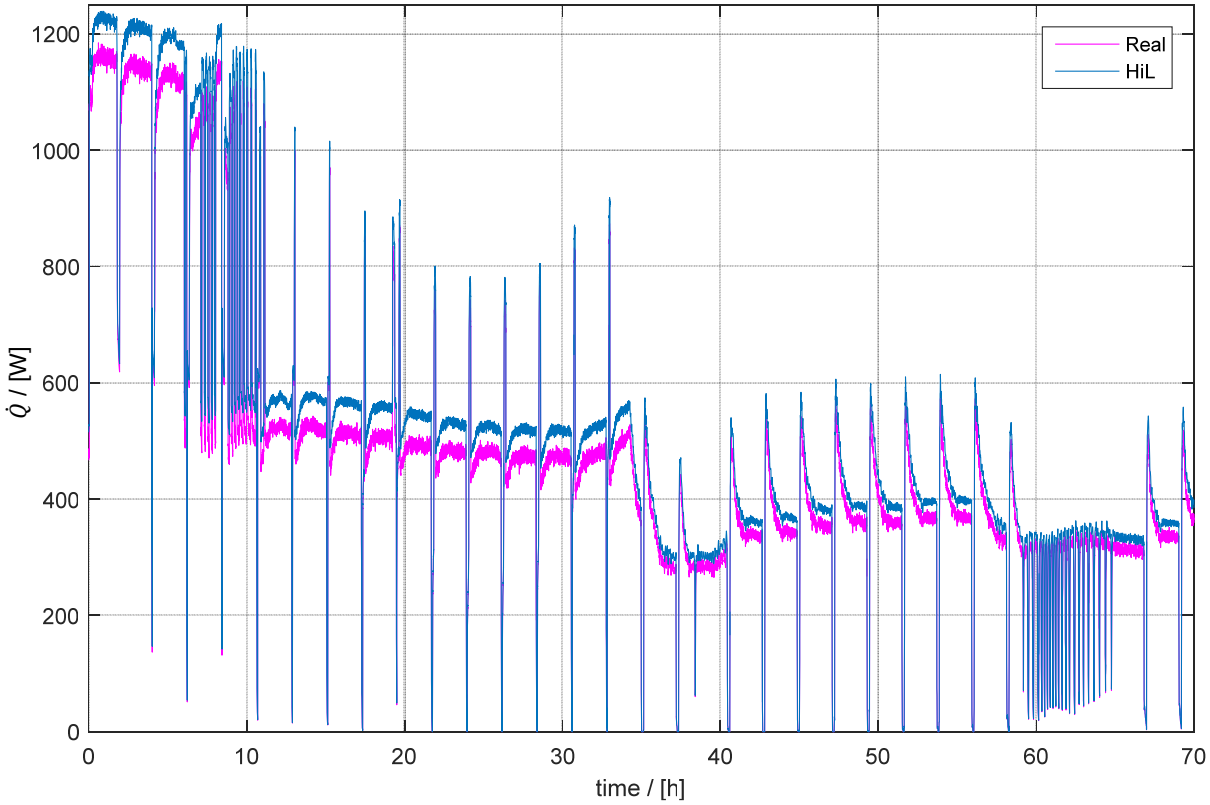

Figure A2-4: HiL simulation and real heating system powers

APPENDIX 2.2: SCENARIO 4

APPENDIX 2.1.1: Test Room Temperature error

Figure A2-5 shows the comparison between the test room temperature (blue) and the test room set point temperature (magenta) that corresponds to the extract air temperature, measured in the scenario 4.

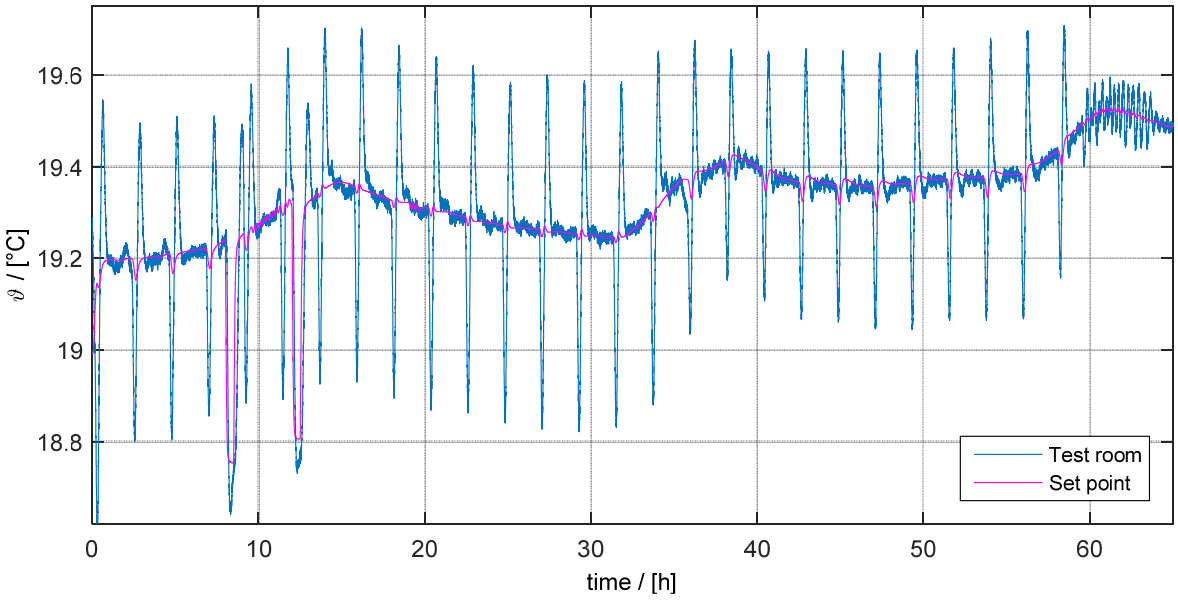

Figure A2-5: Comparison of the measured and set point temperature of the test room (scenario 4)

Table A2-10 shows the maximum, mean and minimum value of $\dot{Q}_{diff,tr}$ and $\dot{Q}_{set\ point,tr}$ calculated according to the equations (5.7), (5.8) and (5.9). The mean value of $\dot{Q}_{diff,tr}$ and $\dot{Q}_{set\ point,tr}$ are calculated by considering the absolute values.

Table A2-10: Maximum, mean and minimum value of $\dot{Q}_{diff,tr}$ and $\dot{Q}_{set\ point,tr}$ for the balance over the test room (scenario 4)

	$\dot{Q}_{diff,tr}$ [W]	$\dot{Q}_{set\ point,tr}$ [W]
Max	12.31	894.60
Mean	2.0911	332.4590
Min	-17.75	-126.39

The energy can be obtained by integration of the powers over the considered period, as it is shown in the equations (5.10), (5.11) and (5.12), and these values are listed in Table A2-11.

Table A2-11: Energy values of the balance over the test room (scenario 4)

	Q_{tr} [Wh]
$Q_{set\ point,tr}$	21407.6
$Q_{mea,tr}$	21408.4
$Q_{diff,tr}$	-0.80

The balance already explained in section 5.5.1 is now applied to the most critical point around the hour 12.5. Figure A2-6 shows the zoom of Figure A2-5 around the hour 12.5.

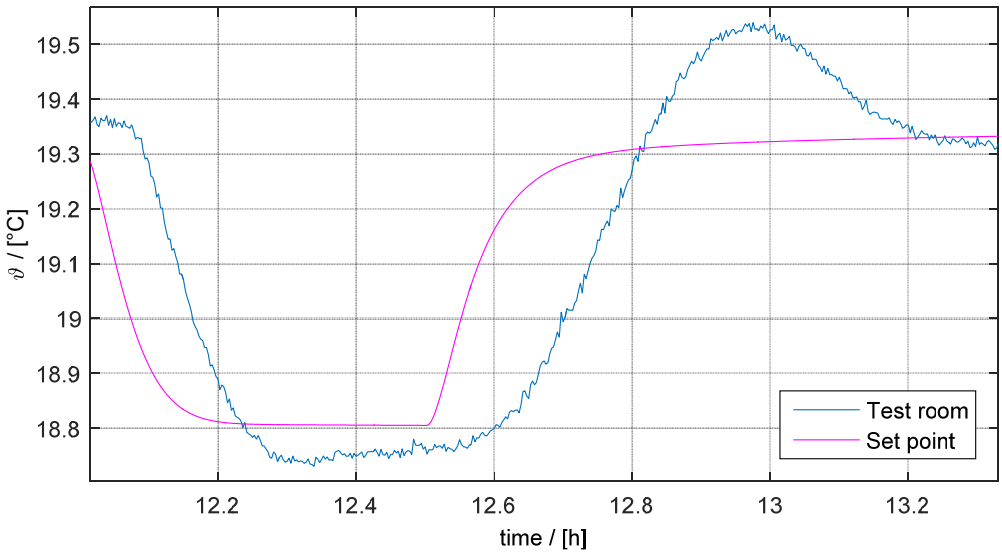

Figure A2-6: Zoom of Figure A2-5

With the equations (5.7), (5.8) and (5.9) the power differences are calculated and the results are listed in Table A2-12: Maximum, mean and minimum value of $\dot{Q}_{diff,tr}$. The mean value of $\dot{Q}_{diff,tr}$ and $\dot{Q}_{set\ point,tr}$ are calculated by considering the absolute values.

Table A2-12: Maximum, mean and minimum value of $\dot{Q}_{diff,tr}$ for a section of period of the scenario 4

	$\dot{Q}_{diff,tr}$ [W]	$\dot{Q}_{set\ point,tr}$ [W]
Max	12.30	369.70
Mean	4.40	322.11
Min	-12.24	279.70

The energy values can be obtained by integration of the powers, as shown in the equations (5.10), (5.11) and (5.12), and these values are listed in Table A2-13.

Table A2-13: Energy of the balance over the test room for a section of period of the scenario 4

	Q_{tr} [Wh]
$Q_{set\ point,tr}$	424.07
$Q_{meas,tr}$	423.82
$Q_{diff,tr}$	0.25

From these results, it is possible to conclude that the temperatures deviations which occur in the test room are not significant in the considered case.

APPENDIX 2.2.2: Coldbox Temperature Error

Figure A2-7 shows the measured and the set point coldbox temperatures.

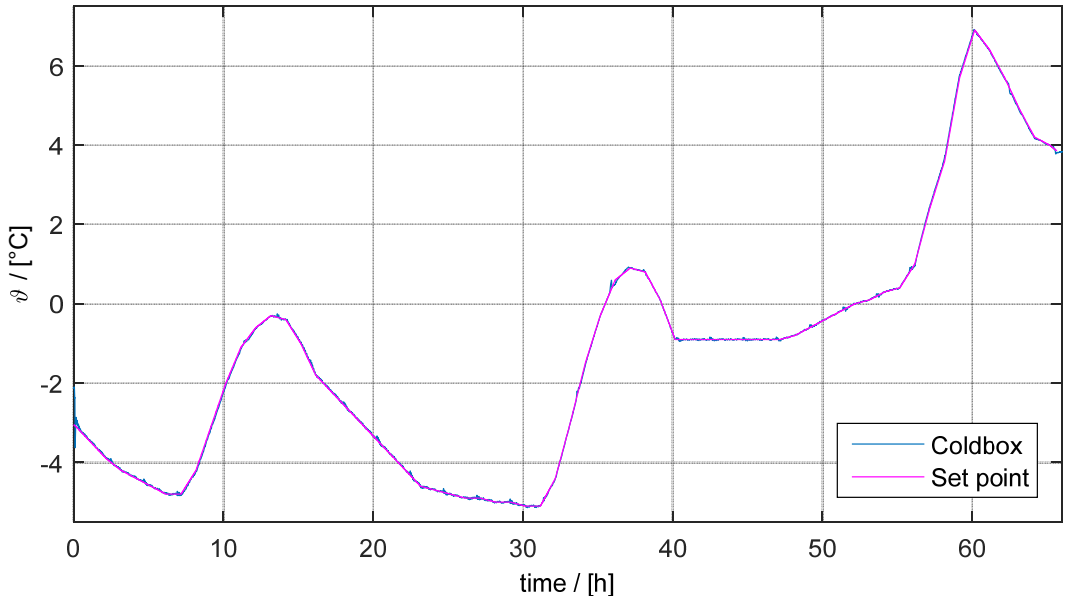

Figure A2-7: Comparison of the measured and set point temperature of the Coldbox for the scenario 4

Table A2-14 shows the maximum, mean and minimum values of $\dot{Q}_{diff,cb}$ and $\dot{Q}_{set\ point,cb}$. The mean value of $\dot{Q}_{diff,cb}$ is calculated by considering the absolute values.

Table A2-14: Maximum, mean and minimum value of $\dot{Q}_{diff,cb}$ and $\dot{Q}_{set\ point,cb}$ for the balance over the coldbox (scenario 4)

	$\dot{Q}_{diff,cb}$ [W]	$\dot{Q}_{set\ point,cb}$ [W]
Max	0.939	1159.9
Mean	0.108	506.4
Min	-0.8207	0

The energy values can be obtained by integration of the powers, as it is shown in the equations (5.16), (5.17) and (5.18), and these values are listed in Table A2-15.

Table A2-15: Energy values of the balance over the coldbox (scenario 4)

	$Q_{diff,cb}$ [Wh]
$Q_{set\ point,cb}$	33240.5
$Q_{meas,cb}$	33239.6
$Q_{diff,cb}$	0.90

As for the other scenarios it is possible to conclude that the coldbox temperatures deviations are not significant in the considered case.

APPENDIX 2.2.3: Total Error

$\dot{Q}_{set\ point}$, $\dot{Q}_{meas}$ and $\dot{Q}_{diff}$ are calculated by means of the equations (5.19), (5.20) and (5.21). The maximum, minimum and mean value of $\dot{Q}_{diff}$ and of $\dot{Q}_{set\ point}$ are shown in Table A2-16.

Table A2-16: Maximum, mean and minimum value of $\dot{Q}_{diff}$ and $\dot{Q}_{set\ point}$ the scenario 4

	$\dot{Q}_{diff}$ [W]	$\dot{Q}_{set\ point}$ [W]
Max	17.74	358.62
Mean	2.13	180.23
Min	-12.43	59.09

The energy values can be obtained by integration of the powers, as it is shown in the equations (5.22), (5.23) and (5.24) and these values are listed Table A2-17.

Table A2-17: Energy values calculated from the whole balance for the scenario 4

	$Q_{diff,cb}$ [Wh]
$Q_{set\ point}$	11830.0
Q_{meas}	11828.2
Q_{diff}	1.8

The overall error calculated during the three day of the HiL simulation is minor compared to the involved powers, so the set point temperatures are reproduced with high accuracy inside the cold box and the test room.

APPENDIX 2.3: SCENARIO 5

APPENDIX 2.3.1: Test Room Temperature error

Figure A2-8 shows the comparison between the test room temperature (blue) and the test room set point temperature (magenta) that corresponds to the extract air temperature, measured in the scenario 5.

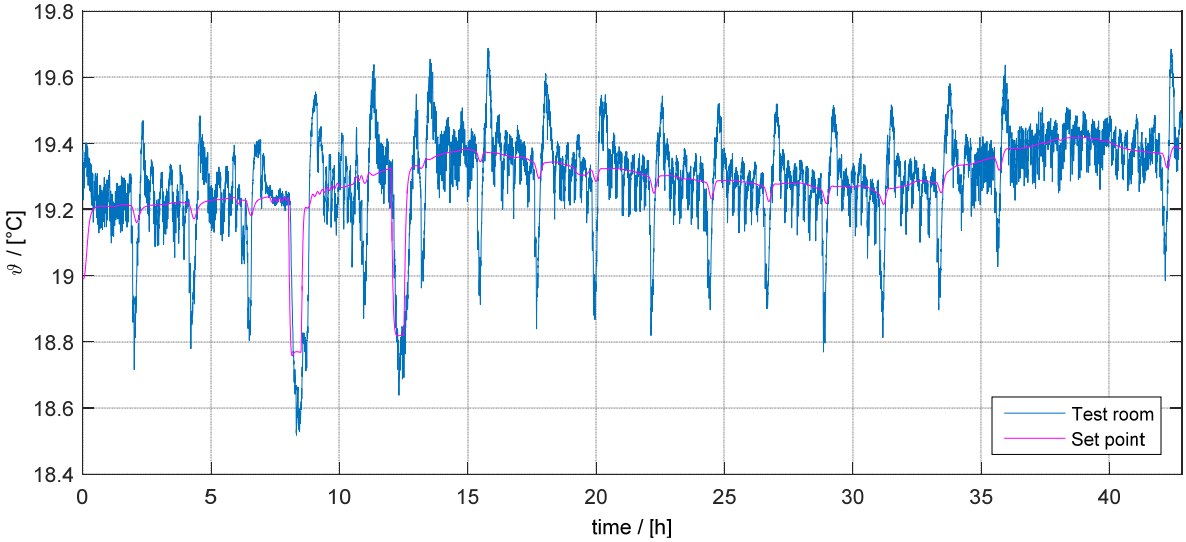

Figure A2-8: Comparison of the measured and set point temperature of the test room (scenario 5)

Table A2-18 shows the maximum, mean and minimum value of $\dot{Q}_{diff,tr}$ and $\dot{Q}_{set\ point,tr}$ calculated according to the equations (5.7), (5.8) and (5.9). The mean value of $\dot{Q}_{diff,tr}$ and $\dot{Q}_{set\ point,tr}$ are calculated by considering the absolute values.

Table A2-18: Maximum, mean and minimum value of $\dot{Q}_{diff,tr}$ and $\dot{Q}_{set\ point,tr}$ for the balance over the test room (scenario 5)

	$\dot{Q}_{diff,tr}$ [W]	$\dot{Q}_{set\ point,tr}$ [W]
Max	12.72	1029.70
Mean	2.51	405.15
Min	-15.02	-174.84

The energy can be obtained by integration of the powers over the considered period, as it is shown in the equations (5.10), (5.11) and (5.12), and these values are listed in Table A2-19.

Table A2-19: Energy values of the balance over the test room (scenario 5)

	Q_{tr} [Wh]
$Q_{set\ point,tr}$	17131.6
$Q_{mea,tr}$	17128.8
$Q_{diff,tr}$	2.8

The balance already explained in section 5.5.1 is now applied to the most critical point around the hour 12.5. Figure A2-9 shows the zoom of the Figure A2-8 around the hour 12.5.

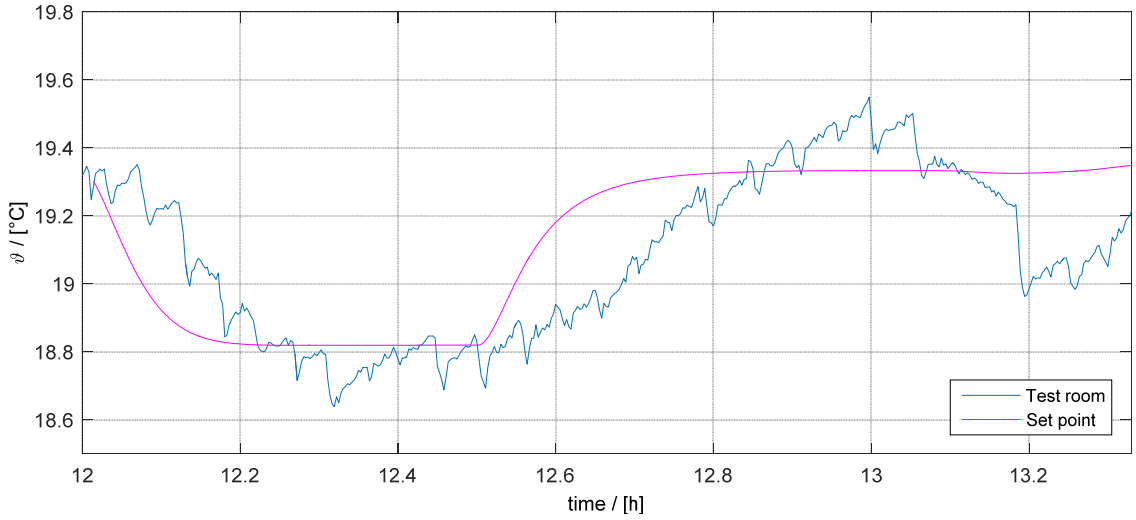

Figure A2-9: Zoom of Figure A2-5

With the equations (5.7), (5.8) and (5.9) the power differences are calculated and the results are shown in Table A2-20. The mean values of $\dot{Q}_{diff,tr}$ and $\dot{Q}_{set\ point,tr}$ are calculated by considering the absolute values.

Table A2-20: Maximum, mean and minimum value of $\dot{Q}_{diff,tr}$ for a section of period of the scenario 5

	$\dot{Q}_{diff,tr}$ [W]	$\dot{Q}_{set\ point,tr}$ [W]
Max	11.06	692.83
Mean	4.37	399.84
Min	-12.71	-98.22

The energy values can be obtained by integration of the powers, as shown in the equations (5.10), (5.11) and (5.12), and these values are listed in Table A2-21.

Table A2-21: Energy values of the balance over the test room for a section of period of the scenario 5

	Q_{tr} [Wh]
$Q_{set\ point,tr}$	522.9
$Q_{meas,tr}$	525.0
$Q_{diff,tr}$	-2.1

From these results, it is possible to conclude that the temperatures deviations which take places in the test room are not significant in the considered case.

APPENDIX 2.3.2: Coldbox Temperature Error

Figure A2-10 shows the measured and the set point coldbox temperatures.

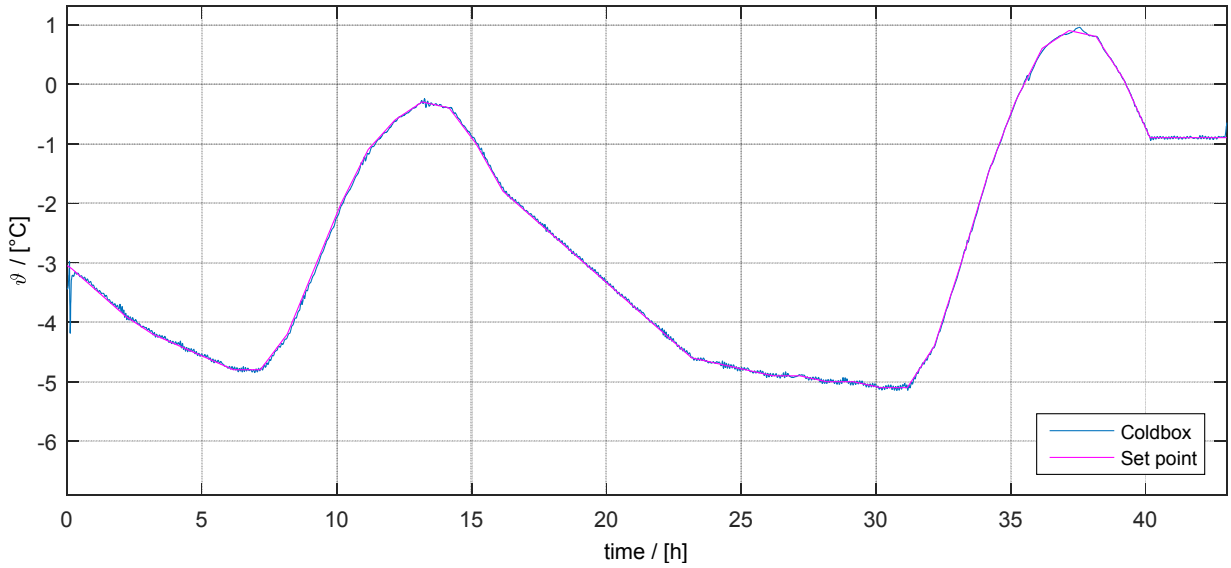

Figure A2-10: Measured and set point coldbox temperatures for the scenario 5

Table A2-22 shows the maximum, mean and minimum values of $\dot{Q}_{diff,cb}$ and $\dot{Q}_{set\ point,cb}$. The mean value of $\dot{Q}_{diff,cb}$ is calculated by considering the absolute values.

Table A2-22: Maximum, mean and minimum value of $\dot{Q}_{diff,cb}$ and $\dot{Q}_{set\ point,cb}$ for the balance over the coldbox (scenario 5)

	$\dot{Q}_{diff,cb}$ [W]	$\dot{Q}_{set\ point,cb}$ [W]
Max	0.6764	1277.4
Mean	0.0795	606.46
Min	-0.7388	0

The energy values can be obtained by integration of the powers, as it is shown in the equations (5.16), (5.17) and (5.18), and these values are listed in Table A2-23.

Table A2-23: Energy values of the balance over the coldbox (scenario 5)

	$Q_{diff,cb}$ [Wh]
$Q_{set\ point,cb}$	25968.3
$Q_{meas,cb}$	25968.7
$Q_{diff,cb}$	0.4

As for the other scenarios, it is possible to conclude that the coldbox temperatures deviations are not significant in the considered case.

APPENDIX 2.3.3: Total Error

$\dot{Q}_{set\ point}$, $\dot{Q}_{meas}$ and $\dot{Q}_{diff}$ are calculated by means of the equations (5.19), (5.20) and (5.21). The maximum, minimum and mean value of $\dot{Q}_{diff}$ and of $\dot{Q}_{set\ point}$ are shown in Table A2-24.

Table A2-24: Maximum, mean and minimum value of $\dot{Q}_{diff}$ and $\dot{Q}_{set\ point}$ for the scenario 5

	$\dot{Q}_{diff}$ [W]	$\dot{Q}_{set\ point}$ [W]
Max	15.0167	375.5919
Mean	2.5100	206.3801
Min	-12.7084	97.6939

The energy values can be obtained by integration of the powers, as it is shown in the equations (5.22), (5.23) and (5.24) and these values are listed Table A2-25.

Table A2-25: Energy values calculated from the whole balance for the scenario 5

	$Q_{diff,cb}$ [Wh]
$Q_{set\ point}$	8836.7
Q_{meas}	8839.9
Q_{diff}	-3.2

The overall error calculated during the three days of the HiL simulation is minor compared with the involved powers, so the set point temperatures are reproduced with high accuracy inside the coldbox and the test room.

7 REFERENCES

Enerclima. (2016). Retrieved 02 08, 2016, from http://www.enerclima.it.

iNSPIRe. (2016). Retrieved 02 16, 2016, from http://www.inspirefp7.eu.

meteonorm. (2016). Retrieved 10 1, 2015, from http://www.meteonorm.com.

Wikipedia. (2016). Retrieved 01 14, 2016, from https://en.wikipedia.org/wiki/PID_controller.

AB, S. I. (2016). *SWEP*. Retrieved 02 26, 2016, from http://handbooks.swep.net/.

Bhattacharya, S. K. (2013). *Control Systems Engineering.*

Borghetti, A. (2012). Centrali elettriche e generazione distribuita. *Education material*. Bologna.

Commisssion of the European Communities. (1990). *The Passys Test Cells.* Brussels: Directorate-General XII for Science, Research and Developement.

Davies, M. G. (2004). *Building Heat Transfer.*

Dermentzis, G., Ochs, F., Siegele, D., & Feist, W. (2014). A FAÇADE INTEGRATED MICRO-HEAT PUMP – ENERGY PERFORMANCE. *BauSIM*, 8.

Feist, W. (1994). *Thermische Gebäudesimulation, Kritische Prüfung unterschiedlicher Modellansätze.* C.F. Müller.

Glück, P. D.-I. (1990). *Wärmeübertragung; Wärmeabgabe von Raumheizflächen und Rohren.*

iNSPiRe. (2014). D3.3. Report on Ventilation and active Heating/Cooling Devices integrated in the Facade. *Report*.

J. A. , H., J. B. , R., & Kun Li , C. (1952). *On the Automatic Control of Generalized Passive Systems.*

Juelich, S.-I. (2016). CARNOT toolbox.

Leonardi, E. (2016). Micro-Heat Pump for Renovated Multi Family House – Simulation Based Analysis of the Performance and Thermal Comfort. *Masterthesis*.

Ochs, F., Dermentzis, G., Siegele, D., & Wolfgang, F. (2014). Feasibility of a Micro-heat Pump - Energy Performance Simulations. *Report*. Bressanone, Italy.

RCGroup. (2013). Il COP delle pompe di calore evaporanti ad aria. *Education material*.

SaLüH! (2016). FFG-Project. *Project*.

SAMSON. (2003). Controllers and Controlled System. *Education material*.

Siegele, D. (2013). Modellierung und Simulation von fassadenintegrierten aktiven Komponenten. *Bachelorthesis*.

Siegele, D. (2015). Measurement and Simulation of the Performance of a Façade-integrated MVHR with Micro Heat Pump. *Masterthesis*.

Wetter, M. (2010). Co-simulatioin of building energy and control systems with the Building Controls virtual Test Bed. *Journal of Building Performance Simulation*.

Zanchini, E. (2012). Moto dei fluidi e termocinetica. *Education material*.